



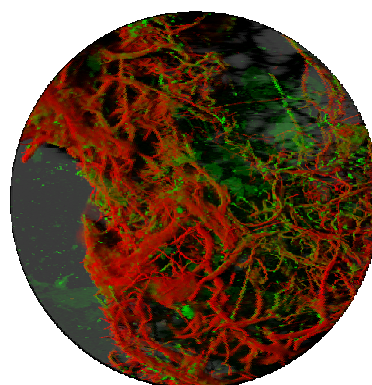
**Facultat de Farmàcia**  
**Dept. de Productes Naturals, Biologia Vegetal i Edafologia**

# **Caracterització de biofilms fototròfics d'ambients hipogeus**

**MÒNICA ROLDÁN MOLINA**

**2008**

## Resultats



*Resultats*

---

## Capítol 4

### Resultats

---

4.1. Mètodes de microscòpia aplicats a la recerca dels cianobacteris.	89
4.2. Fluorescència de biofilms i anàlisi d'imatge en l'estudi de monuments hipogeus.	99
4.3. Identificació de pigments en cèl·lules individuals procedents de biofilms fototròfics mitjançant espectrofotometria confocal.	119
4.4. Morfologia de biofilms fototròfics en baixa il·luminació. El cas de l'avenc de Puigmoltó.	127
4.5. Distribució de biofilms fototròfics en cavitats	147
4.6. Per què n'hi ha un creixement exuberant de microorganismes fototròfics en els ambients hipogeus?.	173
4.7. Els polisacàrids produïts per cèl·lules necrídiques porten a terme l'adherència dels hormogonis al substrat.	187
4.8. Pot influir la llum verda en les propietats de la fluorescència i l'estructura dels biofilms fototròfics?.	201
4.9. La influència de la llum verda en l'ultraestructura dels cianobacteris: la seva aplicació en ambients de baixa il·luminació.	209
4.10. L'eficàcia dels biocides i els tractaments de neteja en els treballs de restauració de monuments hipogeus.	233

*Resultats*

---

#### **4.1. Mètodes de microscòpia aplicats a la recerca dels cianobacteris**

Es revisen tècniques adequades per l'examen microscòpic dels cianobacteris. S'inclou la microscòpia electrònica de rastreig (SEM), la microscòpia electrònica de transmissió (TEM) i la microscòpia de rastreig làser confocal (CSLM). Es presenten avantatges i exemples de cadascuna d'elles. La combinació d'aquestes tècniques proporciona eines eficients per a la identificació i la caracterització dels cianobacteris. Amb el seu ús es pot comprovar la seva presència i viabilitat i definir la citomorfologia i l'estructura tridimensional de les comunitats que formen. Aquestes tècniques són complementàries i permeten la descripció física i fisiològica dels cianobacteris i les comunitats que constitueixen.

Els resultats detallats d'aquest capítol s'inclouen en el següent article:

Microscopy methods applied to cyanobacteria. *Limnetica* (2004), 23 (1-2): 179-185.

*Resultats*

---

## Microscopy methods applied to research on cyanobacteria

M. Hernández Mariné, E. Clavero & M. Roldán

Unitat de Botànica, Facultat de Farmàcia, Universitat de Barcelona, Av Joan XXIII s/n, Barcelona E-08028.  
E-mail: marionahernandez@ub.edu, mroldan@farmacia.far.ub.es, eclavero@farmacia.far.ub.es

### ABSTRACT

Several techniques for microscopic examination of cyanobacteria were reviewed. These included transmission electron microscopy (TEM), scanning electron microscopy (SEM) and confocal laser scanning microscopy (CLSM). Advantages and examples of individual techniques are presented. Their combination provides an efficient way for determining the presence and viability of cyanobacteria, characterization of taxa, observation of cytomorphology and definition of 3-D structure within communities.

**Keywords:** cyanobacteria, transmission electron microscopy, scanning electron microscopy, laser scanning microscopy

### RESUMEN

Se revisan técnicas para el examen microscópico de las cianobacterias. Se incluyen la microscopía electrónica de barrido (SEM), la microscopía electrónica de transmisión (TEM) y la microscopía de barrido láser confocal (CLSM). Se presentan ventajas y ejemplos de cada una de las técnicas. Su combinación proporciona herramientas eficientes para la identificación y caracterización de las cianobacterias. Con su uso se puede comprobar su presencia y viabilidad y definir la citomorfología y la estructura tridimensional de las comunidades que forman.

**Palabras clave:** cianobacterias, microscopía electrónica de barrido, microscopía electrónica de transmisión, microscopía de barrido láser confocal

### INTRODUCTION

Cyanobacteria are abundant throughout the world and contribute significantly to global primary productivity from which picoplanktonic marine and aridland terrestrial components account for a large proportion (García-Pichel *et al.* 2003). The advent of the electron microscopy (history reviewed by McMullan, 1995) revealed that blue-green algae were bacteria, presenting a well-defined submicroscopic organization with a lacking membrane-bound organelles. Their cells are surrounded by a more or less defined exopolysaccharide covering and a cell envelope of Gram-negative type. Pores of different sizes, orderly arranged or not, perforate the cell wall. What differences them from other prokaryotes is their ability to perform oxygenic photosynthesis, localized

in the thylakoid membranes. Thylakoids consist of a double unit membrane enclosing an intrathylakoidal space and their arrangement is characteristic of groups of strains. Thylakoids support two membrane-bound protein complexes, photosystem I (PSI) and photosystem II (PSII), which contain chlorophyll-binding subunits functioning as an internal antenna. In addition, there are rows of phycobilisomes on the thylakoid membrane that act as peripheral antenna systems.

The microscopy techniques most frequently used to determine the diversity of microorganisms in terms of morphology, ecology and physiological adaptations include, scanning electron microscopy (SEM), transmission electron microscopy (TEM) and confocal laser scanning microscopy (CLSM), apart from the classical light microscopy.



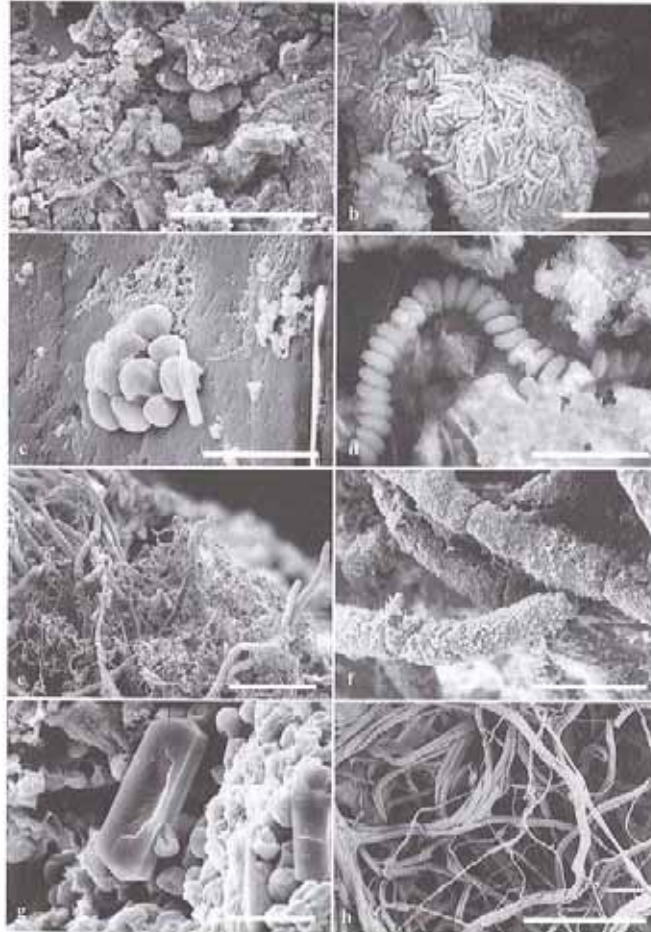


**Figure 1.** Scanning electron photomicrographs. **a, b,** colonisation inside gypsum crevices. Air drying. **a,** global view. Scale bar = 50  $\mu$ m. **b,** high magnification of microscopic colonies of *Synecococcus* sp. Scale bar = 5  $\mu$ m. **c,** small colony of *Chlorococcus* sp. developed on limestone. Conventional chemical fixation. Scale bar = 10  $\mu$ m. **d,** *Halospirulina* sp. from hypersaline microbial mats. Chemical fixation with 2% glutaraldehyde added to the hypersaline water. Scale bar = 10  $\mu$ m. **e, f,** biofilm on a calcareous stone surface. It consisted of *Scytonema julianum* and *Leptolyngbya* sp. Freeze fixation followed by freeze-drying and critical point drying. **e,** global view. Scale bar = 200  $\mu$ m. **f,** high magnification of calcified filaments of *S. julianum* with triradiate calcite crystals. Scale bar = 50  $\mu$ m. **g,** rod-shaped cyanobacteria boring a calcite crystal. Scale bar = 10  $\mu$ m. **h,** biofilm growing on plaster built by erected filaments of *Leptolyngbya* sp. Prefixation in acrolein vapour followed by addition of osmium tetroxide vapour and air drying. Scale bar = 50  $\mu$ m. **Microfotografías de barrido. a, b,** colonización en el interior de grietas en yesos. Secado al aire. **a,** visión de conjunto. Escala = 50  $\mu$ m. **b,** aumento de las colonias microscópicas de *Synecococcus* sp. Escala = 5  $\mu$ m. **c,** pequeñas colonias de *Chlorococcus* sp. sobre piedra calcárea. Fijación química convencional. Escala = 10  $\mu$ m. **d,** *Halospirulina* sp. procedente de tapetes microbianos hipersalinos. Escala = 10  $\mu$ m. **e, f,** biofilm sobre piedra calcárea. Fijado por *Scytonema julianum* y *Leptolyngbya* sp. Fijación mediante congelación seguida de desecado a bajas temperaturas. **e,** visión de conjunto. Escala = 200  $\mu$ m. **f,** aumento de los filamentos calcificados *S. julianum*, recubiertos de agujas trirradiadas de calcita. Escala = 50  $\mu$ m. **g,** cianobacteria coval perforando un cristal de calcita. Escala = 10  $\mu$ m. **h,** biofilm sobre mortero formado por filamentos erectos de *Leptolyngbya* sp. Prefixación con vapores de acroleína seguida de vapores de osmio y secado al aire. Escala = 50  $\mu$ m.

We illustrate a few practical examples, among the great variety of these techniques, to survey cyanobacterial specimens and to determine their intrinsic features. Protocols may require modifications according to organism characteristics.

### SCANNING ELECTRON MICROSCOPY (SEM)

SEM is used to examine surface topology and distribution of specimens as well as relationship among organisms at a high magnification.

Conventional SEM preparation techniques include air drying; chemical fixation followed by critical point drying or freeze fixation followed by freeze-drying and critical point dried. A general overview of them is found in Goldstein *et al.* (1981) and Hyatt (1989).

A standard procedure includes chemical fixation with 2% glutaraldehyde (1,5-glutar-di-aldehyde) in a 0.1 M cacodylate buffer overnight, dehydration in ethanol and critical point dried. The conductivity of biological material may be increased by the impregnation of the whole material with heavy metal salts. Afterwards, specimens are placed on stubs and coated with carbon or gold sputtered. For samples prone to collapse when submerged in liquid medium, a pre-fixation in acrolein vapour followed by addition of osmium tetroxide vapour results in adequate preservation of the three-dimensional structures (Hernández-Mariné *et al.*, 2001). Small stones or filters may also be mounted on the stubs with a biadhesive tape and coated.

Clean samples or calcareous investments work well and the procedure is especially helpful for calcite crystals deposited on sheaths or any outer surface (Fig. 1f). However, as biological material, cyanobacteria tend to be susceptible to dehydration. Sheaths and mucilaginous outer layers may be condensed or blurry the surface of the specimens. Examples of the above protocols are shown in Figure 1.

Other types of SEM (not shown) overcome some of the processing inconveniences of conventional SEM. For example, Environmental

Scanning Electron Microscopy allows the observation of fresh samples at low magnification without modification or preparation (Urzi & Albertano 2001). On the other hand, low temperature scanning electron microscopy (LTSEM), allows the observation of cryofractured samples without further process or alteration (Ascaso *et al.* 2002).

### TRANSMISSION ELECTRON MICROSCOPY (TEM)

TEM provides morphological information about the size, shape and arrangement of organelles inside the cells and the relationship among microorganisms in areas a few nanometers in diameter. A beam of electrons is focused through the sample, producing a map of light and dark areas, which depends on the disposition of heavy metals absorbed selectively in the sample.

Chemical fixation is the most widely used method to preserve biological specimens for TEM. General fixation and embedding methods have been described elsewhere (Hayat, 1989; Bettarel *et al.*, 2000). Samples must be in excellent conditions prior fixation and their ionic strength taken into account, unless the observation of some kind of damage is wanted. For non saline samples 2% glutaraldehyde in 0.1 M cacodylate buffer and post-fixation with 1% osmium tetroxide in the same buffer yield acceptable results. Saline samples, that have higher osmolality, may be fixed with a mixture of 2% glutaraldehyde and variable concentration of formaldehyde solution, according to the osmolality of the medium or the salinity. Next steps are dehydration, embedding in resin, and sectioning. Sections are stained with heavy metals *ex. with* 2% uranyl acetate and lead citrate.

Sometimes the chemical fixation is unsatisfactory. This is mainly revealed by a collapsed cytoplasm. In such a case, or when immunocytochemical and microanalytical studies must be performed, a rapid freeze fixation followed by freeze substitution that replaces cellular water at low temperatures is helpful (Quintana, 1994; Porta *et al.*, 2000). Both methods are appropri-

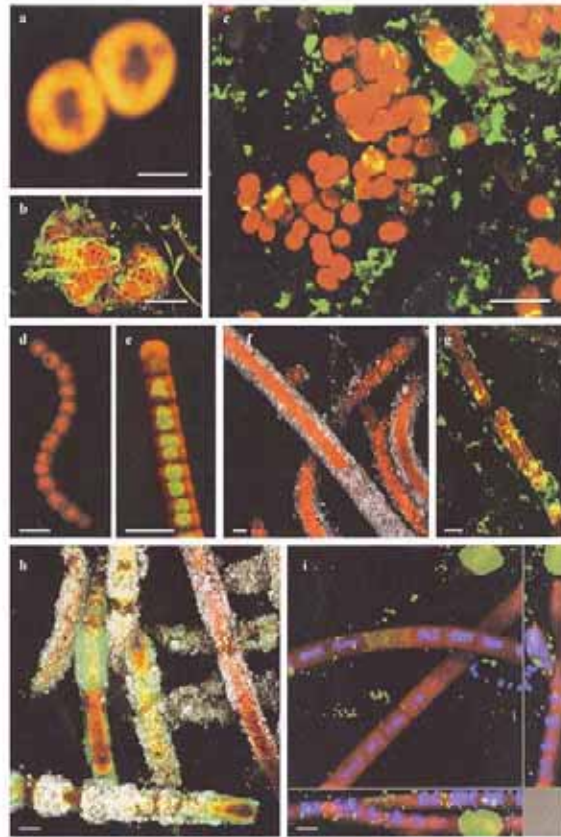


**Figure 2.** Confocal Laser Scanning photomicrographs. **a**, *Cyanoshece* PCC 8303, *xy* single optical thin section. Pigment fluorescence, mainly located at the cell periphery, provides evidence of the thylakoid arrangement. Scale bar = 1  $\mu$ m. **b**, *Aphanothece* sp. from hypogean habitats. Two-channel (pigment fluorescence in red and EPS in green) maximum intensity projection. Scale bar = 10  $\mu$ m. **c**, Thin biofilm of *Gloeocapsopsis* sp. from hypogean habitats. Two-channel (pigment fluorescence in red and EPS in green) maximum intensity projection. Scale bar = 5  $\mu$ m. **d**, filament of *Nostoc* sp. *xy* single optical thin section of pigment fluorescence. Scale bar = 10  $\mu$ m. **e**, *Crinalium* PCC 9333, single section. In dividing cells the nucleoid figures depends on the stage of the division. Two-channel (pigment fluorescence in red and DNA (SYTOX Green) in green). **f**, **g**, **h**, *Seytonema julianum* from limestone caves. Scale bar = 5  $\mu$ m. **f**, two-channel (pigment fluorescence in red and reflection image in white) maximum intensity projection, showing the calcite needles. Scale bar = 10  $\mu$ m. **g**, false branching by trichome fragmentation and lateral protrusion. Two-channel (pigment fluorescence in red EPS in green) maximum intensity projection. Scale bar = 10  $\mu$ m. **h**, three-channel maximum intensity projection (pigment fluorescence in red and EPS in green and calcite needles in white). Scale bar = 10  $\mu$ m. **i**, three-dimensional extended focus projections in *x-y*, *x-z* and *y-z* views, bilinear interpolated *x-y* CLSM sections in the *z*-direction of the biofilm (pigment fluorescence in red, DNA (Hoechst 33258) in blue and EPS in green). Scale bar = 10  $\mu$ m. **Microfotografías de CLSM. a**, *Cyanoshece* PCC 8303, secciónd *xy*. La fluorescencia de los pigmentos, mayoritariamente localizada en la periferia de la célula, evidencia la disposición de los tilacoides. Escala = 1  $\mu$ m. **b**, *Aphanothece* sp. de hábitats hipogeos. Proyección de intensidad máxima con doble canal (fluorescencia de los pigmentos en rojo y EPS en verde). Escala = 10  $\mu$ m. **c**, biofilm de *Gloeocapsopsis* sp. procedente de hábitats hipogeos. Proyección de intensidad máxima con doble canal (fluorescencia de los pigmentos en rojo y EPS en verde). Escala = 5  $\mu$ m. **d**, filamento de *Nostoc* sp. secciónd *xy* de la fluorescencia de pigmentos. Escala = 10  $\mu$ m. **e**, *Crinalium* PCC 9333, secciónd única. Las figuras de los nucleoides dependen del estado de división. Doble canal (fluorescencia de los pigmentos en rojo y ADN (SYTOX Green) en verde). **f**, **g**, **h**, *Seytonema julianum* procedente de cuevas calcáreas. Escala = 5  $\mu$ m. **f**, Proyección de intensidad máxima con doble canal (fluorescencia de los pigmentos en rojo y reflexión en blanco), mostrando las agujas de calcita. Escala = 10  $\mu$ m. **g**, Falsa ramificación por fragmentación del trichoma y protrusión lateral. Proyección de intensidad máxima con doble canal (fluorescencia de los pigmentos en rojo y EPS en verde). Escala = 10  $\mu$ m. **h**, Proyección de intensidad máxima con triple canal (fluorescencia de los pigmentos en rojo, EPS en verde y agujas de calcita en blanco). Escala = 10  $\mu$ m. **i**, Proyección tridimensional "extended focus" en planos *x-y*, *x-z* and *y-z*. interpolación bilinear de las secciones *x-y* de CLSM en dirección *z* de un biofilm (fluorescencia de los pigmentos en rojo, ADN (Hoechst 33258) en azul y EPS en verde). Escala = 10  $\mu$ m.

ate to localise chemicals or organules at the sub-cellular level, using cytochemical stains.

Examples of cell wall layers and porefields, exopolysaccharide covering and sheath structure, cellular division behaviour, intercellular relationships and thylakoid arrangement, using the above described protocols, are shown in Figure 2.

### CONFOCAL LASER SCANNING MICROSCOPY (CLSM)

CLSM is a tool for 3-D localization of fluorescent organisms or items dyed with fluorescent labels. The technique provides an efficient way to determine the presence, the viability and the spatial organization of specific organisms. It offers the possibility for non-invasive optical sectioning by subtracting out-of-focus planes of the image. It allows the *in situ* observations, that is, to examine the surface and the in depth structure of the sample with minimal preparation and without disturbing the structure (Neu & Lawrence, 1997; Roldán *et al.*, 2004).

Advantages are the inherent specificity and sensitivity of fluorescent probes and labelling protocols (Haugland, 1999). CLSM has become a standard tool and its capabilities and use for biological applications are summarized elsewhere (Pawley, 1995). We used a combination of natural pigment fluorescence and fluorescence probes for imaging the *in situ* 3D structure of cyanobacteria and their extracellular polymeric substances (EPS).

The CLSM equipments provide series of thin optical sections of the sample. Optical sections are 2D images obtained at different intervals (*z* step) along the optical axis. The *z* profile is obtained by setting the start position above the sample and the stop position below the layers of interest. CLSMs are equipped with different lasers and detection channels. Laser light sources are monochromatic and the most usual include argon (488 and 514 nm), argon-krypton (488, 568, and 647 nm), helium-neon (543, 596, and 633 nm), and ultraviolet (UV)-argon (351-364 nm) excitation laser beams.

Samples must be fluorescent to be observed in the CLSM. The cyanobacterial photosynthetic pigments, chlorophyll *a* and phycobilins, have an inherent fluorescence at 543 and 633 nm excitation and 590-800 nm emission. To target other specific elements many fluorescent dyes and labels can be used. We use Hoechst 33258 to localize nucleoids, in living or death cells, that fluoresce in blue when excited by ultraviolet light (351 and 364 nm) and SYTOX Green S-7020 that fluoresce in green when excited by blue light (488 nm). SYTOX Green has a high affinity for nucleic acids, but cannot cross the membranes of the living cells which must be fixed before observation. Either glutaraldehyde in 0.2 M cacodylate buffer (pH=7.2) or 4% paraformaldehyde in phosphate buffered saline (PBS) solution 0.15 M (pH=7.4) may be used for fixation. However, glutaraldehyde must be used with caution due to its inherent fluorescence in a wide range of wavelengths.

EPS are revealed with the carbohydrate recognising lectin Concanavalin-A (Con-A from *Canavalia ensiformis*) or Wheat Germ Agglutinin (WGA from *Triticum vulgare*), both need to be conjugated with a fluorophore such as Alexa Fluor 488, among other labels (all fluorescent stains from Molecular Probes, Inc. Leiden). To avoid interference or overlapping of labels that fluoresce in the same wavelengths of pigments, samples are first fixed and then they are discoloured with a 3:1 mixture of ethanol and glacial acetic acid and rinsed in distilled water.

Reflection image (grey channel, excitation at 488 nm and emission at 480-490 nm) was employed to visualise the external surfaces, mineral particles and other compounds, which had a different refractive index from organic matter.

The different optical series can be processed to obtain a single compound image (512 x 512 pixel series and 24 bytes per pixel) by means of different algorithms from the microscope software (Leica) and Imaris software package (Bitplane AG, Zurich). In the figure 3 we present images of a single optical sections and others processed by means of the following algorithms: i) Maximum intensity projection: two-

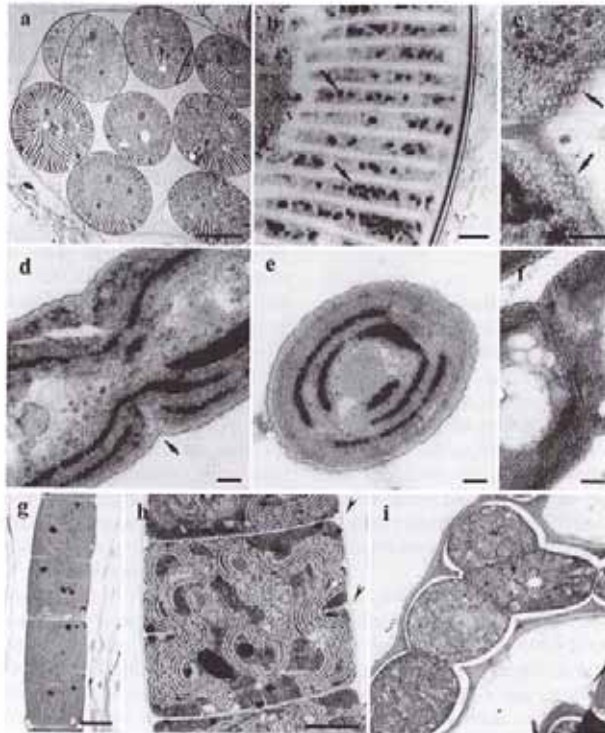


**Figure 3.** Transmission electron photomicrographs. a, b, *Microcoleus chthonoplastes* from a surface microbial mat. Rapid freeze fixation and freeze substitution. a, cross section through a bundle inside a common sheath. Scale bar = 2  $\mu\text{m}$ . b, enlarged view showing the mucilaginous covering, the Gram-negative cell wall and the radial arrangement of the thylakoids. Black spots between thylakoidal membranes are glycogen granules (arrow). Scale bar = 0.1  $\mu\text{m}$ . c, *M. chthonoplastes*. Thin section in the septum region showing the rows of pores at both sides. Chemical fixation. Scale bar = 0.1  $\mu\text{m}$ . d, e, f, *Halomicrocnema excentricum* from hypersaline ponds. Chemical fixation. d, longitudinal section. The outer membrane of the cell wall is not involved in the formation of the septum. A slightly constriction is found between cells along the trichome length (small arrow). Scale bar = 0.1  $\mu\text{m}$ . e, cross section. The thylakoids are concentric and parallel to the cell wall. Scale bar = 0.1  $\mu\text{m}$ . f, group of gas vesicles close to the septum. Scale bar = 0.1  $\mu\text{m}$ . g, longitudinal thin section of a *Oscillatoria lacus-solaris* trichome. Chemical fixation. Thylakoids are disposed more or less parallel to the longitudinal walls. However, some of them cross the nucleoid area. Discontinuous cell division, daughter cells divide and grow into the mother cell size before the next division. Scale bar = 1  $\mu\text{m}$ . h, *Lyngbya* sp. Chemical fixation. Thylakoids are whorled or arranged in parallel groups. Cyanophycin granules are scattered among thylakoids. Continuous cell division, since a new septum formation began before the former one is finished (arrows). Scale bar = 1  $\mu\text{m}$ . i, *Fischerella* sp. from a hypogean habitat. Chemical fixation. The trichomes can be either slightly constricted at the cell walls or torulose. Note the true lateral branching that originates from the change of division plane from transversal to longitudinal; intercalary cell (white asterisk) is in contact with three other cells. Scale bar = 1  $\mu\text{m}$ . *Microfotografías de transmisión.* a, b, *Microcoleus chthonoplastes* procedente de la superficie de un tapete microbiano. Fijación mediante congelación y criosustitución. a, Sección transversal de un haz de filamentos. Escala = 2  $\mu\text{m}$ . b, Vista longitudinal de la envoltura mucilaginosa, la pared celular Gram-negativa y la disposición radial de los tilacoides. Gránulos de glicógeno entre las membranas tilacoidales (flecha). Escala = 0.1  $\mu\text{m}$ . c, *M. chthonoplastes*. Sección en la región del septo que muestra las filas de poros a ambos lados. Fijación química. Escala = 0.1  $\mu\text{m}$ . d, e, f, *Halomicrocnema excentricum* de cubetas hipersalinas. Fijación química. d, Sección longitudinal. La membrana exterior de la pared celular no interviene en la formación del septo. Se observa una ligera constricción en los tubos (flecha pequeña). Escala = 0.1  $\mu\text{m}$ . e, Sección transversal. Tilacoides concéntricos y paralelos a la pared celular. Escala = 0.1  $\mu\text{m}$ . f, Grupo de vesículas de gas cerca del septo. Escala = 0.1  $\mu\text{m}$ . g, Sección longitudinal de un trichoma de *Oscillatoria lacus-solaris*. Fijación química. Los tilacoides se disponen de forma más o menos paralela a la pared longitudinal. Sin embargo, algunos de ellos cruzan el área del nucleóide. División celular discontinua, una sola división intercalar por célula. Escala = 1  $\mu\text{m}$ . h, *Lyngbya* sp. Fijación química. Tilacoides espiralados o en grupos paralelos. Gránulos de cianoficina distribuidos entre los tilacoides. División celular continua, más de una división intercalar por célula (flechas). Escala = 1  $\mu\text{m}$ . i, *Fischerella* sp. procedente de hábitats hipogeos. Fijación química. Trichomas torulosos o con una ligera constricción a nivel del septo. Fijarse en la ramificación lateral verdadera que origina un cambio de plano de división del transversal al longitudinal: la célula intercalar (asterisco blanco) está en contacto con tres células. Escala = 1  $\mu\text{m}$ .

dimensional compound image that integrates the maximum fluorescence intensities of each x, y point of all the optical series along the z-axis.

ii) Extended focus: the image is divided into three frames that represent the maximum intensity projection for the x-y, x-z and y-z planes.

iii) Simulated fluorescence processing (SFP): a three-dimensional simulation that enhances the fluorescence of surface layers and embosses all channels, as if they were illuminated from an oblique angle (Messerli *et al.*, 1993).

Extended focus images of unmodified stone fragments (Fig. 3i), built with the maximum intensity projections of the x-y, x-z, and y-z planes, evidenced gross spatial distribution of microorganisms, EPS and substratum, but also the disposition of microorganisms (e. g. erected vs. prostrate filaments) exhibiting the stratification of the biofilm.

These microscopy techniques (SEM, TEM and CLSM) complemented each other to build a complete physical and physiological description of the cyanobacteria and the communities they constitute.

#### ACKNOWLEDGEMENTS

This work was supported by EU Programme Energy, Environment and Sustainable Development in the frame of CATS Project, contract EVK4-CT-2000-00028. The facilities of SEM, TEM and Confocal Microscopy provided by the Scientific and Technical Services of the University of Barcelona are gratefully acknowledged.

#### REFERENCES

- ASCASO, C., J. WIERZCHOS, V. SOUZA-EGIPSY, A. DE LOS RÍOS & J. DELGADO RODRIGUES. 2002. In situ evaluation of the biodeteriorating action of microorganisms and the effects of biocides on carbonate rock of the Jeronimos Monastery (Lisbon). *International Biodeterioration & Biodegradation*, 49: 1-12.
- BETTAREL, Y., T. SIMENGANDO, C. AMBLARD, & H. LAVERAN. 2000. A comparison of methods for counting viruses in aquatic systems. *Appl. Environ. Microbiol.*, 66: 2283-2289.
- GARCÍA-PICHEL, F., J. BELNAP & S. NEUER. 2003. How much cyanobacteria? Estimates of total biomass and its distribution. *Arch. Hydrobiol./Suppl.*, 148. *Algological studies*, 109: 213-227.
- GOLDSTEIN, J. I., D. E. NEWBURY, P. ECHLIN, D. C. JOY, C. FIORI & E. LIFSHIN. 1981. *Scanning Electron Microscopy and X-Ray Microanalysis*. Plenum Press. New York and London.
- HAUGLAND, R. P. 1999. *Handbook of Fluorescent Probes and Research Chemicals*, 7<sup>th</sup> Ed. Eugene: Molecular Probes, Inc.
- HAYAT M. A. 1989. *Principles and techniques of electron microscopy. Biological applications*. Macmillan Press LTD. Houndmills and London.
- HERNÁNDEZ-MARINÉ, M., G. MARTINEZ, A. DOMINGUEZ, R. FONTARNAU & N. CORTADELLAS. 2001. SEM studies of arborescent aerophytic biofilms. Use of acrolein and osmium vapour impregnation. In: *Microscopy*: 334-335, Universitat de Barcelona, Barcelona.
- MCMULLAN, D. 1995. Scanning electron microscopy 1928-1965. *Scanning*, 17: 175-185.
- NEU, T. & J. R. LAWRENCE. 1997. Development and structure of microbial biofilms in river water studied by confocal laser scanning microscopy. *FEMS Microbiology Ecology*, 24: 11-25.
- PAWLEY, J. B. 1995. *Handbook of biological confocal microscopy*. Plenum Press, New York and London).
- PORTA, D., R. RIPPKA & M. HERNÁNDEZ-MARINÉ. 2000. Unusual ultrastructural features in three strains of *Cyanothece* (cyanobacteria). *Archives of Microbiology* 173: 154-163.
- QUINTANA, C. 1994. Cryofixation, cryosubstitution, cryoembedding for ultrastructural, immunocytochemical and microanalytical studies. *Micron*, 25: 63-99.
- ROLDÁN, M., E. CLAVERO, S. CASTEL & M. HERNÁNDEZ-MARINÉ. 2004. Biofilms fluorescence and image analysis in hypogean monuments research. *Arch. Hydrobiol./Suppl.* 150. *Algological studies*, 111: 127-143.
- URZI, C. & P. ALBERTANO. 2001. Studying phototrophic and heterotrophic microbial communities on stone monuments. In R.J. Doyle (ed.), *Methods in Enzymology* 336: 340-355. San Diego CA. Academic Press.



---

## 4.2. Fluorescència de biofilms i anàlisi d'imatge en l'estudi de monuments hipogeu

La caracterització de l'arquitectura dels biofilms, així com la interacció entre els microorganismes i les superfícies a les quals s'adhereixen, ha estat escassament estudiada, malgrat que és fonamental per resoldre problemes associats al biodeteriorament i per escollir mètodes de control i eliminació adequats. La combinació del CSLM amb diferents sondes fluorescents va proporcionar informació detallada de la composició i l'estructura dels biofilms, la seva morfologia i el metabolisme cel·lular dels seus components. Es va utilitzar el microscopi de rastreig làser confocal per estudiar biofilms fototròfics aerofítics que es desenvolupaven en superfícies il·luminades artificialment en monuments hipogeu, com les catacumbes romanes, concretament les Catacumbes de Domitilla i St. Callistus (Roma, Itàlia). La fluorescència natural de les clorofil·les i les ficobiliproteïnes va ser utilitzada per conèixer la distribució en fondària de les microalgues i els cianobacteris que són fotosintètics. Es van efectuar tincions dobles per determinar la relació entre els pigments, els àcids nucleics i els EPS. Els àcids nucleics van ser marcats específicament amb el fluorocrom Hoechst 33258. Les substàncies polimèriques extracel·lulars (EPS o mucíl·lag) van ser marcades amb la lectina Concanavalina A (Con-A), d'ampli espectre, conjugada amb el fluorocrom Alexa 488 (Molecular Probes, Inc). La Con-A és una lectina que s'uneix als residus de carbohidrats  $\alpha$ -D-mannosa i  $\alpha$ -D-glucosa amb alta especificitat. Atesa la riquesa dels diferents substrats sobre els quals es desenvolupen aquests biofilms, es van detectar altres components autofluorescents, com el carbonat càlcic. Per aquesta raó, en alguns casos es va utilitzar el canal de reflexió per visualitzar superfícies externes, partícules minerals i/o beines calcificades.

Els diferents tipus d'imatges tridimensionals van permetre caracteritzar l'estructura dels biofilms. Les projeccions "Extended" eren molt útils per comparar biofilms. Aquest tipus de reconstrucció mostrava la distribució



espacial dels microorganismes, els EPS i el substrat respecte als eixos x, y i z, així com la disposició i la morfologia dels microorganismes, el que permet observar l'estratificació i la porositat del biofilm. Les projeccions en perspectiva mostren les característiques de la superfície de la mostra, tant del biofilm com del substrat.

La informació aportada pel CSLM complementa la de les tècniques microscòpiques clàssiques. El seu major avantatge és l'observació de l'interior de mostres intactes. EL CSLM permet l'anàlisi de l'estructura a partir de la visualització tridimensional i simultània d'elements específics en l'interior dels biofilms causant la mínima perturbació: molècules (DNA), estructura (superfícies, matriu...) i propietats (creixement i senescència). La tècnica de representació tridimensional, usant diferents algorismes per al processament d'imatges digitals, ha permès obtenir la descripció de l'estructura dels biofilms i una visió més realista i fidel, gràcies a la informació conjunta obtinguda mitjançant reconstruccions 2D i 3D. També va ser possible l'avaluació de la disposició espacial dels microorganismes creixent sobre materials, informació útil en els estudis de biodeterioració.

Els resultats detallats d'aquest capítol s'inclouen en el següent article:

Biofilms fluorescence and image analysis in hypogean monuments research. **Arch. Hydrobiol./Suppl. Algological studies** (2004), 111: 127-143.

Algological Studies 111	127–143	Stuttgart, February 2004
-------------------------	---------	--------------------------

## Biofilms fluorescence and image analysis in hypogean monuments research

By MÓNICA ROLDÁN<sup>1</sup>, ESTER CLAVERO<sup>1</sup>, SUSANNA CASTEL<sup>2</sup> and MARIONA HERNÁNDEZ-MARINÉ<sup>1</sup>

<sup>1</sup>Universitat de Barcelona, Facultat de Farmàcia, Barcelona, Spain

<sup>2</sup>Serveis Científicotècnics, Universitat de Barcelona, Barcelona, Spain

With 20 figures and 1 table in the text

**Abstract:** Confocal Laser Scanning Microscopy (CLSM) was used to investigate aerophytic phototrophic biofilms thriving on artificially illuminated surfaces in Roman hypogean monuments, particularly the St. Callistus and Domitilla Catacombs (Rome, Italy). Phototrophic organisms were visualized by their *in vivo* pigment fluorescence, whereas extrapolymeric substances (EPS) and DNA structures of both photo- and heterotrophic microorganisms were revealed respectively with the carbohydrate recognising lectin Concanavalin-A conjugated with the fluorophore Alexa Fluor 488 and the fluorochrome Hoechst 33258 labels. Inherent fluorescences other than pigment fluorescence such as CaCO<sub>3</sub> fluorescence of the substratum were also detected. Distribution of microorganisms and EPS in biofilms and their relationship with substratum was evidenced with the application of diverse kinds of image analyses. Detailed localization of certain structures or taxa was achieved with the examination of gallery images. On the other hand, particular image analyses enlightened one or several partial aspects of the biofilm heterogeneity. Extended focus images built with the maximum intensity projections of the x–y, x–z, and y–z planes were best to compare among biofilms and to reveal their porosity and stratification. 3D-reconstructions of biofilms as perspective images gave an account of the surface characteristics such as roughness or coverage of the substratum surface. Topographic reconstruction was used to measure geometrical and biological heterogeneity parameters like sample thickness or surface roughness. What makes CLSM so powerful is the ability to analyse samples with minimal preparation and non-disturbing architectural observation, the use of multiple excitation and detection wavelengths at different depths of focus, and the large pool of digital image processing algorithms with which one can effectively target specific elements in the biofilm sample, such as molecules (e.g. DNA and pigments), structure (e.g. surfaces, matrix, sheaths and filaments) and properties (e.g. stage of cell division, growth and senescence), with the capability to fully visualise them all in 3D image.

**Keywords:** Biofilms, Roman Catacombs, Confocal laser scanning microscopy (CLSM), cyanobacteria, Con-A, EPS, hypogean environments, Hoechst 33258, 3D-image structure of biofilms.

0342-1123/04/0150-127 \$ 4.25

© 2004 E. Schweizerbart'sche Verlagsbuchhandlung, D-70176 Stuttgart  
Algological Studies 111 – Arch. Hydrobiol. Suppl. 150

### Introduction

In the past decade the study of biofilms has emerged as a powerful new approach for the research of microorganisms. It has been established, by direct observation of natural habitats, that a multi-species community can persist attached to surfaces in a relatively complex and coordinated manner (LAWRENCE et al. 1991). The microorganisms building a biofilm are embedded within a matrix formed by their own, which constitutes a protected mode of growth easing survival in hostile environments (COSTERTON et al. 1999, WIMPENNY 2000 and references therein).

In the special case of hypogean monuments, biofilms are acrophytic (living on air), that is, they grow attached to the interface air/surface, playing an important role in the erosion of several substrata. Phototrophic organisms are the main components of these structured communities, when light is available (LAWRENCE et al. 1991, DANIN & CANEVA 1990, ORTEGA et al. 1993, GÓMEZ-ALARCÓN et al. 1995, ALBERTANO et al. 1994, HERNÁNDEZ-MARINÉ et al. 2001).

Up to now most of the methodological approaches to study microbial communities on stone monuments have dealt with the quantification and identification of the different types of microorganisms whereas the biofilm architecture has been poorly studied, mainly by scanning and transmission electron microscopy (URZI & ALBERTANO 2001). However, as these techniques require sample dehydration and fixation, they do not allow non-disturbing architectural observation (DAVEY et al. 2000).

Recent advances in microscopy, especially in confocal laser scanning microscopy (CLSM) and molecular techniques, facilitate the examination of such communities (LAWRENCE & NEU 1999 and references therein). CLSM, due to its optical sectioning features, high spatial resolution and minimal sample manipulation, is a very powerful tool for the non-destructive study of thick biological samples (CALDWELL et al. 1992, LAURENT et al. 1994). CLSM has been successfully applied to different aspects of microbial ecology, such as spatial arrangement, composition and the properties of different types of biofilms (LAWRENCE et al. 1991, WOLFAARDT et al. 1994, NEU & LAWRENCE 1997). However, CLSM techniques have been mostly addressed to aquatic biofilms and sessile communities responsible for bacterial infections (COSTERTON et al. 1999), whereas acrophytic biofilms have been scarcely studied.

In the frame of a European project that focuses on the control, prevention and monitoring of cyanobacteria dominated communities that cause damage to rock surfaces in Roman hypogea (CATS), we studied the biofilms formed in the St. Callistus and Domitilla Catacombs. The main objective of this work was to develop a protocol for obtaining the maximum information on the spatial organisation of specific organisms, the distribution of exopolymer components, the interactions of biofilms with the colonised surfaces toward, eventually, control of biofilm development.

### Material and methods

Our biofilm samples come from artificially illuminated surfaces in Roman hypogean monuments, in particular the St. Callistus and Domitilla Catacombs (Rome, Italy). Fragments of biofilms were obtained by detaching from several substrata (plaster, bricks, frescoes and tufa) and, rarely, they were taken together with small pieces of their support. The samples were collected on March 2001 and maintained on a 2 mm layer of BG11 medium (RIPPKA 1988) at a 10% nutrient concentration, solidified with agar (1%, Merck). This setup kept the samples alive and protected the biofilm architecture.

#### Preparation and staining of material

Undamaged biofilm fragments were transferred to microcapsules or onto cavity microscope slides. Nucleic acids were specifically stained with the DNA-selective dye Hoechst 33258 (0.008  $\mu\text{m}$ ) (Sigma-Aldrich). EPS were labelled with the broad-spectrum carbohydrate recognizing lectin Concanavalin-A conjugated with the fluorophore Alexa Fluor 488 (Con-A, Molecular Probes, Inc.) at a final concentration 0.8 mM. The samples were incubated at the same time in Con-A and Hoechst 33258 solution for 40 min at 16°C and darkness. After staining, the samples were washed 3 times with phosphate buffered saline (PBS) solution 0.15 M adjusted pH of 7.4, which was finally drained.

#### Confocal Laser Scanning Microscopy

Two different CLSMs were used: 1. TCS4D Leica Confocal Scanning Microscope equipped with three ArKr 75 mV lasers and two detection channels; the wavelengths of the excitation lasers were 488 nm, 568 nm and 674 nm. Images were acquired in two channels simultaneously, red channel for pigment fluorescence and green channel for EPS labelled with Con-A. The reflection image (grey channel, excitation at 488 nm and emission at 480–490 nm) was employed to visualise the external surfaces, mineral particles and other compounds, which had a different refractive index from organic matter. 2. TCS-SP2 Leica Confocal Scanning Microscope equipped with four laser beams and three detection channels; wavelengths of the excitation lasers were in the UV Ar (351 nm and 364 nm), blue Ar (458, 476, 488 nm), green Ar (514 nm); green HeNe (543 nm) and red HeNe (633 nm). Images were acquired in the three channels simultaneously (red channel for pigment fluorescence, blue channel for nucleic acids Hoechst 33258 label and green channel for the labelled EPS). The Leica TCS-SP2 combines confocal microscopy with spectrophotometric detection. A prism in the beam path splits the light emitted from the specimen into its spectral components. A slit with two movable mirrored plates, placed directly in front of the photomultiplier of each detector, allows for a wavelength-specific selection of the fluorescent signals out of the overall spectrum; in the system the detection bandwidth can be changed to fit a specific emission and thus minimise crosstalk among fluorophores. Samples were observed with the following lenses: x10 (0.4 Numerical Aperture or NA), x20 (0.7 NA), x40 (1.25–0.75 NA), x63 (1.32 NA) and x100 (1.4–0.7 NA) Plan Apochromat oil immersion objective.

Image acquisition was performed with the software package delivered with the instruments: Leica TCS-4D and TCS-SP2 Confocal Software. These equipments provide series of thin optical sections of the sample. We acquired optical sections in both x–y and x–z planes. The optical sections are 2D images obtained at different intervals (z step) along the optical axis. The image size was 512 x 512 pixels with 8-bit greyscale (the intensity of each pixel was set to 255 levels of grey).

The z profile was obtained by setting the start position above the sample and the stop position below the layers of interest. The thickness of the sample was established as the distance from the uppermost to the lowest position of inherent pigment fluorescence. The maximum depth that could be measured was 166.6  $\mu\text{m}$  for the TCS-4D and 3.00 mm for the TCS-SP2.

**Image analysis and processing**

Image analyses were performed using the Imaris software package (Bitplane AG, Zürich) and the Leica Confocal software (LCS). A 3-D image is processed voxel-by-voxel (pixel in 3D). The different optical series were processed to obtain a single compound image (512 x 512 pixel series and 24 bites per pixel) by means of different algorithms:

1) Maximum intensity projection: two-dimensional compound image that integrates the maximum fluorescence intensities of each x,y point of all the optical series along the z-axis.

2) Gallery: two-dimensional compound images consisting on a series of selected sections, ordered correlatively from the top to the bottom of the acquisition.

3) Perspective image: the series of optical sections obtained along the sample depth are stacked to generate a 3-D representation, which can be visualised from any desired angle. Two basic algorithms are used for this kind of reconstruction (HALL, P. M. & WATT, A. H. 1991, CABRAL et al. 1994): raytrace and perspective projection. The 3-D representations can concern selected depth subregions or the whole depth of the sample.

4) Extended focus: the image is divided into three frames that represent the maximum intensity projection for the x-y, x-z and y-z planes.

5) Simulated fluorescence processing (SFP): a three-dimensional simulation that enhances the fluorescence of surface layers and embosses all channels, as if they were illuminated from an oblique angle (MESSERLI et al. 1993).

6) Topographic reconstruction: from each of the x-y-z sampling points, the one with the center of mass of intensities is displayed in a map, which gives information on the characteristics of the surface. We chose the red channel to observe the surface of pigment fluorescence. Figures are shown in a false colour scale that represents depth from red to violet. Variation in the colour indicated irregularity of the surface. The image can be rotated around the x, y or z axis. Measures of thickness and roughness of biofilms were obtained from these images. Roughness was calculated as arithmetic average and root mean square of the profile ordinates within the measured section ( $R_a$  and  $R_q$  respectively) by means of the LCS program.

$$R_a = \frac{1}{A} \int_0^A Z(x, y) dA \text{ with } Z(x, y) = Z_i - \bar{Z} \tag{1}$$

$$R_q = \frac{1}{A} \int_0^A Z^2(x, y) dA \text{ with } Z(x, y) = Z_i - \bar{Z} \tag{2}$$

## Results

The illuminated tufa and plaster surfaces were irregularly covered by biofilms, composed of mixed organisms and EPS. Identified taxa are listed in HERNÁNDEZ-MARINÉ et al. 2003.

We made simultaneous and sequential acquisition of images, using the range of excitation wavelengths described above and selective emission filters.

### Observation at 543 and 633 nm excitation and 590–800 nm emission (red channel)

The photosynthetic pigments, chlorophylls and phycobilins, of the phototrophic organisms fluoresce in red at this setting so that neither staining nor coupling to fluorescent probes is necessary. Fig. 1 shows the maximum intensity projection of pigment fluorescence. The organism responsible of the biofilm structure was the filamentous *Scytonema julianum* (MENECH EX A. B. FRANK) RICHTER, and few thin filaments of *Leptolyngbya* sp. crept over them (Fig. 1).

### Observation at 351 and 364 nm excitation and 400–480 nm emission (blue channel)

The fluorophore Hoechst 33258 stained DNA both in living and dead cells (Fig. 2).

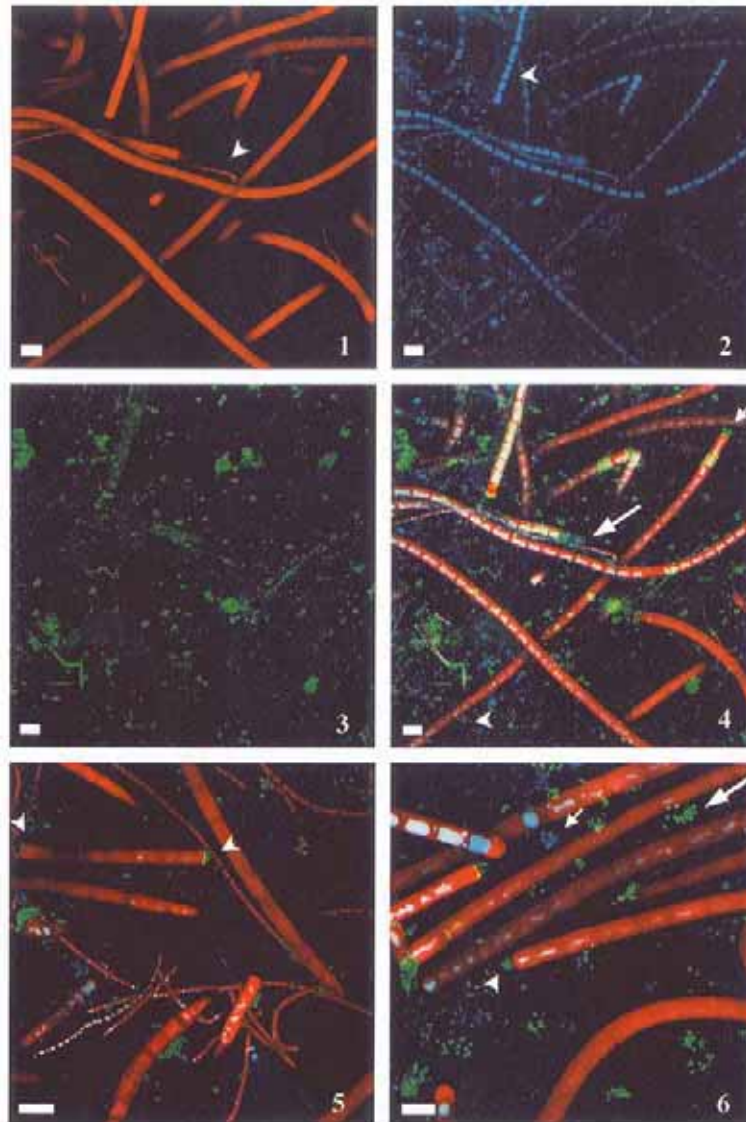
The stage of cell division could be ascertained by means of the size and shape of nucleoids. For example (Fig. 2) dividing cells of cyanobacterial filaments were recognized by their hourglass shaped nucleoids, whereas interphase cells had centered nucleoids. The intensity of blue fluorescence was variable, depending on cell and sheath conditions. Low blue intensity may represent low penetration of the fluorophore into the cells (e.g. thick sheathed cells) but also cells that had already lost most of their nucleic acids (e.g. dead cells). High blue intensity meant easy penetration (e.g. thin sheathed or senescent cells).

### Observation at 488 nm excitation and 490–543 nm emission (green channel)

Con-A labelled acidic polysaccharides of the extrapolymeric matrix. Their distribution was heterogeneous and limited, appearing as green points, spots, masses and tubes, sometimes clearly defined and sometimes diffuse (Fig. 3).

## Multiple channels

The overlay of the red, blue and green channels, via combination of two or all three together, reveals additional information (Figs 4–10). For better understanding the description in the text is presented as combinations of two channels, although some images are overlays of three channels (Figs 4–7, 9–10).



**Figs 1-4.** CLSM micrographs. Maximum intensity projection of 53 x-y optical sections ( $z$  step = 0.41  $\mu\text{m}$ ), 21.17  $\mu\text{m}$  total thickness of a biofilm of *Scytonema julianum*, *Leptolyngbya* sp. and heterotrophic microorganisms in *St. Callistus*. **1** - PF localisation (chlorophyll *a* and phycobilins) inside the cells. Note *Leptolyngbya* sp. filaments (arrowhead). **2** - NA stain. Note division of nucleoids (arrowhead). **3** - EPS. **4** - Overlay of the three channels shown in Figs 1-3. Three-channel maximum intensity projection showing

#### Pigment fluorescence of phototrophic microorganisms coupled to Hoechst 33258

Both phototrophic and heterotrophic organisms were visualised and could be distinguished by their coloration. The former presented both red and blue fluorescence, while the latter fluoresced only in the blue channel. The state of the phototrophic organisms was better perceived with this dichotomy than using the blue channel alone. Cells with high blue intensity and low auto-fluorescence indicated that the easy penetration of the fluorophore was due to senescence. Some terminal cells were blue fluorescent but without pigment fluorescence (Fig. 4). On the other hand, cells with high red fluorescence and ongoing division figures indicated active growth. Actively dividing and post-divisional cells, like those forming hormogonia or in apical areas, were shorter (Fig. 5). Post-divisional disposition of nucleic acids in different levels were visualised inside Chroococcalean cells (Fig. 7).

#### Combination of pigment fluorescence and Con-A

This combination correlates the non-homogeneous distribution of phototrophic organisms with EPS (Fig. 4). The cyanobacterial outer mucilaginous envelopes were irregularly distributed, according to species or to the condition of the specimen. EPS was also observed to remain for a long time after the producing organisms had died. In filamentous cyanobacteria the sheath could be thin or thick, even around the same trichome (Fig. 8). Strong green fluorescent dashes were bound to the hormogonia as mucilage apical pads (Figs 4–6) in *Leptolyngbya* sp. and *Scytonema julianum*.

#### Combination of Con-A and Hoechst 33258

EPS was irregularly distributed in the biofilms and, occasionally, was present in cell-free areas.

the apical pads (small arrow), terminal cells of *Scytonema julianum* with blue fluorescence (large arrow) and colonies of bacteria (arrowhead). Unless specified, colour allocation in the figures is red for pigment fluorescence (PF), blue for nucleic acids (NA) and green for Con-A lectin-stained extracellular polymeric substances (EPS). [Scale bar = 10  $\mu$ m.]

**Fig. 5.** Three-channel maximum intensity projection (PF, EPS and NA) of 31 x-y optical sections (z step = 0.3  $\mu$ m). *Scytonema julianum* and *Leptolyngbya* sp. in St. Callistus. Apical pads (arrowheads) displayed a strong Con-A fluorescence. 9  $\mu$ m total thickness of the biofilm. [Scale bar = 10  $\mu$ m.]

**Fig. 6.** Three-channel maximum intensity projection (PF, EPS and NA) of 109 x-y optical sections (z step = 0.4  $\mu$ m). *Scytonema julianum* and heterotrophic microorganisms in St. Callistus. *S. julianum* exhibits apical pads (arrowhead). Heterotrophic microorganisms (bacteria and actinobacteria) were also evidenced by NA (small arrow). Some bacteria, which nucleoids were labelled with Hoechst 33258, were embedded in EPS (long arrow). 20.7  $\mu$ m total thickness of the biofilm. [Scale bar = 10  $\mu$ m.]



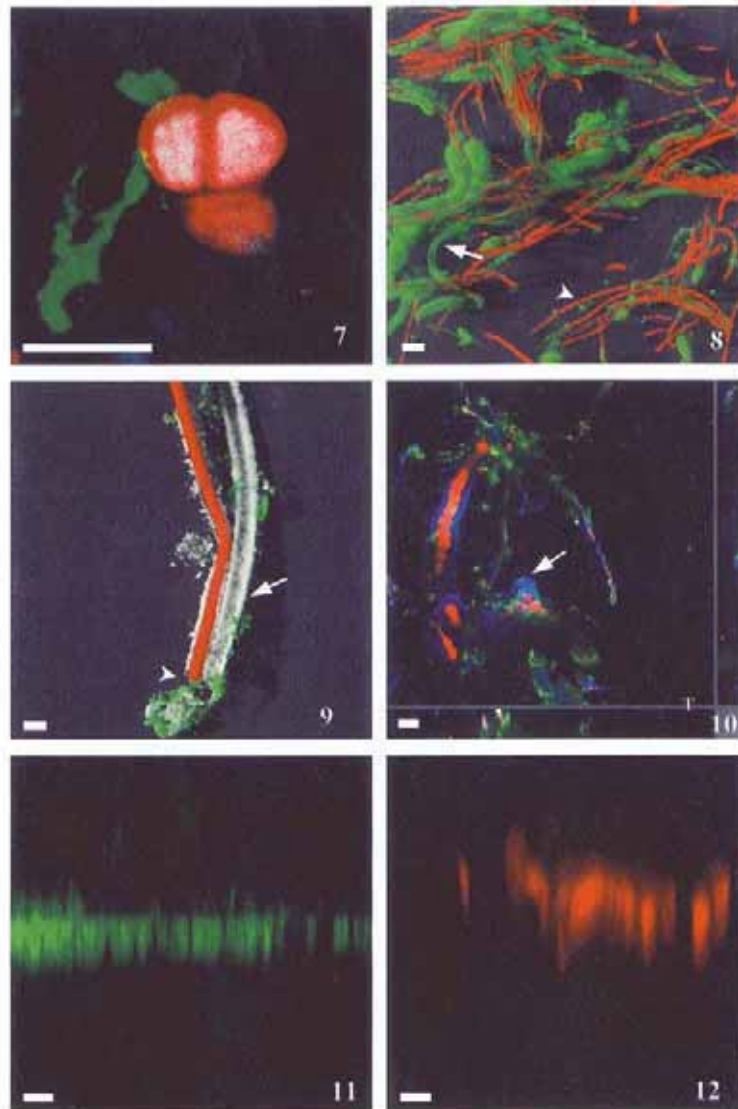


**Fig. 7.** Three-channel maximum intensity projection (PF, EPS and NA) of 55  $x$ - $y$  optical sections ( $z$  step = 0.3  $\mu\text{m}$ ) showing the spherical NA inside Chroococcales cells. [Scale bar = 10  $\mu\text{m}$ .]

**Fig. 8.** Two-channel image of PF and EPS created by the Simulated Fluorescence Process (SFP) method of 46  $x$ - $y$  optical sections ( $z$  step = 0.99  $\mu\text{m}$ ) in *Domitilla*. Note

## Biofilms fluorescence and image analysis in hypogean monuments 135

**Observation at 488 nm excitation and 480–495 nm emission (grey channel)  
in combination with other channels**

The grey channel evidenced thickness of calcified sheaths, in this case around *Scytonema julianum* (Fig. 9). Coupled to pigment fluorescence it discriminates empty calcified sheaths from calcified live filaments. Con-A labelled sheaths and EPS debris covering filaments, calcified sheaths and substratum were also visualised.

**Unexpected fluorescence**

The sheaths of *Fischerella* sp. (Fig. 10) and some terminal cells of *Scytonema julianum* (Fig. 4) showed fluorescence in blue light (excitation at 351 and 364 nm and emission at 400–480 nm). CaCO<sub>3</sub> presented a weak and diffuse fluorescence at 505–515 nm (green channel, Fig. 11) and red channel (580–800 nm, data not shown) when excited at 488 nm. It was observed on plaster and fresco substrata but also on cyanobacteria calcified sheaths or debris in untreated samples. The unexpected fluorescence was helpful to reveal the colonisation of calcified substrata by phototrophic organisms (Figs 11, 12).

**Gallery**

As an example of gallery a sample 203 µm deep, growing on a base of plaster and tufa was chosen. This gallery consists of compound images from the red and green channels (Fig.13). Each optical section details the particular depth at which it was imaged. The upper left sections (0–22.5 µm deep) show scattered red filaments of cyanobacteria and some green spots. At deeper levels (22.5–45 µm deep) the number of red filaments increases and green spots become bigger. The background of the images changed from black (empty space) to dull green (inherent fluorescence of plaster). Filamentous cyanobacteria were concentrated at the left and upper right zones of the images. Both zones appear more crowded at deeper levels (45–52 µm deep) and then (67.5–90 µm deep) become striped yellow.

*Leptolyngbya* sp. filaments either sheathed (arrow) or unsheathed (arrowhead). 45.5 µm total thickness of the biofilm. [Scale bar = 10 µm.]

**Fig. 9.** Three-channel SFP (PF, EPS and reflection) of 41 x-y optical sections (z step = 0.52 µm). *Scytonema julianum* in Domitilla. EPS was present recovering substrata and at greyish calcified sheaths (arrow). The living filament (red fluorescence) presented an attachment pad at one side (arrowhead). 20 µm total thickness. [Scale bar = 10 µm.]

**Fig. 10.** Three-dimensional extended focus projections in x-y, x-z and y-z views of 51 (step = 0.4 µm) bilinear interpolated x-y CLSM sections in the z-direction of the biofilm. *Fischerella* sp. in Domitilla, in this case blue colour corresponds to an inherent fluorescence of the sheaths (arrow). 20 µm total thickness. T = surface of sample. [Scale bar = 10 µm.]

**Figs 11–12.** xz optical thin section (confocal spectral imaging) of cyanobacterial PF and inherent fluorescence of substratum (green) in St. Callistus. These views show the inherent fluorescence of substratum, without stain. [Scale bar = 10 µm.]

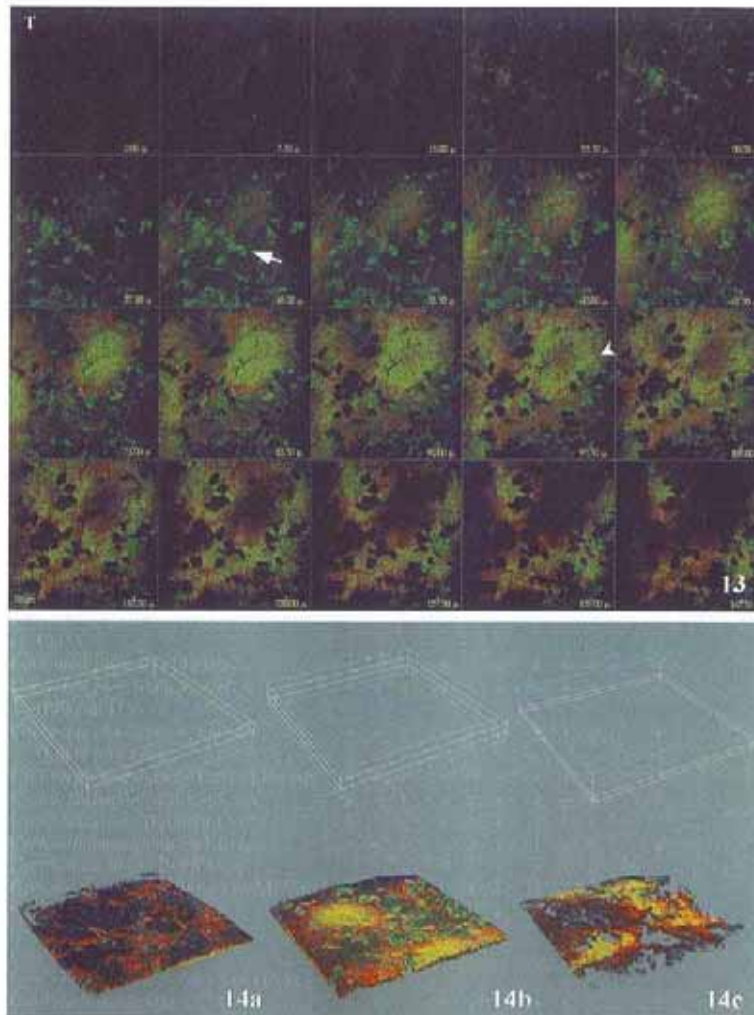


**Fig. 13.** Gallery of double-fluorescence: PF and EPS (strong green, arrow) of filamentous cyanobacteria in Domitilla. In addition the dull green inherent fluorescence of plaster is revealed (arrowhead). 20 representative images of 81 x-y optical sections (z step = 2.5  $\mu$ m). 203  $\mu$ m total thickness. **T** = surface of the biofilm.

**Fig. 14.** 3D perspective projection in the ray-tracing method of 81 x-y optical sections (z step = 2.5  $\mu$ m) shown in Fig.13. Selected regions from top, middle and bottom levels. Each level has a particular microbial composition (filamentous cyanobacteria) and mucilage abundance. **a.**– The surface level of the biofilm (0–27 x-y optical sections) is composed by phototrophic filaments and microbial aggregates embedded in EPS. **b.** – The middle level (27–54 x-y optical sections) corresponds to the zone in which PF and EPS was higher, also inherent fluorescence of plaster was observed. **c.** – At the bottom level (54–81 x-y optical sections) phototrophic microorganisms surrounding plaster irregularities were evidenced. 203  $\mu$ m total thickness of the biofilm.

## Biofilms fluorescence and image analysis in hypogean monuments 137

low zones surrounded by red filaments as a result of the juxtaposition of fluorescence from the two channels. At this same level (67.5–90  $\mu\text{m}$  deep) the green spots of upper images are substituted by black spaces. The amount of black spaces increases in subsequent images (105–135  $\mu\text{m}$  deep) and the yellow zones are darker and more reddish. These spaces devoid of fluorescence correspond to the tufa substratum. Sections at deeper levels (142.5–203  $\mu\text{m}$ ) contained progressively less fluorescence (not shown).

**Image analysis and processing**

Application of diverse analytical packages helped to extract different information from the same serial sections.

**Perspective image**

The reconstruction of the biofilm in Fig. 13 in various 3D-subregions displayed better evidence of the gross shape and the stratification of the sample (Fig. 14 a–c).

Cyanobacterial filaments were entangled, both at the biofilm surface (Fig. 14a) and inside the biofilm (Fig. 14b). The irregularity of the tufa base was visualized as spaces devoid of fluorescence among colonised plaster (yellow zones) in the lowest subregion (54–81  $\mu\text{m}$  deep, Fig. 14c) and as mounds covered by plaster that emerged at the median subregion (27–54  $\mu\text{m}$ , Fig. 14b). The filamentous biofilm covered the surface of the substratum moulding on its irregularities (red filaments around the plaster mounds) but also colonising the inside of the plaster layer.

The relationship biofilm-substratum was also evidenced in a perspective image including all optical sections (Fig. 15). In this case, a thin biofilm moulded on a strongly rough substratum. The roughness of the substratum was ostensible due to its inherent green fluorescence.

**Extended focus**

Extended focus evidenced the differential distribution in depth of the microorganisms in the biofilm. The architecture of the biofilm in Fig. 16 was sustained by entangled filaments of *Leptolyngbya* sp. (main frame, x–y plane). On the right hand side in the main frame various thick-sheathed *Gloeotheca* sp. cells were attached to the basic structure, on the left *Gloeotheca* sp. cells devoid of sheath appeared isolated. Maximum intensity projections of the y–z and x–z planes (right and lower frames) revealed that thick sheathed cells were mainly concentrated on the top of the biofilm while unsheathed cells were mainly at the bottom.

**Simulated fluorescence processing (SFP)**

Using shadow imaging, specialised cells (Fig. 17), small nucleoids and thin filaments (0.3  $\mu\text{m}$ ) stained with Con-A (Fig. 18) were evidenced. For the filamentous

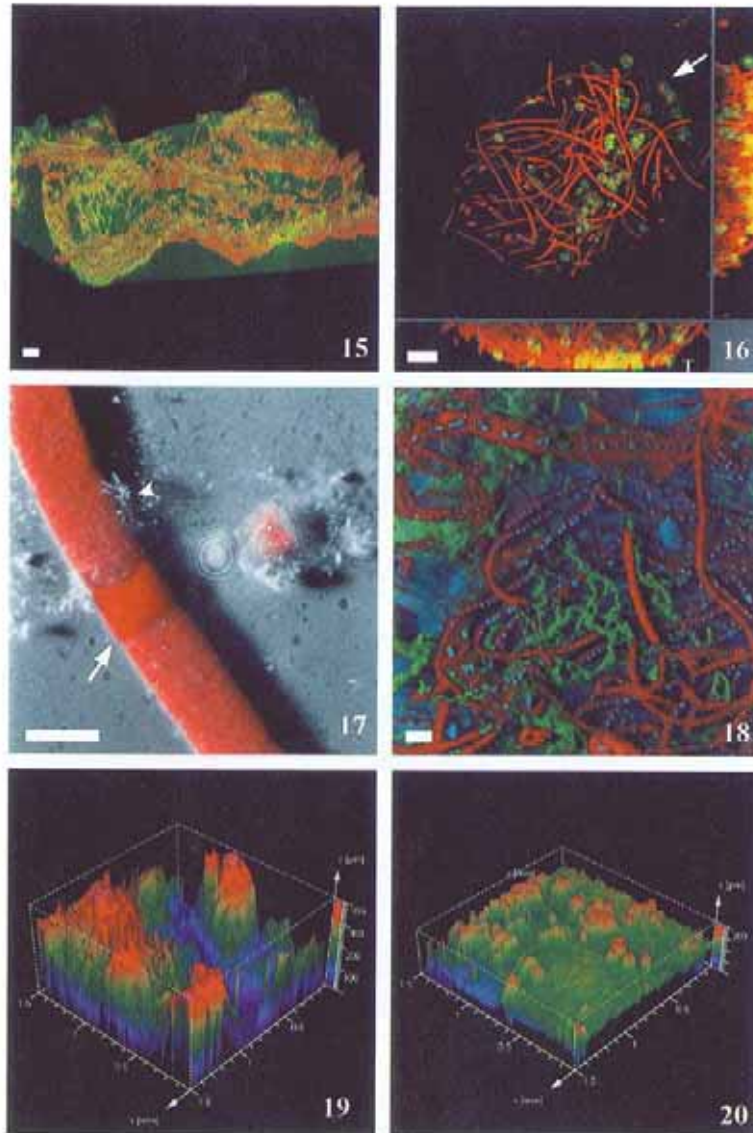


**Fig. 15.** 3D Perspective projection of the imaged volume. Two-channel (PF and EPS) of 159 x-y optical sections (z step = 2.48  $\mu\text{m}$ ), 395  $\mu\text{m}$  total thickness of the biofilm. Epilithic phototrophic microorganisms (in red) moulded on strongly irregular substratum (in green). Zones with steep slope are less colonised. [Scale bar = 50  $\mu\text{m}$ .] **Fig. 16.** Three-dimensional extended focus projections in x-y, x-z and y-z views of 27 (z step = 0.83  $\mu\text{m}$ ) bilinear interpolated x-y CLSM sections in the z-direction of the biofilm

## Biofilms fluorescence and image analysis in hypogean monuments 139

species present in the catacombs, trichome breakage and hormogonia formation was helped either by cells that disintegrate without specialised changes in structure or by necridia. Necridia increased their pigment fluorescence while becoming concave (Fig. 17).

#### Topographic reconstruction

Topographical images (Figs 19, 20) of the biofilms shown in Figs 14 and 15 were compared. Roughness and other characteristics of the biofilms from these topographical images are given in Table 1. The average roughness ( $R_a$ ) was highest in one biofilm from St. Callistus (Csc16c) (Figs 14 and 18) than in another from Domitilla (Cd13d) (Figs 15 and 19). The  $R_q$  was also superior in the case of Csc16c, as well as the ratio  $A'/A$ .

#### Discussion

The use of a non-invasive tool as the CLSM has become indispensable in studies of the distribution of microorganisms and biodeterioration where the microbial relationships, tridimensional structure and pattern of attachment to substratum should be preserved (NEU & LAWRENCE 1997, LAWRENCE & NEU 1999). The observation of pigment auto-fluorescence *in vivo* allowed us to localise phototrophic organisms but also helped in their identification by recognising various features such as planes of division in aggregates, branching-types or localisation of special cells. The combination of two labels for either nucleic acids or EPS together with pigment auto-fluorescence allowed us to properly characterise the biofilms of the Catacombs with their different organisms whether photo- or heterotrophic.

composed of *Leptolyngbya* sp. and Chroococcales with sheath (arrow) in St. Callistus. 22.41  $\mu\text{m}$  thickness. T = surface of biofilm. [Scale bar = 10  $\mu\text{m}$ .]

**Fig. 17.** Two-channel image of PF and reflection (grey) created by the Simulated Fluorescence Process (SFP) method of 92 x-y optical sections (z step = 0.3  $\mu\text{m}$ ). Note a necridic cell (arrow) and debris of the sheath (arrowhead) of *Scytonema* sp. 27.74  $\mu\text{m}$  total thickness. [Scale bar = 10  $\mu\text{m}$ .]

**Fig. 18.** Three-channel SFP image (PF, NA and EPS) of 103 x-y optical sections (z step = 0.4  $\mu\text{m}$ ). Biofilm from Domitilla, composed of *S. julianum* and *Leptolyngbya* sp. 40.8  $\mu\text{m}$  total thickness. [Scale bar = 10  $\mu\text{m}$ .]

**Figs 19–20.** Topographic reconstruction of PF. Figures are shown in a false colour scale that represents total depth from red to violet. Irregularities in the surface are reflected in colour changes. **19** – Biofilm from St. Callistus. 159 x-y optical sections (z step = 2.48  $\mu\text{m}$ ) corresponding to the Fig. 15. The strong variation in colour indicated strong irregularity of the surface. 395  $\mu\text{m}$  total thickness. **20** – Biofilm from Domitilla, 81 x-y optical sections (z step = 2.5  $\mu\text{m}$ ) corresponding to Figs 13 and 14. The evenness in colour reflects the uniformity of the surface. The thin biofilm is almost homogeneously moulding on the regular plaster surface (green) except for small warts, represented in red. 203  $\mu\text{m}$  total thickness.

Table 1. Roughness and thickness values of the biofilms from CD13d and Csc 16c shown in Figs. 14 and 15 as calculated from the topographic reconstruction of pigments fluorescence.

	Csc16c	Cd13d
Thickness [ $\mu\text{m}$ ]	395	203
$R_a$ [ $\mu\text{m}$ ]	118.81	22.25
$R_q$ [ $\mu\text{m}$ ]	186.40	104.45
A [ $\text{mm}^2$ ]	2.24	2.24
A' [ $\text{mm}^2$ ]	41.73	6.0
Ratio A'/A	18.62	2.68

A = Area of the acquired image; A' = Area of the total surface of the pigments fluorescence

The capability of Con-A to bind to diverse polysaccharides such as dextran, glycogen, mannose and amylopectin (GOLDSTEIN et al. 1965), has been successfully applied to reveal mannose rich protein layers present on the walls of actinobacteria (GAD et al. 1997), germinating conidia of filamentous fungi (BRUL et al. 1997, BOURETT et al. 1998) and alginate in bacterial biofilms (GOVAN 1990, STRATHMANN et al. 2002). Therefore, the application of this wide-spectrum EPS label ensured we were observing the EPS from the various possible sources of the Catacomb biofilms. When coupled to pigment auto-fluorescence, Con-A revealed the form, organisation and thickness of external mucilaginous envelopes around phototrophic microorganisms and by this way we obtained further information to identify them and characterise their physiological state. Shape and position of EPS is characteristic for various species and genera of cyanobacteria (KOMÁREK & ANAGNOSTIDIS 1998), but also related to the ability of cyanobacteria to modulate the response to external factors (ALBERTANO & BELLEZZA 2001): nutrient limitations and water stress may reduce or increase the quantity of released polysaccharides in aqueous environment (NICOLAUS et al. 1999, DE PHILIPPIS et al. 1991) besides light-related stress reduces the polysaccharide release in diatoms but has not been proved in cyanobacteria (DE WINDER et al. 1999). On the other hand, the combination of DNA (blue channel) and EPS (green channel) discriminated the EPS located around organisms from EPS isolated remains (localised versus seldom).

Substratum composition has to be taken into account when studying labelled but intact field samples. Inherent green fluorescence, that has been reported for calcified sheaths and calcium carbonate grains (DECHO & KAWAGUCHI 1999), could mask or increase green fluorescence of Con-A labelled EPS.

Features for the characterisation of biofilm structure were obtained from the various compound images of tridimensional reconstruction. Distribution of microorganisms and EPS in biofilms and their relationship with substratum was evidenced by the various kinds of compound images. Gallery images were adequate for the careful examination of biofilms, allowing detailed localization of certain structures or taxa. Extended focus images built with the maximum inten-

## Biofilms fluorescence and image analysis in hypogean monuments 141

sity projections of the x-y, x-z, and y-z planes were best to compare among biofilms. Such images evidenced gross spatial distribution of microorganisms, EPS and substratum, but also the disposition of microorganisms (e. g. erected vs. prostrate filaments), overall, exhibiting the stratification and porosity of the biofilm. Perspective images gave an account of surface characteristics such as roughness or coverage of the substratum surface that could be quantified by means of topographic reconstruction. Confocal Laser Scanning Microscopy is a very versatile tool for the study of biofilm *in situ*. What makes CLSM so powerful is the ability to analyse samples with minimal preparation or disturbance, the use of multiple excitation and detection wavelengths at different depths of focus, and the large pool of digital image processing algorithms with which one can effectively target specific elements in the biofilm sample, such as molecules (eg. DNA and pigments), structure (eg surfaces, matrix, sheaths and filaments) and properties (eg. stage of cell division, growth and senescence), with the capability to fully visualise them all in 3D.

## Acknowledgements

This work was supported by EU Programme Energy, Environment and Sustainable Development in the frame of CATS Project, contract EVK4-CT-2000-00028. The authors also acknowledge Miss R. GARCÍA from the Scientific and Technical Services of the University of Barcelona, for her helpful assistance with the CLSM.

## References

- ALBERTANO, P. & BELLEZZA, S. (2001): Cytochemistry of cyanobacterial exopolymers in biofilms from Roman hypogea. – *Novi Hedwigia, Beih.* **123**: 501–518.
- ALBERTANO, P.; KOVÁČIK, L. & GRILLI-CAIOLA, M. (1994): Preliminary investigations on epilithic cyanophytes from a Roman Necropolis. – *Arch. Hydrobiol./Algological Studies* **75**: 71–74.
- BOURETT, T. M.; CZYMEK, K. J. & HOWARD, R. J. (1998): An improved method for affinity probe localization in whole cells of filamentous fungi. – *Fungal Genet. Biol.* **24**: 3–13.
- BRUL, S.; NUSSBAUM, J. & DIEHLANDHOESING, S. K. (1997): Fluorescent probes for wall porosity and membrane integrity in filamentous fungi. – *J. Microbiol. Methods* **28**: 169–178.
- CABRAL, B.; CAM, N. & FORAN, J. (1994): Accelerated Volume Rendering and Tomographic Reconstruction Using Texture Mapping Hardware. – In: 1994 Symposium on Volume Visualization, ACM SIGGRAPH, p. 91–98.
- CALDWELL, D. E.; KORBER, D. R. & LAWRENCE, J. R. (1992): Imaging of bacterial cells by fluorescence exclusion using scanning confocal laser microscopy. – *J. Microbiol. Methods* **15**: 249–261.
- COSTERTON, J. W.; STEWART, P. S. & GREENBERG, E. P. (1999): Bacterial biofilms: a common cause of persistent infections. – *Science* **284**: 1318–1322.
- DANIN, A. & CANEVA, G. (1990): Deterioration of limestone walls in Jerusalem and marble monuments in Rome caused by cyanobacteria and cyanophilous lichens. – *Int. Biodeterior.* **26**: 397–417.
- DAVEY, M. E. & O'TOOLE, G. A. (2000): Microbial biofilms: from ecology to molecular genetics. – *Microbiol. Mol. Biol. Rev.* **64**: 847–867.



- DECHO, A. W. & KAWAGUCHI, T. (1999): Confocal imaging of *in situ* natural microbial communities and their extracellular polymeric secretions using nanoplast (R) resin. – *Biotechniques* **27**: 1246–1252.
- DE PHILIPPIS, D.; SILL, C.; TASSINATO, G.; VICENZINI, M. & MATERASSI, R. (1991): Effects of growth conditions on exopolysaccharides production by *Cyanospira capsulata*. – *Biores. Technol.* **38**: 101–104.
- DE WINDER, B.; STAATS, N.; STAL, L. J. & PATERSON, D. M. (1999): Carbohydrate secretion by phototrophic communities in tidal sediments. – *J. Sea Res.* **42** (2): 131–146.
- GAD, M.; ITOH, A. & IKAI, A. (1997): Mapping cell wall polysaccharides of living microbial cells using atomic force microscopy. – *Cell Biol. Int.* **21**: 697–706.
- GÓMEZ-ALARCÓN, G.; CILLEROS, B.; FLORES, M. & LORENZO, J. (1995): Microbial communities and alteration processes in monuments at Alcalá de Henares, Spain. – *Sci. Total Environ.* **167**: 231–239.
- GOVAN, J. R. W. (1990): Characteristics of mucoid *Pseudomonas aeruginosa* *in vitro* and *in vivo*. – In: GACESA, P. & RUSSELL, N. J. (eds.): 701 *Pseudomonas* Infection and Alginate Biochemistry, Genetics and Pathology, p. 50–75. Chapman & Hall, London.
- GOLDSTEIN, I. J.; HOLLERMAN, C. E. & MERRICK, J. M. (1965): Protein-carbohydrate interaction: I. The interaction of polysaccharides with 698 concanavalin A. – *Biochim. Biophys. Acta.* **97**: 68–76.
- HALL, P. M. & WATT, A. H. (1991): Rapid volume rendering using a boundary-fill guided raycast algorithm. – In: PATRIKALAKIS, N. M. (ed.): Scientific Visualization of Physical Phenomena (Proceedings of CG International '91), p. 235–249, Springer-Verlag.
- HERNÁNDEZ-MARINÉ, M.; CLAVERO, E. & ROLDÁN, M. (2003): Why there is such luxuriant growth in the hypogean environments. – *Arch. Hydrobiol./Algological Studies* **109**: 229–239.
- HERNÁNDEZ-MARINÉ, M.; ROLDÁN MOLINA, M.; CLAVERO, E.; CANALS, A. & ARIÑO, X. (2001): Phototrophic biofilm morphology in dim light. The case of the Puigmoltó sinkhole. – In: ELSTER, J.; SECKBACH, J.; VINCENT, W. P. & LHOTSKÝ, O. (eds.): Algae and extreme environments. – *Nova Hedwigia, Beih.*, **123**: 237–253.
- KOMÁREK, J. & ANAGNOSTIDIS, J. (1998): Cyanoprokaryota. 1. Chroococcales. – In: ETTI, H.; GÄRTNER, G.; HEYNIIG, H. & MÖLLENHAUER, D. (eds.): Süßwasserflora von Mitteleuropa. – Bd. **19**: 547 pp., Gustav Fischer, Jena.
- LAURENT, M.; JOHANNIN, G.; GILBERT, N.; LUCAS, L.; CASSIO, D.; PETIT, P. & FLEURY, A. (1994): Power and limits of laser scanning confocal microscopy. – *Biol. Cell* **80**: 229–240.
- LAWRENCE, J. & NEU, T. R. (1999): Confocal Laser Scanning Microscopy for Analysis of Microbial Biofilms. – In: DOYLE, R. J. (ed.): Methods in Enzymology: Biofilms **310**: 131–144, Academic Press, San Diego.
- LAWRENCE, J. R.; KORBER, D. R.; HOYLE, B. D.; COSTERTON, J. W. & CALDWELL, D. E. (1991): Optical sectioning of microbial biofilms. – *J. Bacteriol.* **173**: 6558–6567.
- MESSERLI, J. M.; VAN DER VOORT, H. T. M.; RUNGGER-BRÄNDLE, E. & PERRIARD, J. C. (1993): Three-Dimensional Visualization of Multi-Channel Volume Data: The am SFP Algorithm. – *Cytometry* **14**: 725–735.
- NEU, T. R. & LAWRENCE, J. R. (1997): Development and structure of microbial biofilms in river water studied by confocal laser scanning microscopy. – *FEMS Microbiol. Ecol.* **24**: 11–25.
- NICOLAUS, B.; PANICO, A.; LAMA, L.; ROMANO, I.; MANCA, M. C.; DE GIULIO, A. & GAMBACORTA, A. (1999): Chemical composition and production of exopolysaccharides from representative members of heterocystous and non-heterocystous cyanobacteria. – *Phytochemistry* **52**: 639–647.
- ORTEGA, J. J.; HERNÁNDEZ-MARINÉ, M. & SAIZ-JIMÉNEZ, C. (1993): Cyanobacteria and algae on historic buildings and monuments. – In: GARG, K. L.; ARAI, H. & RAI, B. (eds): Recent Advances in Biodeterioration and Biodegradation. 1–2, p. 173–203, Calcutta.
- RIPPKA, R. (1988): Isolation and purification of cyanobacteria. – In: PACKER, L. & GLAZER, A. N. (eds), Methods in Enzymology. **167**: 3–28, Academic Press, Inc., San Diego.

## Biofilms fluorescence and image analysis in hypogean monuments 143

- STRATHMANN, M.; WINGENDER, J. & FLEMMING, H. C. (2002): Application of fluorescently labelled lectins for the visualization and biochemical characterization of polysaccharides in biofilms of *Pseudomonas aeruginosa*. – *J. Microbiol. Methods* **50**: 237–248.
- URZI, C. & ALBERTANO, P. (2001): Studying phototrophic and heterotrophic microbial communities on stone monuments. – In: DOYLE R. J. (ed.): *Microbial growth in biofilms. Part A: Developmental and molecular biological aspects*. – *Methods in Enzymology*, **336**: 340–355, Academic Press, Inc., San Diego.
- WIMPENNY, J. (2000): An overview of biofilms as functional communities. – In: ALLISON, D.; GILBERT, P.; LAPPIN-SCOTT, H. & WILSON, M. (eds.): *Community structure and co-operation in biofilms*, p. 1–24, Cambridge University Press, Cambridge.
- WOLFAARDT, G. M.; LAWRENCE, J. R.; ROBARTS, R. D.; CALDWELL, S. E. & CALDWELL, D. E. (1994): Multicellular organization in a degradative biofilm community. – *Appl. Environ. Microbiol.* **60**: 434–446.

Manuscript received July, 4, 2002, accepted November, 18, 2002.

## The authors' addresses:

MÓNICA ROLDÁN,  
ÉSTER CLAVERO,  
MARIONA HERNÁNDEZ-MARINÉ,  
Universitat de Barcelona,  
Facultat de Farmàcia,  
Unitat de Botànica,  
Av. Joan XXIII s/n,  
E-08028, Barcelona, Spain.  
e-mail: mroldan@farmacia.far.ub.es

SUSANNA CASTEL,  
Serveis Científicotècnics,  
Universitat de Barcelona,  
Barcelona Science Park,  
Josep Samitier 1–5,  
E-08028, Barcelona, Spain.

*Resultats*

---

### **4.3. Identificació de pigments en cèl·lules individuals procedents de biofilms fototròfics mitjançant espectrofotometria confocal**

Es presenta una nova tècnica d'imatge per a l'anàlisi de pigments fotosintètics presents a una sola cèl·lula en mostres gruixudes vives i intactes. Aquesta tècnica es basa en un microscopi de rastreig làser confocal acoblat a mètodes espectrofotomètrics. La capacitat espectral del microscopi confocal permet mesurar el senyal de fluorescència emès d'una àrea seleccionada de la mostra, rastrejat en tot el rang d'emissió a través d'un conjunt de passos d'emissió prèviament seleccionats. Les possibilitats i les limitacions d'aquesta tècnica varen ser estudiades utilitzant pigments purs, cultius d'un cianobacteri i una alga verda i biofilms naturals procedents d'ambients hipogeus. Els espectres dels pigments purs es correlacionaren bé amb els espectres publicats dels pigments extrets. Espècies pertanyents a diferents grups filogenètics, com Cyanobacteria, Bacillariophyta o Chlorophyta, van presentar una morfologia i unes propietats de fluorescència dels seus pigments característiques que en permetien la discriminació respecte d'altres grups filogenètics. Així mateix foren separades les espècies de cianobacteris amb ficoeritrina i sense. Aquesta nova tècnica permet:

- (i) Analitzar el senyal fluorescent procedent d'un sol píxel o d'un conjunt.
- (ii) Analitzar de forma directa els pigments fluorescents pertanyents a una sola cèl·lula en mostres gruixudes.
- (iii) Establir simultàniament la relació entre l'anàlisi de pigments *in vivo*, la morfologia de l'espècimen i la localització tridimensional a l'interior de la comunitat microbiana intacta.

Els resultats detallats d'aquest capítol s'inclouen en el següent article:

Non invasive pigment identification in living phototrophic biofilms by confocal imaging spectrofluorometry. ***Appl. Environ. Microbiol.*** (2004), 70 (6): 3745-3750

## Noninvasive Pigment Identification in Single Cells from Living Phototrophic Biofilms by Confocal Imaging Spectrofluorometry

M. Roldán,<sup>1</sup> F. Thomas,<sup>2</sup> S. Castel,<sup>3</sup> A. Quesada,<sup>4</sup> and M. Hernández-Mariné<sup>1\*</sup>

*Departament de Productes Naturals, Biologia Vegetal i Edafologia<sup>1</sup> and Serveis Científicotècnics, Barcelona Science Park,<sup>3</sup> Universitat de Barcelona, and Institut de Robòtica i Informàtica Industrial (CSIC-UPC),<sup>2</sup> E-08028 Barcelona, and Departamento de Biología, Universidad Autónoma de Madrid, E-28049 Madrid,<sup>4</sup> Spain*

Received 1 October 2003/Accepted 20 February 2004

**A new imaging technique for the analysis of fluorescent pigments from a single cell is reported. It is based on confocal scanning laser microscopy coupled with spectrofluorometric methods. The setup allows simultaneous establishment of the relationships among pigment analysis in vivo, morphology, and three-dimensional localization inside thick intact microbial assemblages.**

Phototrophic organisms produce a number of photosynthetic pigments that act as photoactivated fluorescent markers that switch on in response to light at a particular wavelength. A fraction of the energy absorbed by pigments may be emitted immediately at a longer wavelength, which is known as fluorescence (7). Fluorescence allows the description of a complex community in terms of physiological state (17), discrimination among phylogenetic groups (8), quantification of biomass (2), energy transfer, and cell evolution (4). Approaches to improve the use of cellular fluorescence techniques with subsequent localization of the organisms in two dimensions (2D) or 3D (15, 10) have been reported.

Here we propose a new application of the confocal scanning laser microscope (CSLM) coupled with a spectrofluorometric detector. Confocal imaging spectrofluorometry provides simultaneous 3D information on photosynthetic microorganisms and their fluorescence signatures within thick assemblages (as in microbial mats, biofilms, etc.) because of their multiple excitation wavelengths ( $\lambda_{exc}$ ) and free detection of emitted wavelengths. We report our results on pigments, pure cultures, and biofilms from dim-light environments.

**Pigments.** The pure pigments chlorophyll *a* (Chl *a*) and Chl *b*, xanthophyll (Xant), R-phycoerythrin, allophycocyanin-XL (APC-XL), and C-phycoerythrin (C-PC), all obtained from Sigma-Aldrich (St. Louis, Mo.), were used as controls. Pigment solutions were set at a final concentration of 1 mg/ml, and scans were done as described below.

**Culture and biofilm preparation.** Two cultures of *Nostoc humifusum* Carm. (*Cyanobacteria*) and *Muriellopsis* sp. (*Chlorophyta*) at distinct stages of growth (exponential phase, 1 week; stationary phase, 3 weeks) and three stratified aerophytic biofilms from dim habitats, BF1, BF2, and BF3, which are described and identified elsewhere (6), were tested. The

biofilms contained several photosynthetic phylogenetic groups (*Cyanobacteria*, *Chlorophyta*, and *Bacillariophyta*).

**CSLM.** CSLM was performed with a Leica TCS-SP2 (Leica Microsystems, Mannheim, Germany). The wavelengths of the excitation lasers were in the UV Ar (351 and 364 nm), blue Ar (458, 476, and 488 nm), green Ar (514 nm), green HeNe (543 nm), and red HeNe (633 nm) spectra. Each image sequence (wavelength scans or lambda scan function of the system) was obtained by scanning the same *x-y* optical section with a  $\lambda$  step size of 20 nm for emission wavelengths between 360 and 800 nm. The *x, y, \lambda* data set was acquired at the *z* position at which the fluorescence was maximal, and acquisition settings were not altered throughout the experiments. The variation in intensity of a particular spectral component, encoded with 8 bits, is represented on the screen with a pseudocolor lookup table. 3D maximum-intensity projections were made with Imaris software (version 2.7; Bitplane AG, Zürich, Switzerland).

**Fluorescence analysis.** The mean fluorescence intensity (MFI) of the *x-y-\lambda* data sets was measured with the Leica Confocal Software, version 2.0. The region-of-interest (ROI) function of the software was used to determine the spectral signature of a selected area of the scanned image. For pigment solutions, we analyzed ROIs of 1,000  $\mu\text{m}^2$  (10 regions). For cell culture and biofilm analysis, ROIs of 1  $\mu\text{m}^2$ , taken from the fluorescent thylakoid region inside the cell, were set in each *x-y-\lambda* stack of images. A patent application related to this technology has been filed (no. 200302905, 27 November 2003, Spain).

Lambda scans of *N. humifusum* (21 ROIs), *Muriellopsis* sp. (50 ROIs), and biofilms (5 ROIs for each species in the biofilm) were obtained for each  $\lambda_{exc}$  in three independent experiments. 3D plots—MFI to longer-wavelength emission versus cell number—were obtained with Matlab 6.0 (Mathworks, Inc.). The mean and standard error for all of the regions or cells examined in each  $\lambda_{exc}$  were calculated. The maxima of the pigments corresponded to their dispersion range at the distinct  $\lambda_{exc}$ .

Lambda scans of the pure pigments (Fig. 1 and 2) correlated well with published spectra of extracted pigments (11, 13, 14).

\* Corresponding author. Mailing address: Departament de Productes Naturals, Biologia Vegetal i Edafologia, Universitat de Barcelona, Av. Joan XXIII s/n, E-08028 Barcelona, Spain. Phone: (34) 93 4024490. Fax: (34) 93 4035879. E-mail: hernande@farmacia.far.ub.es.

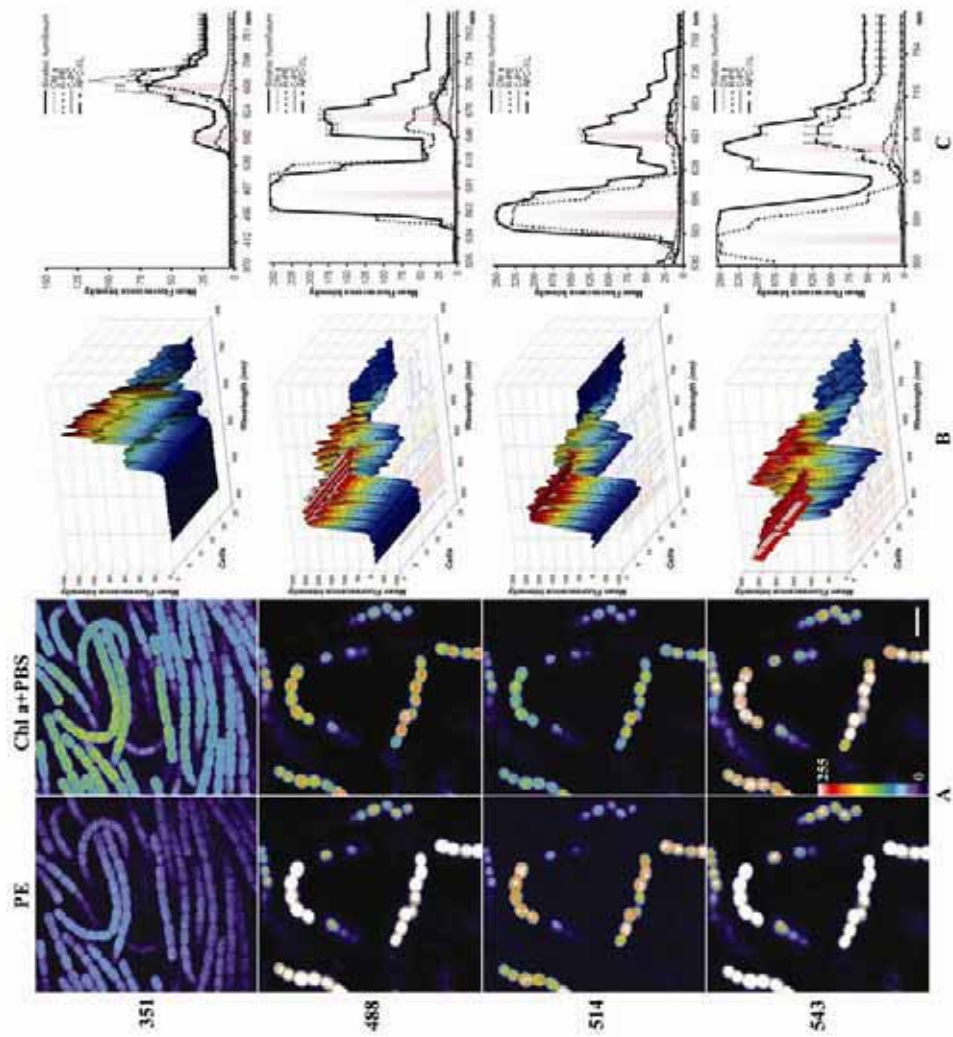


FIG. 1. CSLM images and lambda scans of *N. humifusum* in vivo. These optical sections and spectral profiles were derived at  $\lambda_{exc}$ s of 351, 488, 514, and 543 nm. (A) Pseudocolor confocal  $x$ - $y$ - $z$  single sections corresponding to the  $\lambda_{max}$  autofluorescence of C-PE (first maximum) and Chl *a* plus phycobiliproteins (PBS) (second maximum) at each of the four  $\lambda_{exc}$ s. The pseudocolor scale is shown at the bottom left. Warm colors such as white and red represent maximum intensities, whereas cold colors like blue are representative of low intensities (the intensity of each pixel was set to 255 levels of grey). Such optical sections correspond to the maximum peaks when excited at the corresponding  $\lambda_{exc}$  shown in C plots (shady areas). (B) 3D surface pseudocolor plots of fluorescence spectra; emission wavelength,  $x$ ; MFI,  $y$ ; number of cells,  $z$ . The  $\lambda_{exc}$  position of each cell showed practically no variability at each  $\lambda_{exc}$  even if the cultures were in different states of growth. (C) 2D plots representing the MFI spectra of *N. humifusum* and pure pigments. Standard errors ( $n = 2$ ) cells and R-phycoerythrin, C-PC, APC-XL, and Chl *a* ( $n = 10$  regions) MFI spectra at these  $\lambda_{exc}$ s are represented. Ratios of C-PC and APC-XL fluorescence had to be multiplied by a factor of 2 owing to the weak fluorescence signal received by the CSLM. Each value shown is the average MFI from three independent experiments carried out under the same conditions. Scale bar = 10  $\mu$ m.

All species had a Chl *a* fluorescence maximum at 680 to 690 nm, while those belonging to the same phylogenetic group, Cyanobacteria, Chlorophyta, or Bacillariophyta, showed similar spectra (Fig. 1 to 3) because of the presence of characteristic pigments (8).

Fluorescence properties of single  $x$ - $y$ - $z$  sections of *N. humifusum*, corresponding to the emission peak ( $\lambda_{max}$ ), were obtained for each pigment at each  $\lambda_{exc}$  (Fig. 1). From these sections, the ROIs used to plot 3D and 2D spectral data (Fig. 1B and C) were obtained. The emission maximum of Chl *a* was observed at a 351-nm  $\lambda_{exc}$  and showed a weak shoulder when close to the phycobiliprotein fluorescence maximum at  $663 \pm 1.5$  nm (Fig. 1C) (4). The 488-, 514-, and 543-nm  $\lambda_{exc}$ s absorbed essentially by C-phycoerythrin (C-PE), resulted in strong orange fluorescence emission at  $579 \pm 1.6$  nm in vivo. These results are consistent with those previously reported (12, 16, 15).

*Muriellopsis* sp. (Fig. 2) showed a prominent Chl *a* fluorescence peak at  $696.5 \pm 2.4$  nm when excited at any  $\lambda_{exc}$  (Fig. 2C). This Chl *a* peak shifted ( $\sim 10$  nm) to a longer wavelength than generally reported for  $\lambda_{exc}$ . This shift may be a result of the interaction of the Xant lutein (5) with Chl *a* (1, 18). Furthermore, the presence of Chl *b* affected the state of the longer-wavelength-absorbing forms of Chl *a* (3, 9).

3D maximum-intensity projections of three biofilms showed the differential distribution in depth of the forming microorganisms (Fig. 3A) and emission spectra (Fig. 3B). In biofilm BF1, thin filaments of *Leptolyngya* sp. were horizontally oriented on top of wide *Scytonema julianum* (Fig. 3A). Both cyanobacteria had a wide  $658.4 \pm 3$ -nm  $\lambda_{max}$  emission peak from the overlap of Chl *a* and phycobiliproteins (Fig. 3B). In addition, the emission peak ( $579.7 \pm 3.8$  nm) of *Leptolyngybya* sp., but not that of *S. julianum*, was attributable to the presence of C-PE (Fig. 3B). In biofilm BF2, *Diademsis gallica* (Bacillariophyta) was mainly on the top of the biofilm while chroococcal cyanobacteria formed a discontinuous bottom layer (Fig. 3A). The  $\lambda_{max}$  of *D. gallica*, at  $676.2 \pm 5$  nm (Fig. 3B), did not coincide with the  $\lambda_{max}$  of the other groups because of the presence of Chl *c*. The chroococci showed spectra similar to those of *Leptolyngybya* sp. and *N. humifusum* (Fig. 1 and 3). Biofilm BF3 was also stratified, with a continuous upper layer of *Chlorella*-like organisms and isolated colonies of *Cyanosarcina parthenonensis* in deeper parts (Fig. 3A). Their  $\lambda_{max}$  matched those of the related groups Chlorophyta and Cyanobacteria, respectively (Fig. 1 to 3).

**Statistical test.** A parallel experiment to compare the MFIs of species in culture at distinct  $\lambda_{exc}$ s was carried out. The emission ranges used were 640 to 700 nm (351-nm  $\lambda_{exc}$ ), 555 to 605 nm (488-nm  $\lambda_{exc}$ ), and 580 to 620 nm (543-nm  $\lambda_{exc}$ ). Twenty-five replicates of each taxon, each composed of 20 optical sections at a  $z$  step of 0.45  $\mu$ m, were obtained. These sections were processed by Metamorph image analysis software to obtain a composite image in which the total fluorescence was quantified. Differences between the MFIs of species in culture at different  $\lambda_{exc}$ s were evaluated by two-way analysis of variance (fixed factors) with statistical significance set to 0.05. When significant differences were observed, means were compared by the least significant differences of Fisher's multirange test. The MFI was significantly different between species ( $F_{1, 137} = 413.49, P < 0.0001$ ) and between  $\lambda_{exc}$ s ( $F_{2, 137} =$



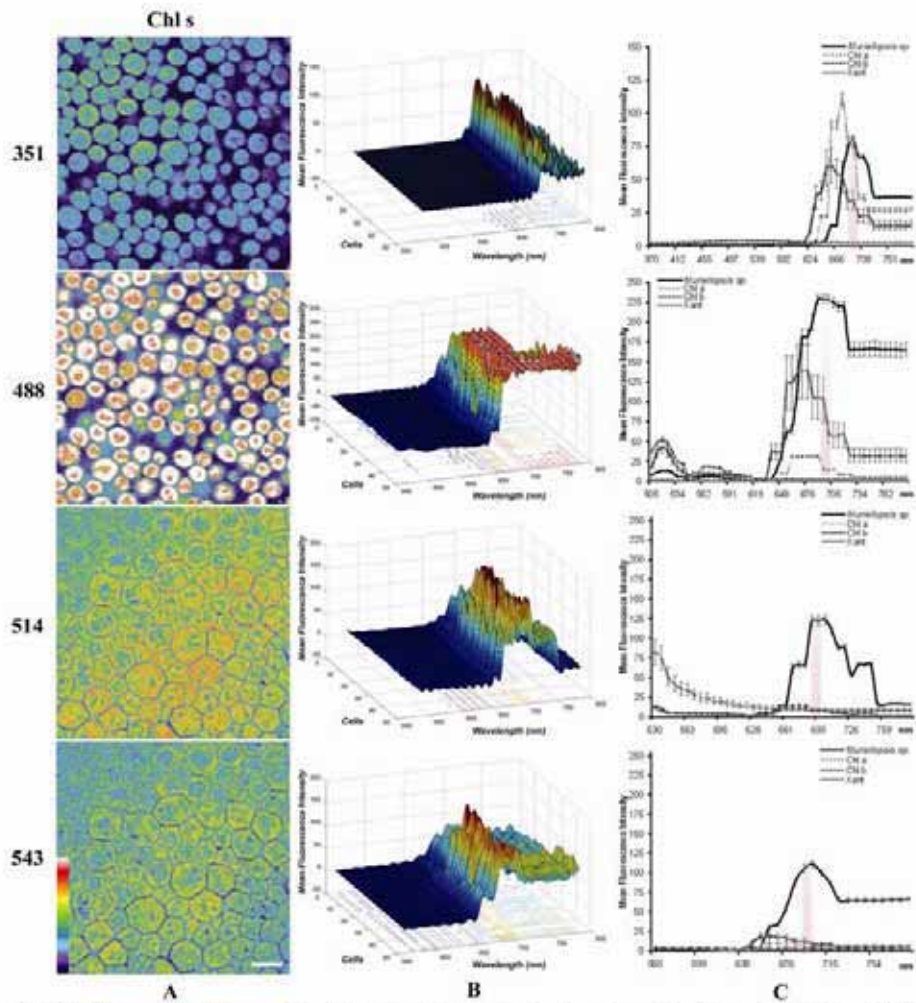


FIG. 2. CSLM images and lambda scans of *Mariellopsis* sp. in vivo. These optical sections and spectral profiles were derived at  $\lambda_{exc}$ s of 351, 488, 514, and 543 nm. (A) Pseudocolor confocal  $x$ - $y$ - $z$  single sections corresponding to the  $\lambda_{exc}$  autofluorescence of Chl *a* and Chl *b* for each of the four  $\lambda_{exc}$ s. The pseudocolor scale is shown at the bottom left. Such optical sections correspond to the maximum peaks when excited at the corresponding  $\lambda_{exc}$ s, shown in C plots (shady areas). (B) 3D surface pseudocolor plots of fluorescence spectra: emission wavelength,  $x$ ; MFI,  $y$ ; number of cells,  $z$ . The  $\lambda_{exc}$  position of each cell showed practically no variability in the  $\lambda_{exc}$ , even if the cultures were at different stages of growth. (C) 2D plots representing the MFI spectra for *Mariellopsis* sp. and pure pigments. Emission spectra are the mean  $\pm$  standard error ( $n = 50$  cells), and Xant, Chl *a*, and Chl *b* pigments ( $n = 10$  regions) in each  $\lambda_{exc}$  are represented. The ratio of Xant fluorescence had to be multiplied by a factor of 2 owing to the weak fluorescence signal received by the CSLM. Scale bar = 10  $\mu$ m.

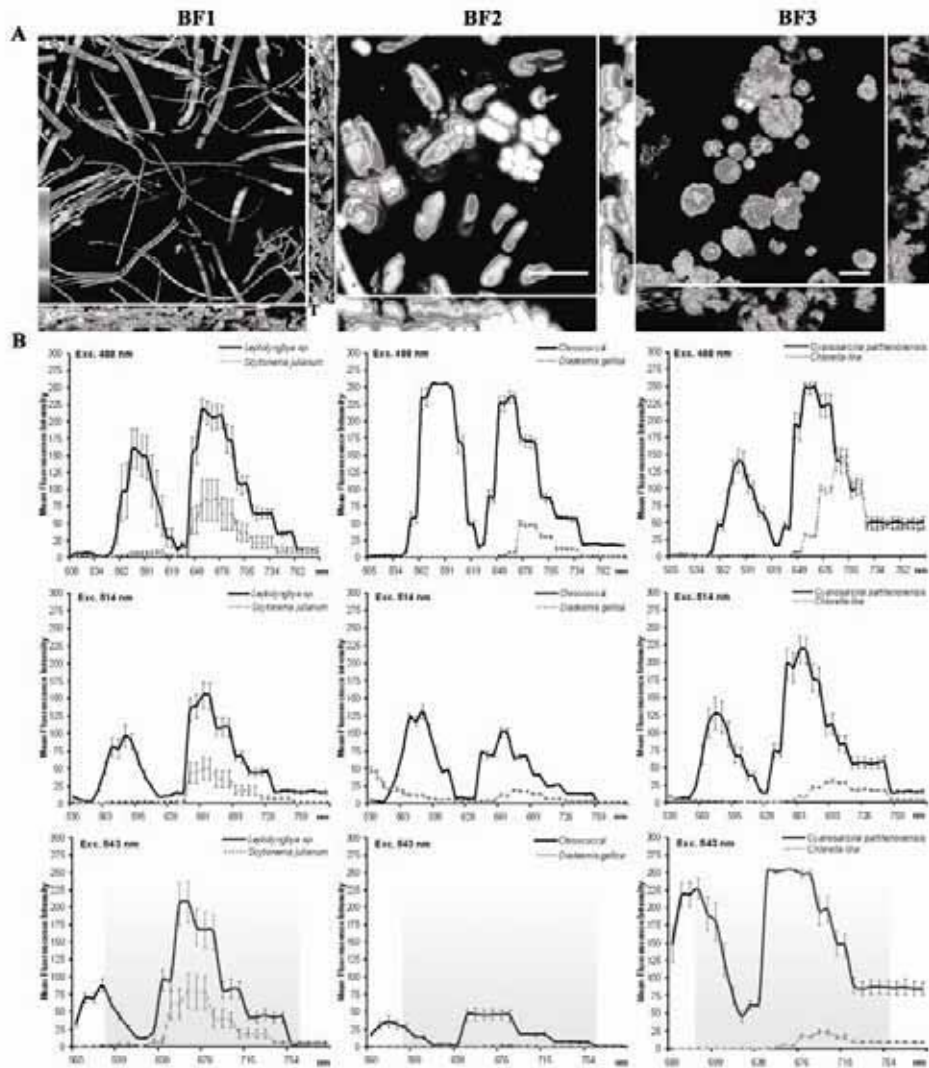


FIG. 3. CSLM images and lambda scans of three *in vivo* aerophytic biofilms from the Roman catacombs (BF1 and BF2) and Zuhers (BF3). Optical sections and spectral profiles derived from  $\lambda_{exc}$ s of 351, 488, 514, and 543 nm. (A) 3D maximum-intensity projections in the *x-y* direction and orthogonal views in the *z* direction of the biofilm. Each image represents the maximum autofluorescence emitted in the range of 590 to 775 nm (shady area) when excited at 543 nm. The pseudocolor scale is shown at the bottom left. T = surface of the sample. Scale bar = 10  $\mu$ m. BF1, 49 *x-y* optical sections of *S. julianum* and *Leptolyngbya* sp. The voxel size is 465.03 by 465.03 by 398.73  $nm^3$ , *z* step, 0.4  $\mu$ m. Thickness, 19.54  $\mu$ m. BF2, 66 *x-y* optical sections of a stratified biofilm consisting of two strata, an upper epilithic layer composed of colonies of *D. gulfua* and an understory layer formed by chroococcal colonies. The voxel size is 75.82 by 75.82 by 98.51  $nm^3$ , *z* step, 0.1  $\mu$ m. Thickness, 6.6  $\mu$ m. BF3, 98 *x-y* optical sections of a stratified biofilm with a continuous upper layer of *Chlorella*-like organisms and a discontinuous bottom layer of *C. parthenoceros* (arrow). The voxel size is 146.77 by 146.77 by 300  $nm^3$ , *z* step = 0.2  $nm^3$ . Thickness, 19.4  $\mu$ m. (B) *In vivo* mean emission spectra of the different species present in the biofilms of panel A and the standard error (live cells). The emission difference profiles of the biofilms indicate the presence of different groups of algae and cyanobacteria.

14.57,  $P < 0.0001$ ). The interaction term was also significant ( $F_{2, 137} = 99.65$ ,  $P < 0.0001$ ) owing to the different set of pigments of each species. For MFI at a 351-nm  $\lambda_{exc}$ , which corresponds mainly to chlorophyll fluorescence, the results were similar for *N. humifusum* and *Muriellopsis* sp. In contrast, for MFI at 488- and 543-nm  $\lambda_{exc}$ , the outcome for *N. humifusum* was higher than that for *Muriellopsis* sp. The  $\lambda_{exc}$ s used here are reported to be the most suitable for detecting phycobiliproteins (8). The *Cyanobacteria* in field samples presented a higher MFI for the range of 640 to 740 nm at any of the  $\lambda_{exc}$ s compared to *Chlorophyta* and *Bacillariophyta* (Fig. 3B). The *Cyanobacteria* also showed a high MFI at  $\lambda_{max}$ s of 577 to 580 nm (Fig. 3B) because of the C-PE. We did not observe changes in the  $\lambda_{max}$  of particular taxa—*N. humifusum*, *S. julianum*, or *C. parthenonensis*—when they were covered by thick sheaths, exopolymeric substances, or calcareous investments.

**Conclusions.** The combination of CSLM with spectrofluorometry techniques provides a powerful tool that extends the application fields of these two methodologies. This setup allows (i) direct analysis for global and single fluorescent pixels and their 3D localization in vivo, thus minimizing the artifacts associated with a small sample size, and (ii) discrimination of cells with particular fluorescence signatures within a colony and correlation with morphology and individual cell states.

This work was supported by the EU Program Energy, Environment, and Sustainable Development in the frame of CATS Project contract EVK4-CT-2000-00028.

We thank Herminia Rodríguez for supplying species in culture and the Scientific and Technical Services of the University of Barcelona for helpful assistance with the CSLM. We thank Elisabet Yuste for her contribution to the experimental work.

## REFERENCES

- Andersson, P. O., T. Gillbro, A. E. Asato, and R. S. H. Liu. 1992. Dual singlet state emission in a series of mini-carotenes. *J. Lumin.* **51**:11–20.
- Becker, G., H. Hoffeld, A. T. Hasselrot, D. M. Fiebig, and D. A. Menzler. 1997. Use of a microscope photometer to analyze in vivo fluorescence intensity of epilithic microalgae grown on artificial substrata. *Appl. Environ. Microbiol.* **63**:1318–1325.
- Bialek-Bylka, G. E., and J. S. Brown. 1986. Spectroscopy of native chlorophyll-protein complexes embedded in polyvinyl alcohol films. *Photobiophys.* **13**:63–71.
- Campbell, D., V. Hurry, A. K. Clarke, P. Gustafsson, and G. Öquist. 1998. Chlorophyll fluorescence analysis of cyanobacterial photosynthesis and acclimation. *Microbiol. Mol. Biol. Rev.* **62**:667–683.
- Del Campo, J. A., J. Moreno, H. Rodríguez, M. A. Vargas, J. Rivas, and M. G. Guerrero. 2000. Carotenoid content of chlorophycean microalgae: factors determining lutein accumulation in *Muriellopsis* sp. (*Chlorophyta*). *J. Biotechnol.* **76**:51–59.
- Hernández-Marín, M., E. Clavero, and M. Roldán. 2003. Why there is such luxuriant growth in the hypogean environments. *Arch. Hydrobiol. Algol. Stud.* **148**:229–240.
- Keränen, M., E.-M. Aro, and E. Tyystjärvi. 1999. Excitation-emission map as a tool in studies of photosynthetic pigment-protein complexes. *Photosynthetica* **37**:225–237.
- Millie, D. F., O. M. E. Schofield, G. J. Kirkpatrick, G. Johnsen, and T. J. Evens. 2002. Using absorbance and fluorescence spectra to discriminate microalgae. *Eur. J. Phycol.* **37**:313–322.
- Mullet, J. E., J. J. Burke, and C. J. Arntzen. 1980. A developmental study of photosystem I peripheral chlorophyll proteins. *Plant Physiol.* **65**:823–827.
- Neu, T. R., U. Kuhllicke, and J. R. Lawrence. 2002. Assessment of fluorochromes for two-photon laser scanning microscopy of biofilms. *Appl. Environ. Microbiol.* **68**:901–909.
- Ong, L. J., and A. N. Glazer. 1987. R-phycocyanin II, a new phycocyanin occurring in marine *Synechococcus* species. Identification of the terminal energy acceptor bilin in phycocyanins. *J. Biol. Chem.* **262**:6323–6327.
- Rodríguez, H., J. Rivas, M. G. Guerrero, and M. Losada. 1989. Nitrogen-fixing cyanobacterium with a high phycoerythrin content. *Appl. Environ. Microbiol.* **55**:758–760.
- Talarico, L., and G. Maranzana. 2000. Light and adaptive responses in red macroalgae: an overview. *J. Photochem. Photobiol. B Biol.* **56**:1–11.
- Tjioe, L., T. Legerton, J. Wegstein, L. A. Herzenberg, and M. Roederer. 2001. Phycoerythrin-allophycocyanin: a resonance energy transfer fluorochrome for immunofluorescence. *Cytometry* **44**:24–29.
- Wiggli, M., A. Smallcombe, and R. Bachofen. 1999. Reflectance spectroscopy and laser confocal microscopy as tools in an ecophysiological study of microbial mats in an alpine bog pond. *J. Microbiol. Methods* **34**:173–182.
- Wyman, M. 1992. An *in vivo* method for the estimation of phycoerythrin concentrations in marine cyanobacteria (*Synechococcus* spp.). *Limnol. Oceanogr.* **37**:1300–1306.
- Ying, L., X. Huang, B. Huang, J. Xie, J. Zhao, and X. S. Zhao. 2002. Fluorescence emission and absorption spectra of single *Anabaena* sp. strain PCC7120 cells. *Photochem. Photobiol.* **76**:310–313.
- Young, A. J., and H. A. Frank. 1996. Energy transfer reactions involving carotenoids: quenching of chlorophyll fluorescence. *J. Photochem. Photobiol. B Biol.* **36**:3–15.

---

#### 4.4. Morfologia de biofilms fototròfics en baixa il·luminació. El cas de l'avenc de Puigmoltó

Les cavitats càrstiques constitueixen un ambient molt especialitzat amb una distribució disjunta i cosmopolita. Es tracta d'ambients estables caracteritzats per temperatures uniformes durant tot l'any, humitat constant i il·luminació escassa, especialment a les zones més profundes. Només es coneix la distribució i els requeriments ecològics d'algunes de les espècies que habiten en aquests ambients. Els microorganismes fototròfics que viuen a l'entrada de les cavitats també es troben, en general, en hàbitats terrestres aerofítics, com monuments.

La present memòria es va iniciar amb l'estudi de biofilms que es desenvolupen a l'avenc càrstic de Puigmoltó, a la costa est de la Península Ibèrica, amb els objectius següents: (1) determinar l'estructura dels biofilms fototròfics referent a la composició d'espècies i a la forma de creixement i (2) determinar-ne la distribució espacial en funció de les condicions ambientals. Els biofilms fototròfics que cobreixen la superfície calcària de l'avenc es van examinar mitjançant microscòpia òptica, de rastreig làser confocal, electrònica de rastreig i de transmissió. Els biofilms es desenvolupen a la superfície del substrat, aparentment organitzats segons un gradient decreixent d'il·luminació i, generalment presentaven un gruix inferior a 150 µm. No es van observar ni creixement endolític ni casmoendolític. A la part superior de l'avenc, els biofilms formen un cinturó discontinu de color verd clar format principalment per *Scytonema julianum* i formes cocals envoltades per grans quantitats d'EPS. A la part inferior de l'avenc, per sota de 5 m, els biofilms presenten una distribució en mosaic sobre el substrat suau i porós i molt pocs organismes van ser capaços de créixer sota condicions estables de temperatura i humitat però amb llum decreixent. *Scytonema ocellatum* va ser l'espècie dominant junt amb protonemes de molses i el líquen *Macentina stigonemoides*. La fase inicial de colonització per part dels cianobacteris filamentosos es va portar a terme

## *Resultats*

---

mitjançant hormogonis amb l'evidència que eren necessaris per a la unió inicial a la superfície els extrems recoberts de mucílag o restes de cèl·lules necrídiques amb substàncies polimèriques extracel·lulars que funcionaven com agent adhesiu.

Els resultats detallats d'aquest capítol s'inclouen en el següent article:

Phototrophic biofilm morphology in dim light. The case of the Puigmoltó sinkhole. ***Nova Hedwigia, Beih.*** (2001), 123:237-253.

---

Nova Hedwigia, Beiheft 123, p. 237–253. December 2001  
Algae and extreme environments

---

## Phototrophic biofilm morphology in dim light. The case of the Puigmoltó sinkhole

MARIONA HERNÁNDEZ-MARINÉ<sup>1</sup>; MÓNICA ROLDÁN<sup>1</sup>; ESTER CLAVERO<sup>1</sup>;  
ANTONI CANALS<sup>1</sup> & XAVIER ARIÑO<sup>2</sup>

with 36 figures

---

**Abstract:** A study of sinkhole biofilms, in the East coast of the Iberian peninsula was undertaken with the following aims: (1) to determine the structure of phototrophic biofilms in terms of species composition and growth forms, and (2) to determine their spatial distribution as a function of environmental conditions. The phototrophic biofilm coating the limestone surface in the sinkhole was examined using LM (Light Microscopy), SEM (Scanning Electron Microscopy), TEM (Transmission Electron Microscopy) and CLSM (Confocal Laser Scanning Microscopy). The biofilms develop on the substrate surface, apparently organized following the decreasing irradiance. Endolithic or chasmoendolithic growth was not observed. In the uppermost part of the sinkhole, the biofilm formed a discontinuous light green belt mainly built up by *Scytonema julianum* and coccoid forms surrounded by large amounts of EPS. Below 5 m in depth, biofilm occurred in patches on soft and porous substrate and very few organisms were able to grow along the whole gradient of conditions. *Scytonema ocellatum* was the prevalent species together with the moss protonemata and the lichen *Macentina stigonemoides*. The initial colonization phase of filamentous cyanoprokaryota was mediated by gliding hormogonia, with the evidence indicating that pad tips or necridic cell remnants that functioned as a pasting agent were required for the initial surface attachment. Living photosynthetic biofilms on the walls of the sinkhole were actually very thin, always less than 150 µm thick. In addition, filaments were loosely arranged and the space between them empty. The main difference between highly hydrated biofilms and sinkhole biofilms seems to be related to the lack of a matrix, that is, EPS and water.

**Key words:** Cyanoprokaryota/Cyanobacteria, confocal laser scanning microscopy, cave, lichen, algae, polysaccharide, lectin, fluorescence, biofilm structure.

### Introduction

Biofilms are open systems of cells, exopolimeric material and extracellular spaces (LAWRENCE et al. 1991). The biofilm functions primarily to protect the micro-organisms from hostile environments and as a trap for nutrient acquisition (MACKAY et al. 1999).

---

#### Authors' addresses:

<sup>1</sup> Facultad de Farmacia, Botánica, Av. Joan XXIII, s/n., E-08028 Barcelona, Spain. E-mail: hernandez@farmacia.far.ub.es.

<sup>2</sup> Universitat Pompeu Fabra, IDEC, Balmes 132, E-08008 Barcelona, Spain.

1438-9134/01/0123-237 \$ 4.50  
© 2001 J. Cramer in der Gebr. Borntraeger Verlagsbuchhandlung, D-70176 Stuttgart

Limestone caves and sinkholes are very specific environments with a greatly disjoint and world-wide distribution. They usually have stable temperatures throughout the year, constant humidity and low light particularly toward the deepest zones. Sinkholes present a vertical, gradual stratification of temperature and humidity, whereas light depends mainly on the walls' irregularities (HERRERO-BORGOSÓN 1986).

Phototrophic biofilms thrive on the walls, giving them a grey, dusty feel. The biofilms are made of mosses and lichens together with microalgae and cyanoprokaryota as significant components (GARBACKI et al. 1999, HOFFMANN 1989, NIENOW 1996, VINOGRADOVA et al. 1998). Despite the extensive literature dealing with phototrophic microorganisms in caves, knowledge is incomplete and investigations of organisms and community structure in response to environmental conditions are scarce. The occurrence, distribution and ecological requirements are known for just a handful of species (ARIÑO et al. 1997, COUTÉ 1989, FRIEDMANN 1979, GARBACKI et al. 1999, HERNÁNDEZ-MARINÉ et al. 1999).

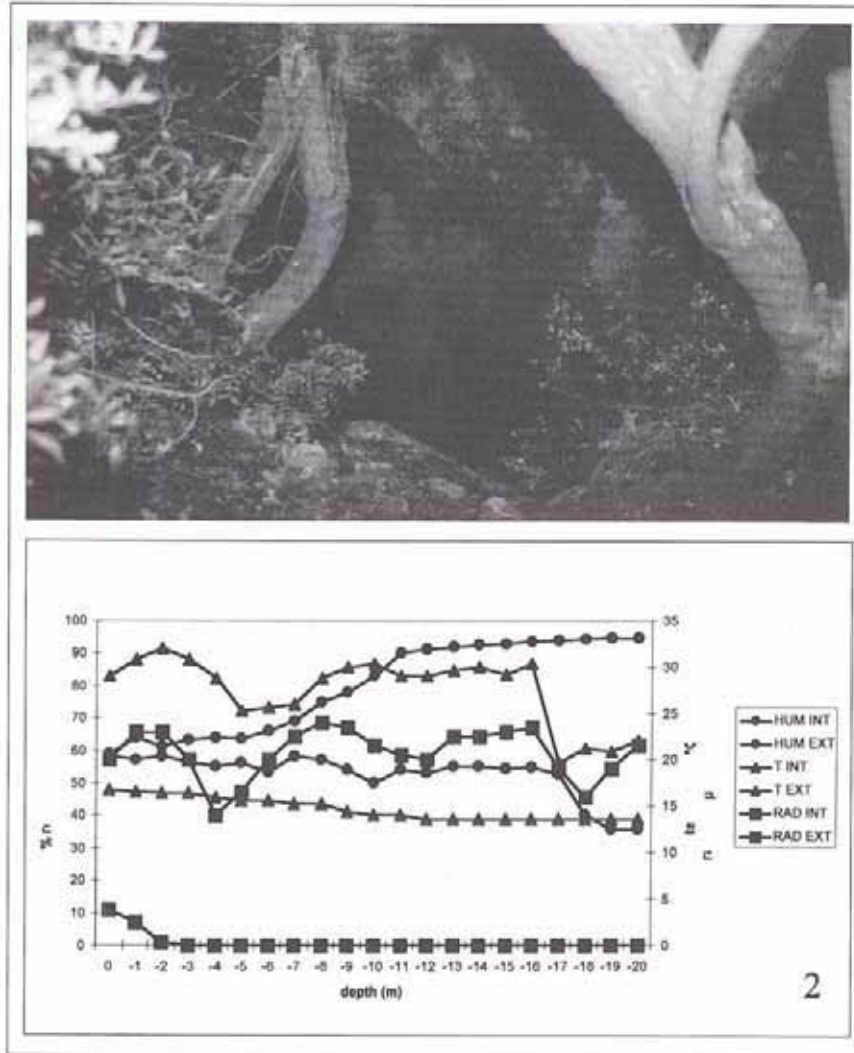
A study of biofilms thriving in a limestone sinkhole in the East coast of the Iberian peninsula was performed with the following aims: (1) to determine the structure of phototrophic biofilms in terms of species composition and growth forms and (2) to determine their distribution as a function of the environmental conditions.

## Materials and methods

The material for study was collected from a limestone sinkhole (Puigmoltó, Garraf UTM 31TDF07/41°13'16"N, 1°52'00"W, near Barcelona) in the East coast of the Iberian Peninsula. Calcite is the dominant mineral (95 %), both in the form of a soft substrate and of hard stone blocks. The sinkhole has an irregular mouth (Fig. 1). It is 2 m in diameter at its opening and descends sub-vertically down to 32 m. Air temperature was measured by means of thermistors (Grant, Cambridge), relative humidity by means of hygrometers (Vaisala, Helsinki) and photosynthetically active radiation (P.A.R.) with a LICOR quantum photometer (Lincoln, Nebraska). All the probes were connected to a Squirrel Data Logger (Grant, Cambridge) and were logged every ten minutes. Average temperature, relative humidity and irradiance were measured from the cave entrance down to a depth of 20 m (07/10/99).

Samples were obtained by scrapping the substrates on two different survey days. On 07/10/99 sampling was performed from the entrance down to a depth of 25 m, in places where colonisation by phototrophic microorganisms was evident. On 12-Mar-2000 samples were collected following a transept, at intervals of 1m down to 5m and then every 2 m down to 20 m. Cultures were grown on 1 % agarised (ADSA-MICRO) BG11 (RIPPKA 1988).

Selected fragments of the biofilms growing on the sinkhole walls and cultures were studied by means of LM (light microscopy), CLSM (Confocal Laser Scanning Microscopy), SEM (Scanning Electron Microscopy) and TEM (Transmission Electron Microscopy). LM was carried out with a NIKON Optiphot-2. Rock chips for SEM were submerged in liquid nitrogen and freeze-dried, then placed on stubs and gold sputtered. Specimens were viewed using a HITACHI S-2300 microscope. Chemical fixation and preparation for TEM was made according to HERNÁNDEZ-MARINÉ (HERNÁNDEZ-MARINÉ 1996). Thin sections were viewed using a HITACHI H800 MT transmission electron microscope.



Figs 1-2. 1 – Entrance to the Puigmoltó limestone sinkhole. 2 – Evolution of microclimatic parameters.

A LEICA TCS 4D CLSM equipped with an ArKr laser (75 mW) was used to produce high-resolution images of autofluorescence, reflection, labelled nucleic acids and EPS. Nucleic acids were specifically stained with SYTOX Green (Molecular Probes, Inc.) in samples



previously fixed with 2,5 % glutaraldehyde in cacodilate buffer. EPS was labelled with the carbohydrate recognizing lectin Concanavalin-A. FITC-conjugated Con A (Succ-Con-A, Molecular Probes, Inc.) was used at a final concentration of  $10 \mu\text{g ml}^{-1}$  to  $30 \mu\text{g ml}^{-1}$ , and samples were not washed. Samples were observed either for autofluorescence and SYTOX fluorescence or for autofluorescence and Con-A fluorescence. In addition, unstained samples were scanned in the reflection and fluorescent mode. The reflection images were obtained with laser light of 488 nm and were used to examine the outer layer for the presence of mineral particles and calcified sheaths. Natural fluorescence of chlorophyllous pigments was examined by exciting samples with a laser light of 568 nm and capturing the fluorescence emitted at  $>590 \text{ nm}$ . An excitation of 488 nm, and emission fluorescence of 520 nm were used for the detection of both SYTOX and FITC-conjugated lectin Concanavalin A. By design, autofluorescence could not be detected at this setting, thus preventing interference with induced fluorescence.

Images were taken with 20x and 63x objectives (numerical apertures 0,4 and 1,4 respectively) and collected as Z-series (3D imaging) in order to map the spatial distribution of fluorescence in the samples. Images showing reflection, pigment fluorescence, nucleic acids label, Con-A or combinations of these are presented in maximum intensity projection unless stated otherwise. Observations on in-depth distribution of the organisms were obtained from undamaged fragments transferred to microcapsules. The thickness of the biofilm was established using the distribution of natural fluorescence of chlorophyllous pigments as a marker. Top and bottom were fixed at the first and last image showing fluorescence. Reconstruction of pre-established series to obtain "lateral projections" was achieved by means of Imaris software (Bitplane AG, Zürich).

To ensure accurate species identification, CLSM, TEM and SEM images were cross-referenced with LM images of identified phototrophic organisms.

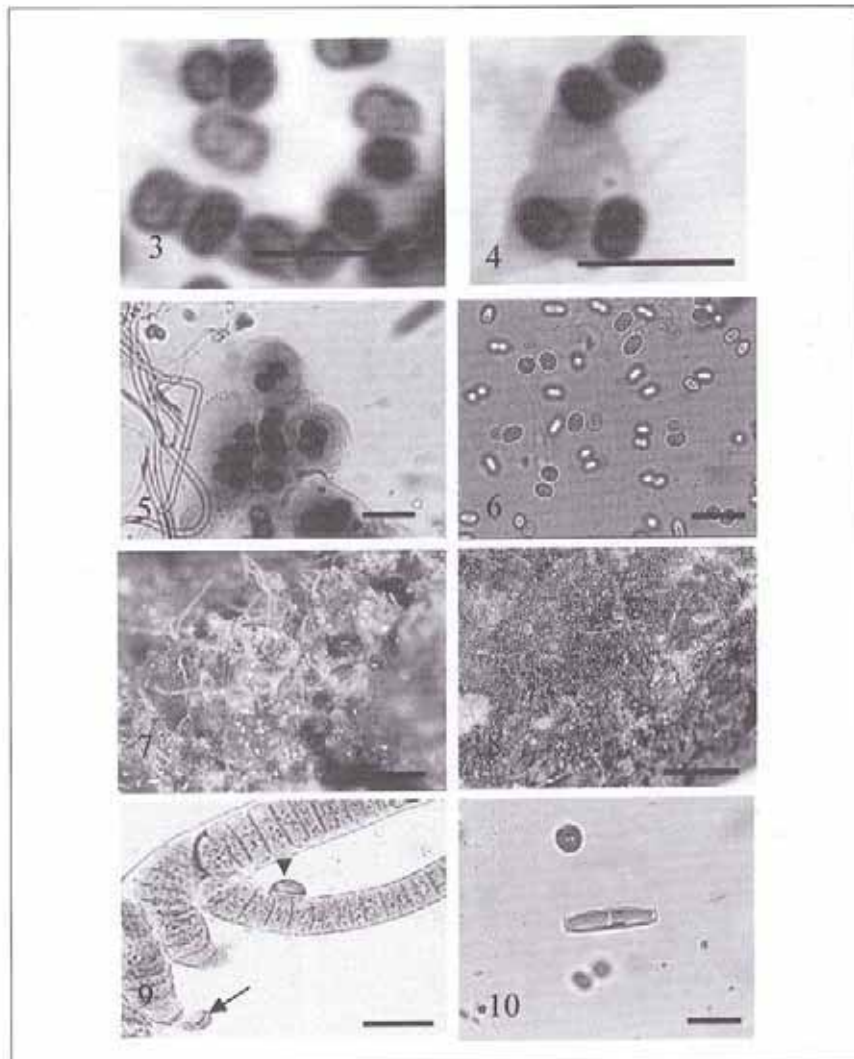
## Results

### Environmental conditions

The evolution of microclimatic parameters is presented in Figure 2. Temperature fluctuations in the Puigmoltó sinkhole were attenuated with respect to the outside and, below 4.5 m depth, temperature was nearly constant throughout the year. Humidity was above 80% at 4.5 m depth and near the dew point at 10 m. The light at 3 m was detectable at  $5 \mu \text{ einstein m}^{-2} \text{ s}^{-1}$ , whereas at 4 m it was below the detection threshold of the instrument (Fig. 2).

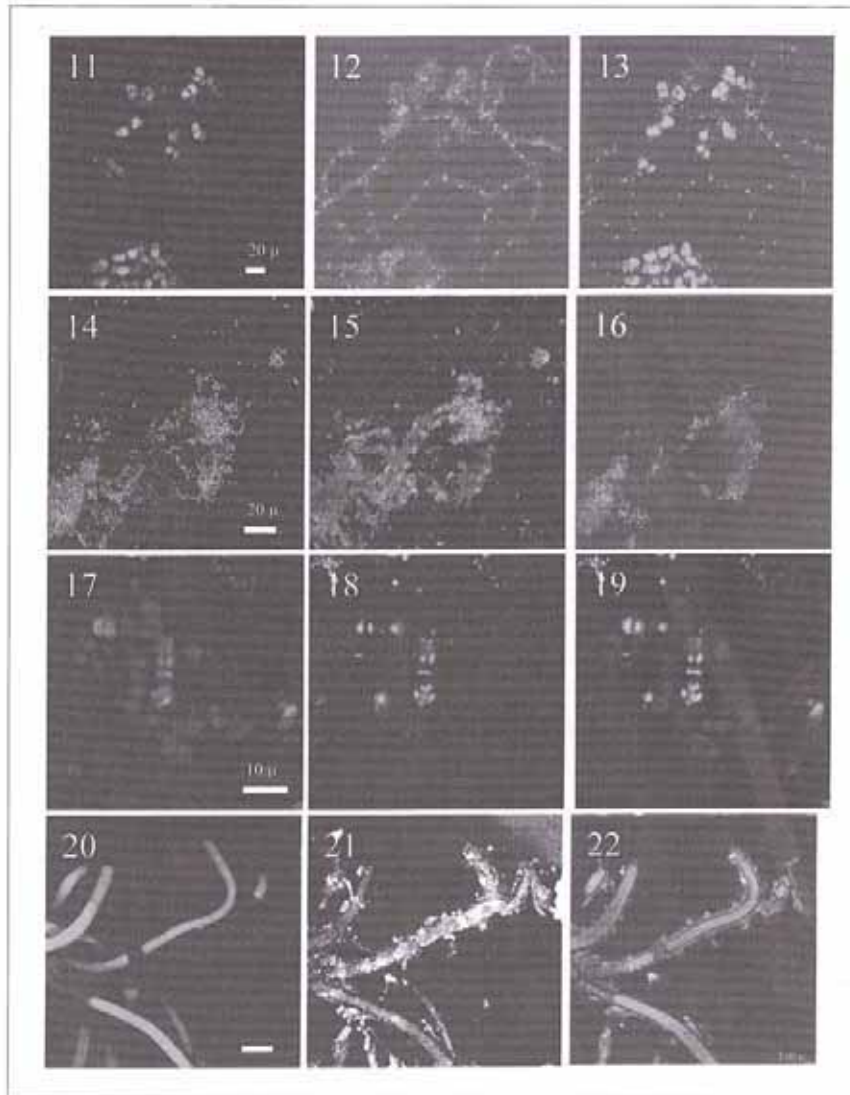
### Species composition

A photosynthetic biofilm presenting an irregular distribution covered the walls of Puigmoltó sinkhole and formed belt-like biofilms built by few separate species. No seasonal variation was observed. In the samples scraped off the walls we identified six species of cyanoprokaryota [*Aphanothece smithii* KOMÁRKOVÁ-LEGNEROVÁ et CRONBERG (Figs 3, 4), *Geitleria calcarea* FRIEDMANN, *Gloeothece rupestris* (LYNGBYE) BORNET (Figs 5, 6), *Phormidium ambiguum* FRÉMY, *Scytonema julianum* (KÜTZ.) MENECH. (Fig. 7), *Scytonema ocellatum* LYNGB. (Figs 8,



**Figs 3–10.** Light micrographs of phototrophic sinkhole organisms.

**3** – *Aphanothece smithii*. **4** – *A. smithii* after staining with Methylene blue for mucilage presentation, illustrating the course of cell division. **5** – *Leptolyngbya* sp. and *Gloeotheca rupestris* with visible envelopes around cells. Methylene blue staining. **6** – *G. rupestris*. **7** – Biofilm from the cave mouth mainly composed by *Scytonema julianum*. **8** – Biofilm from 10 m depth mainly composed by *Scytonema ocellatum*. **9** – Part of a filament of *S. ocellatum* showing a terminal cell still laterally attached (arrow) and after settling of the isolated tip (arrow head). **10** – *Hantzschia amphioxys*. [Scale bar = 10  $\mu\text{m}$ .]



**Figs 11–22.** Confocal laser scanning micrographs. Simultaneous sampling.  
**11–13** – Z series projection of *Botryolepraria lesdainii*. **11** – Pigment autofluorescence. **12** – SYTOX Green labelling. **13** – Two channel maximum intensity projection of fungal hyphae nucleus and terminal bunches of algal cells. **14–16** – Unidentified cyanoprokaryota Coccoid 1. **14** – Z series projection of pigment autofluorescence. **15** – z series projection of Con-A labelling. **16** – Optical thin section illus-

9)], two species of Bacillariophyta [*Diadesmis contenta* (GRUN.) D.G.MANN, *Hantzschia amphioxys* (EHRENBERG) GRUNOW (Fig.10)], five Chlorophyta [*Coccolobos verrucariae* (R. CHODAT) VISCHER, *Klebsormidium flaccidum* (KÜTZING) SILVA, MATTOX et BLACKWELL, *Leptostira obovata* VISCHER, *Myrmecia* sp., *Trentepohlia* sp.] and two lichens [*Botryolepraria lesdani* (HUE) CANALS et al. (Figs 11–13), *Macentina stigonemoides* A. ORANGE]. We also observed moss protonemata, several thin filaments assigned to the genus *Leptolyngbya*, one unidentified coccoid cyanoprokaryota (Figs 15–17) and microbial non-photosynthetic cells (Figs 17–19). *L. obovata* was observed both free-living and lichenized in *M. stigonemoides*. Among the different organisms found only three filamentous cyanoprokaryota (*G. calcarea*, *S. julianum* and *S. ocellatum*) had calcified sheaths. In *G. calcarea* the cover was composed of small calcite needles radially orientated and embedded in the polysaccharide sheath. Both *Scytonema* species presented calcite embeddings only on the sheath surface, in the form of crystals on *S. julianum* and as grainy crumbs on the thin sheath of *S. ocellatum* (Figs 20–24). Motile hormogonia of calcified filaments were separated from the main filament by means of necrotic cells or mucilaginous pads (Figs 25–27). In the case of *S. ocellatum*, terminal cells could also behave as hormogonia; when separated, they remained laterally attached for a while (Fig. 9) and later grew and developed as any other independent juvenile filament when attached to mature filaments (Figs 9, 24) or to any other organism or inorganic surface.

### Spatial variation

The biofilms developed on the substrate surface, apparently organized following the decreasing irradiance. Neither endolithic nor chasmoendolithic growth were observed. In the uppermost part, from the threshold down to 5 m depth, the biofilm formed a discontinuous light green belt, mainly composed of moss protonemata, the lichen *Botryolepraria lesdani* and green algae (mainly *Trentepohlia* sp. and *Myrmecia biatorellae*). The most common diatom, *Diadesmis contenta*, was also found, on the biofilm surface. Cyanoprokaryota occurred in grey patches mainly built up by coccoid forms surrounded by large amounts of extracellular polymeric substances (EPS). *Gloeotheca rupestris* (Fig. 5), *Aphanothece smithii* (Fig. 4) and one unidentified coccoid (Coccoid 1) were widespread only down to 4 m, and isolated specimens with thinner sheaths or devoid of sheaths could be found down to 15 m. *Scytonema julianum* grew on all surfaces not directly exposed to long periods of sunlight except on the hardest calcareous rocks. *S. julianum* and moss protonemata were entangled along with substrate grains and with diatoms on top. At a depth of 3 m the lichen *B. lesdani* outnumbered all other organisms, forming dusty green patches on its own.

trating that pigment autofluorescence was discontinuous, and developed only on the limestone mineral particle's surface. 17–19 – Z series projection of *Aphanothece smithii*. 17 – Pigment autofluorescence. 18 – SYTOX Green labelling. 19 – Two-channel maximum intensity projection showing that nucleoids of bacterial cells were dyed with Sytox Green but did not exhibit pigment fluorescence (top left corner above number). 20–22 – *Scytonema ocellatum*. 20 – Z series projection of pigment autofluorescence. 21 – Z series projection in reflection mode showing the calcified sheaths. 22 – Optical thin section illustrating the separation between mineral particles and the photosynthetic layer.

Below 5 m the phototrophic biofilm was uneven; in some places it was well-developed and in other places it was almost absent. Even in the places colonized by organisms the delimitation between different belts was weak and the number of species declined towards the end of the sinkhole. Transept samples from 5 to 15 m of depth revealed that the substrate was irregular in hardness. Only few patches of phototrophic biofilm were found in these samples, at 5 to 10 m depth and always occurring on soft or porous substrates. The species found at these depths were present down to the end although their abundance varied. The organisms forming the biofilm were long and thin moss protonemata, *Macentina stigonemoides*, *Scytonema ocellatum* and *Phormidium ambiguum*. In addition, diatoms, coccoid forms and occasional filaments of *Leptolyngbya* ssp. grew on the entangled biofilm surface built mainly by *S. ocellatum* and protonemata moss. The hard calcite areas of the walls were not colonized.

In the transept from 10 m down to 15 m discontinuous patches covered extensive zones. The violet penicillate thallus of *Scytonema ocellatum* was the prevalent component of the biofilm, entangled with *Phormidium ambiguum* and *Macentina stigonemoides*. Below that, the sheaths of coccoid cyanoprokaryota and some filaments of *S. ocellatum* and *Phormidium ambiguum* were strongly colonized by adhering bacteria. TEM observation revealed disorganized thylakoids in those organisms (Figs 32,33).

*Geitleria calcarea* was distributed in small patches down to 20 m depth, although no instances were found in the path of the transept.

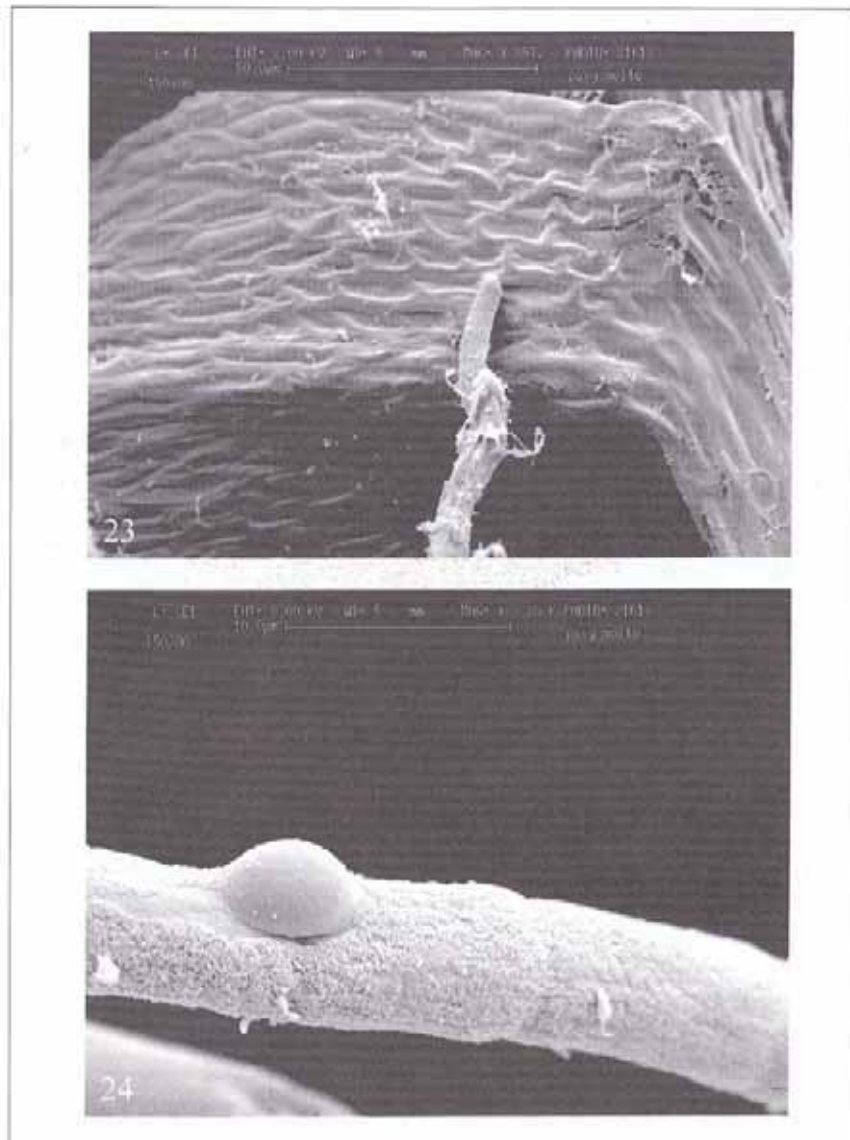
A variety of actinomycetes occurred throughout the biofilm. At 2.5 m they were yellow and hidden under spongy material, whereas deeper down in the sinkhole (at 15 to 25 m, the deepest zone sampled) they were dusty and blue-grey. Despite their showing characteristic traits, it was not possible to identify which exact variety of actinomycetes they belonged to.

The differential distribution of polysaccharide sheaths in colonies and filaments was studied through labelling of EPS with con-A lectin, in combination with natural fluorescence images. Near the entrance, the colonies of coccoid forms were enrobed by EPS. Living colonies and the remains of sheaths coated the surface of sand, small calcite grains and muddy soil, but did not penetrate inside the mineral (Figs 15–17). Hormogonia and filamentous forms were irregularly sheathed. The sheaths of *Scytonema julianum* were thicker than those of *Scytonema ocellatum* and *Phormidium ambiguum*. Pad tips and the regions around necridic cells displayed stronger con-A fluorescence than any other part of the sheath, indicating their polysaccharidic composition (Figs 25–27).

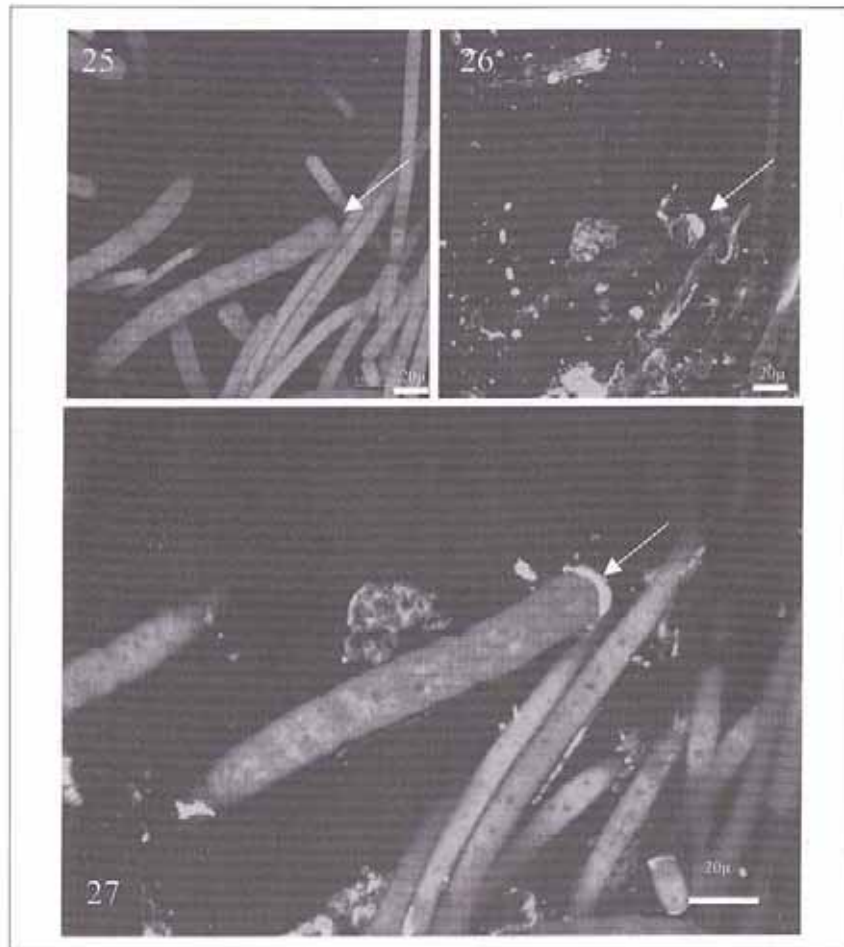
The presence of bacterial microcolonies with irregular distribution was found in images collected in the 2-channel mode, by overlaying pigment fluorescence and nucleic acid stain.

Nucleoids of bacterial cells were dyed with Sytox Green but did not exhibit pigment fluorescence unlike in the case of small cyanoprokaryota (Figs 17–19).

Images of unstained samples were scanned in reflection and fluorescence for the presence of mineral particles and are shown in maximum intensity projection (Figs 20–21), except for Figure 22 which is an optical slice. In this one image the separation between mineral particles and the photosynthetic layer indicated that in *Scytonema ocellatum* the calcite cover was on the sheath surface.



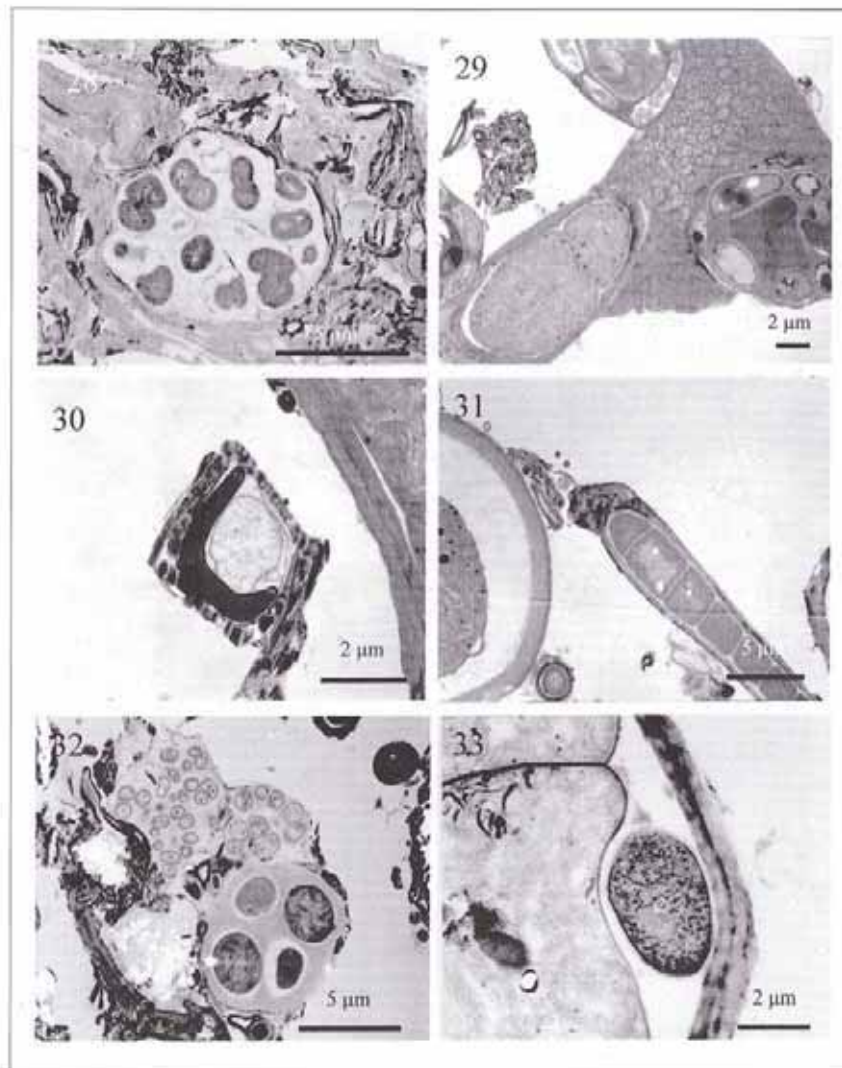
**Figs 23–24.** SEM micrographs of *Scytonema ocellatum*.  
**23** – Hormogonia on the surface of a protonemata moss. **24** – Terminal cut-off cell attached to a mature filament. The sheath surface is covered with grainy crumbs of calcite.



**Figs 25–27.** Confocal laser scanning micrographs of *Scytonema ocellatum*. Simultaneous sampling. **25** – Z series projection of pigment autofluorescence. **26** – Z series projection with Con-A labelling. **27** – Two-channel maximum intensity projection showing that pad tips (arrow) displayed stronger Con-A fluorescence than any other part of the sheath.

#### Attachment

Near the sinkhole entrance, colonial coccoid forms that were enclosed in large amounts of EPS (Figs 15–19) were stuck by their whole polysaccharide sheath (Fig. 28) on both calcareous stones and hard surfaces. Filamentous forms, as well as protonemata mosses and the



Figs 28-33. TEM micrographs.

28 – Colonial Coccoid 1, enclosed in EPS, appeared attached to the substrate along their whole sheath. 29 – *Macentina stigonemoides* and *Scytonema ocellatum* attached to debris. 30 – Transversal section of *Diadesmis contenta* attached by a stalk. 31 – *Phormidium ambiguum* filament attached by a pad tip. 32 – Colonial Coccoid 1 closely adhered to some bacterial cells. 33 – Sheaths of *Scytonema ocellatum* colonized by bacteria.



lichen *Macentina stigonemoides* were thriving only on soft limestone surfaces and debris (Fig. 29). Diatoms presented a stalk (Fig. 30). The hormogonia of both *Scytonema julianum* and *Phormidium ambiguum* were the only components of the filament that were able to move. The initial colonization phase was mediated by the actively gliding hormogonia, evidence indicating that the ending tip pad was required for the initial surface attachment. It functioned as a pasting agent, capable of attaching to abiotic materials as well as other organisms. The mature filaments of *Scytonema ocellatum* and *P. ambiguum* were attached by pad tips or by necrotic cell remnants (Figs 29, 31). These structures were the only point of contact between the nearly erect filaments and the wall surface. On the other hand, the mature filaments of *S. julianum* were attached by the sheath of two or three end cells that were dead and not covered with calcite needles. Thin *Leptolyngbya*-like filaments growing on top of the biofilm had no special attachment structures.

### Biofilm's architecture

The combination of techniques used, CLSM, SEM and TEM, reveals the 3-dimensional architecture of the biofilms. In particular, the use of CLSM permitted the observation of intact biofilms, the form and arrangement of organisms and the differentiation between dead and living cells. Since only living photosynthetic cells were fluorescent, pigment fluorescence offered a real picture of the thickness of the photosynthetic layer. Living photosynthetic biofilms on the walls of the sinkhole were actually very thin. Reconstruction from image sequences of fluorescent fragments of intact attached biofilms from 5 m depth down to 15 m (horizontal thin sections cut through the biofilm from the wall's surface to the exterior), showed that biofilms were always less than 150  $\mu\text{m}$  thick (Figs 34–36). In addition, when con-A labelling was employed the filaments were found to be loosely arranged and the space between the filaments was found to be empty.

### Discussion

The phototrophic microorganisms that built the biofilm can be found in terrestrial, aerophytic and atmophytic habitats or associated with lichens and mosses in cryptogamic crusts (BUDEL 1999, EVANS & JOHANSEN 1999, JOHANSEN 1993, KOMÁREK & ANAGNOSTIDIS 1999, ORTEGA et al. 1993). The observed assemblages are rather similar to the flora found in other low light environments such as catacombs and tombs (ALBERTANO et al. 1993, ALBERTANO & URZI 1999, ARIÑO et al. 1997) as well as caves (GARBACKI et al. 1999, VINOGRADOVA et al. 1998).

The biofilm present in the sinkhole was very thin and formed exclusively by epilithic species, even near the entrance. This behaviour indicates stress due to low light, and otherwise green algae and cyanoprokaryota would colonize pores and endolithic habitats (ASENCIO & ABOAL 2000, BELL 1993). Below a depth of 5 m *Gloeothece rupestris*, *Aphanothece smithii* and Coecoid 1 appeared mixed with the biofilm and presented cells that were isolated or in small colonies nearly devoid of sheaths, which also indicates unfavourable growth conditions (NICOLAUS et al. 1999). Light-related stress reduces biofilm thickness and species diversity. Before its total disappearance with depth, the phototrophic biofilm becomes lax and thin and shows symptoms of senescence, and in addition the sheaths of cyanoprokaryota and *Leptosira*



**Fig. 34.** Confocal laser scanning micrographs. Simultaneous sampling of autofluorescence signal of chlorophyll (568 nm excitation, 590 nm mission) and SYTOX Green and Con-A (488 nm excitation and 520 nm emission). Gallery of Z series projection of double-fluorescence images from 10 m dept biofilm, mainly composed of *Scytonema ocellatum* and *Phormidium ambiguum*. 12 representative images of 54 (2.51  $\mu\text{m}$  interval) from the surface of the biofilm to the last fluorescent image. 135  $\mu\text{m}$  total thickness of the biofilm.

*ovobata* are colonized by bacteria and the lichen's fungal and algal partners split. With such evident deficiencies, ecological microniches could only be occupied by specific organisms with a high degree of specialization. Among these are *Geltleria calcarea* and *Scytonema ocellatum*. *G. calcarea*, as described in other dim light habitats (LECLERC et al. 1983), seemed adapted to thrive alone in the deepest zone. *S. ocellatum* is widespread in aerophytic habitats (GIBTLER 1932, SANT'ANNA 1984) with less available water. It was able to accumulate an antifungal secondary metabolite (PATTERSON & BOLIS 1997), to quickly colonize with hormogonia and cutting off of terminal cells, and was capable of dealing with the sinkhole habitat. The cutting off of the tips is not exclusive to *S. ocellatum* since it has also been described in other members of the Scytonemataceae (PANDEY & MITRA 1972 and references herein).

Below 5 m, biofilms were not found in belts but in patches, and their distribution in the transept samples was irregular in depth, indicating that low photosynthetic active radiation was only one of the limiting stress factors. Assuming that air temperature and humidity were constant inside the sinkhole, the settlement in patches of filamentous cyanoprokaryota hinted that biofilm organisms were dependent on other environmental conditions, resulting in specific organizational features (TOLKER-NIELSEN & MOLIN 2000).

The attachment of organisms to the walls depends on the presence of polysaccharidic substances. Coccoid forms that colonize the sinkhole entrance possess the capacity to produce enough EPS to adhere to hard surfaces and initiate the colonization process. The ability of biofilms to thrive towards the deep dim light zones without seeping water was nearly restricted to the porous surfaces, probably enhancing water absorption. This could be due to limited polymeric substances, scarce on the filamentous forms (*Scytonema ocellatum* or *Phormidium ambiguum*), or to the small adhesion surface that these filamentous forms present. Both possibilities, added to the availability of hygroscopic water in porous substrates, could help in the understanding of the unstructured, patchy distribution that biofilms display in the deepest zones. On the other hand, the ability to utilize water vapour may be as low in these limited biofilms as it is in cryptoendolithic habitats where cyanoprokaryota photosynthesize at very high matrix water potentials (PALMER & FRIEDMANN 1990).

Calcified filaments of *Scytonema ocellatum* and *Scytonema julianum* were not able to attach. Only hormogonia and terminal cells of *S. ocellatum* could initiate a new filament. Con-A lectin labelling of EPS, in combination with pigment fluorescence, helps in the understanding of the attachment of phototrophic organisms to the substrate (LAWRENCE et al. 1991). In fact, cyanoprokaryota are known to produce qualitatively and quantitatively different EPS depending on the physiological state of the cells and from one strain to another (HOAGLAND et al. 1993, NICOLAUS et al. 1999). The strong signal shown by the pad tips of the hormogonia, when labelled with con-A, indicates that the observed filaments may secrete several types of EPS. The polysaccharides forming the sheath could be used to retard water loss, to trap nutrients or for gliding (HOICZYK 2000), whereas others, extruded by end cells or as a result of necrotic cell disintegration, may be quite different and may help in the release of hormogonia and in the attachment to the surfaces.

In intertidal systems, biofilms form protective environments in which single microorganisms and microcolonies are immobilized in a common polymeric matrix (NEU 2000). Through an extensive network of channels, gas and nutrient exchange is maintained in the film matrix (LAWRENCE et al. 1991). The EPS matrix acts as a stabilizing anchor and possesses physical and chemical properties that contribute a protective effect to the cells from high irradiance (SABA-

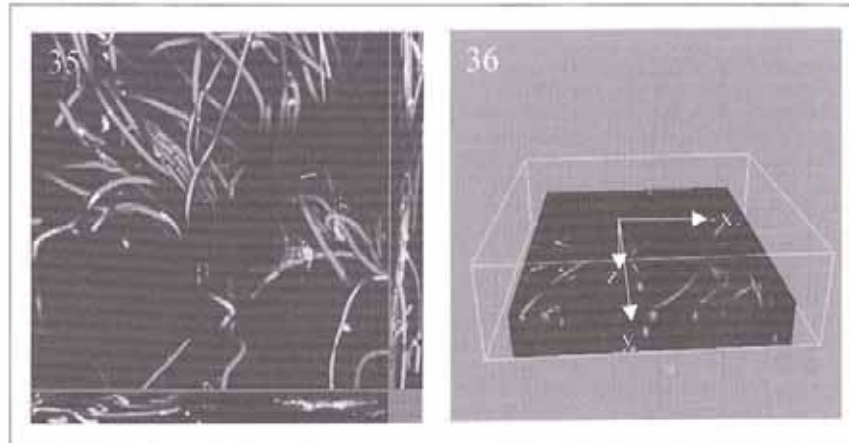


**Fig. 35.** Three-dimensional extended focus image and orthogonal view of 54 (2.51  $\mu\text{m}$  interval) bilinear interpolated x-y CLSM sections in z-directions of the biofilm. The extended focus x-y image was made from the selected volume by collapsing the z direction. Orthogonal views are cuts through selected regions of interest (arrowheads in the xy image) in the z-direction. All three images were made in the contrast optimised average mode.

**Fig. 36.** Perspective projection of the imaged volume. The wireframe box corresponds to the total sample volume and the three arrows to the reference axes (Z points down and Y points towards the reader).

TER 2000), afford organisms a potential for resiliency during periods of stress, and may enhance the overall physiological activities (DECHO 2000). The main difference when comparing highly hydrated biofilms and sinkhole biofilms seems to be related to the lack of a matrix, thus to water and EPS. The influx of nutrients, transfer of waste and establishment of micro-environmental conditions (LAWRENCE et al. 1991) must be very different with empty space in between the biological constituents. The combination of external environmental conditions and interactions among the organisms thriving in cave-like environments makes it a special habitat that deserves better understanding.

#### Acknowledgements

The authors thank the Scientific and Technical Services of the University of Barcelona. Supported by the Spanish DGESIC Program PB97-0957

## References

- ALBERTANO, P.; KOVÁČIK, L. & GARDAVSKÝ, A. (1993): Cross-gradient cultures of filamentous cyanophytes. – *G. Bot. Ital.* **127**: 386–392.
- ALBERTANO, P. & URZÌ, C. (1999): Structural interactions among epilithic cyanobacteria and heterotrophic microorganisms in Roman hypogea. – *Microbial Ecol.* **38**: 244–252.
- ARIÑO, X.; HERNÁNDEZ-MARINÉ, M. & SAIZ-JIMÉNEZ, C. (1997): Colonization of Roman tombs by calcifying cyanobacteria. – *Phycol.* **36**: 366–373.
- ASENCIO, A. D. & ABOAL, M. (2000): A contribution to knowledge of chasmoendolithic algae in cave-like environments. – *Arch. Hydrobiol./Algolog. Studies* **98**: 133–151.
- BELL, R. A. (1993): Cryptoendolithic algae of hot semiarid lands and deserts. – *J. Phycol.* **29**: 133–139.
- BÜDEL, B. (1999): Ecology and diversity of rock-inhabiting cyanobacteria in tropical regions. – *Eur. J. Phycol.* **34**: 361–370.
- COUTÉ, A. (1989): *Geitleria calcarea* Friedmann (Cyanophyceae, Hormogonophycidae, Stigonematales, Stigonemataceae): un cas d'adaptation à un milieu extrême. – *Bull. Soc. bot. Fr., Actual. bot.*, **136**: 113–130.
- DECHO, A. W. (2000): Microbial biofilms in intertidal systems. – *Cont. Shelf Res.* **20**: 1257–1273.
- EVANS, R. D. & JOHANSEN, J. R. (1999): Microbiotic crusts and ecosystem processes. – *Crit. Rev. Plant Sci.* **18**: 183–225.
- FRIEDMANN, I. (1979): The genus *Geitleria* (Cyanophyceae or Cyanobacteria): Distribution of *G. calcarea* and *G. floridana* n. sp. – *Pl. Syst. Evol.* **131**: 169–178.
- GARBACKI, N.; ECTOR, L.; KOSTIKOV, I. & HOFFMANN, L. (1999): Contribution à l'étude de la flore des grottes de Belgique. – *Belg. J. bot.* **132**: 43–76.
- GEITLER, L. (1932): Cyanophyceae. – 1195 pp., Akad. Verlagsgesell., Leipzig.
- HERNÁNDEZ-MARINÉ, M. (1996): Electron microscopic characterization of *Microcoleus chthonoplastes* Thur. (Cyanobacteria). – *Arch. Hydrobiol./Algolog. Studies* **83**: 347–365.
- HERNÁNDEZ-MARINÉ, M.; ASENCIO-MARTÍNEZ, A.; CANALS, A.; ARIÑO, X.; ABOAL, M. & HOFFMANN, L. (1999): Discovery of populations of the lime incrusting genus *Loriella* (Stigonematales) in Spanish caves. – *Arch. Hydrobiol./Algolog. Studies* **94**: 121–138.
- HERRERO-BORGOÑO, J. J. (1986): La flora de la simas valencianas. – 301 pp., Federación Territorial Valenciana de Espeleología, Valencia.
- HOAGLAND, K. D.; ROSOWSKI, J. R.; GRETZ, M. R. & ROEMER, S. C. (1993): Diatom extracellular polymeric substances: Function, fine structure, chemistry, and physiology. – *J. Phycol.* **29**: 537–566.
- HOFFMANN, L. (1989): Algae of terrestrial habitats. – In: CRONQUIST, A. (ed.): *The Botanical Review* **55**: 77–105, The New York Bot. Garden, Bronx, NY.
- HOICZYK, E. (2000): Gliding motility in cyanobacteria. Observations and possible explanations. – *Arch. Microbiol.* **174**: 11–17.
- JOHANSEN, J. R. (1993): Cryptogamic crusts of semiarid and arid lands of North America. – *J. Phycol.* **29**: 140–147.
- KOMÁREK, J. & ANAGNOSTIDIS, J. (1999): Cyanoprokariota. 1. Chroococcales. – In: Ettl, H.; Gärtner, G.; Heynig, H. & Mollenhauer, D. (eds.): *Süßwasserflora von Mitteleuropa*, Bd. 19/1: 1–547. Gustav Fischer, Jena.
- LAWRENCE, J. R.; KÖRBER, D. R.; HOYLE, B. D.; COSTERTON, J. W. & CALDWELL, D. E. (1991): Optical sectioning of microbial biofilms. – *J. Bacteriol.* **173**: 6558–6567.
- LECLERC, J. C.; COUTÉ, A. & DUPUY, P. (1983): Le climat annuel de deux grottes et d'une église du Poitou, où vivent des colonies pures d'algues sciaphiles. – *Cryptogamie, Algologie* **4**: 1–19.
- MACKAY, W. G.; GRIBBON, L. T.; BARER, M. R. & REID, D. C. (1999): Biofilms in drinking water systems: a possible reservoir for *Helicobacter pylori*. – *J. appl. Microbiol., Symposium Suppl.*, **85**: 52S–59S.
- NEU, T. R. (2000): In situ cell and glycoconjugate distribution in river snow studied by confocal laser scanning microscopy. – *Aquat. Microb. Ecol.* **21**: 85–95.

## Phototrophic biofilm morphology in dim light. The case of the Puigmoltó sinkhole. 253

- NICOLAUS, B.; PANICO, A.; LAMA, L.; ROMANO, I.; MANCA, M. C.; DE GIULIO, A. & GAMBACORTA, A. (1999): Chemical composition and production of exopolysaccharides from representative members of heterocystous and non-heterocystous cyanobacteria. – *Phytochemistry* **52**: 639–647.
- NIENOW, J. A. (1996): Ecology of subaerial algae. – *Nova Hedwigia Beih.* **112**: 537–552.
- ORTEGA, J. J.; SÁNCHEZ-CASTILLO, P. M.; HERNÁNDEZ-MARINÉ, M. & SAIZ-JIMÉNEZ, C. (1993): Isolation and characterization of epilithic chlorophytes and cyanobacteria from two Spanish cathedrals (Salamanca and Toledo). – *Nova Hedwigia* **57**: 239–253.
- PALMER, R. J. & FRIEDMANN, E. I. (1990): Water relations and photosynthesis in the cryptoendolithic microbial habitat of hot and cold deserts. – *Microbial Ecol.* **19**: 111–118.
- PANDEY, D. C. & MITRA, A. K. (1972): Interesting observations on a new species of *Scytonematopsis* (*S. ghazipurensis* n. sp.). – In: DESIKACHARY, T. V. (ed.) *Taxonomy and biology of blue-green algae*, p. 58–61. The Bangalore Press, India.
- PATTERSON, G. M. L. & BOLIS, C. M. (1997): Fungal cell-wall polysaccharides elicit an antifungal secondary metabolite (phytoalexin) in the cyanobacterium *Scytonema ocellatum*. – *J. Phycol.* **33**: 54–60.
- RIPPKA, R. (1988): Isolation and purification of cyanobacteria. – In: PACKER, L. & GLAZER, A. N. (eds.), *Methods in Enzymology* **167**, p. 3–28. Acad. Press, Inc., San Diego.
- SARATER, S. (2000): Structure and architecture of a stromatolite from a mediterranean stream. – *Aquat. Microb. Ecol.* **21**: 161–168.
- SANT'ANNA, C. (1984): Flora de cyanophyceae associada a briófitas, município de Campina Verde, MG. – *Rickia* **11**: 129–142.
- TOLKER-NIELSEN, T. & MOLIN, S. (2000): Spatial organization of microbial biofilm communities. – *Microbial Ecol.* **40**: 75–84.
- VINOGRADOVA, O. N.; KOVALENKO, O. V.; WASSER, S. P.; NEVO, E. & WEINSTEIN-EVRON, M. (1998): Species diversity gradient to darkness stress in blue-green algae/cyanobacteria: a microscale test in a prehistoric cave, Mount Carmel, Israel. – *Isr. J. Plant Sci.* **46**: 229–238.

*Resultats*

---

#### 4.5. Distribució de biofilms fototròfics en cavitats (Garraf, Espanya)

La distribució dels biofilms, la diversitat dels organismes fototròfics i la seva relació amb les condicions ambientals es van estudiar a tres cavitats del massís càrstic del Garraf (Barcelona, NE Espanya). Es van identificar 63 tàxons: 28 Cyanobacteria (42,8 % Chroococcales, 21,4 % Oscillatoriales, 7,1 % Nostocales i 28,6 % Stigonematales), 11 Chlorophyta, 16 Bacillariophyta i 8 líquens. Són noves cites en cavitats: *Aphanothece caldariorum* Richter, *Asterocapsa* sp., *Gloeocapsa caldariorum* Rabenhorst, *Chroococcus ercegovicii* Komárek & Anagnostidis, *Calothrix parietina* (Nägeli) Thuret, *Achnanthes curtissima* H. J. Carter, *Amphora pediculus* (Kützing) Grunow, *Gomphonema clavatum* Ehrenberg, *Navicula bryophila* J. B. Petersen, *Tryblionella hungarica* (Grunow) D. G. Mann, *Simonsenia delognei* Lange-Bertalot, *Chlorella minutissima* Fott & Nováková, *Muriella terrestris* J. B. Petersen i *Ctenocladus circinnatus* Borzí.

Les dades ambientals es van obtenir a les tres cavitats, mesurant la temperatura, la humitat relativa i la llum, i es va observar un clar gradient des de l'entrada fins a una certa profunditat on les condicions romanen constants. Encara que el patró microclimàtic va ser similar a les tres cavitats estudiades, la profunditat a la qual es van establir les condicions abiòtiques va ser diferent a cada cavitat, ja que aquestes presentaven característiques estructurals diferents. Globalment, es van distingir tres nivells diferents:

- a) Nivell de l'entrada: el microclima estava molt influït per l'exterior. La llum atenuada i els factors abiòtics van fluctuar al llarg de l'any. A les pedres seques molt il·luminades, les colònies de microflora eren molt riques, amb una abundància especial de biofilms mucilaginosos compostos d'algues i cianobacteris, típic d'hàbitats terrestres aerofítics o atmofítics. La comunitat dominada per *Scytonema julianum* va créixer



en àrees protegides de la pluja. *Trentepohlia* spp i líquens crustacis, que tenien aquesta alga com a fotobiont, eren molt abundants.

- b) El nivell intermedi presentava oscil·lacions de temperatura i humitat moderades i poca llum (25-0,5 mV) sense esdevenir un factor d'estrès. Els biofilms estaven formats per una barreja d'espècies. Els cianobacteris van ser el grup dominant, ocasionalment barrejats amb algues verdes i diatomees. L'abundància dels biofilms disminueix amb el decreixement de la irradiància.
- c) Nivell profund (<1 mV) fins a l'extinció total de la llum, amb factors abiòtics estables (10°C i 100 % d'humitat relativa). Només algunes espècies van ser capaces de colonitzar aquesta zona de poca il·luminació. La presència de restes d'organismes i beines buides va incrementar-se amb la il·luminació decreixent, i amb excepció de *Geitleria calcarea* i *Loriella osteophila*, els cianobacteris i les algues van ser fortament colonitzades per bacteris i fongs filamentosos.

Les estratègies protectores contra la dessecació i la irradiació desapareixien gradualment de l'entrada al fons: biofilms formats per cianobacteris cocals mucilaginosos i de color fosc es van tornar més prims amb la disminució de la llum i gradualment van ser substituïts per biofilms formats per cianobacteris filamentosos calcificats amb beines transparents que produïen taques blanques a les parets. Els líquens crustacis van ser substituïts per altres de tal·lus leprós, com *Botryolepraria lesdainii* i *Macentina stigonemoides*. Els biofilms es van distribuir en mosaic en els avencs, mentre que a les coves es distribuïen en forma de cinturons més o menys continus. Les diferències en la disponibilitat de l'aigua i la duresa del substrat podrien explicar les variacions en la composició de les espècies i la distribució en mosaic.

Els resultats detallats d'aquest capítol s'inclouen en el següent article:

Distribution of phototrophic biofilms in cavities (Garraf, Spain). ***Nova Hedwigia Beih*** (2004), 78 (3-4): 329-351.

**Distribution of phototrophic biofilms in cavities (Garraf, Spain)**

by

M. Roldán<sup>1</sup>, E. Clavero<sup>1</sup>, T. Canals<sup>1</sup>, A. Gómez-Bolea<sup>2</sup>, X. Ariño<sup>3</sup>  
and M. Hernández-Marín<sup>1</sup><sup>1</sup>Facultat de Farmàcia, Secció Botànica, Universitat de Barcelona  
Av. Joan XXIII, s/n, E-08028 Barcelona, Spain<sup>2</sup>Facultat de Biologia, Secció Botànica, Universitat de Barcelona  
Diagonal, 645, E-08028 Barcelona, Spain<sup>3</sup>Universitat Pompeu Fabra, IDEC, Balmes, 132, E-08008 Barcelona, Spain

With 56 figures and 3 tables

Roldán, M., E. Clavero, T. Canals, A. Gómez-Bolea, X. Ariño & M. Hernández-Marín (2004):  
Distribution of phototrophic biofilms in cavities (Garraf, Spain). - Nova Hedwigia 78: 329-351.**Abstract:** The distribution of biofilms, the diversity of phototrophic organisms, and their relation to environmental conditions were studied in three limestone cavities in the karstic Garraf massif (Barcelona, NE Spain). Sixty-two taxa: 28 Cyanobacteria (42.8% Chroococcales, 21.4% Oscillatoriales, 7.1% Nostocales and 28.6% Stigonematales), 11 Chlorophyta, 16 Bacillariophyta and 7 lichens were identified. The environmental data obtained at three cavities by measuring temperature, relative humidity and light, showed a clear gradient from the entrance to a certain depth beyond which they remained stable. In a broad sense, the existence of three different levels can be assumed:

- a) Entrance level. The microclimate was strongly influenced by the outdoors. Scarcely attenuated light and abiotic factors fluctuated throughout the year. On the highly illuminated dry rocks the microflora colonies were quite rich, with special abundance of mucilaginous biofilms composed of algae and cyanobacteria typical of terrestrial aerophytic or atmophytic habitats. The community dominated by *Scytonema julianum* thrived in areas protected from rain. *Trentepohlia* sp. and many crustose lichens, which had this alga as a photobiont, were abundant.
- b) Intermediate level, with moderate abiotic oscillations and low light (25-0.5 mV) that was not yet a stress factor. A mixture of species formed biofilms. Cyanobacteria were their most visible constituents, occasionally mixed with green algae and diatoms. Biofilm abundance diminished with decreasing irradiance.
- c) Deep level (< 1 mV) until light extinction, with stable abiotic factors (10°C and dew point humidity). Only a few species were able to colonize this dim light zone. The presence of remains and empty sheaths increased with decreasing irradiance, and except for *Geitleria calcarea* and *Loriella osteophila*, the algae were heavily colonized by bacteria and filamentous fungi.

\*Corresponding author: Mónica Roldán, e-mail: mroldan@farmacia.far.ub.es

DOI: 10.1127/0029-5035/2004/0078-0329

0029-5035/04/0078-0329 \$ 5.75  
© 2004 J. Cramer in der Gebrüder Borntraeger  
Verlagsbuchhandlung, D-14129 Berlin · D-70176 Stuttgart

The protective strategies displayed by the phototrophic species against desiccation and irradiation gradually changed from the entrance to the bottom. Biofilms formed of mucilaginous and dark coloured coccoid cyanobacteria became thinner with decreasing light and were gradually replaced by biofilms formed of calcified filaments with uncoloured sheaths, which to the naked eye appeared as pale stains on the walls. Crustose lichens were replaced by others with a leprose thallus, such as *Botryoleprarialesdainii* and *Macentina stigonemoides*. Biofilms were distributed in a mosaic in the sinkholes, whereas they formed continuous belts on the cave walls. Differences in the availability of liquid water and substratum coherence might explain the variations in species composition and patchiness observed in these cavities.

### Introduction

Limestone cavities are highly specific environments scattered all over the world (Hernández-Mariné et al. 1999). Cavities are stable environments characterized by uniform temperatures through the year, constant humidity and low illumination, especially at the deepest zones. The balance of light, humidity and temperature determines the growth, development and reproduction of cyanobacteria and microalgae. However, they can also be affected by other physical factors such as the dimensions, morphology and direction of the mouth of the cavity or the colour and nature of the rock (Bellés 1989). The gradient of these factors has been associated with the zonation of the microflora, regarding both diversity and abundance (Gèze 1965, Herrero-Borgoñon 1986, Nienow & Friedmann 1993).

Ecological requirements and distribution are only known for a few cavity inhabiting species (Couté 1989, Sant' Anna et al. 1991, Ariño et al. 1998, Garbacki et al. 1999, Vinogradova et al. 1998, 2000, Asencio & Aboal 2000a, b), even if many of these species are common in other low light environments such as catacombs and tombs (Albertano & Grilli-Caiola 1989, Albertano 1993, Albertano et al. 1994, Ariño et al. 1997).

Phototrophic microorganisms living at the entrance of cavities are usually found in terrestrial aerophytic habitats (Komárek & Anagnostidis 1999, Hernández-Mariné et al. 2001). Towards the deepest zone of the cavity the vegetation is built by a few species adapted to low light conditions, the overall community becoming less dense and less diverse (Hoffmann 1989, Albertano et al. 1994).

The Mediterranean landscape displays an abundance of calcareous bulks, which are suitable for the development of different subterranean cavities. Near Barcelona (NE Spain) the karstic Garraf massif provides a great variety of sinkholes and caves, which have been scarcely studied from a botanical point of view (Ariño et al. 1998). The distribution of biofilms, the diversity of phototrophic organisms, and their relation to environmental conditions were studied in three Garraf massif limestone cavities. Two of them were sinkholes formed with vertical dry walls (Puigmoltó and Papellona), and the third was a horizontal cave with highly moisturized, loose substratum and flooded bottom (Corral Nou).

### Study area

The studied materials were collected from three cavities in Garraf massif, near Barcelona (Table 1). Papellona (Fig. 1) and Corral Nou (Fig. 2) exhibited special characteristics. The coherence of the substratum in all cavities is heterogeneous with compact

Table 1. Geographical coordinates of the cavities localised in the municipal term of Begues (Garraf, Spain) with their type of rocks, features of morphology and dates of sampling and measurements.

CAVITIES	LATITUDE (N)	LONGITUDE (E)	ALTITUDE	DEPTH	TYPE OF ROCKS	ORIENTATION	DIMENSION OF THE MOUTH	DATES SAMPLING MEASUREMENTS
Papellona	41°17'10"	1°54'49.5"	503 m	3 m	Aptian calcareous	36°N	7.5 m of longitude	03/10/98 02/03/99 21/02/01
Corral Nou	41°18'6"	1°51'17"	244 m	6 m	Aptian calcareous and concrete substratum	10°N	2 x 3 m	03/10/98 02/03/99 21/02/01
Puigmoltó	41°18'49.5"	1°55'27"	512 m	29 m	Dolomite calcareous	.	2 x 2 m	07/10/99



Figs 1-2. Entrance to the different cavities (Gurraf). 1. Cave Corral Nou. 2. Sinkhole Papellona.

and loose areas irregularly distributed. Calcite is the dominant mineral except in Corral Nou (Table 1). Corral Nou is distinguished by its one spring at the bottom, which feeds a permanent pool with seasonal variations of water level (water depth ranges from 0.5 to 1 m approximately). Papellona is a sinkhole with a wide and shallow entrance (about 3 m) which is bifurcated at its end in two wings (the wings of the *Papellona*, which is Catalan for butterfly). One wing is practically horizontal and the other is a well of 3 m. Due to its morphology, the entrance of this cavity has a microclimate very similar to the exterior, unlike the other cavities.

#### Materials and methods

The abiotic conditions of the cavities: temperature, humidity and light were monitored and compared to external conditions (Figs 3-5). Air temperature was measured by means of thermistors (Grant, Cambridge), relative humidity by hygrometers (Vaisala, Helsinki) and irradiance with a LICOR quantum photometer (Lincoln, Nebraska). All probes were connected to a Squirrel Data Logger (Grant, Cambridge) and logged every ten minutes. The sensors faced the phototrophic surfaces, but it was not always easy to control their position.

The sinkhole Papellona and the cave Corral Nou were sampled along their total depth, while Puigmoltó sinkhole was sampled down to 20 metres. Two types of sampling were made so as to gather extensive information on diversity and autoecology of the species forming the biofilms. In the first place, those zones where algal growth was observed were sampled in all cavities to assemble a

floristic catalogue as complete as possible. After that, wall samples were collected at different depths of the cavities: entrance level, intermediate level and deep level, noting abiotic conditions. In addition, samples from the water, walls above water level (0 and 40 cm), the ceiling of the entrance, and the external wall were obtained at Corral Nou.

Sample aliquots were both observed directly and cultured. BG11 (Rippka et al. 1988) with or without carbonate (12g/l) and BBM (Chantanachat & Bold 1962), solid media were used (0.6% Agar-agar Merck).

Selected fragments of the biofilms and cultured colonies were studied by means of Light Microscopy (LM), Confocal Laser Scanning Microscopy (CLSM) and Scanning Electron Microscopy (SEM). LM observations were carried out with a NIKON Optiphot-2. Samples for SEM were fixed in a solution of 2% glutaraldehyde in a 0.1 M cacodylate buffer overnight. A second 24-hour fixation was carried out with osmium tetroxide (1%) and then samples were dehydrated, dried at a critical point (CPD), placed on stubs, and gold coated. For the diatom SEM studies material was processed as in Merino et al. (1995), air dried on membrane filters, placed onto aluminium stubs and gold coated. Specimens were viewed using a HITACHI S-2300 microscope. For CLSM photosynthetic pigments were visualized by their inherent fluorescence. DNA was labeled with the specific fluorochrome dye SYTOX Green dead cell stain-S-7020 (Molecular Probes, Inc.). Extracellular polysaccharides (EPS) were labeled with the broad-spectrum carbohydrate-recognizing lectin Concanavalin-A conjugated with the fluorophore Alexa Fluor 488 (Con-A, Molecular Probes, Inc.). Other techniques, sample processing, and observations for CLSM were as described in Hernández-Marín et al. (2001). Optical sections were processed with the maximum intensity projection algorithm in which the maximum fluorescence intensities of each x,y point of all the optical series along the z-axis are integrated in a two-dimensional compound image.

Identification was performed according to several systematic manuals (Geitler 1932, Desikachary 1959, Anagnostidis & Komárek 1988, 1990, Komárek & Anagnostidis 1989, 1999, Krammer & Lange-Bertalot 1986, 1988, 1991, Round et al. 1990, Ettl & Gärtner 1995) and specific publications for particular species.

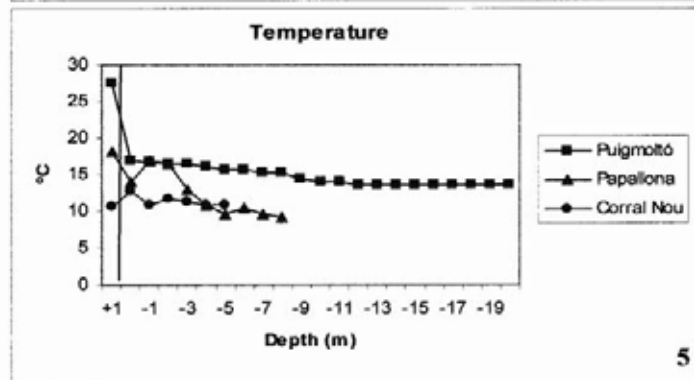
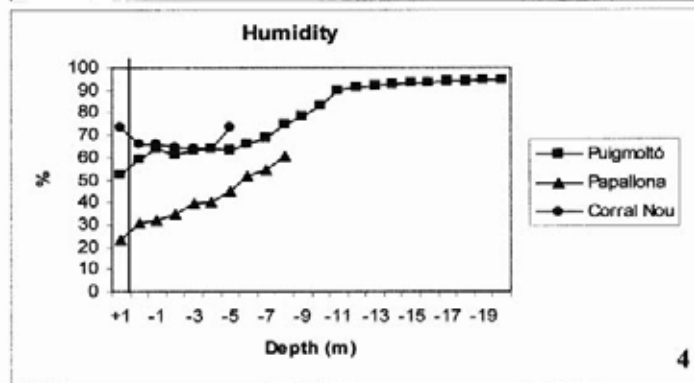
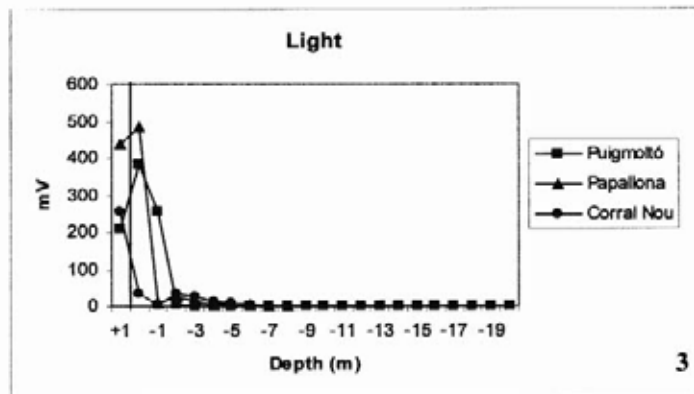
## Results

### Environmental measurements

The environmental data obtained at the three cavities (temperature, relative humidity, and light) demonstrated the existence of a gradient from the entrance to a certain depth where they remained stable (Figs 3-5). The microclimate inside the cavities was relatively stable all year round (data not shown). Temperature oscillated in the first few metres near the entrance but gradually stabilized; relative humidity increased until saturation point and light decreased until extinction (below the sensor's threshold).

Although the pattern of microclimate was similar at the studied cavities, especially if we compare it to outdoor data, the depth where abiotic conditions became stabilized, or at which the light disappeared, was different for each cavity, since they had different structural characteristics (Table 1). Due to its structure, the upper part of the cave Corral Nou was the least stable, and environmental changes outside, mainly wind or clouds, caused strong oscillations of its microclimate in very short intervals of time. The deepest sinkhole, Puigmoltó, with a narrow entrance, had a steep gradient of relative humidity and rapidly reached environmental stability, whereas Papellona, which has the widest diameter at the entrance, was heterogeneous.

In any case, and comparing the microclimatic data of the studied cavities, three levels could be distinguished according to abiotic factors. At the first level, from the



Figs 3-5. Abiotic factors ( light, humidity and temperature) in the three cavities: Papellona, Puigmoltó and Corral Nou. Temperature, humidity and light measures were performed at the interior and exterior of the cavities in order to monitor the oscillations between both environments.

entrance to a few metres depth, oscillations of temperature, humidity and overall light were directly related to the outdoors. At the second level (3-6 m), there were slight variations and the effect of the outdoor oscillations was attenuated. Finally, at the third level in the deepest zone of the cavity (>6 m), abiotic conditions remained stable (Figs 3-5).

#### Algae, cyanobacteria and lichens

Table 2 shows a list of the identified taxa at the three studied cavities, with selected specimens shown in Figs 6-37. Of the total, Cyanobacteria were most species rich, with 28 taxa, of which 12 were Chroococcales (42.8%), 6 were Oscillatoriales (21.4%), 2 were Nostocales (7.1%) and 8 were Stigonematales (28.6%). Only 11 taxa were Chlorophyta. Only one of the 16 Bacillariophyta, *Orthoseira roeseana*, was a centric diatom. Due to their importance in the developed communities, lichens were also included (7 species identified). The most common were *Botryolepraria lesdainii* (Fig. 21) and *Macentina stigonemoides*.

Cyanobacteria were thriving at every level of the cavity. Among all identified species, *Scytonema julianum* was the most widespread. Among other cyanobacteria, the most frequent were *Leptolyngbya* sp., *Myxosarcina* sp. and *Phormidium* spp. Some species were very abundant locally, such as *Scytonema ocellatum* and *Phormidium ambiguum* in the sinkhole Puigmoltó and *Chroococcus ercegovicii* (Fig. 14) in the cave Corral Nou. *Asterocapsa* sp. (Figs 7, 8), *Scytonema arcangelii* and *S. crispum* were found in very small amounts, only in Corral Nou and Papellona, respectively.

Chlorophyta were almost absent in Corral Nou cave, but were abundant at the entrance and first few metres of Papellona and Puigmoltó. *Trentepohlia* sp. together with other species from soil and rocks, such as *Bracteacoccus minor*, *Chlorella minutissima*, *Choricystis chodatii* (Fig. 18) and *Stichococcus bacillaris* (Fig. 22) were generally abundant. Some Chlorophyta species were simultaneously observed as free-living organisms and as photobionts of leprose lichens: *Coccolobrya verrucariae* (Fig. 20) (photobiont of *Botryolepraria lesdainii*) and *Leptosira obovata* (photobiont of *Macentina stigonemoides*). On the other hand, *Trentepohlia* sp, which was found as a photobiont of various crustose lichens (such as *Lithothelium triseptatum*, *Ramonia calcicola*, *Encephalographa ellisae*, *Strigula calcarea* and *Petractis thelotremella*) was primarily in the photobiont status at the entrance of the cavities, becoming mostly free-living at intermediate levels and absent at deep levels (Table 3).

Diatom species, many of which are typically aquatic, were mostly confined to Corral Nou cave, where samples came from water, soil and epiphytes. Some species were found indiscriminately on the three substrata: *Achnanthes* sp. (Figs 23, 24), *Achnantheidium minutissimum* (Fig. 25), *Amphora pediculus* (Fig. 26), *Diploneis oblongella* (Fig. 27), *Diploneis ovalis* (Fig. 28), *Adlafia bryophila* (Figs 29, 30) and *Nitzschia perminuta*. Typically aquatic or epiphytic species were (Table 2): *Craticula halophila*, *Gomphonema clavatum* (Figs 31-33), *Simonsenia delognei* (Fig. 34, aquatic) and *Luticola nivalis* (epiphyte). *Diademsis contenta* (Fig. 35) and *Hantzschia amphioxys*, which were the most abundant species in all the studied cavities, were found both underwater and on walls. *Tryblionella hungarica* (Figs 36, 37) and



Resultats

Table 2. Distribution of cyanobacteria, microalgae and lichens in the cavities

Taxon	Cavities			Level
	Papellona	Corral Nou	Puigmoltó	
<b>Cyanobacteria</b>				
<i>Aphanothece caldariorum</i> P.G. Richt.	-	+	-	I
<i>Aphanothece saxicola</i> Nägeli	-	+	-	I
<i>Aphanothece smithii</i> Komárk.-Legn. & Cronberg	-	-	+	I, D
<i>Asterocapsa</i> sp.	-	+	-	E
<i>Calothrix parietina</i> (Nägeli) Thur. ex Bornet & Flahault	-	+	-	E
<i>Chroococcus ercegovicii</i> Komárek & Anagnost.	-	+	-	E, I
<i>Cyanosarcina parthenonensis</i> Anagnost.	+	+	-	I
<i>Geitleria calcarea</i> Friedmann	+	+	+	D
<i>Gloeocapsa caldariorum</i> Rabenh.	-	+	-	E
<i>Gloeocapsa decorticans</i> (A. Braun) P.G. Richt. in Wille	-	+	-	E
<i>Gloeocapsa gelatinosa</i> (Menegh.) Kütz.	-	+	-	E
<i>Gloeocapsa novacekii</i> Komárek & Anagnost.	-	+	-	E, I
<i>Gloeothece rupestris</i> (Lyngb.) Bornet in Wittr. & Nordst.	+	+	+	E, I
<i>Herpyzonema pulverulentum</i> Hern.-Mar. & Canals	+	-	-	I, D
<i>Leptolyngbya</i> sp.	+	+	+	E, I, D
<i>Leptolyngbya perelegans</i> (Lemmerm.) Anagnost. & Komárek	+	+	-	ND
<i>Loriella osteophila</i> Borzí	+	+	-	D
<i>Myxosarcina</i> sp.	+	+	-	I, D
<i>Nostoc microscopicum</i> Carmich. ex Bornet & Flahault	+	+	+	E, I
<i>Nostoc paludosum</i> Kütz. ex Bornet & Flahault	-	+	-	E
<i>Phormidium ambiguum</i> Gomont	-	-	+	I, D
<i>Phormidium autumnale</i> C. Agardh ex Gomont	+	+	-	E, I
<i>Pseudophormidium purpureum</i> (Gomont) Anagnost. & Komárek	+	-	-	I
<i>Scytonema arcangelii</i> Bornet & Flahault	+	-	-	E
<i>Scytonema crispum</i> (C. Agardh) Bornet	+	-	-	E
<i>Scytonema julianum</i> Menegh. ex P.G. Richt.	+	+	+	E, I
<i>Scytonema ocellatum</i> Lyngb. ex Bornet & Flahault	+	-	+	I, D
<i>Stigonema minutum</i> Hassall ex Bornet & Flahault	-	+	-	E
<b>Chlorophyta</b>				
<i>Bracteacoccus minor</i> (Chodat) J. Petrová	+	-	-	E
<i>Chlorella minutissima</i> Fott & Nováková	+	-	+	E
<i>Choricystis chodatii</i> (Jaag) Fott	+	-	-	E
<i>Coccolobos verrucariae</i> Chodat em. Vischer	+	-	-	I
<i>Ctenocladus circinnatus</i> Borzí	+	+	-	E
<i>Klebsormidium flaccidum</i> (Kütz.) P.C. Silva, Mattox & W.H. Blackw.	-	-	+	E
<i>Leptosira obovata</i> Vischer	-	-	+	ND
<i>Muriella terrestris</i> J.B. Petersen	+	-	-	E, I
<i>Myrmecia biatorellae</i> J.B. Petersen	-	-	+	E, I, D
<i>Stichococcus bacillaris</i> Nägeli	+	-	+	I
<i>Trentepohlia</i> sp.	+	+	-	E, I
<b>Bacillariophyta</b>				
<i>Achnanthes</i> sp.	-	+ <sup>1,2,3</sup>	-	E, I

Taxon	Cavities			Level
	Papellona	Corral Nou	Puigmoltó	
<i>Achnanthydium minutissimum</i> (Kütz.) Czarn.	-	+ <sup>1,2,3</sup>	-	E, I
<i>Adlafia bryophila</i> (J. B. Petersen) Lange-Bert. in Moser et al.	-	+ <sup>1,2,3</sup>	-	E, I
<i>Amphora pediculus</i> (Kütz.) Grunow	-	+ <sup>1,2,3</sup>	-	E, I
<i>Craticula halophila</i> (Grunow ex Van Heurck) D.G. Mann	-	+ <sup>2,3</sup>	-	E, I
<i>Diademsis contenta</i> (Grunow) D.G. Mann	-	+ <sup>2</sup>	+ <sup>1</sup>	E, I, D
<i>Diploneis oblongella</i> (Naegeli) A. Cleve	-	+ <sup>1,2,3</sup>	-	E, I
<i>Diploneis ovalis</i> (Hilse) Cleve	-	+ <sup>1,2,3</sup>	-	E, I
<i>Encyonopsis microcephala</i> (Grunow in Van Heurck) Krammer	-	+ <sup>2</sup>	-	E, I
<i>Gomphonema clavatum</i> Ehrenb.	-	+ <sup>2,3</sup>	-	E, I
<i>Hantzschia amphioxys</i> (Ehrenb.) Grunow in Cleve & Grunow	-	+ <sup>1,2</sup>	+ <sup>1</sup>	E, I
<i>Luticola nivalis</i> (Ehrenb.) D.G. Mann	-	+ <sup>3</sup>	-	E, I
<i>Nitzschia perminuta</i> (Grunow) Perag.	-	+ <sup>1,2,3</sup>	-	E, I
<i>Orthoseira roeseana</i> (Rabenh.) O' Meara	+ <sup>1</sup>	-	-	I
<i>Simonsenia delognei</i> Lange-Bert.	-	+ <sup>2</sup>	-	E, I
<i>Tryblionella hungarica</i> (Grunow) D.G. Mann	-	+ <sup>1</sup>	-	E, I
<b>Lichens</b>				
<i>Botryolepraria lesdainii</i> (Hue) Canals et al.	+	+	+	E, I, D
<i>Encephalographa ellisae</i> Massal	+	-	-	E
<i>Lithothelium triseptatum</i> (Nyl.) Aptroot	+	-	-	E
<i>Macentina stigonemoides</i> Orange	+	+	+	I, D
<i>Petractis thelotremella</i> (Bagl.) Vězda	+	+	-	E
<i>Ramonia calcicola</i> Canals & Gómez-Bolea	+	-	+	I
<i>Strigula calcarea</i> Bricaud & Roux	+	+	+	E, I
Total number of species	31	42	19	

<sup>1</sup>Soil, <sup>2</sup>Water, <sup>3</sup>Epiphyte

E: Entrance level (0-3 m)

I: Intermediate level (3-6 m)

D: Deep level (>6 m)

ND: Not determined

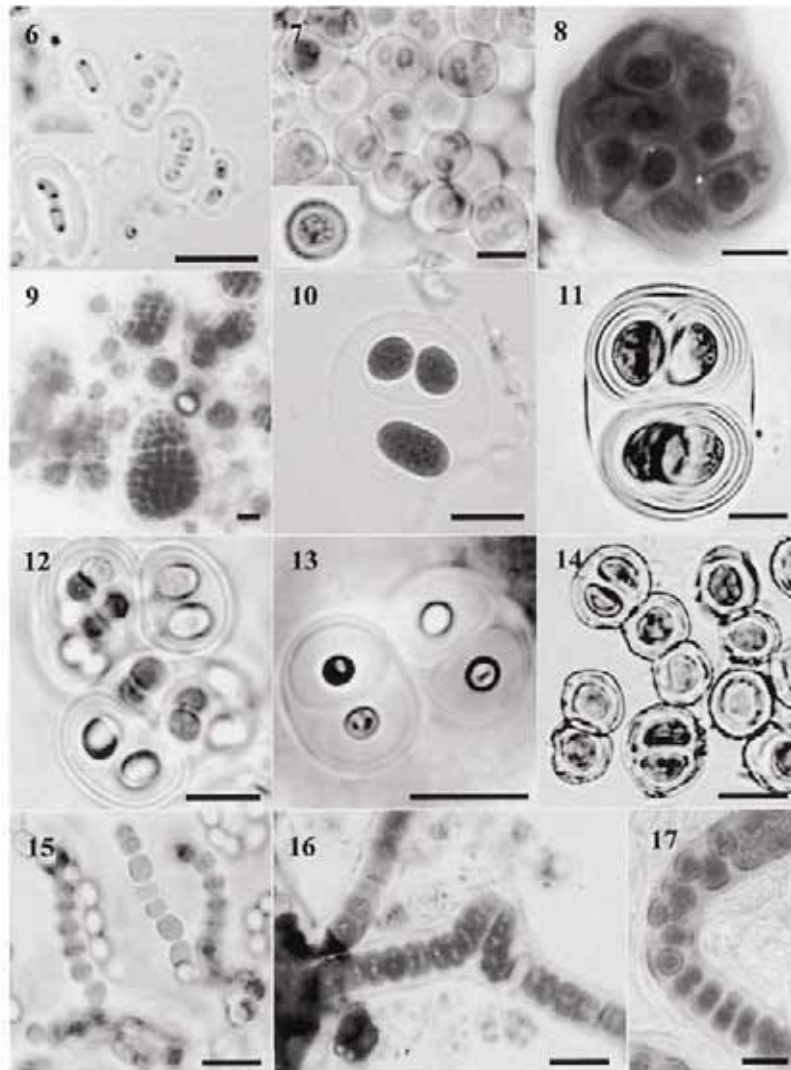
*Orthoseira roeseana* were only found on the walls. Of these taxa, several have been reported repeatedly from aerial habitats: *Achnanthydium minutissimum*, *Adlafia bryophila*, *Diademsis contenta*, *Gomphonema clavatum*, *Hantzschia amphioxys*, *Luticola nivalis*, and *Orthoseira roeseana*.

#### Biofilm Composition and Distribution

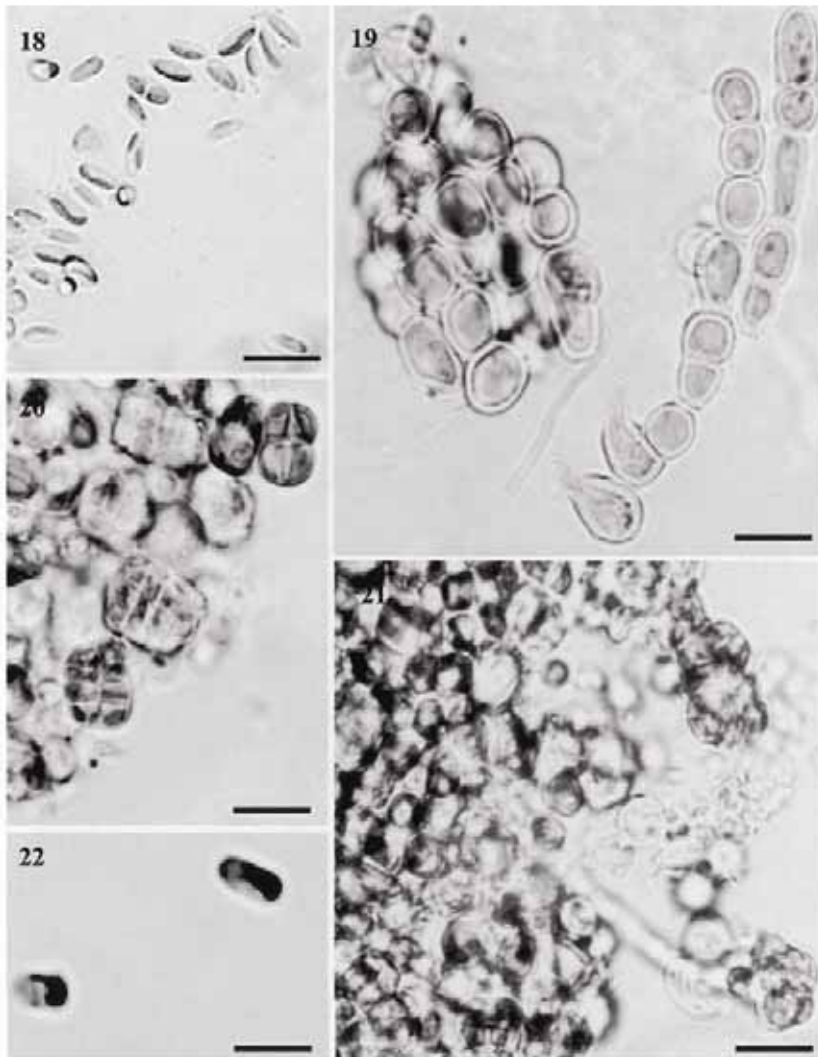
Table 3 and Figs 38-56 show the distribution and growth habit of the more abundant species forming biofilms at different levels - entrance, intermediate and deep - at each one of the studied cavities. In all the studied cavities, the phototrophic communities developed biofilms. They were macroscopically visible as defined bands or mosaics, which were predominantly found on loose substrata.

Table 3. Phototrophic species forming the biofilms. Sample numbers are ordered by cavities and depth levels. E: Entrance level (0-3 m), I: Intermediate level (3-6 m), D: Deep level (6 m-bottom). Numbers in bold are the sample sites for which the locations in the cavities are given in Figs 38-40.

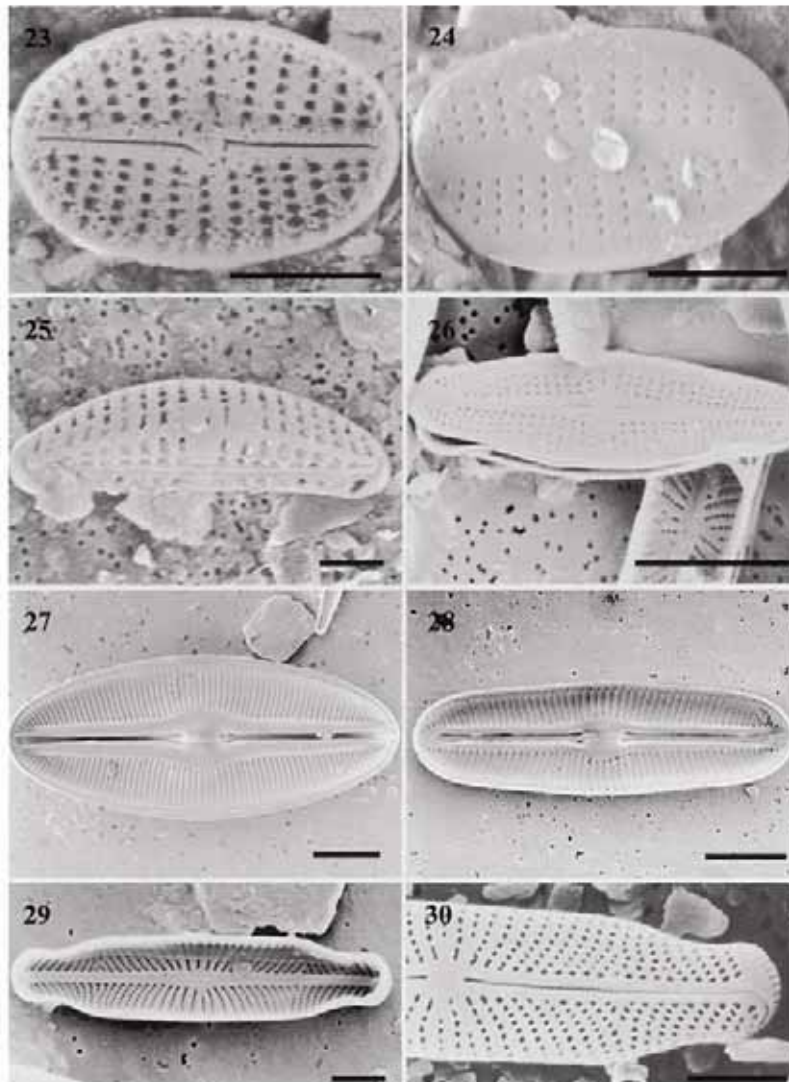
Level	Cavity	Main Organisms
E	Papellona	1: Phanerogams, ferns, mosses, moss protonemata, <i>Encephalographa ellisae</i> , <i>Lithothelium triseptatum</i> , <i>Petractis thelotremella</i>
	Corral Nou	2 (Out side): <i>Scytonema julianum</i> , <i>Nostoc microscopicum</i> , moss protonemata, <i>Petractis thelotremella</i> and <i>Strigula calcarea</i> 3 (Ceiling): <i>Gloeocapsa novacekii</i> , <i>Scytonema julianum</i> , <i>Trentepohlia</i> sp., moss protonemata, <i>Chroococcus ercegovicii</i> and other Chroococcales
	Puigmoltó	4: <i>Gloeotheca rupestris</i> and other Chroococcales, <i>Leptolyngbya</i> sp., <i>Nostoc microscopicum</i> and <i>Scytonema julianum</i> 5: <i>Chlorella minutissima</i> and <i>Diademsis contenta</i> 6: <i>Botryolepraria lesdainii</i>
I	Papellona	7: <i>Scytonema julianum</i> , <i>Botryolepraria lesdainii</i> and <i>Orthoseira roseana</i> 8: <i>Botryolepraria lesdainii</i> , <i>Macentina stigonemoides</i> , mosses, filamentous fungi and Chroococcales <i>Myxosarcina</i> -like 9: Chroococcales <i>Myxosarcina</i> -like, <i>Gloeotheca rupestris</i> , <i>Leptolyngbya</i> sp., <i>Scytonema julianum</i> , <i>Trentepohlia</i> sp., filamentous fungi, <i>Cocobotrys verrucariae</i> , <i>Botryolepraria lesdainii</i> , <i>Ramonia calcicola</i> and <i>Strigula calcarea</i>
	Corral Nou	10 (40 cm): Moss protonemata, <i>Leptolyngbya</i> spp., <i>Trentepohlia</i> sp., <i>Gloeocapsa novacekii</i> , <i>Aphanothece caldarium</i> and other Chroococcales 11 (Water): Moss protonemata, <i>Scytonema julianum</i> , <i>Diploneis ovalis</i> , <i>Chroococcus ercegovicii</i> , <i>Myxosarcina</i> sp. and other Chroococcales 12 (40 cm): <i>Nostoc microscopicum</i> , <i>Leptolyngbya</i> sp., <i>Phormidium autumnale</i> , <i>Chroococcus ercegovicii</i> and other Chroococcales 13 (Water): <i>Aphanothece saxicola</i> , <i>Cyanosarcina parthenonensis</i> , <i>Gloeotheca rupestris</i> and other Chroococcales, <i>Leptolyngbya</i> sp., <i>Scytonema julianum</i> , <i>Diploneis ovalis</i> , <i>Diploneis oblongella</i> , <i>Trentepohlia</i> sp. and moss protonemata
	Puigmoltó	14: <i>Aphanothece smithii</i> , <i>Gloeotheca rupestris</i> and other Chroococcales 15: Moss protonemata, <i>Botryolepraria lesdainii</i> , <i>Trentepohlia</i> sp., <i>Myrmecia biatorellae</i> , <i>Diademsis contenta</i> , <i>Ramonia calcicola</i> and <i>Strigula calcarea</i> 16: Moss protonemata, <i>Stichococcus bacillaris</i> , <i>Scytonema ocellatum</i> , <i>Diademsis contenta</i> and <i>Leptolyngbya</i> sp. 17: <i>Scytonema ocellatum</i> , <i>Phormidium ambiguum</i> , <i>Macentina stigonemoides</i> and moss protonemata
D	Papellona	18: <i>Geitleria calcarea</i> , <i>Loriella osteophila</i> and Chroococcales <i>Myxosarcina</i> -like
	Corral Nou	19: <i>Geitleria calcarea</i> , <i>Loriella osteophila</i> , <i>Botryolepraria lesdainii</i> and <i>Macentina stigonemoides</i>
	Puigmoltó	20: <i>Scytonema ocellatum</i> , <i>Phormidium ambiguum</i> , <i>Macentina stigonemoides</i> , moss protonemata, <i>Leptolyngbya</i> sp. and <i>Diademsis contenta</i> 21: <i>Myrmecia biatorellae</i> , <i>Phormidium ambiguum</i> , <i>Scytonema ocellatum</i> and <i>Macentina stigonemoides</i> 22: <i>Scytonema ocellatum</i> and <i>Phormidium ambiguum</i> 23: <i>Geitleria calcarea</i> , filamentous fungi and actinobacteria



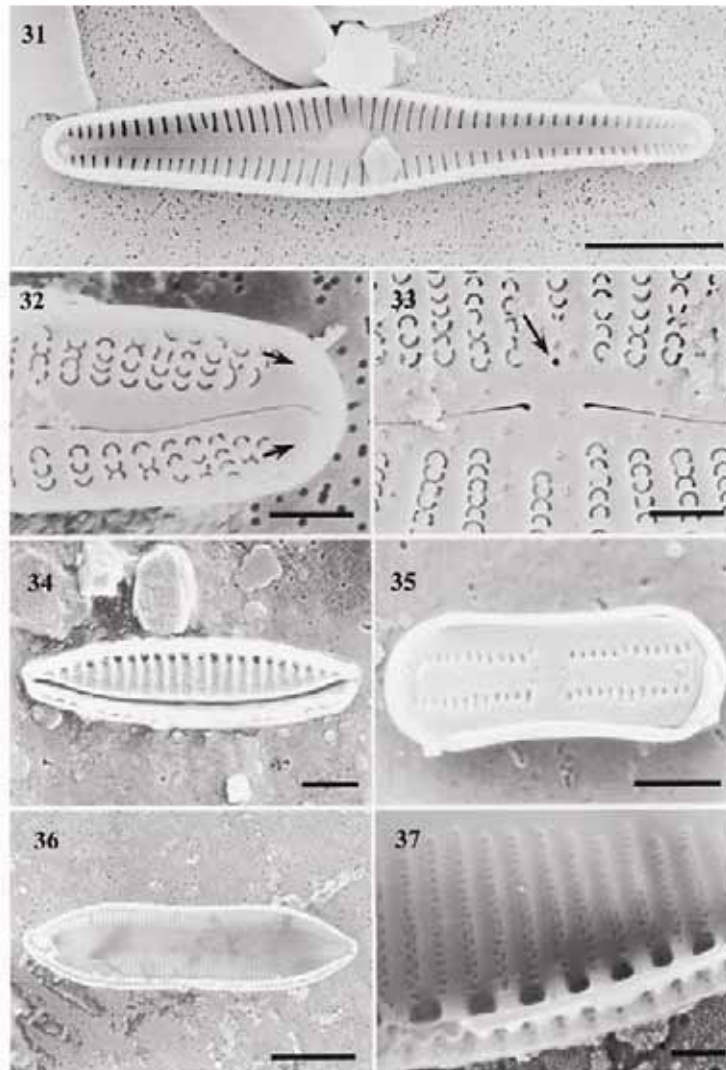
Figs 6-17. Light micrographs of cyanobacteria. 6. *Aphanothece caldariorum*. 7. *Asterocapsa* sp. Insert: arthrospora with sheath covered by wart-like processes. 8. *Asterocapsa* sp. 9. *Cyanosarcina parthenonensis*. 10. *Gloeotheca rupestris*. 11. *Gloeocapsa decorticans*. 12. *Gloeocapsa caldariorum*. 13. *Gloeocapsa gelatinosa*. 14. *Chroococcus ercegovicii*. 15. *Nostoc paludosum*. 16. *Herpyzonema pulverulentum*. 17. *Stigonema minutum*. Scale bars = 10 μm (Figs 6-10), 20 μm (Figs 11, 12).



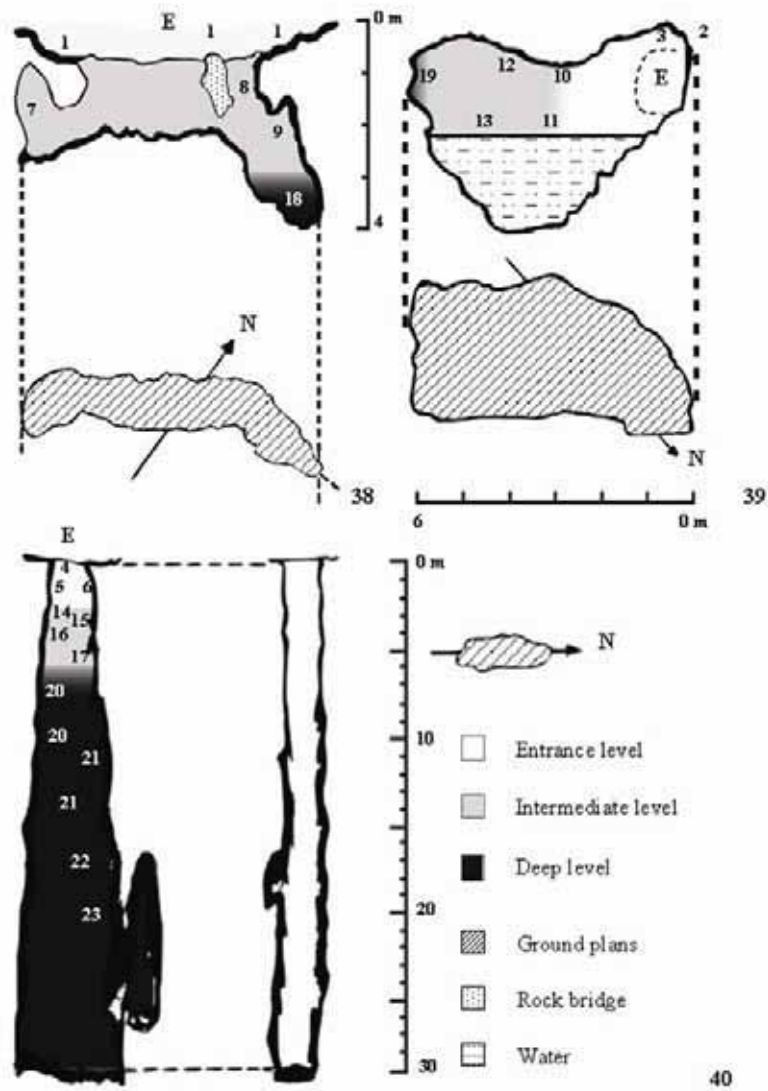
Figs 18-22. LM micrographs. 18. *Choricystis chodatii*. 19. *Ctenocladius circinnatus*. 20. *Cocobotrys verrucariae*. 21. *Botryoleprarialesdainii*. 22. *Stichococcus bacillaris*. Scale bars = 10  $\mu$ m (Figs 18-21), 5  $\mu$ m (Fig. 22).



Figs 23-30. SEM micrographs of diatoms. 23, 24. *Achnanthes* sp., internal view of valve and external view of rapheless valve, respectively. 25. *Amphora pediculus*, external view of valve. 26. *Achnanthidium minutissimum*, external view of valve. 27. *Diploneis ovalis*, internal view of valve. 28. *Diploneis oblongella*, internal view of valve. 29. *Adlafia bryophila*, internal view of valve. 30. *Adlafia bryophila*, external view of valve apex. The striae at the centre are radial and at the ends convergent. Scale bars = 2  $\mu\text{m}$  (Figs 23, 24, 25, 29, 30), 5  $\mu\text{m}$  (Figs 26, 28), 10  $\mu\text{m}$  (Fig. 27).

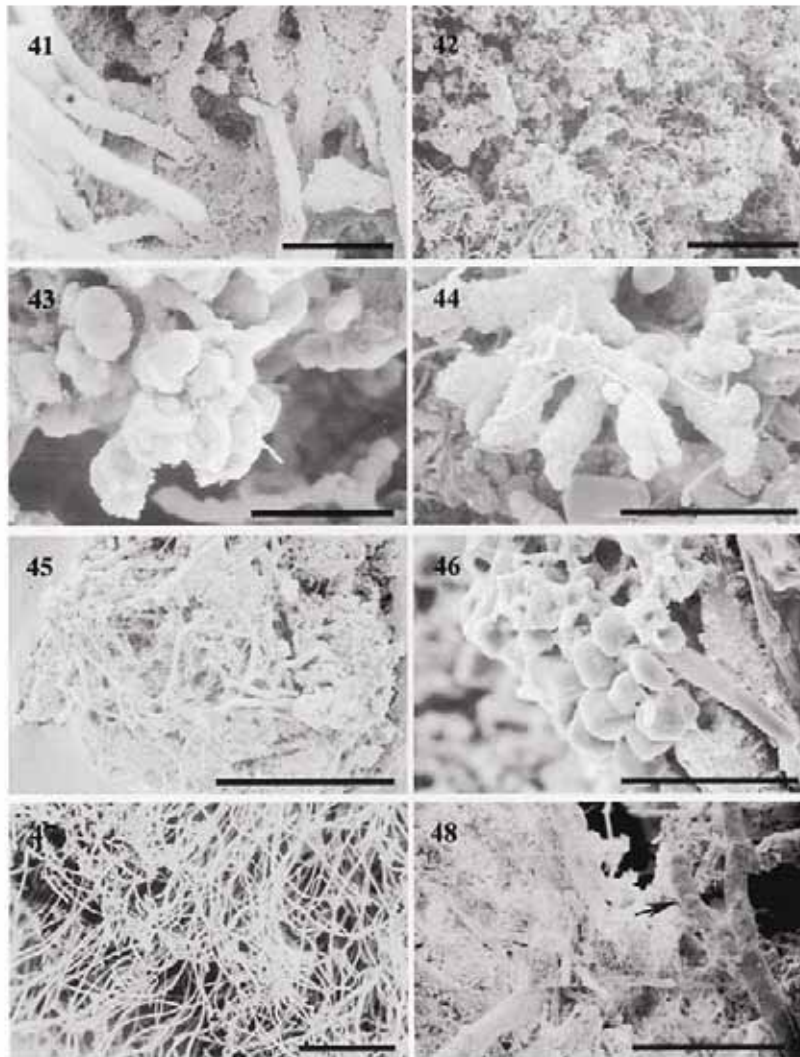


Figs 31-37. SEM micrographs of diatoms. 31. *Gomphonema clavatum*, internal view of valve. 32. *Gomphonema clavatum*; external view of the end of the valve showing pore field (arrows). 33. *Gomphonema clavatum*; external view of central portion of valve showing rounded stigmal opening (arrow). 34. *Simonsenia delognei*; external view of valve showing the external costae. 35. *Diadesmis contenta*, external view of valve. 36. *Tryblionella hungarica*, external view of valve. 37. *Tryblionella hungarica*, external view of area where there can be observed fibulae squat and striae biseriata. Scale bars = 10  $\mu\text{m}$  (Figs 31, 36 ), 2  $\mu\text{m}$  (Figs 32, 33, 34, 35), 1  $\mu\text{m}$  (Fig. 37).



Figs 38-40. Ground plans and profiles of the studied cavities showing the distribution of biofilms in three levels (entrance, intermediate and deep). Sampling sites are marked as numbers on the profiles and correspond to the numeration given in Table 3. 38. Papellona Sinkhole. 39. Corral Nou cave. 40. Puigmoltó Sinkhole. The localisation of sampling sites is only marked on the profile in the northern direction. E: Cavity entrance N = North.





Figs 41-48. SEM micrographs of biofilms in different levels. 41. Biofilm of *Scytonema julianum* at entrance level. 42. Biofilm of *Botryoleprarialesdainii* at entrance level. 43. Details of algal cells and fungal hyphae of *Botryoleprarialesdainii*. 44. Biofilm of *Macentina stigonemoides* at intermediate level. 45. Biofilm of *Scytonema julianum* and Chroococcales at entrance level. 46. Magnified view of the bottom left from Fig. 45. 47. Biofilm of *Scytonema ocellatum* at deep level. 48. Biofilm of *Geitleria calcarea* and *Loriella osteophila* at deep level. Scale bars = 10  $\mu\text{m}$  (Figs 31, 36 ), 2  $\mu\text{m}$  (Figs 32, 33, 34, 35), 1  $\mu\text{m}$  (Fig. 37).

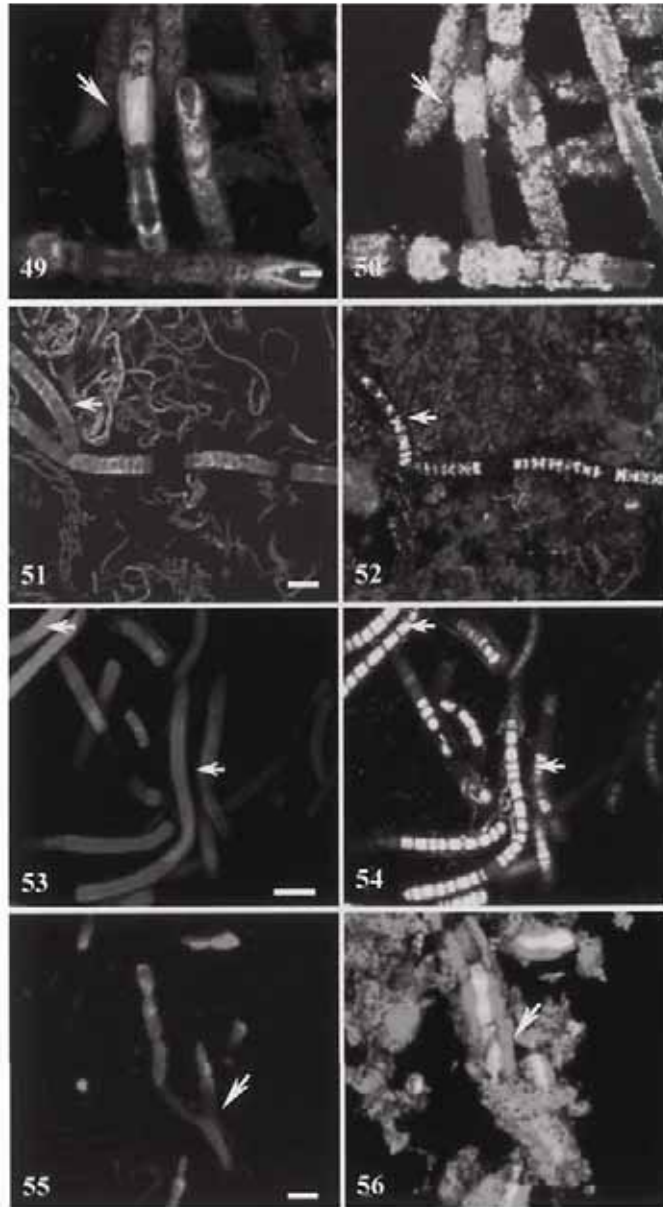
At the end of the entrance of Papellona sinkhole (Fig. 38), there are two small wings. A well-developed community grew in the wing oriented to the west (Fig. 38:7), dominated by *Scytonema julianum*, which was gradually replaced by the lichen *Botryolepraria lesdainii* deeper in the cavity (Figs 42, 43). A biofilm mainly consisting of patches of *B. lesdainii* and *Macentina stigonemoides* (Fig. 44) developed at the wing oriented to the east in the intermediate zone (Fig. 38:8). On the same wall, 2 m deeper, biofilms were composed mainly of cyanobacteria and free-living *Coccolobus verrucariae*. The latter species also occurred as a photobiont of the lichen *Botryolepraria lesdainii*.

The communities of phototrophic organisms at Corral Nou (Fig. 39) formed thick and dense biofilms, rich in mucilage, all year round. At the run-off water tracks on the outdoor walls of the cave, there was a biofilm composed of *Scytonema julianum*, *Nostoc microscopicum* and moss protonema. The concrete wall at the left of the entrance had scarce development of microorganisms. The ceiling at the entrance was mainly colonized by a biofilm consisting of Chroococcales and *S. julianum* (Figs 41, 45, 46).

The biofilms at the intermediate zone and below the entrance were carbonated and mucilaginous, often formed by *S. julianum*. Carbonate needles covered its mucilaginous sheath. Compound images of pigments and EPS (Fig. 49) compared to simultaneously acquired pigments and reflection images (Fig. 50) demonstrated that the carbonate distribution was positively related with EPS. Diatoms only thrived when liquid water was available (Table 3) except for the aerophytic taxa *Hantzschia amphioxys* and *Diademsia contenta*. Some communities changed during the year, in summer the water level was lower and several bands with different colours could be observed. They were composed by the species *Stigonema minutum* (Fig. 12) and *Ctenocladus circinnatus* (Fig. 14), which were not present in winter-spring, when the level of water had risen and the bands were not visible. Then there was only a continuous biofilm covering the entire wall with slight variations in colour.

At the entrance of Puigmoltó (Fig. 40) the biofilm was mainly composed by Chroococcales, *Leptolyngbya* sp., and *Scytonema julianum* (Figs 41, 45, 46, 49-52), whereas at four metres it was basically *Botryolepraria lesdainii*. This biofilm was gradually replaced by another mainly composed by filamentous cyanobacteria, including *Scytonema ocellatum* (Fig. 47), *Leptolyngbya* sp., *Phormidium ambiguum*, and patches of the lichen *Macentina stigonemoides*, that covered the entire cavity until a maximum depth of 15 m. Towards the end of the intermediate zone phototrophic organisms (Fig. 51, pigment fluorescence) were still actively dividing though heavily surrounded by bacteria (Fig. 52, DNA label). *Scytonema ocellatum* (Figs 53, 54) and *Geitleria calcarea* were almost free of heterotrophic organisms.

The phototrophic communities in the darkest area of all cavities were very simple and always composed of *Geitleria calcarea*. Strongly calcified filaments were still alive at these low light conditions as revealed by pigment fluorescence (Fig. 55) and its coupling with the reflection images (Fig. 56). In some cases, there were other filamentous calcified cyanobacteria such as *Loriella osteophila* (Fig. 48). Lichens, if present, were only leprose.



### Discussion

In general, all the cavities sampled presented communities of cyanobacteria and green algae, as well as diatoms and lichenized algae. Most of the species found in this study have been reported in different biotopes (aerophytic, edaphic and fresh waters) (Flechtner et al. 1998, Hoffmann 2001, Nienow & Friedmann 1993). First reports for cavities included the cyanobacteria *Aphanothece caldariorum*, *Asterocapsa* sp., *Gloeocapsa caldariorum*, *Chroococcus ercegovicii*, *Calothrix parietina*, the diatoms *Amphora pediculus*, *Gomphonema clavatum*, *Adlafia bryophila*, *Tryblionella hungarica* and *Simonsenia delognei* and the chlorophytes *Chlorella minutissima*, *Muriella terrestris* and *Ctenocladus circinnatus*. The microclimate inside the cavities was controlled by temperature (that stabilized at depth from 10°C to 15°C) and relative humidity (that increased downward up until saturation). Light was attenuated and finally disappeared at depth.

The gradient of microclimatic conditions was closely related to the colonizing communities of photosynthetic organisms. In a broad sense, three different levels relating abiotic factors to phototrophic organisms were assumed.

a) Entrance level. The microclimate was strongly influenced by the outdoors. Light was scarcely attenuated and abiotic factors fluctuated throughout the year. The microflora colonies were quite rich, with a special abundance of mucilaginous biofilms composed of algae, cyanobacteria typical from terrestrial aerophytic or atmophytic habitats, crustose lichens and mosses. In fact, all the identified species are well known from these environments (Johansen 1993, Garbacki et al. 1999, Komárek & Anagnostidis 1999 and references herein). A community dominated by *Scytonema julianum* developed in some areas that were protected from the rain. The presence of *Trentepohlia* sp. in many crustose lichens was also remarkable.

b) Intermediate level. This portion of the cavities had moderate oscillations and low light (25-0.5 mV); algal biofilms became thin and less mucilaginous but still had

Figs 49-56. Pairs of CLSM micrographs captured from the same locations. 49, 50. Two-channel maximum intensity projections of 10 x-y optical sections (z step = 1.9 µm) from a biofilm composed by *Scytonema julianum* at entrance level. Co-localisation of EPS and inorganic calcareous material. 49. Pigment fluorescence and EPS forming sheaths (arrow). 50. Pigment fluorescence and reflection showing the inorganic calcareous material (arrow) co-localized roughly with the EPS. Compare arrows in both images. 51, 52. Maximum intensity projections of 41 x-y optical sections (z step = 0.37 µm) from biofilm composed by *Scytonema julianum* and *Leptolyngbya* sp. 51. Pigment fluorescence. 52. SYTOX GREEN labelling showing the X-shape division pattern of nucleoids (arrow). Outside fluorescent filaments, the DNA label revealed heterotrophic organisms. 53, 54. Maximum intensity projection of 53 x-y optical sections (z step = 2.5 µm) from a biofilm composed by *Scytonema ocellatum* var. *purpureum* at intermediate level. 53. Pigment fluorescence. 54. SYTOX GREEN labelling showing cell division pattern (arrow). This species was almost free of heterotrophic organisms. 55, 56. Maximum intensity projection of 69 x-y optical sections (z step = 0.5 µm) from a biofilm composed by *Geitleria calcarea* at the deepest level. 55. Pigment fluorescence showing true branching (arrow). 56. Pigment fluorescence and reflection channel showing the fluorescent trichomes were contained inside thick calcified sheaths (arrow). Scale bars = 10 µm (Figs 49-52, 55, 56), 20 µm (Figs 53, 54).

diverse communities. The communities were a mixture of species from both the upper and lower levels. Leprose lichens (*Botryolepraria lesdainii* and *Macentina stigonemoides*) were more frequent whereas crustose lichens decreased in number and species. *Trentepohlia* sp. was found mainly in the free-living form. Cyanobacteria were the most visible constituents, occasionally mixed with green algae and diatoms.

c) Deep level. This portion had very low light (< 1 mV) until light extinction, with stable abiotic factors. The decrease in light had evident effects on the community. Only very few species were able to colonize the low light zone. The presence of remnants and empty sheaths increased with decreasing irradiance. The individuals were heavily colonized by bacteria and filamentous fungi except for *Geitleria calcarea* and *Loriella osteophila*, the dominant phototrophic species, which were actually restricted to the deepest zone, as in other dim light habitats (Abdelahad & Bazzichelli 1988, Couté 1989, Hernández-Mariné et al. 1999). Lichens, if present, were leprose.

Changes of abiotic factors were strong along the vertical axis, while at the horizontal level the conditions were relatively constant. Therefore, the aforementioned stratification was better observed inside sinkholes, which presented a vertical orientation, than in Corral Nou cave, with nearly a horizontal disposition.

The influence of the gradient of microclimatic conditions, especially light and relative humidity, on the communities was not only reflected on their species composition but on the aspect of the biofilms. The protective strategies displayed by the species against desiccation and irradiation gradually changed from the entrance to the bottom. Biofilms formed by mucilaginous and dark coloured coccoid cyanobacteria were gradually substituted by biofilms built by calcified filaments with uncoloured sheaths, which were macroscopically visualized as pale stains on the walls. Similar adaptive strategies promote crustose lichens to be substituted by others with leprose thallus. The development of dark coloured sheaths (as in most Chroococcales), probably functioning as an UV sunscreen (Garcia-Pichel & Castenholz 1991, Van Liere & Walsby 1982), was useless or even a nuisance at the bottom of the cavities. On the other hand, the persistence of humidity at the dew point throughout the year made the excretion of mucilaginous material as a water reservoir unnecessary.

Besides the gradient of microclimatic conditions, other factors affected the presence and distribution of phototrophic microorganisms. Locally, in Corral Nou, the presence of liquid water was associated with the presence of species not found in other cavities. The availability of liquid water retained within the substratum is essential to perform net photosynthesis (Lange et al. 1993; Büdel & Lange 1991) and could explain the high number of species of Corral Nou cave and the higher proportion of Chroococcales and diatoms (Vinogradova 1998, Hoffmann 2001).

On the other hand, growth of microorganisms was not continuous but patchy, though conditions in relative humidity and light were comparable. The absence of growth coincided with the presence of coherent substratum. This could be related to the water retention properties of the substrate (De Winder et al. 1989) or to the microorganisms' aptitude to attach to surfaces (Guillitte & Dreesen 1995, Hernández-Mariné et al. 2001).

Changes in the communities are reported to be mainly caused by light and relative humidity (Nienow & Friedmann 1993, Ariño et al. 1997). However, factors related with substratum coherence (Nienow & Friedmann 1993, Hernández-Mariné et al. 2001) or the interaction among species (Costerton 2000) have been poorly studied, although they play an important role in the development of hypogean biofilms.

#### Acknowledgements

This work was supported by the Spanish DGEIC Program PB97-0957. The facilities of SEM and CLSM by the Scientific and Technical Services of the University of Barcelona are gratefully acknowledged. We would like to thank Jordi Camprubí for his help in map design and Jeff Johansen who offered sage advice.

#### References

- ABDELAHAD, N. & G. BAZZICHELLI (1988): *Geitleria calcarea* Friedmann, Cyanophycée cavernicole nouvelle pour l'Italie. - Nova Hedwigia, Beih. **46**: 265-270.
- ALBERTANO, P. (1993): Epilithic algal communities in hypogean environments. - Giorn. Bot. Ital. **127**: 386-392.
- ALBERTANO, P. & M. GRILLI-CAIOLA (1989): A hypogean algal association. - Braun-Blanquetia **3**: 287-292.
- ALBERTANO, P., L. KOVÁČIK & M. GRILLI-CAIOLA (1994): Preliminary investigations on epilithic cyanophytes from a Roman Necropolis. - Arch. Hydrobiol./Suppl. **105** (Algological Studies **75**): 71-74.
- ANAGNOSTIDIS, K. & J. KOMÁREK (1988): Modern approach to the classification system of cyanophytes. 3 - Oscillatoriales. - Arch. Hydrobiol./Suppl. **80** (Algological Studies **50-53**): 327-472.
- ANAGNOSTIDIS, K. & J. KOMÁREK (1990): Modern approach to the classification system of cyanophytes. 5 - Stigonematales. - Arch. Hydrobiol./Suppl. **86** (Algological Studies **59**): 1-73.
- ARIÑO, X., A. CANALS & M. HERNÁNDEZ-MARINÉ (1998): Cianofícies i algues aerofítiques de substrats carbonatats. - Acta Bot. Barcinon. **45**: 133-140.
- ARIÑO, X., M. HERNÁNDEZ-MARINÉ & C. SAIZ-JIMÉNEZ (1997): Colonization of Roman tombs by calcifying cyanobacteria. - Phycologia **36**: 366-373.
- ASENCIO, A.D. & M. ABOAL (2000a): Algae from La Serreta cave (Murcia, SE Spain) and their environmental conditions. - Arch. Hydrobiol./Suppl. **131** (Algological Studies **96**): 59-78.
- ASENCIO, A.D. & M. ABOAL (2000b): A contribution to knowledge of chasmoendolithic algae in cave-like environments. - Arch. Hydrobiol./Suppl. **133** (Algological Studies **98**): 133-151.
- BELLÉS, X. (1989): Els sistemes cavernícoles. - In: FOLCH I GUILLEN, R. (ed.): Història Natural dels Països Catalans **14**. Els sistemes naturals: 320-326. Enciclopèdia Catalana, S.A., Barcelona.
- BÜDEL, B. & O.L. LANGE (1991): Water status of green and blue-green phycobionts in lichen thalli after hydration by water vapour uptake: Do they become turgid? - Bot. Acta **104**: 361-366.
- CHANTANACHAT, S. & H.C. BOLD (1962): Phycological studies II. Some algae from arid soils. Publication no. 6218. University of Texas, Austin, Texas.
- COSTERTON, J.W. (2000): Biofilms in the New Millennium: musings from a peak in Xanadu. - In: ALLISON, D.G., P. GILBERT, H.M. LAPPIN-SCOTT & M. WILSON (eds): Community structure and co-operation in biofilms: 330-344. Cambridge University Press, Cambridge.

- COUTÉ, A. (1989): *Geitleria calcarea* Friedmann (Cyanophyceae, Hormogonophycidae, Stigonematales, Stigonemataceae): un cas d'adaptation à un milieu extreme. - Bull. Soc. Bot. France, Actual. Bot. **136**: 113-130.
- DE WINDER, B.D., H.C.P. MATTHIJS & L.R. MUR (1989): The role of water retaining substrate on the photosynthetic response of three drought tolerant phototropic microorganisms isolated from a terrestrial habitat. - Arch. Microbiol. **152**: 458-462.
- DESIKACHARY, T.V. (1959): Cyanophyta. - Indian Council of Agricultural Research, New Delhi.
- ETTL, H. & G. GÄRTNER (1995): Syllabus der Boden-, Luft- und Flechtenalgen. - Gustav Fischer Verlag, Stuttgart.
- FLECHTNER, V.R., J.R. JOHANSEN & W.H. CLARK (1998): Algal composition of microbiotic crusts from the central desert of Baja California, Mexico. - Great Basin Naturalist **58**: 295-311.
- GARBACKI, N., L. ECTOR, I. KOSTIKOV & L. HOFFMANN (1999): Contribution à l'étude de la flore des grottes de Belgique. - Belg. J. Bot. **132**: 43-76.
- GARCIA-PICHEL, F. & R.W. CASTENHOLZ (1991): Characterization and biological implications of scytonemin, a cyanobacterial sheath pigment. - J. Phycol. **27**: 395-409.
- GEITLER, L. (1932): Cyanophyceae. - In: L. Rabenhorst's Kryptogamen-Flora von Deutschland, Österreich und der Schweiz, vol. **14**: 1-1196. Akademische Verlagsgesellschaft, Leipzig.
- GÉZE, B. (1965): La spéléologie scientifique. Collección: Le Rayon de la Science. - Éditions du Seuil, Paris.
- GUILLITTE, O. & R. DREESEN (1995): Laboratory chamber studies and petrographical analysis as bioreceptivity assessment tools of building materials. - Sci. Total Environm. **167**: 365-374.
- HERNÁNDEZ-MARINÉ, M., A. ASECIO-MARTÍNEZ, A. CANALS, X. ARIÑO, M. ABOAL & L. HOFFMANN (1999): Discovery of populations of the lime incrusting genus *Loriella* (Stigonematales) in Spanish caves. - Arch. Hydrobiol./Suppl. **129** (Algological Studies **94**): 121-138.
- HERNÁNDEZ-MARINÉ, M., M. ROLDÁN MOLINA, E. CLAVERO, A. CANALS & X. ARIÑO (2001): Phototrophic biofilm morphology in dim light. The case of the Puigmoltó sinkhole. - In: ELSTER, J., J. SECKBACH, W.P. VINCENT & O. LHOTSKÝ (eds): Algae and extreme environments. Nova Hedwigia, Beih. **123**: 237-253.
- HERRERO-BORGÓN, J.J. (1986): La flora de la simas valencianas. - Federación Territorial Valenciana de Espeleología, Valencia.
- HOFFMANN, L. (1989): Algae of terrestrial habitats. - Bot. Rev. **55**: 77-105.
- HOFFMANN, L. (2001): Caves and other low-light environments: aerophytic photoautotrophic microorganisms. - In: COLLINS, G. (ed.): Encyclopedia of Environmental Microbiology: 835-843. John Wiley & Sons, New York.
- JOHANSEN, J.R. (1993): Cryptogamic crusts of semiarid and arid lands of North America. - J. Phycol. **29**: 140-147.
- KOMÁREK, J. & K. ANAGNOSTIDIS (1989): Modern approach to the classification system of Cyanophytes. 4 - Nostocales. - Arch. Hydrobiol./Suppl. **82** (Algological Studies **56**): 247-345.
- KOMÁREK, J. & K. ANAGNOSTIDIS (1999): Cyanoprokaryota 1. Chroococcales. - In: Ettl, H., G. GÄRTNER, H. HEYNIG & D. MOLLENHAUER (eds): Süßwasserflora von Mitteleuropa **19** (1): 1-548. Gustav Fischer, Jena.
- KRAMMER, K. & H. LANGE-BERTALOT (1986): Bacillariophyceae 1. Naviculaceae. - In: Ettl, H., J. GERLOFF, H. HEYNIG & D. MOLLENHAUER (eds): Süßwasserflora von Mitteleuropa. **2** (1): 1-876. Gustav Fischer, Stuttgart.

- KRAMMER, K. & H. LANGE-BERTALOT (1988): Bacillariophyceae. 2. Bacillariaceae, Epithemiaceae, Surirellaceae. - In: Ettl, H., J. Gerloff, H. Heynig & D. Mollenhauer (eds): Süßwasserflora von Mitteleuropa. 2 (2): 1-596. Gustav Fischer, Stuttgart.
- KRAMMER, K. & H. LANGE-BERTALOT (1991): Bacillariophyceae. 4. Achnanthaceae. Kritische Ergänzungen zu *Navicula* (Lineolatae) und *Gomphonema*. - In: Ettl, H., G. Gärtner, J. Gerloff, H. Heynig & D. Mollenhauer (eds): Süßwasserflora von Mitteleuropa. 2 (4): 1-437. Gustav Fischer, Stuttgart.
- LANGE, O.L., B. BÜDEL, A. MEYER & E. KILIAN (1993): Further evidence that activation of net photosynthesis by dry cyanobacterial lichens requires liquid water. - *Lichenologist* 25: 175-189.
- MERINO, V., E. CLAVERO, J. GRIMALT & M. HERNÁNDEZ-MARINÉ (1995): Diatoms from la Trinitat salt works, Ebre Delta (Spain). Considerations about *Amphora hyalina*. - *Vie Milieu* 45: 265-272.
- NIENOW, J.A. & E.I. FRIEDMANN (1993): Terrestrial lithophytic (rock) communities. - In: Friedmann, E.I. (ed.): Antarctic microbiology: 343-412. Wiley-Liss, Inc., New York.
- RIPPKA, R. (1988): Isolation and purification of cyanobacteria. - *Methods Enzymol.* 167: 3-28.
- ROUND, F.E., R.M. CRAWFORD & D.G. MANN (1990): The diatoms. Biology and morphology of the genera. - Cambridge University Press, Cambridge.
- SANT'ANNA, C.L., S.M.F. SILVA & L.H.Z. BRANCO (1991): Cyanophyceae da gruta-quechora, município de Utbatuba, Estado de São Paulo, Brasil. - *Hoehnea* 18: 75-97.
- VAN LIERE, L. & A.E. WALSBY (1982): Interactions of cyanobacteria with light. - In: Carr, N.G. & B.A. Whitton (eds): The biology of cyanobacteria: 9-47. Blackwell Scientific Publ., Oxford.
- VINOGRADOVA, O.N., O.V. KOVALENKO, E. NEVO, S.P. WASSER & M. WEINSTEIN-EVRON (2000): Cyanoprocaryotes/Cyanobacteria of Jamal Cave, Nahal Me'arot Nature Reserve, Mount Carmel, Israel. - *Int. J. Algae* 2: 41-50.
- VINOGRADOVA, O.N., O.V. KOVALENKO, S.P. WASSER, E. NEVO & M. WEINSTEIN-EVRON (1998): Species diversity gradient to darkness stress in blue-green algae/cyanobacteria: a microscale test in a prehistoric cave, Mount Carmel, Israel. - *Israel J. Plant Sci.* 46: 229-238.

Received 28 March 2002, accepted in revised form 01 July 2003.



*Resultats*

---

---

#### 4.6. Per què hi ha un creixement exuberant de microorganismes fototròfics en els ambients hipogeu?

Els organismes formadors de biofilms tenen un gran interès en el context de la degradació del patrimoni cultural. Particularment, els ambients hipogeu exposats a la llum artificial són colonitzats per comunitats microbianes, les quals en deterioren les parets i els frescos. Per descobrir les estratègies que els biofilms fototròfics utilitzaven per desenvolupar-se en aquestes condicions es van estudiar, a les Catacumbes romanes de St. Callistus i Domitilla, l'estructura tridimensional d'aquestes comunitats i les espècies que els formaven. Els principals organismes van ser cianobacteris filamentosos amb beina i les molses. L'estructura dels biofilms era heterogènia, especialment en gruix, densitat i composició d'organismes, però podien ser classificats en funció dels principals organismes que els formaven. Es va observar una diversitat decreixent en els biofilms fototròfics a baixes irradiàncies. Els biofilms a més baixa il·luminació estaven formats únicament per filaments erectes de *Leptolyngbya* sp. Llevat d'aquest biofilm, la composició dels organismes no estava clarament relacionada amb un gradient decreixent d'il·luminació. Malgrat això, els biofilms procedents de mostres sota escassa il·luminació van ser porosos i formats per cianobacteris filamentosos erectes. *Leptolyngbya* sp., l'espècie més ubiqüista, conté un alt nombre de ficobilisomes i els seus hormogonis presenten un moviment lliscant que permet la colonització del substrat. Aquests mecanismes poden jugar un paper important per desenvolupar-se sota condicions de baixa il·luminació a les Catacumbes.

Els resultats detallats d'aquest capítol s'inclouen en el següent article:

Why there is such luxurious growth in the hypogean environments?.  
**Arch. Hydrobiol. 148/ Algological studies** (2003), 109: 229-240.

*Resultats*

---

Algological Studies 109 (Cyanobacterial Research 4)	229–239	Stuttgart, August 2003
--	---------	------------------------

## Why there is such luxurious growth in the hypogean environments

By MARIONA HERNÁNDEZ-MARINÉ, ESTER CLAVERO and MÓNICA ROLDÁN

Universitat de Barcelona, Facultat de Farmàcia, Unitat de Botànica, Barcelona, Spain

With 16 figures and 1 table in the text

**Abstract:** Organisms building biofilms are of considerable interest in the context of degradation of cultural heritage. Particularly, hypogean environments exposed to artificial light are colonized by microbial communities, which damage walls and frescoes. In order to ascertain the mechanisms by which phototrophic biofilms thrive under the particular conditions of hypogea, the organism composition and three-dimensional structure of biofilms from the Roman catacombs St. Callistus and Domitilla were studied. The main phototrophic organisms forming the biofilms were filamentous sheathed cyanobacteria and mosses. Biofilms were spatially very heterogeneous in thickness, density and organism composition but could be classified as regards their main organisms. There was a trend of decreasing diversity in the phototrophic composition of the biofilms under lower irradiances, the one at the lowest irradiance being uniquely built by erected filaments of *Leptolyngbya* sp. Except for this biofilm, the main organism composition was not clearly related with decreasing irradiance. However, biofilms from dim light samples were porous and the filamentous cyanobacteria in them were erected. *Leptolyngbya* sp., the most ubiquitous species, displayed a high number of phycobilisomes and its hormogonia a gliding movement that allowed colonization of substrata. Such mechanisms may have an important role for thriving under the low light conditions of the catacombs.

**Key words:** Biofilms, catacombs, CLSM, cyanobacteria, EPS, hypogean environments, low irradiance, three-dimensional structure of biofilms.

### Introduction

Roman catacombs are hypogean monuments that preserve very valuable material of the history of the early Christians (1<sup>st</sup> to 9<sup>th</sup> centuries). After the opening of the catacombs to the public, growth of microorganisms on their frescoes and walls have formed yellow to blue or dark green patinas that disgust curators and public visiting the works of art. Such patinas not only present an unaesthetic appearance but they can contribute to the deterioration of the murals (ORTEGA et al. 1993 a, b). As previous studies have described (ALBERTANO & URZI 1999), the environmental conditions of these catacombs are relatively invariant and pre-

0342-1123/03/0148-229 \$ 2.75

© 2003 E. Schweizerbart'sche Verlagsbuchhandlung, D-70176 Stuttgart  
Algological Studies 109 = Arch. Hydrobiol. Suppl. 148

dictable, high environmental humidity (RH 90–99 %), low and constant temperature (16–19 °C) and low illumination provided by the lamps set for the display to the public. Low light conditions allow the growth of very few phototrophic organisms, mainly cyanobacteria, which are able to absorb almost all visible wavelengths emitted by these lighting systems (BRUNO et al. 2001). Such phototrophs, together with actinobacteria and fungi build complex structured communities, called biofilms, that conform the macroscopic patinas. Biofilms are aggregated and sustained by an extracellular matrix of polymeric substances (EPS) that is synthesized by some of the organisms. Depending on the type and activity of the organisms and the gradient of physico-chemical factors present in their environment, a diverse range of biofilms is formed.

In the frame of a European project, that focuses on the control, prevention and monitoring of cyanobacteria dominated communities that cause damage to rock surfaces in Roman hypogea (CATS), we studied the biofilms formed in St. Callistus and Domitilla catacombs. The monitoring and improved knowledge of biofilm structure and diversity of species will lead to better understanding, interpretation and prediction of the effect that biofilms may have on those special substrata.

### Material and methods

Sampling was performed in Domitilla and St. Callistus, two catacombs neighbouring and underneath the via Appia Antica (Rome, Italy) during the first week in March 2001. Biofilms were collected from different substrata (plaster, fresco, tufa, bricks and mortar) in eight localities consisting of rooms or corridors (Table 1).

Selected fragments of biofilms were both directly observed and maintained in enrichment cultures. Biofilms were cultured in BG11 solid medium (RIPPKA 1988) at 1/10 strength, with 1 % agar (Merck), at 19 °C.

Biofilms were studied by means of LM (light microscopy), fluorescence stereomicroscope, SEM (Scanning Electron Microscopy), TEM (Transmission Electron Microscopy) and CLSM (Confocal Laser Scanning Microscopy).

Rock chips for SEM were processed with an acrolein-osmium fixation technique developed for this project (HERNÁNDEZ-MARINÉ et al. 2001a) and observed using a Hitachi S-2300 microscope. Chemical fixation and preparation for TEM was made according to HERNÁNDEZ-MARINÉ (1996). Thin sections were observed using a HITACHI H800 MT transmission electron microscope.

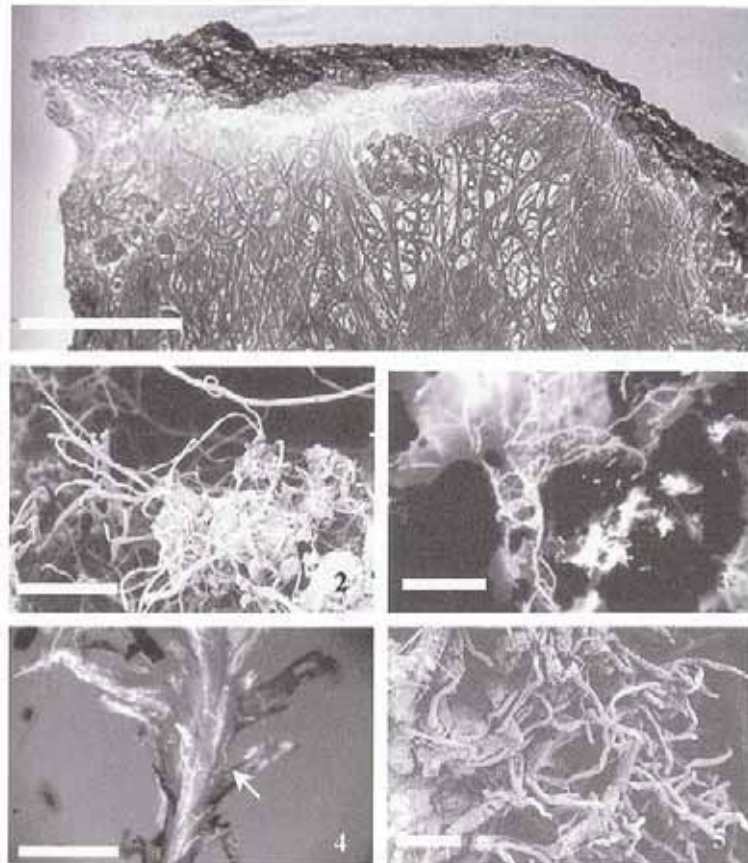
Pigment autofluorescence, nucleic acids and EPS of undamaged biofilm fragments were studied with CLSM. Nucleic acids were specifically stained with Hoechst 33258 (Molecular Probes, Inc.) and EPS was labelled with the carbohydrate recognizing lectin Concanavalin-A (Alexa-conjugated Con A (Succ-Con-A, Molecular Probes, Inc).

Two different CLSM devices were used: The TCS-SPII LEICA Confocal Scanner Microscope equipped with four laser beams and three detection channels; excitation wavelengths of the laser beams were in the UV (351 nm and 364 nm; UVA<sub>r</sub>), blue (488 nm; Ar), green (514 nm and 543 nm; Ar/HeNe) and red (633 nm; Ar/HeNe) ranges. And the TCS LEICA Confocal Scanner Microscope with three laser ArKr 75 mV and two detection channels; excitation wavelengths of the laser beams were 488 nm; 568 nm and 674 nm. Optical sections of biofilms were collected separately in multi-channels as Z-series (3D imaging), in order to map the spatial distribution of fluorescence of pigments, DNA and EPS in the samples. Optical sections were subsequently processed with either Imaris software (Bitplane AG, Zurich) or LEICA Confocal software (LCS) to obtain com-

## Why there is such luxurious growth in the hypogean environments 231

Table 1. Sampled biofilms from Domitilla (CD) and St. Callisto (CSC) roman hypogea. The type of the substratum, the phototrophic organism composition and the thickness of the pigment fluorescent layer are described for each sampling site.

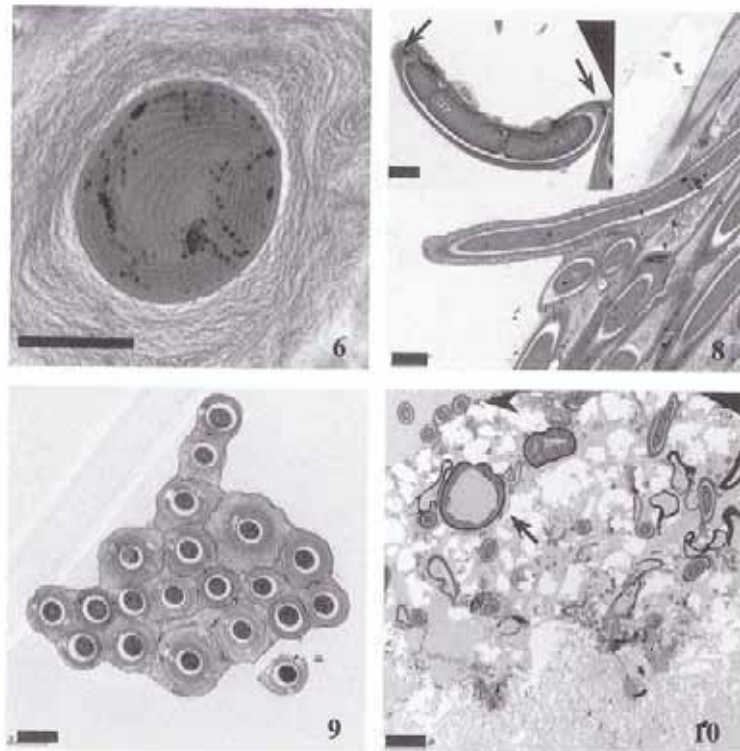
Sample	Substratum	Composition of Biofilm	Mean Biofilm Thickness ( $\mu\text{m}$ )
<b>CD12: Arcosolium near Basilica</b>			
CD12a	Plaster	Moss protonemata and rhizoids, <i>Stichococcus</i> -like, <i>Leptolyngbya</i> , <i>Scytonema</i> , <i>Fischerella</i> , <i>Pseudostaurastrum</i> , Bacteria, Fungi	364
CD12c	Plaster	Moss protonemata and rhizoids, <i>Leptolyngbya</i> sp., Bacteria, Chroococcales, <i>Phormidium</i> , <i>Fischerella</i> .	396
CD12e	Plaster	Mosses, <i>Leptolyngbya</i> , Actinobacteria, Bacteria	
<b>CD13: Cubiculum of "Apostoli Piccoli"</b>			
CD13a	Fresco	Mosses, <i>Leptolyngbya</i> , <i>Fischerella</i> , Bacteria	
CD13b	Fresco	<i>Leptolyngbya</i> , Calcified filaments	167.5
CD13c	Fresco	<i>Leptolyngbya</i>	330
CD13d	Plaster-Tufa	<i>Leptolyngbya</i> , <i>Scytonema</i> , <i>Pseudostaurastrum</i> , <i>Diademsis gallica</i> , <i>Stichococcus</i> -like, Chroococcales	188.4
CD13dv		Mosses, <i>Scytonema</i> , <i>Leptolyngbya</i> , <i>Fischerella</i> , Fungi	
<b>CD15: Wall in the Corridor before the "Ipogeo dei Flavi"</b>			
CD15a	Bricks	<i>Fischerella</i> , <i>Scytonema</i> , <i>Leptolyngbya</i> , <i>Phormidium</i> , Chroococcales, Fungi	
CD15b	Bricks	Mosses, Chroococcales, Calcified filaments, <i>Leptolyngbya</i>	227.5
CD15c1	Bricks	Moss protonemata, <i>Leptolyngbya</i> , <i>Scytonema</i> , <i>Fischerella</i> , Chroococcales, <i>Aphanocapsa</i> , <i>Pseudostaurastrum</i> , <i>Diademsis gallica</i> , Bacteria, Fungi	
CD15c2	Mortar	Protonemata mosses, <i>Scytonema</i> , <i>Leptolyngbya</i> , <i>Fischerella</i> , Chroococcales, <i>Aphanocapsa</i> , <i>Pseudostaurastrum</i> , <i>Diademsis gallica</i>	
CD15f	Tufa	Mosses, Chroococcales, Calcified filaments	287.5
CD15g	Plaster	<i>Aphanocapsa</i> , <i>Gloeotheca</i> , <i>Scytonema</i> , <i>Fischerella</i> , <i>Pseudostaurastrum</i> , Fungi, Bacteria, Actinobacteria	
CD15h	Plaster	Mosses, <i>Leptolyngbya</i> , <i>Fischerella</i> , Chroococcales, <i>Pseudostaurastrum</i> , <i>Phormidium</i> , Actinobacteria	
<b>CSC13: Cubiculum of "Oceano"</b>			
CSC13a	Fresco	<i>Leptolyngbya</i> , <i>Fischerella</i>	
CSC13b	Fresco	<i>Leptolyngbya</i>	
<b>CSC16: Wall in the Corridor of Cubiculum "Caio and Eusebio"</b>			
CSC16a	Plaster	<i>Leptolyngbya</i>	
CSC16b	Plaster	<i>Leptolyngbya</i> , Chroococcales	
CSC16b'	Plaster	Protonemata mosses, <i>Scytonema</i> , <i>Leptolyngbya</i> , Chroococcales	332.5
CSC16c	Plaster	<i>Leptolyngbya</i> , Chroococcales	397.5
CSC16d	Plaster	<i>Leptolyngbya</i> , <i>Fischerella</i> , Fungi	
CSC16e	Plaster	<i>Leptolyngbya</i> , Protonemata mosses	415
<b>CSC17: Last Arcosolium, on the left before the exit stairs.</b>			
CSC17a	Plaster	Calcified thin filaments, <i>Scytonema</i> , <i>Stichococcus</i> -like, <i>Phormidium</i> , <i>Leptolyngbya</i> , Fungi	84.8
<b>CSC19: Arcosolium</b>			
CSC19b	Plaster	Calcified filaments, <i>Scytonema</i> , Fungi, <i>Fischerella</i> , Mosses, Protonemata mosses, <i>Leptolyngbya</i> , Chroococcales	
CSC19c	Plaster	<i>Scytonema</i> , <i>Leptolyngbya</i> , <i>Fischerella</i> , Mosses	116



Figs 1-5: **1** – SEM. General aspect of a biofilm of the Roman Catacombs, mainly built by filamentous cyanobacteria with erected filaments. **2** – SEM. *Leptolyngbya* sp. biofilm. **3** – Fluorescence stereomicroscope micrograph of a *Leptolyngbya* sp. biofilm with gorgonia-like shape. **4** – Fluorescence stereomicroscope micrograph. *Leptolyngbya* sp. (arrow) filaments on mosses. **5** – SEM. *Leptolyngbya* sp. on *Scytonema julianum*. [Scale bar = 200  $\mu$ m (Figs 1, 4), 50  $\mu$ m (Figs 2, 3, 5).]

pound images of fluorescence and/or spatial structure. A general view of the whole sample was obtained with a LEICA MZFLIII fluorescence stereomicroscope or at 100X with either of the two CLSM devices. Then, finer structure of the biofilm was observed at 630X, 1000X.

Why there is such luxurious growth in the hypogean environments 233



Figs 6–10. TEM. **6** – Transversal thin section of a *Leptolyngbya* sp. trichome, close to the septum, with high number of phycobilisomes. Thylakoids in *Leptolyngbya* sp. dispose parallel to the longitudinal walls. However, in this section, oblique thylakoids correspond to those that ingrow parallel to the septum during the cell division. **7** – Longitudinal thin section of *Leptolyngbya* sp. covered by a sheath (arrows). **8** – Thin section of a *Leptolyngbya* sp. bundle. Filaments are arranged in different directions, the longitudinally cut filament is gliding over the others. **9** – Transversal thin section of a *Leptolyngbya* sp. bundle. The polysaccharide sheaths of the filaments are joined to each other, sustaining the 3D structure of the bundle. **10** – Thin section of a fragment of deteriorated plaster. Mosses (arrow) are penetrating into the substratum. *Leptolyngbya* sp. filaments are on the surface (arrowhead) and inside the substratum. [Scale bars = 1  $\mu\text{m}$  (Figs 6,7), 2  $\mu\text{m}$  (Figs 8, 9), 5  $\mu\text{m}$  (Fig. 10).]

## Results

Biofilms developed adhered to all the solid surfaces studied (plaster, fresco, tufa, bricks or mortar) and at low irradiances. Water availability was related to the porosity of the substratum, though some biofilms could be sporadically exposed to dripping water.



The main phototrophic organisms forming the biofilms were mosses and filamentous sheathed cyanobacteria (Fig. 1): *Leptolyngbya* sp., *Phormidium* sp., *Scytonema julianum* (MENEGHINI ex FRANK) RICHTER and *Fischerella* sp., although few species of Chroococcales were specially abundant in bricks and mortars (Table 1). Accompanying organisms were diatoms (*Diadesmis gallica* W. SMITH, *Pseudostaurosira* sp.), fungi hyphae and actinobacteria. A general trend of decreasing diversity in the phototrophic composition of the biofilms under lower irradiances was observed.

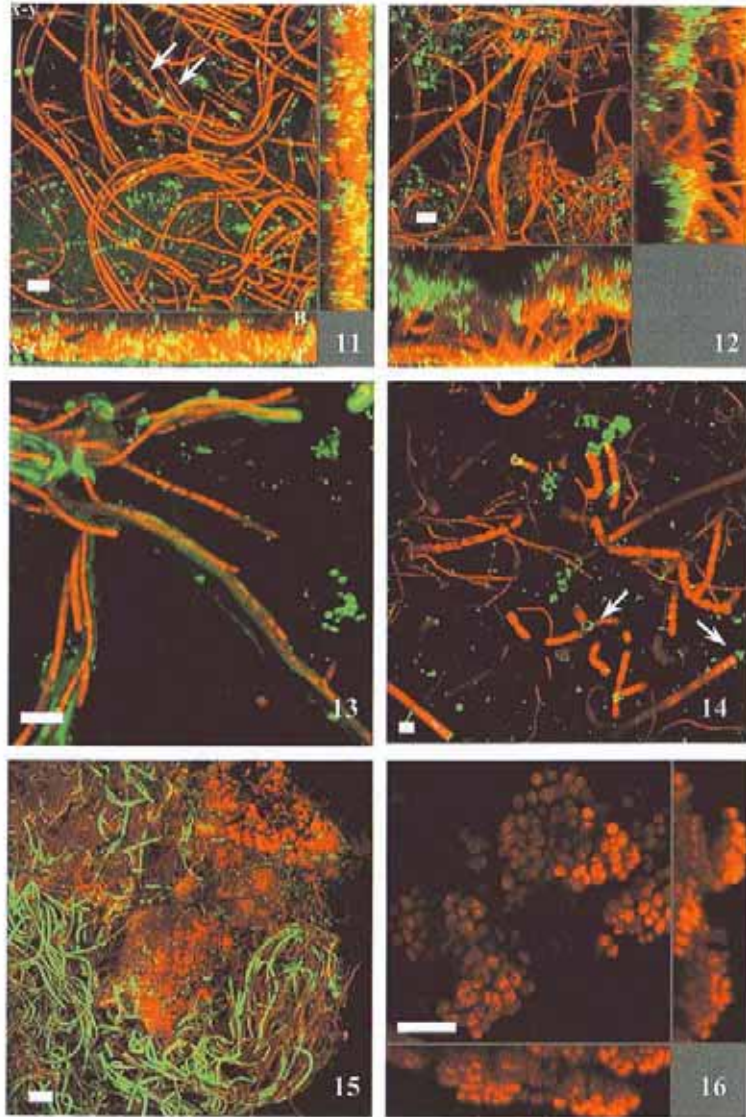
*Leptolyngbya* sp. was the most widespread species. Present in all but two samples, it thrived in all the substrata and localities. It was the only phototroph (Fig. 2) building the greenish patinas under the lowest photon flux density at which phototrophic growth was still present. In this case, it presented many erected filaments, overall forming hairy biofilms (Fig. 3). But it also developed close to the lamps as a part of a community and then lay on moss protonemata (Fig. 4), or other cyanobacteria such as *Scytonema julianum* (Fig. 5).

*Leptolyngbya* sp. specimens collected from low light conditions presented a large amount of phycobilisomes (Figs 6 and 7). In general, fluorescence was higher in any cyanobacteria species than in mosses under same conditions of excitation. Furthermore, first results of laser induced fluorescence profiles of chlorophyll and phycobilin pigments (CLSM function), showed that cyanobacteria were able to harvest a wide range of wavelengths, emitting fluorescence when excited at wavelengths from 351–633 nm (data not shown).

*Leptolyngbya* appeared as erected filaments, under low light, or in compact biofilms (Figs 8 and 9).

Figs 11–16. Compound images of CLSM. (red = pigment fluorescence, green = Con-A labelled EPS, blue = Hoechst 33258 stained nucleic acids). **11–12**. Confocal double-fluorescence (autofluorescence and EPS) images. Three-dimensional extended focus images and orthogonal views of bilinear interpolated x-y CLSM sections in the z-directions of the biofilms. The extended focus x-y image was made from the selected volume by collapsing the z-direction. The orthogonal views are cuts through selected regions of interest in the z-direction. T=top, B=bottom. **11** – Compound image of 30x-y optical sections (0.95 µm interval). Compact biofilm of *Leptolyngbya* sp. (28 µm total thickness). Necrotic cells surrounded by EPS (arrows). **12** – Compound image of 50 x-y optical sections (1.47 µm interval). Porous biofilm of *Leptolyngbya* sp. (73.5 µm total thickness). **13** – Two-channel maximum intensity projection (autofluorescence and EPS) of 59 x-y optical sections (0.2 µm interval). Dispersion of *Leptolyngbya* sp. bundles in a biofilm. **14** – Three-channel maximum intensity projection (autofluorescence, EPS and nucleic acids) of 109 x-y optical sections (0.4 µm interval). Complex biofilm formed by different species of filamentous cyanobacteria: *Leptolyngbya* sp., *Scytonema julianum* and *Fischerella* sp. The apical pads display stronger Con-A fluorescence than any other parts of the sheath. **15** – Two-channel maximum intensity projection (autofluorescence and EPS) of 115 x-y optical sections (2.5 µm interval) showing a patina formed by filamentous cyanobacteria with isolated aggregates of Chroococcales. Some cyanobacteria filaments are covered by green sheaths, labelled with Con-A. **16** – Three-dimensional extended focus image and orthogonal view of 35 bilinear interpolated x-y CLSM sections in the z-direction of the biofilms (1 µm interval). Biofilm of small Chroococcales (ca. 1 µm). [Scale bar = 10 µm (Figs 11–14, 16), 100 µm (Fig 15)].

Why there is such luxurious growth in the hypogean environments 235



Necrotic cells in old *Leptolyngbya* sp. filaments produced large amounts of EPS that contributed in the split-off of hormogonia from the trichomes. Hormogonia could glide along the inside of sheaths to the edges of the colony and grow past the first attaching point, making the resulting filament longer. They also could glide over the colony and attach to filaments of the same species. As a result the colonies of *Leptolyngbya* sp. could take a *gorgonia*-like shape (Fig. 2). Besides, hormogonia could glide over and attach to other species or any suitable substratum and, in this manner, colonize new surfaces.

The secretion of EPS around trichomes was very irregular, thin (Figs 7, 8) or very thick in some filaments, forming concentric layers (Figs 6, 9). EPS helped each filament to join to neighbouring filaments; so that EPS (Figs 8, 9) gave structure and coherence to the biofilm.

The macroscopical patinas appeared to be spatially very heterogeneous in thickness, density and organism composition. As a rule, they were usually thin, except near the lamps. At low magnification, three types of patina could be differentiated. Patinas formed by filamentous cyanobacteria, patinas formed by filamentous cyanobacteria with isolated aggregates of Chroococcales, and heterogeneous patinas very diverse in organism composition, constituted mainly by moss, moss protonemata and filamentous cyanobacteria (Fig. 10).

Except for the third type, at higher magnification the organism composition of the patinas changed fairly abruptly in space, so that different subregions (we will call them biofilms) could be established. Filamentous cyanobacteria-patinas could be formed by *Leptolyngbya* sp. biofilms (Figs 11, 12, 13), biofilms of entangled filaments of *Leptolyngbya* sp. and *Phormidium* sp. (3 µm in diameter) or *Fischerella* sp., and biofilms of entangled *Leptolyngbya* sp. and *Scytonema julianum* (Fig. 14). In the biofilms of *Leptolyngbya* sp. and *S. julianum*, heterotrophic organisms were also notably represented. Patinas formed by filamentous cyanobacteria and Chroococcales (Fig. 15), could contain any of the filamentous cyanobacteria mentioned above, biofilms of small (ca. 1 µm diameter) Chroococcales (Fig. 16), biofilms of large Chroococcales with thick slime sheaths, and biofilms with mixed Chroococcales. Heterogeneous patinas contained mosses, with their rhizoids penetrating into the substratum (Fig. 10), and entangled with filamentous cyanobacteria, sparse individuals of Chroococcales and diatoms.

This third type of patina occurred mainly in samples from dripping zones. No special preferences for a particular substratum were observed in any of the types. Neither was a clear trend in distribution of the patinas in relation to light, except for the biofilm exclusively of *Leptolyngbya* sp. at the lowest irradiance. However, biofilms from dim light samples were hollow and the filamentous cyanobacteria in them were erected (Fig. 12). The *Leptolyngbya*-dominated biofilms were thin and velvety, adopting the *gorgonia*-like a tridimensional architecture.

The EPS was heterogeneously distributed in the biofilms (Fig. 11), sometimes being more abundant at the bottom due to sheath remains (Fig. 12).

### Discussion

The artificial illumination allowed a luxurious photosynthetic growth and formation of biofilms, in St. Callistus and Domitilla catacombs.

A relatively small number of photosynthetic organisms were found to be responsible for the development of those biofilms. The main representatives were sheathed cyanobacteria as *Phormidium* sp., *Leptolyngbya* sp., *Fischerella* sp. or the heavily calcified *Scytonema julianum*. As a group, filamentous cyanobacteria do equally well in other low light environments that are occasionally wet. They have been reported from catacombs before (ALBERTANO & URZI 1999) and also from other dim light aerophytic environments such as sinkholes and caves (ARIÑO et al., 1997, HERNÁNDEZ-MARINÉ 2001b). However, no representatives of some of the most successful groups of subaerial algae (NIENOW 1996) were found. Photobionts of lichens, such as *Trebouxia*, *Coccomyxa* and *Leptosira* were not found. Coccoid green algae and the *Apatococcus-Pleurastrum* group, common in tree barks and dry rocks, were neither represented.

The combination of cultures, morphological characterization by microscopic techniques, in particular CLSM, use of fluorescent probes and the generation of three-dimensional digitalized image represented an advance in the understanding of the features of the biofilm. Conjugated lectins helped to reveal the structural heterogeneity in the polysaccharides distribution.

The community structure and organisms cooperation of different types of aquatic biofilms has been fully documented (NEU 2000, WIMPENNY 2000). In aquatic habitats the architecture that biofilms develop may be more or less porous depending on the physico-chemical characteristics of the environment in which they grow (WIMPENNY 2000). The aerophytic biofilms differ from the aquatic ones in the surface, that is solid-gas, and voids instead of liquid water or watery substances among the organisms. In the case of the biofilms in the murals of the catacombs, EPS could be regulated in response to a variety of environmental factors, probably forming thicker sheaths related to low water availability (ORTEGA-MORALES et al. 2001).

Low irradiance appeared to be the main stress factor shaping the biofilms. To cope with low irradiance, cyanobacteria increase the number and size of phycobilisomes (COUTÉ & BURY 1988) and have the ability of harvesting at nearly all wavelengths. Erected filamentous organisms mainly composed the biofilms grown at the lowest light levels, and the community formed hollow and velvety structures. The porous structure of the biofilms allowed all the filaments to obtain the maximum amount of light. Impoverishment of the diversity may have occurred due to population shifts in the community in response to changes/reduction in the irradiance levels.

Motility (HOICZYK & WOLFGANG 1998, HOICZYK 2000) and colony formation is associated with the production of mucilage. In the case of *Leptolyngbya* sp. the growth of the filaments and the motility of the hormogonia is responsible for the formation and spatial organization of biofilms. Hormogonia colonize adjacent organisms or clean surfaces, in a dissemination strategy.

The polysaccharidic apical pads used for the filament fixation of *Leptolyngbya* sp. are formed by necridic cells and previously to the attachment. This contrasts with the mechanism of fixation in *Pseudomonas aeruginosa*, in which polysaccharide production is switched on when the surface is contacted (DAVIES et al. 1993).

The particular hypogean habitat is not extreme regarding temperature and water conditions (humidity) (ALBERTANO & URZI 1999). Therefore light appears as the main stress factor and responsible for the low diversity of photosynthetic life. Cell signalling has been found to be important in regulating the biodiversity in bacterial biofilms (DAVIES et al. 1998). However, nothing is known about complex physiological regulation or the putative control through production of cell signals or quorum substances in subaerial biofilms.

Although dim light may affect the community composition and diversity, it did not prevent the development of photosynthetic biofilms. The photosynthetic organisms thriving in the catacombs have the mechanisms to live under low light (chromatic adaptation, porous biofilms) and colonize new surfaces. The best theory that explains this luxurious photosynthetic growth was formulated by CALDWELL et al. (1997) pointing out that success at any level comes as a result of the ability to grow and reproduce, with those that grow fastest in a particular set of physico-chemical conditions inevitably surviving best.

#### Acknowledgements

This work was supported by EU Programme Energy, Environment and Sustainable Development in the frame of CATS Project, contract EVK-4-CT-2000-00028. The facilities of SEM, TEM and Confocal Microscopy provided by the Scientific and Technical Services of the University of Barcelona are gratefully acknowledged.

#### References

- ALBERTANO, P. & URZI, C. (1999): Structural interactions among epilithic cyanobacteria and heterotrophic microorganisms in Roman hypogea. – *Microbial Ecol.* **38**: 244–252.
- ARIÑO, X.; HERNÁNDEZ-MARINÉ, M. & SAIZ-JIMÉNEZ, C. (1997): Colonization of Roman tombs by calcifying cyanobacteria. – *Phycologia* **36**: 366–373.
- BRUNO, L.; PIERMARINI, S. & ALBERTANO, P. (2001): Characterisation of spectral emission by cyanobacterial biofilms in the Roman Catacombs of Priscilla in Rome (Italy). – In: ELSTER, J., SECKBACH, J., VINCENT, W. P. & LHOŤSKÝ, O. (eds.): *Algae and extreme environments*. – *Novi Hedwigia. Beih.*, **123**: 229–236.
- CALDWELL, D. E.; WOLFAARDT, G. M.; KÖRBER, D. R. & LAWRENCE, J. R. (1997): Do bacterial communities transcend Darwinism? – *Adv. Microbial Ecol.* **15**: 105–191.
- COUTÉ, A. & BURY, E. (1988): Ultrastructure d'une cyanophycée aérienne calcifiée cavernicole : *Scytonema julianum* (FRANK) RICHTER (Hormogonophycideae, Nostocales, Scytonemataceae). – *Hydrobiologia* **160**: 219–239.
- DAVIES, D. G.; CHAKRABARTY, A. M. & GEESEY, G. G. (1993): Exopolysaccharide production in biofilms-substratum activation of alginate gene expression by *Pseudomonas aeruginosa*. – *Appl. environ. Microbiol.* **59**: 1181–1186.

## Why there is such luxurious growth in the hypogean environments 239

- DAVIES, D. G.; PARSEK, M. R.; PEARSON, J. P.; JGLEWSKI, B. H.; COSTERTON, J. W. & GREENBERG, E. P. (1998): The involvement of cell-to-cell signals in the development of a bacterial biofilm. – *Science* **280**: 295–298.
- HERNÁNDEZ-MARINÉ, M. (1996): Electron microscopic characterization of *Microcoleus chthonoplastes* THUR. (Cyanobacteria). – *Arch. Hydrobiol./Algological Studies* **83**: 347–365.
- HERNÁNDEZ-MARINÉ, M.; MARTINEZ, G.; DOMÍNGUEZ, A.; FONTARNAU, R. & CORTADELLAS, N. (2001a): SEM studies of arborescent aerophytic biofilms. Use of acrolein and osmium vapour impregnation. – In: *Microscopy*, p. 334–335. Universitat de Barcelona, Barcelona.
- HERNÁNDEZ-MARINÉ, M.; ROLDÁN MOLINA, M.; CLAVERO, E.; CANALS, A. & ARIÑO, X. (2001b): Phototrophic biofilm morphology in dim light. The case of the Puigmoltó sinkhole. – In: ELSTER, J.; SECKBACH, J.; VINCENT, W. P. & LHOTSÝ, O. (eds.): *Algae and extreme environments*. – *Nova Hedwigia, Beih.*, **123**: 237–253.
- HOJCZYK, E. (2000): Gliding motility in cyanobacteria: Observations and possible explanations. – *Arch. Microbiol.* **174**: 11–17.
- HOJCZYK, E. & WOLFGANG, B. (1998): The junctional pore complex, a prokaryotic secretion organelle, is the molecular motor underlying gliding motility in cyanobacteria. – *Curr. Biol.* **8**: 1161–1168.
- NEU, T. R. (2000): In situ cell and glycoconjugate distribution in river snow studied by confocal laser scanning microscopy. – *Aquat. Microb. Ecol.* **21**: 85–95.
- NIENOW, J. A. (1996): Ecology of subaerial algae. – *Nova Hedwigia, Beih.*, **112**: 537–552.
- ORTEGA, J. J.; HERNÁNDEZ-MARINÉ, M. & SAIZ-JIMÉNEZ, C. (1993a): Cyanobacteria and algae on historic buildings and monuments. – In: GARG, K. L.; ARAI, H. & RAI, B. (eds.): *Recent Advances in Biodeterioration and Biodegradation*, **1–2**: 173–203, Calcutta.
- ORTEGA, J. J.; SÁNCHEZ-CASTILLO, P. M.; HERNÁNDEZ-MARINÉ, M. & SAIZ-JIMÉNEZ, C. (1993b): Isolation and characterization of epilithic chlorophytes and cyanobacteria from two Spanish cathedrals (Salamanca and Toledo). – *Nova Hedwigia* **57**: 239–253.
- ORTEGA-MORALES, B.; LÓPEZ CORTES, A.; HERNÁNDEZ DUQUE, G.; CRASSOUS, P. & GUEZENNEC, J. (2001): Extracellular polymers of microbial communities colonizing ancient limestone monuments. – In: DOYLE, R. J. (ed.): *Methods in Enzymology. Microbial growth in biofilms. Part A: Developmental and molecular biological aspects*, **336**: 331–339, Academic Press, Inc., San Diego.
- RIPPKA, R. (1988): Isolation and purification of cyanobacteria. – In: PACKER, L. & GLAZER, A. N. (eds.): *Methods in Enzymology*, **167**: 3–28, Academic Press, Inc., San Diego.
- WIMPENNY, J. (2000): An overview of biofilms as functional communities. – In: ALLISON, D.; GILBERT, P.; LAPPIN-SCOTT, H. & WILSON, M. (eds.): *Community structure and cooperation in biofilms*, p. 1–24, Cambridge University Press, Cambridge.

The authors' address:

MARIONA HERNÁNDEZ-MARINÉ,  
 ÉSTER CLAVERO,  
 MÓNICA ROLDÁN,  
 Universitat de Barcelona,  
 Facultat de Farmàcia,  
 Unitat de Botànica,  
 Av. Joan XXIII s/n,  
 E-08028, Barcelona, Spain.  
 e-mail: hernande@farmacia.far.ub.es

*Resultats*

---

---

#### **4.7. Els polisacàrids produïts per cèl·lules necrídiques porten a terme l'adherència dels hormogonis al substrat**

A la majoria de cianobacteris filamentosos, els hormogonis són una forma transitòria d'aturada del creixement que serveix per la dispersió a curtes distàncies, l'adhesió i el subsegüent establiment de biofilms. Els mecanismes que intervenen en aquesta adhesió són complexos, incloent interaccions no específiques i propietats determinades pels organismes i per les condicions ambientals.

L'objectiu va ser l'estudi de la formació de substàncies mucilaginoses que intervenen en els primers passos dels processos d'adhesió dels hormogonis. Es van estudiar biofilms aerofítics, vius i intactes, procedents d'hàbitats amb escassa il·luminació, mitjançant el microscopi electrònic de transmissió i de rastreig làser confocal marcant el DNA i les substàncies polimèriques extracel·lulars. Els biofilms estaven formats principalment per *Leptolyngbya* spp. i *Scytonema* spp. En aquests cianobacteris filamentosos, el primer aspecte visible de la diferenciació dels hormogonis va ser la formació de cèl·lules que ajudaven al trencament del tricoma, anomenades necridia. La investigació revelà canvis en aquestes cèl·lules. Inicialment, presenten un increment de la intensitat de fluorescència i de la producció de polisacàrids intracel·lulars. El trencament del tricoma i l'alliberament dels hormogonis van ser causats per la desintegració d'aquestes cèl·lules necrídiques, que a l'últim pas només mostraven fluorescència de les substàncies polisacàridiques. Els extrems polisacàridics semblen actuar com a mecanismes d'adhesió, com una goma d'enganxar al començament de l'adhesió de l'hormogoni al substrat. Per tant, podem postular que la colonització d'hàbitats per cianobacteris filamentosos és eficient perquè els hormogonis i el seu extrem adhesiu hi estan implicats. Malgrat això, són necessaris més estudis per comprendre la importància de les restes de cèl·lules necrídiques i la seva contribució en la colonització de nous hàbitats.



Els resultats detallats d'aquest capítol s'inclouen en el següent article:

Adherence of hormogonia to substrata is mediated by polisaccharides produced by necridic cells. ***Arch. Hydrobiol./Suppl. Algological studies*** (2005), 117: 1-11.

## Adherence of hormogonia to substrata is mediated by polysaccharides produced by necridic cells

By MARIONA HERNÁNDEZ-MARINÉ and MÓNICA ROLDÁN

Universitat de Barcelona, Facultat de Farmàcia, Unitat de Botànica,  
Barcelona, Spain

With 4 figures in the text

**Abstract:** In most filamentous cyanobacteria the hormogonia are a transient non-growth state that serves in the short-distance dispersal, attachment and subsequent establishment of biofilms. The mechanisms involved in their adhesion are complex, including nonspecific interactions, properties determined by the organisms and the environmental conditions. The aim of this study was to further our knowledge of the formation of the mucilaginous substances that mediate in the first steps of the hormogonium attachment processes. Intact-live biofilms, from aerophytic dim habitats, were processed for Transmission Electron Microscopy and Confocal Scanning Laser Microscopy (CSLM) with and without fluorescent labelling for DNA and polysaccharidic substances. Those biofilms were mainly built by *Leptolyngbya* spp. and *Scytonema* spp.

In the above filamentous cyanobacteria the first visible aspect of hormogonia differentiation was the formation of cells that help trichome breakage, called necridia. The investigation revealed changes in such cells. At the beginning they presented higher pigment fluorescence than the neighbour cells without change in size. While changing to a characteristic cupping glass shape the CSLM revealed the loss of pigment fluorescence and the increased production of intracellular polysaccharides. Trichome breakage and hormogonia liberation were caused by the disintegration of such necridia, that at their final step only presented a strong polysaccharidic fluorescence. The immediate neighbours, that became the newly formed hormogonium, retain those cupping glass polysaccharidic fluorescent remains of necridia attached at one or both tips. These polysaccharidic pads seemed to act as glue-like attachment mechanism at the onset of hormogonia adhesion to substrata. We can then postulate that colonization of habitats and plant infection by filamentous cyanobacteria is efficient because hormogonia and their sticky tip are involved. However more studies are needed to understand the significance of necridia remains and their contribution to the formation of biofilms.

**Keywords:** Adhesion, attachment, biofilms, catacombs, Confocal scanning laser microscopy, CSLM, Con-A, cyanobacteria, EPS, Hoechst 33258, hormogonia, hypogean environments, *Leptolyngbya*, polysaccharides, *Scytonema*.

0342-1120/05/0159-239 \$ 2.75

© 2005 E. Schweizerbart'sche Verlagbuchhandlung, D-70176 Stuttgart  
Algological Studies 117 = Arch. Hydrobiol. Suppl. 159

### Introduction

Cyanobacteria are able to undergo cell differentiation in response to environmental changes, which can be both positive and negative for growth, depending on the taxon (ANAGNOSTIDIS & KOMÁREK 1988, HERDMAN & RIPPKA 1988, MEEKS et al. 2002). As was first proposed by KOHL (1903), some scytonematacean and oscillatoriacean trichomes break delivering short motile fragments called hormogonia. The fragmentation of trichomes occurs at heterocytes, between two vegetative cells, or by the help of dying sacrificed cells called necridia (ANAGNOSTIDIS & KOMÁREK 1988).

Hormogonia are a transient, non-growth state that serves in the short-distance dispersal and colonization (ANAGNOSTIDIS & KOMÁREK 1988). In addition, symbiotically competent filamentous cyanobacteria differentiate hormogonia that act as infective units in the formation of symbiotic associations (MEEKS 1998, MEEKS & ELHAI 2002). The smaller-sized cells of hormogonia result from cell divisions that are not accompanied by an increase in cell biomass; there is no significant net synthesis of DNA (HERDMAN & RIPPKA 1988), protein, or chlorophyll (CAMPBELL & MEEKS 1989) during the differentiation and active gliding periods of the hormogonium cycle. In addition, hormogonia lack heterocytes and do not fix  $N_2$  (TANDEAU DE MARSAC 1994).

Death and lysis of necridia helps in the transcellular trichome breakage (ANAGNOSTIDIS & KOMÁREK 1988) and hormogonia release. Moreover, the release of hormogonia by *Nostoc* symbionts is induced by chemical signals released by the plant partner that influence hormogonium behavior (MEEKS & ELHAI 2002, CAMPBELL et al. 2003). The selection of such cells is generally considered haphazard and accidental in contrast with the pattern of selection and preparation of cells that will differentiate as heterocytes (EL-SHEHAWY & KLEINER 2003 and references therein).

There is a large body of literature about selective advantages for microorganisms to colonize (COSTERTON et al. 1999) and attach to surfaces (BLENKINSOPP & COSTERTON 1991, DE PHILIPPIS & VINCENZINI 1998, DUNNE 2002, BAKKER et al. 2004). Several mechanisms involved in attachment have been suggested. One of the most attractive theories in adhesion is the extended DLVO- model of colloid stability (VAN OSS et al. 1986, JUCKER et al. 1998) in which linkage is regarded as the total sum of Lifshitz-Van der Waals, acid-base, and electrostatic interactions. However, this theory assumes that microorganisms behave as inert particles, which is not the case (HERMANSSON 1999). The production of some substances, such as extracellular polysaccharides (EPS), that can act simultaneously or in distinct steps of the colonization process should be considered (FINLAY & FALKOW 1997, HERMANSSON 1999, SUTHERLAND 2001). Further support comes from a direct link between the biofilm adhesive strength and the polysaccharide content (HOKPUTSA et al. 2003) and colonization of substrata (ALBERTANO et al. 1994, LAMENTI et al. 2000, HU et al. 2003, ORTEGA-CALVO et al. 1995). The EPS composition is also related to the adhesion potential. Hydrophobic exopolysaccha-

rides, excreted by mature filaments of benthic cyanobacteria, have been implicated in cohesion mechanisms (BAKKER et al. 2004). Conversely, EPS secreted by planktonic cyanobacteria and hormogonia are hydrophilic (FATTOM & SHILO 1984) and thereby can reduce the surface tension.

We illustrate a mechanism for hormogonia adhesion that has not been previously observed. We hypothesize that first steps in the attachment processes are mediated by a pad of mucilaginous material constructed by the help of necridic cells. Focus is on the biofilm forming filamentous-sheathed cyanobacteria *Lepidolyngbya* ssp., *Scytonema julianum* (KÜTZ.) MENECH. in KÜTZ. and *S. ocellatum* LYNGBYE.

### Material and methods

Small chips of substrata bearing intact-live biofilms were collected in dim light habitats: the Pupellona cave in Garraf, NE Spain (ROLDÁN et al. 2004a) and St. Callistus catacomb, neighbouring and underneath the via Appia Antica from Rome, Italy (HERNÁNDEZ-MARINÉ et al. 2003). Biofilms were collected from different substrata: limestone from the cave, and plaster, fresco, tufa, bricks, and mortar from the catacombs. General views of the whole sample were obtained with light microscopy. Biofilms developed on the cave wall and hypogean monuments as distinct dusty blue green, up to few millimeters of thickness. Stable temperatures and humidity along the year characterize the habitats studied. Differences in biofilm thickness, cyanobacterial, and microalgal density and composition were observed depending upon light conditions and capacity to retain water from the material that supported the colonized surfaces (HERNÁNDEZ-MARINÉ et al. 2003, ROLDÁN et al. 2004a).

Pigment autofluorescence, nucleic acids and polysaccharides of undamaged biofilm fragments were studied with Confocal scanning laser microscopy (CSLM). Nucleic acids were specifically stained with Hoechst 33258 (Molecular Probes, Inc.), polysaccharides were labeled with the carbohydrate recognizing lectin Concanavalin A-AlexaFluor 488 (Suco-Con-A, Molecular Probes, Inc.). CSLM was performed using a Leica microscope, model TCS-SP2 (Leica Microsystems, Mannheim, Germany). Autofluorescence from photosynthetic pigments was viewed in the red channel (590–800 nm) using 543- and 633-nm excitation wavelengths (Ar/HeNe laser).

Nucleic acids were collected at 400–480 nm (blue fluorescence) using 351- and 364-nm excitation wavelengths from an argon laser. Polysaccharides were observed at 490–530 nm (green fluorescence) using 488-nm excitation wavelength from an argon laser.

In order to map the spatial distribution of fluorescence of pigments, DNA, and polysaccharides in the samples, optical sections of biofilms were collected separately in multi-channels as Z-series (3D imaging).

Image combining and processing were performed with Imaris™ V. 2.7. (Bitplane AG Zürich, Switzerland) image analysis program. Biofilms were observed at 100X, 630X, and 1000X with the CSLM device.

Samples for TEM were fixed in a solution of 2% glutaraldehyde in 0.1 M cacodylate buffer and post-fixed with 1% osmium tetroxide in the same buffer. The sections were viewed using a Hitachi H800MT transmission electron microscope operating at 100kV.

## Results

### LM observations of living biofilms

Many cyanobacterial filaments were interwoven forming 3D structures that left air spaces among them. Individual trichomes of *Scytonema julianum* and *S. ocellatum* had some ends attached to the solid surfaces. Bundles of filaments of *Lepidolyngbya* spp. were mainly creeping on the substrata and on top of other organisms, with some individual trichome extending out of the common sheath.

The first visible sign of hormogonia differentiation in *Scytonema* spp. was the formation of necridic cells that separated short fragments from the main trichome (Fig. 1a). Necridia had a cupping glass shape and faded colour, similar to the colour of dead cells. Hormogonia formation was evidenced by the development of cells that were smaller and differently shaped than vegetative cells. Necridia and hormogonia were scarce, though present along the year. When hormogonia detached from the parental trichome, the debris of necridic cells remained at one or both tips of the newly isolated hormogonia as terminal or subterminal cells (Fig. 1b). Hormogonia of *Scytonema julianum* and *S. ocellatum* moved apparently not at random but with a tip towards the substratum, which may explain their distribution in the biofilm. These species usually were attached at the surface of the substrata, which is at the bottom layer of the biofilm, and grew erect.

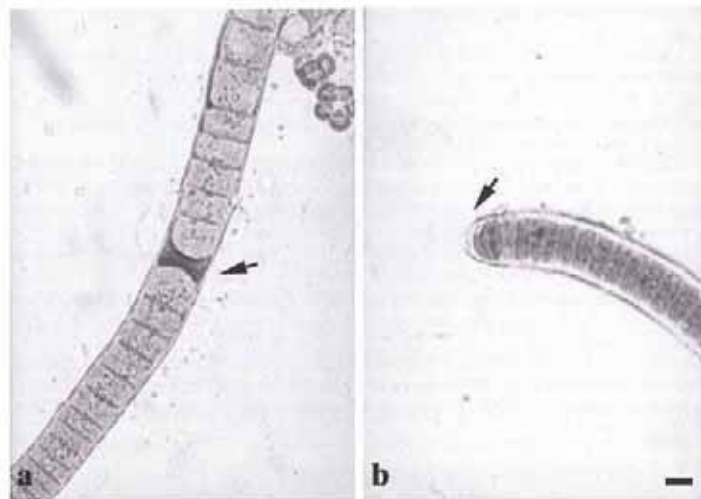


Fig. 1. Light micrographs of *Scytonema ocellatum* var. *purpureum* (a) and *Scytonema julianum* (b). **a** – Necridic cell with cupping glass shape and faded colour (arrow). **b** – Apical pad (arrow). [Scale bar = 10  $\mu$ m.]

Trichomes of *Leptolyngbya* spp. were either isolated or within a common sheath, packed tightly or loosely and twisting around one another. Inside the filaments hormogonia were separated by necridic cells from the rest of the trichome. Free hormogonia could be attached to adjacent organisms or any type of substrata.

#### CLSM observations

The stage of cell division could be ascertained by means of autofluorescence intensity and the shape and size of nucleoids stained in blue with the fluorophore Hoechst 33258. Cells with high red auto-fluorescence or ongoing division figures indicated active growth (Fig. 2). Cells with low auto-fluorescence indicated senescence (ROLDÁN et al. 2004b).

The cells that started to adopt the cupping glass shape characteristic of the necridia presented higher pigment fluorescence than any of the neighbouring cells (Fig. 2a). Next, necridia presented a weak increase of polysaccharides, as revealed by the green Con-A label (Fig. 2b). Meanwhile, nucleoids from the cells that became hormogonia adopted a string of beads appearance, as a result of simultaneous divisions without changes in cell size (Fig. 2b). At the final step of the transformation process, necridia only showed a strong polysaccharidic fluorescence (Fig. 2c), sometimes enhanced by EPS formation in adjacent cells (Fig. 2d). The newly formed hormogonia of *Scytonema* spp. and *Leptolyngbya* spp. still had necridia debris attached to their tips (Figs. 2 e, f). Serial sections of apical pads revealed that they maintained the cupping glass shape of necridia (Figs. 2g-j) and their strong green fluorescence, characteristic of polysaccharides.

#### TEM observations

Figure 3a shows TEM images of *Leptolyngbya* sp. necridic cells that undergo strong changes in their content, the nucleoid was no longer visible and thylakoids were destroyed. In addition its hormogonia presented an attached pad at their tip (Fig. 3b).

In figure 4 the morphological changes in the differentiation and release of necridia and hormogonia and their attachment to a solid substratum are schematised.

#### Discussion

It is well established that hormogonia are the diaspores of filamentous cyanobacteria. The pioneer work of FATTOM & SHILO (1984) described hydrophilic mucilage in hormogonia, which act reducing the surface tension and facilitate their gliding motility. However, little is known in terms of the necridia function and adherence properties of hormogonia with the colonised surfaces. Studies on hormogonia are mostly focused on *Nostoc* symbiosis (COHEN & MEERS 1997,

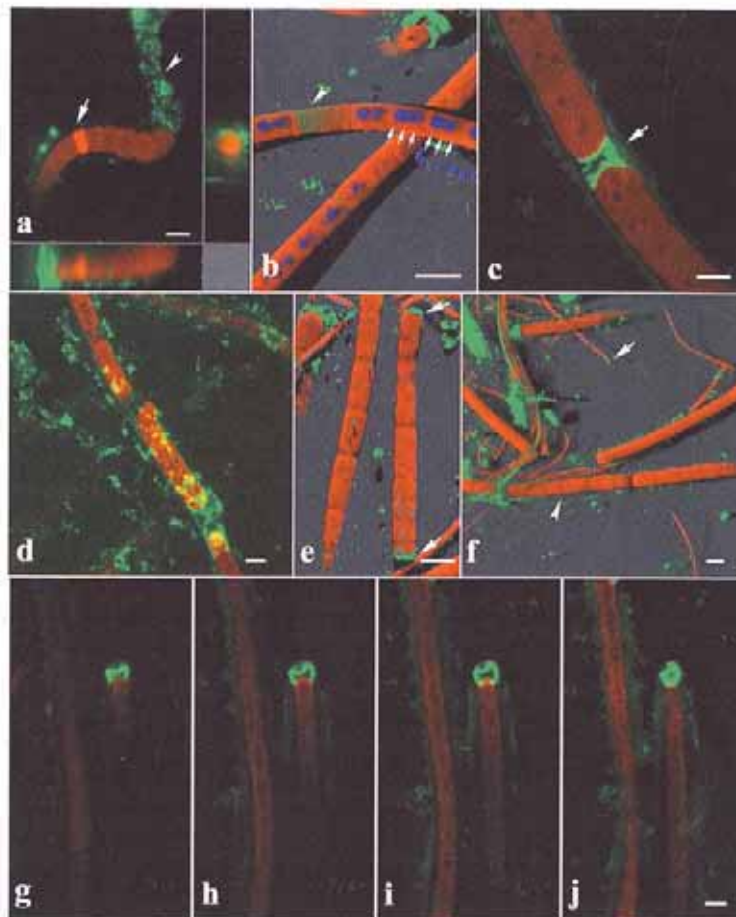


Fig. 2. Confocal microscope images of filaments of *Scytonema* spp. and *Leptolyngbya* spp. in vegetative growth state and different stages of hormogonium cycle. Biofilm samples come from Papellona cave (a, c, d, f-i) and St. Callistus cutacombs (b, e, j). Pigment fluorescence is shown as red colour, polysaccharides labelled with Con-A-AlexaFluor 488 as green colour, and nucleic acids stained with Hoechst 33258 as blue colour. **a** – Extended focus projection showing pigment fluorescence and Con-A-AlexaFluor 488 of *Scytonema ocellatum*. The central image shows the *xy*-projection and the bottom and right images show the *xz*- and *yz*- projections along the depth. The right and bottom side of the *yz*- and the *xz*- section, respectively, correspond to the substratum. Note a necridic cell with high pigment fluorescence (arrow) and debris of the sheath (arrowhead). **b** – Three-channel simulated fluorescence projection (SFP). A necridic cell in a further stage of differentiation is not stained with Hoechst 33258 label and has produced polysaccharides which are labelled with Con-A (arrowhead). An hormogonium is distinguished at the right of the necridium by its dividing nucleoids (small arrows) with a

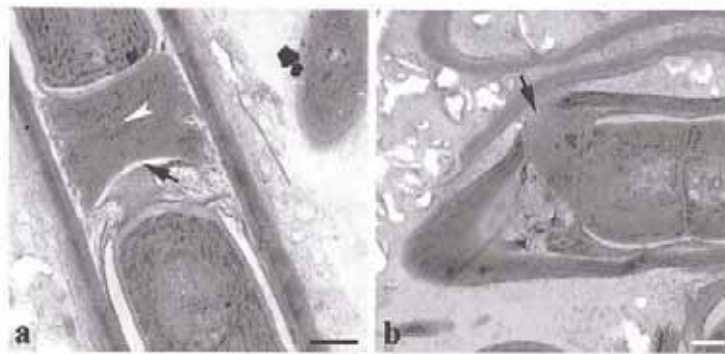


Fig. 3. TEM micrographs of *Leptolyngbya* sp. **a** – Necridic cell showing internal changes, including thylakoidal degradation (arrowhead) and the early stage of the apical pad formation (arrow). **b** – Hormogonium apical pad (arrow). The hormogonium is opening up through a break in the sheath. [Scale bar = 0.5  $\mu\text{m}$ .]

MEEKS & ELHAI 2002, CAMPBELL et al. 2003) that mainly fragment between two vegetative cells or at heterocytes (KOMÁREK & ANAGNOSTIDIS 1989). To date, necridia have only been recognised as responsible for trichome breakage (ANAGNOSTIDIS & KOMÁREK 1988 and references therein) or as a “short segment of trail extending beyond the front of the pre-release hormogonium” (HERNÁNDEZ-MUÑIZ & STEVENS 1987) but their transformation into an apical pad has not been reported.

Further, in the case polysaccharides were reported on hormogonia, they were not localized at their tips but as slime surrounding them, both for motile hormogonia of *Nostoc commune*, (BAZZICHELLI et al. 1985) and for non motile hormogonia of *N. punctiforme* (SCHUESSLER et al. 1997).

In general, fixation and dehydration artefacts associated with the preparation for TEM make difficult the observation of polysaccharides. In the present work the events that led to mucilaginous pad formation were also difficult to interpret.

string of beads appearance as a result of simultaneous divisions. **e** – Two-channel optical section (pigment fluorescence and polysaccharides) of necridic cells showing strong polysaccharide fluorescence. **d** – Two-channel maximum intensity projection (pigment fluorescence and polysaccharides). Hormogonia are liberating out of the parent sheath. **e** – Two-channel simulated fluorescence projection of free hormogonia with apical pads (arrows). Note that hormogonia cells are shorter than those of vegetative filaments at left. **f** – Two-channel simulated fluorescence projection (pigment fluorescence and polysaccharides) of a biofilm. Hormogonia of *Scytonema julianum* (arrowhead) and *Leptolyngbya* sp. (arrow) have polysaccharidic apical pads. **g** – Two-channel (pigment fluorescence and polysaccharides) xy optical sections of *Scytonema julianum*. Four out of 10 optical sections of an apical necridium debris, showing the cupping glass shape of the pad. [Scale bar = 10  $\mu\text{m}$ .]



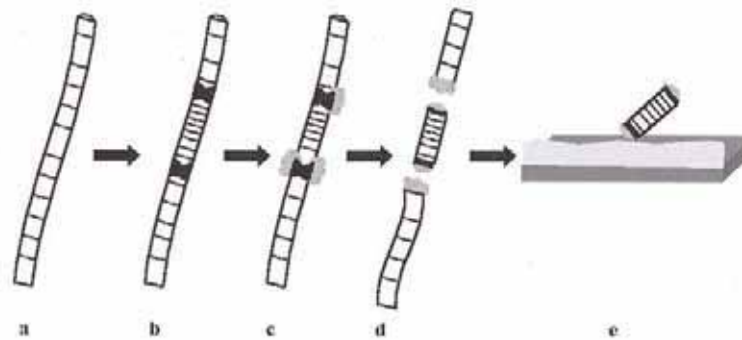


Fig. 4. A simplified schema illustrating the morphological development of hormogonia in some filamentous cyanobacteria.

**a** – The filament consists entirely of vegetative cells. The development of hormogonia is triggered by a variety of environmental changes, both positive and negative for growth. **b** – Vegetative cells at the terminal or subterminal tips of parental filaments divide without simultaneous increase in cell biomass. Some cells differentiate into necridia. Necridia are situated at one side of the hormogonium or both sides, in the case of subterminal hormogonia. Necridia are characterized by their cupping glass shape and increased fluorescence. **c** – During their development necridia transform their content into polysaccharidic substances. **d** – The hormogonium moves out of the parental sheath by active gliding, maintaining the mucilaginous necridium attached at its tip. **e** – Attachment of the hormogonium to the solid substratum.

We have only been able to distinguish the presence of polysaccharides and the cupping glass shape in necridia remains by means of sequential images of autofluorescence and labeling of DNA and polysaccharides. Assessment of CSLM and TEM images suggest that the contents of necridic cells had changed to a mucilaginous pad, maintaining their cupping glass shape. Thus, we propose that changes in necridia may help to stick and attach hormogonia to the substratum due to the glue-like adhesion of polysaccharidic substances. Necridia are not cells that just die to help the release of hormogonia but they transform and adapt themselves for their final function, the attachment of hormogonia. This mechanism can act in conjunction with other adhesion mechanisms.

The differentiation of necridia into specialized cells involves extensive biochemical and structural changes, the molecular bases of which are not known. In contrast, drastic changes also occur during differentiation of heterocytes (HERRERO et al. 2004, MEEKS et al. 2002) that are well understood, at least in symbiotic strains of *Nostoc* (ADAMS & DUGGAN 1999, MEEKS & ELHAI 2002, MEEKS et al. 2002). The first stage in necridium differentiation is a high increase in fluorescence that characterizes the loss of photosystem II activity, which is well described for heterocytes (MEEKS & ELHAI 2002). The transformation of the cupping glass necridium to a polysaccharidic pad, must involve either repression or differential protein synthesis as reported for heterocytes glycolipids that are pro-

duced and used as a barrier to prevent the entry of O<sub>2</sub> (WOLK 1996 and references therein, ZHOU & WOLK 2003). Finally, necridia, as stated for heterocytes, are also "specialized cells specially selected and prepared for their fate" (EL-SHEHAWY & KLEINER 2003) that after the process does not re-enter the cell cycle and are sacrificed.

The application of the techniques here described has helped to illustrate and clarify the role of necridia in the initial attachment of hormogonia to the substrata. We can then postulate that colonization of habitats and plant infection by filamentous cyanobacteria is efficient in part because hormogonia and their sticky tips are involved. However more studies are needed to understand the significance of necridia remains and their contribution to the formation of biofilms.

#### Acknowledgements

This work was supported by EU Programme Energy, Environment and Sustainable Development in the frame of CATS Project, contract EVK4-CT-2000-00028. The authors would like to thank the Scientific and Technical Services of the University of Barcelona for their excellent technical assistance with the CSLM. Fruitful discussions with ESTER CLAVERO are also acknowledged.

#### References

- ADAMS, D. G. & DUGGAN P. S. (1999): Heterocyst and akinete differentiation in cyanobacteria. – *New Phytol.* **144**:1–33.
- ALBERTANO P., KOVÁČIK L. & CAIOLA M. G. (1994): Preliminary investigations on epilithic cyanophytes from a Roman Necropolis. – *Arch. Hydrobiol./Algolog. Stud.* **105**: 71–74.
- ANAGNOSTIDIS K. & KOMÁREK J. (1988): Modern approach to the classification system of cyanophytes. 3-Oscillatoriales. – *Arch. Hydrobiol./Algolog. Stud.* **50–53**: 327–472.
- BAKKER D. P., POSTMUS B. R., BUSSCHER H. J. & VAN DER MEI H. C. (2004): Bacterial strains isolated from different niches can exhibit different patterns of adhesion to substrata. – *Appl. Environ. Microbiol.* **70**: 3758–3760.
- BLENKINSOPP S. A. & COSTERTON J. W. (1991): Understanding bacterial biofilms. – *Trends Biotechnol.* **9**: 138–143.
- BAZZICHELLI G., ABDELAHAD N. & VENTOLA F. (1985): Structural modifications in the extracellular investment of *Nostoc commune* VAUCH. during the life cycle. I. Motile and nonmotile hormogonium, biseriata stage. – *J. Ultrastruct. Res.* **91**: 174–181.
- CAMPBELL E. L. & MEEKS J. C. (1989): Characteristics of hormogonia formation by symbiotic *Nostoc* spp. in response to the presence of *Anthoceros punctatus* or its extracellular products. – *Appl. Environ. Microbiol.* **55**: 125–131.
- CAMPBELL E. L., WONG F. C. Y. & MEEKS J. C. (2003): DNA binding properties of the HrmR protein of *Nostoc punctiforme* responsible for transcriptional regulation of genes involved in the differentiation of hormogonia. – *Mol. Microbiol.* **47**: 573–582.
- COHEN M. F. & MEEKS J. C. (1997): A hormogonium regulating locus, *hrm UA*, of the cyanobacterium *Nostoc punctiforme* strain ATCC 29133 and its response to an extract of a symbiotic partner *Anthoceros punctatus*. – *Mol. Plant - Microbe Int.* **10**: 280–289.
- COSTERTON J. W., STEWART P. S. & GREENBERG E. P. (1999): Bacterial biofilms: a common cause of persistent infections. – *Science* **284**:1318–1322.
- DE PHILIPPIS R. & VINCENZINI M. (1998): Exocellular polysaccharides from cyanobacteria and their possible applications. – *FEMS Microbiol. Rev.* **22**: 151–175.

- DUNNE W. M. JR. (2002): Bacterial Adhesion: Seen Any Good Biofilms Lately? – *Clinical Microbiol. Rev.* **15**: 155–166.
- EL-SHEHAWY R. M. & KLEINER D. (2003): The mystique of irreversibility in cyanobacterial heterocyst formation: parallels to differentiation and senescence in eukaryotic cells. – *Physiol. Plant.* **119**: 49–55.
- FATTOM A. & SHILO M. (1984): Hydrophobicity as an adhesion mechanisms of benthic cyanobacteria. – *Appl. Environ. Microbiol.* **47**: 135–143.
- FINLAY B. B. & FALKOW S. (1997): Common themes in microbial pathogenicity: revisited. – *Microbiol. Mol. Biol. Rev.* **61**: 136–169.
- HERDMAN M. & RIPPKA R. (1988): Cellular differentiation: hormogonia and bacocytes. – *Methods Enzymol.* **167**: 232–242.
- HERMANSSON M. (1999): The DLVO theory in microbial adhesion. – *Colloids Surf., B: Biointerfaces* **14**: 105–119.
- HERNÁNDEZ-MARINÉ M., CLAVERO E. & ROLDÁN M. (2003): Why there is such luxurious growth in the hipogean environments. – *Arch. Hydrobiol./Algolog. Stud.* **109**: 229–239.
- HERNÁNDEZ-MUÑOZ W. & STEVENS E. JR. (1987): Characterization of the motile hormogonia of *Mastigocladus laminosus*. – *J. Bacteriol.* **169**: 218–223.
- HERRERO A., MUÑOZ-PASTOR A. M., VALLADARES A. & FLORES E. (2004): Cellular differentiation and the NtcA transcription factor in filamentous cyanobacteria. – *FEMS Microbiol. Rev.* **28**: 469–487.
- HOKPUTSA S., HU C., PAULSEN B. S. & HARDING S. E. (2003): A physico-chemical comparative study on extracellular carbohydrate polymers from five desert algae. – *Carbohydr. Polym.* **54**: 27–32.
- HU C., LIU Y., PAULSEN B. S., PETERSEN D. & KLAVENESS D. (2003): Extracellular carbohydrate polymers from five desert soil algae with different cohesion in the stabilization of fine sand grain. – *Carbohydr. Polym.* **54**: 33–42.
- JUCKER B. A., ZEHNDER A. B. & HAUKEHARM S. (1998): Quantification of polymer interactions in bacterial adhesion. – *Environ. Sci. Technol.* **32**: 2909–2915.
- KOHL F. G. (1903): Über die Organisation und Physiologie der Cyanophyceenzelle. – Gustav Fischer, Jena, Germany.
- KOMÁREK J. & ANAGNOSTIDIS K. (1989): Modern approach to the classification system of cyanophytes. 4-Nostocales. – *Arch. Hydrobiol./Algolog. Stud.* **56**: 247–345.
- LAMENTI G., TIANO P. & TOMASELLI L. (2000): Biodeterioration of ornamental marble statues in the Boboli Gardens (Florence, Italy). – *J. Appl. Phycol.* **12**: 427–433.
- MEEKS, J. C. (1998): Symbiosis between nitrogen-fixing cyanobacteria and plants. – *Bio-science* **48**: 266–276.
- MEEKS J. C., CAMPBELL E. L., SUMMERS M. L. & WONG F. C. (2002): Cellular differentiation in the cyanobacterium *Nostoc punctiforme*. – *Arch. Microbiol.* **178**: 395–403.
- MEEKS J. C. & ELHAI J. (2002): Regulation of cellular differentiation in filamentous Cyanobacteria in free-living and plant-associated symbiotic growth states. – *Microbiol. Mol. Biol. Rev.* **66**: 94–121.
- ORTEGA-CALVO J. J., ARIÑO X., HERNÁNDEZ-MARINÉ M. & SAIZ-JIMENEZ C. (1995): Factors affecting the weathering and colonisation of monuments by phototrophic microorganisms. – *Sci. Tot. Environ.* **167**: 329–341.
- ROLDÁN M., CLAVERO E., CANALS T., GÓMEZ-BOLFA A., ARIÑO X. & HERNÁNDEZ-MARINÉ M. (2004a): Distribution of phototrophic biofilms in cavities (Garraf, Spain). – *Nova Hedwigia* **78** (3-4): 329–351.
- ROLDÁN M., CLAVERO E., CASTEL S. & HERNÁNDEZ-MARINÉ M. (2004b): Biofilms fluorescence and image analysis in hypogean monuments research. – *Arch. Hydrobiol./Algolog. Stud.* **111**: 127–143.
- SCHUESSLER A., MEYER T., GEHRIG H. & KLUGE M. (1997): Variations of lectin binding sites in extracellular glycoconjugates during the life cycle of *Nostoc punctiforme*, a potentially endosymbiotic cyanobacterium. – *Eur. J. Phycol.* **32**: 233–239.
- SUTHERLAND I. W. (2001): Biofilm exopolysaccharides: a strong and sticky framework. – *Microbiology* **147**: 1–9.

## Adherence of hormogonia to substrata by polysaccharides

249

- TANDEAU DE MARSAC N. (1994): Differentiation of hormogonia and relationships with other biological processes. – In: BRYANT D. A. (ed.): *The molecular biology of cyanobacteria*, p. 825–842, Kluwer Academic Publishers, Boston, Mass.
- VAN OSS C. J., GOOD R. J. & CHAUDHURY M. K. (1986): The role of Van der Waals forces and hydrogen bonds in hydrophobic interactions between biopolymers and low energy surfaces. – *J. Colloid Interface Sci.* **111**: 378–390.
- WOLK C. P. (1996): Heterocyst formation. – *Annu. Rev. Genet.* **30**: 59–78.
- ZHOU R. & WOLK C. P. (2003): A two-component system mediates developmental regulation of biosynthesis of a heterocyst polysaccharide. – *J. Biol. Chem.* **278**: 19939–19946.

## The authors' address:

MARIONA HERNÁNDEZ-MARINÉ,  
MÓNICA ROLDÁN,  
Universitat de Barcelona  
Facultat de Farmàcia  
Unitat de Botànica  
Av. Joan XXIII s/n  
E-08028, Barcelona, Spain.  
marionahernandez@ub.edu

*Resultats*

---

---

#### 4.8. Pot influir la llum verda en les propietats de la fluorescència i l'estructura dels biofilms fototròfics?

La il·luminació artificial pot alterar els monuments hipogeus induint la formació de biofilms fototròfics que causen biodeterioració i/o alteració estètica de les superfícies. Nosaltres examinem l'efecte de la llum blanca (WL) o verda (GL) en biofilms formats per *Gloeotheca membranacea* (Cyanobacteria) i *Chlorella sorokiniana* (Chlorophyta), totes dues espècies presents en hàbitats de baixa il·luminació, amb l'objectiu d'avaluar el potencial de la llum verda per prevenir el creixement del biofilms fototròfics.

Es va utilitzar el microscopi de rastreig làser confocal espectral per examinar fotopigments, DNA i polisacàrids extracel·lulars (EPS) i les sèries obtingudes utilitzades per realitzar l'anàlisi quantitativa de l'estructura dels biofilms. Es van mesurar les característiques de la fluorescència i la mida de l'aparell fotosintètic de cèl·lules individualitzades.

Sota llum verda (GL), les dimensions de les regions dels til·lacoides van ser significativament més petites en ambdues espècies que en llum blanca. L'aparell fotosintètic de cèl·lules en GL presenta significativament menys intensitat de fluorescència mitjana (MFI, acrònim de l'anglès) en ambdues espècies, així mateix la densitat d'EPS en biofilms formats per *G. membranacea* és menor que en els de llum blanca. Mentre que aquests efectes van ser moderats per *G. membranacea* per l'adaptació cromàtica, *C. sorokiniana* va patir gran estrès sota llum verda. La resposta dels biofilms a la llum verda comprèn diferències en la fluorescència dels pigments, el gruix dels biofilms i el biovolum, així com simplificació de la seva estructura tridimensional, si comparem amb els biofilms sota llum blanca (WL). Els resultats suggereixen que la llum verda contribueix al decreixement de la diversitat específica i, per tant, pot esdevenir una estratègia eficient per controlar el desenvolupament dels biofilms fototròfics en monuments hipogeus il·luminats artificialment.

Els resultats detallats d'aquest capítol s'inclouen en el següent article:

Does green light influence the fluorescence properties and structure of phototrophic biofilms? ***Appl. Environ. Microbiol.*** (2006), 72 (4): 3026-3031.

## Does Green Light Influence the Fluorescence Properties and Structure of Phototrophic Biofilms?

M. Roldán,<sup>1</sup> F. Oliva,<sup>2</sup> M. A. González del Valle,<sup>3</sup> C. Saiz-Jimenez,<sup>3</sup> and M. Hernández-Marín<sup>1\*</sup>

*Departament de Productes Naturals, Biologia Vegetal i Edafologia, Universitat de Barcelona, Av. Joan XXIII s/n, 08028 Barcelona, Spain<sup>1</sup>; Departament d'Estadística, Facultat de Biologia, Universitat de Barcelona, Av. Diagonal 645, 08028 Barcelona, Spain<sup>2</sup>; and Instituto de Recursos Naturales y Agrobiología, CSIC, Sevilla, Spain<sup>3</sup>*

Received 26 August 2005/Accepted 2 February 2006

**Artificial illumination can harm works of art by inducing the development of photosynthetic biofilms. With the aim of preventing biodeterioration or esthetic damage to such surfaces, we evaluated and compared the effects of illuminating biofilms formed by *Gloeotheca membranacea* (cyanobacteria) and *Chlorella sorokiniana* (Chlorophyta) using exclusively white or green light.**

Inappropriate artificial illumination of archaeological remains and their interior works of art (1, 2, 3, 4) results in the uncontrolled development of photosynthetic microorganisms, primarily cyanobacteria and microalgae (10, 13, 15, 19, 20), forming greenish biofilms that contribute to surface biodeterioration. These organisms feature a matrix composed primarily of exopolymers (EPS) that are involved in the resistance of biofilms to adverse abiotic conditions as well as in attachment (3, 5, 6, 24). Owing to their hygroscopicity (7, 8, 11, 28), EPS can be particularly harmful to archaeologically valuable surfaces. Control efforts usually focus on cleaning damaged surfaces or on chemical treatments that have little efficacy against biofilms (5, 14). Hence, there is an ever-increasing interest in the development of alternative strategies for preventing and minimizing biofilm development.

Changes in spectral ambient light produce variations in pigment distribution and abundance for cyanobacteria and microalgae (17, 18, 23). In particular, green light (GL) retards growth (9), causes vacuolation in the thylakoidal system (1), and affects pigment composition (25) and fine structure (1). GL is also advantageous since it represents the maximum absorbance of human vision. We thus sought to evaluate the potential for GL to prevent biofilm growth by comparing the responses of artificial biofilms exposed to either GL or white light (WL).

**Biofilm preparation.** Sterilized lime-pozzolana slabs (three slabs, 3 by 1 cm) were inoculated with 1 g of a mixture of *Gloeotheca membranacea* Bornet CCAP1430/3 (Pasteur Culture Collection, Paris, France) and *Chlorella sorokiniana* Shih and Krauss SAG 211-32 (Centro de Investigaciones Científicas, Isla de La Cartuja, Seville, Spain). The slabs were placed in petri dishes and stored at 19 to 22°C under continuous GL (Narva LT 18 W/017 green TT; Narva, Czech Republic) or WL (Chiyoda F 15 S daylight; Chiyoda Corporation, Japan) at a constant photon flux density of 20  $\mu\text{mol} \cdot \text{m}^{-2} \cdot \text{s}^{-1}$  for 60 days. The emission spectra of the lamps were measured with a LICOR (Lincoln, NE) Li-1800 spectroradiometer (Fig. 1).

**CSLM.** Confocal scanning laser microscopy (CSLM) was performed to establish possible differences between GL and WL treatments in morphology, size of thylakoidal areas, and architecture of biofilms (20), for which a Leica TCS-SP2 (Leica Microsystems Heidelberg GmbH, Mannheim, Germany) was used. Autofluorescence from photosynthetic pigments (PP) was excited with the 543- and 633-nm lines of an Ar/HeNe laser and observed in the red channel at an emission range of 590 to 800 nm. EPS were labeled with the carbohydrate-recognizing lectin concanavalin A (ConA)-Alexa Fluor 488 (Molecular Probes, Inc., Eugene, OR), excited with the 488-nm line of an Ar laser, and viewed in the green channel at 490 to 530 nm. Unlabeled organisms were used for a staining control. To determine the spatial relationship between pigment fluorescence and EPS, bichannel images were acquired in the *x-y* plane at different intervals along the *z* axis. The thickness of the sample was established as the distance from the highest position to the lowest position of inherent pigment fluorescence. Image combining and processing were performed with the Imaris software package, version 2.7 (Bitplane AG, Zürich, Switzerland) (20).

**Analysis of organisms.** Slabs maintained under GL exhibited colonies of two to four cells of *G. membranacea* surrounded by a relatively thick sheath in which only the oldest wrecked external layers were labeled by ConA (Fig. 2A). Membrane vacuolated thylakoids were seen as empty spaces inside the cells (Fig. 2C). Slabs kept under WL displayed *G. membranacea* colonies with a larger number of cells (with 54.1% having more than four cells) surrounded by an apparently compact sheath that was strongly labeled in green in all layers (Fig. 2B); *C. sorokiniana* was nearly absent in slabs maintained under GL (Fig. 2A and C), showing negative selection under this spectral quality (27).

Metamorph software (Universal Imaging Corp.) was used to measure pigment fluorescence regions in three-dimensional projections of unlabeled cells. Data sets were exported into Microsoft Excel for analysis. In GL, the mean dimensions (length by width) for *G. membranacea* (26 cells) were 6.23  $\pm$  1.32  $\mu\text{m}$  by 4.52  $\pm$  0.40  $\mu\text{m}$ ; in WL (17 cells), the mean dimensions were 6.91  $\pm$  1.77  $\mu\text{m}$  by 5.42  $\pm$  0.55  $\mu\text{m}$ . For *C. sorokiniana*, the mean dimensions under GL (48 cells) were 3.18  $\pm$  0.52  $\mu\text{m}$  by 2.65  $\pm$  0.57  $\mu\text{m}$ ; in WL, the mean dimen-

\* Corresponding author. Mailing address: Departament de Productes Naturals, Biologia Vegetal i Edafologia, Universitat de Barcelona, Av. Joan XXIII s/n, E-08028 Barcelona, Spain. Phone: (34) 93 4024490. Fax: (34) 93 4035879. E-mail: marionahernandez@ub.edu.



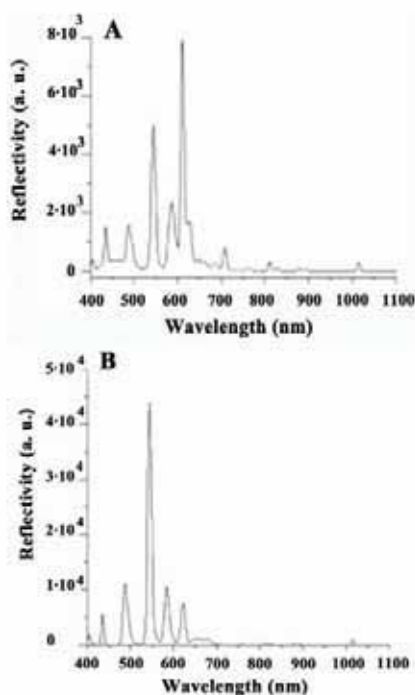


FIG. 1. Spectral emission of the two fluorescent light sources, white (A) and green (B) light, in the 400- to 1,100-nm range at a photon flux density of  $20 \mu\text{mol} \cdot \text{m}^{-2} \cdot \text{s}^{-1}$ . In addition to a peak at 544 nm, the green lamps gave two small shoulders at 425 to 450 nm and at 480 to 510 nm, wavelengths at which PC and PE absorb energy.

sions (54 cells) were  $3.43 \pm 0.71 \mu\text{m}$  by  $2.88 \pm 0.6 \mu\text{m}$ . The results for each species were processed with a one-way analysis of variance (ANOVA) model using SAS software. Thylakoid region width for *G. membranacea* in GL compared to that in WL ( $F_{1,41} = 38.12$ ;  $P = 0.000$ ) and the thylakoid region length ( $F_{1,100} = 4.09$ ;  $P = 0.046$ ) and width ( $F_{1,100} = 3.83$ ;  $P = 0.053$ ) for *C. sorokiniana* were statistically significantly smaller. Both species exhibited restricted cell volume, a strategy used by organisms to decrease energy demands (26).

**Analysis of biofilms.** Quantitative analysis of biofilm structure was carried out with the GNU Public License program (Departament de Llenguatges i Sistemes Informàtics, Universitat Politècnica de Catalunya [https://lafarga.cpl.upc.edu/projects/qbiof/]) based on the Comstat software package (12). Both GL- and WL-grown biofilms (Fig. 2 and Table 1) were formed by a layer of *G. membranacea*, with the colonies being thinner and more compact in WL (Fig. 2A and B). For biofilms exposed to GL, *C. sorokiniana* was scarce (Fig. 2A and C), whereas in WL (Fig. 2B and D), it had an irregular density. PP

biovolume ( $\mu\text{m}^3 \cdot \mu\text{m}^{-2}$ ) was larger for GL biofilms (Table 1), whereas the PP roughness coefficient, which provides a measure of how much the thickness of the biofilm varies, and PP biofilm porosity (16) were much lower than in WL (Table 1). The EPS porosity and roughness coefficient were higher in GL than in WL (Table 1).

ConA labeling of *G. membranacea* grown in WL suggests that its EPS contain  $\alpha$ -D-mannose and/or  $\alpha$ -D-glucose residues, sugars to which ConA binds with high specificity (22). In GL, EPS of this type were not produced; the labeled outer rings correspond to remains from the original culture. The low efficiency of light absorption of chlorophyll (Chl) *a* in GL for *G. membranacea* biofilms and the concomitant changes in EPS production (8, 22) would result in a weaker attachment to the substratum (6, 11) and a reduction in tolerance to desiccation stress (24).

**Analysis of pigment fluorescence: lambda scan function.** The fluorescence spectra of pigments were obtained in single cells from the intact biofilms by a noninvasive method (21) using a Leica TCS-SP2 microscope. Gains and offsets were equal for each field at different excitation wavelengths ( $\lambda_{exc}$ s) and remained constant during the scanning process. To determine the spectral signature of a selected area from the scanned image (Fig. 3A and 4A),  $1\text{-}\mu\text{m}^2$  regions of interest (ROIs) taken from the thylakoid region inside the cell were established for each  $x$ - $y$ - $\lambda$  stack of images.

Lambda scans of both species ( $n = 20$  ROIs) obtained for each  $\lambda_{exc}$  in at least three independent experiments show that mean fluorescence intensity (MFI) and the half-bandwidth of the spectra from both species were different for both light types, whereas the spectrum shapes were identical (Fig. 3 and 4).

In GL, the fluorescence spectra for all pigments in both species at all  $\lambda_{exc}$ s were less intense than those for WL (Fig. 3A and 4A). Both species grown under WL emitted only red fluorescence of Chl *a* when excited with UV light (351 nm) (Fig. 3A and 4A).

***Gloeothece membranacea.*** In both WL and GL, fluorescence was weaker at a  $\lambda_{exc}$  of 488 nm (blue region) than at a  $\lambda_{exc}$  of 543 nm, where the Chl *a* receives its energy from phycobilins (20). C-phycoerythrin (PE) showed fluorescence at an emission wavelength of ca. 580 nm when excited at 488 nm and at its optimum  $\lambda_{exc}$  (543 nm). Upon comparison of the MFI at  $\lambda_{exc}$ s of 488 and 543 nm in both treatments, the MFI was observed to be lower in the blue region (Fig. 3B).

For the GL sample, the highest maximum for *G. membranacea* corresponded to Chl *a* (ca. 670.7 nm), and its strongest emission was at a  $\lambda_{exc}$  of 488 nm. The content of PE pigment was higher than in WL, which has previously been reported as a response to low light or as a chromatic adaptation, allowing the organism to harvest light from the green-yellow bandwidths (18, 28).

The emission bands for WL samples were considerably higher (659.3 to 666.4 nm) than those for GL samples, corresponding to the phycobiliproteins C-phycoerythrin (PC) and allophycocyanin (APC) (Fig. 3B); however, the proportion of Chl *a* fluorescence to total pigment fluorescence was much lower.

***Chlorella sorokiniana.*** At a  $\lambda_{exc}$  of 488 nm, differences in the Chl *a* maximum ( $\lambda_{max} = 687.9$  nm) were not observed for samples of either light type (Fig. 4).

The mean and standard error were calculated for all the ROIs

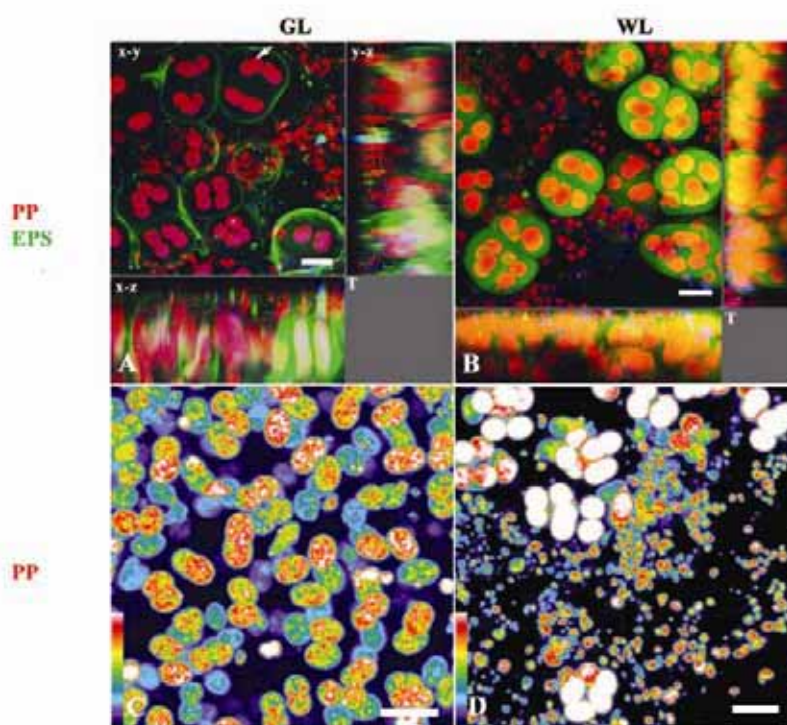


FIG. 2. CSLM three-dimensional images of biofilms under GL and WL conditions. The color assignment in the figures is red for PP and green for ConA lectin conjugated with Alexa Fluor 488-labeled EPS. (A) Detail of *Gloeotheca membranacea* colonies grown in GL. Shown is a bichannel extended-focus projection of 232  $x-y$  optical sections ( $z$  step = 0.2  $\mu\text{m}$ ). (B) Details of *G. membranacea* colonies grown in WL. *Chlorella sorokiniana* was found in the upper layer (T). Shown is a bichannel extended-focus projection of 142  $x-y$  optical sections ( $z$  step = 0.2  $\mu\text{m}$ ). (C and D) False color representation corresponding to the pigment autofluorescence. The color key is shown at the bottom left. (C) Thylakoidal PP in *G. membranacea*. Shown is a bichannel maximum intensity projection of 73  $x-y$  optical sections ( $z$  step = 0.2  $\mu\text{m}$ ). (D) Cells of *G. membranacea* and *C. sorokiniana*. Shown is a maximum intensity projection of 139  $x-y$  optical sections ( $z$  step = 0.2  $\mu\text{m}$ ). T, biofilm surface. Scale bar, 10  $\mu\text{m}$ .

examined at each  $\lambda_{exc}$ . For each species and line, the significance of the results was evaluated with a repeated measures ANOVA model. Three factors were taken into account: light treatment, emission wavelength, and cell. The cell factor is nested into the light treatment, and emission wavelength is the repeated measures factor ("within-subject effects" due to the fact that every cell is measured at all wavelengths). All three factors had statistically

significant differences ( $P < 0.05$  in all cases) for the two species at every line (351, 488, and 543 nm).

At a  $\lambda_{exc}$  of 351 nm, significant differences in MFI were found for the emission range of 649.5 to 683.4 nm, in which PC, APC, and Chl *a* emit. At a  $\lambda_{exc}$  of 488 nm, significant differences in MFI were found for the emission range of 573.6 to 590.7 nm, in which PE emits, and 653.6 to 659.3 nm, in which

TABLE 1. Quantitative analysis of biofilm structure<sup>a</sup>

Characteristic	PP-GL	PP-WL	EPS-GL	EPS-WL
Biovolume ( $\mu\text{m}^3 \cdot \mu\text{m}^{-2}$ )	7.12 $\pm$ 4.41	1.97 $\pm$ 0.38	4.91 $\pm$ 4.59	5.43 $\pm$ 2.50
Biofilm porosity (16)	1,046.1 $\pm$ 511.92	1,823.9 $\pm$ 990.57	37,863.23 $\pm$ 32,507.66	625.75 $\pm$ 334.57
Mean thickness ( $\mu\text{m}$ ) <sup>b</sup>	21.27 $\pm$ 11.36	6.6 $\pm$ 1.40	22.67 $\pm$ 19.03	20.27 $\pm$ 6.81
Roughness (12)	1.16 $\pm$ 0.15	1.35 $\pm$ 0.04	1.29 $\pm$ 0.24	0.55 $\pm$ 0.19

<sup>a</sup> Listed in the table are mean values from a total of 24 image stacks.

<sup>b</sup> Biofilm thickness in the different channels was calculated without considering the empty spaces that exist along the biofilm  $z$  axis.

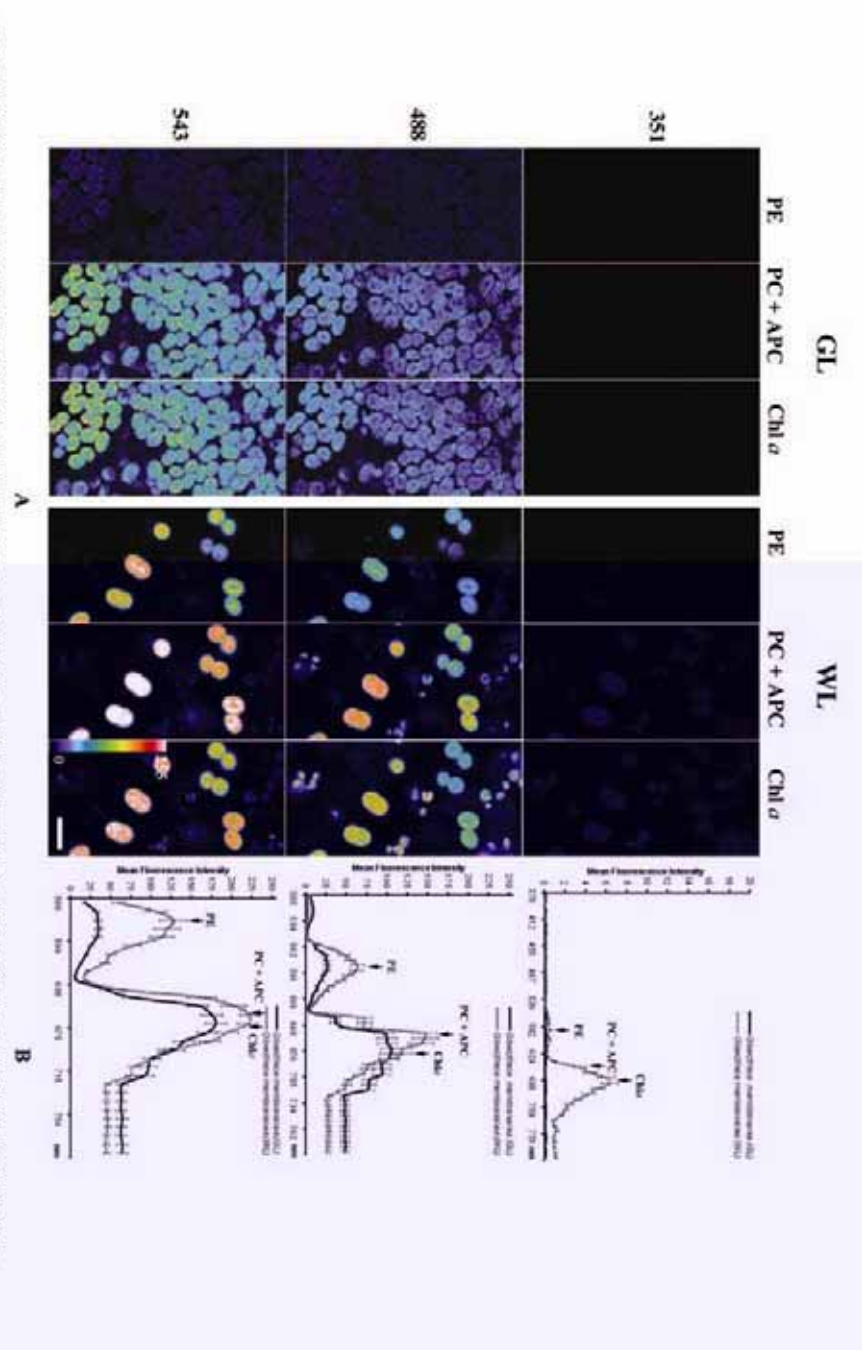


FIG. 3. In vivo CSLM images and lambda scans of *Gloeobacter moniliformis*. Optical sections and spectral profiles derived from  $\lambda_{exc}$ s of 351, 488, and 543 nm under WL- and GL-conditions. (A) False color representation corresponding to the  $\lambda_{exc}$  and fluorescence of Chl a and phycoerythrin from WL- and GL-spectral data sets for each of the three  $\lambda_{exc}$ s. The color key is shown at the bottom right. Each optical section corresponds to the maximum peak when excited with the corresponding  $\lambda_{exc}$  shown in the plots in B. (arrow). (B) Two-dimensional plots representing the MFI spectra for *G. moniliformis* under WL- and GL-conditions. Data are the means  $\pm$  standard errors from 20 cells of the three fields examined in each treatment. PE = APC, phycoerythrin plus allophycocyanin. Scale bar: 10  $\mu$ m.

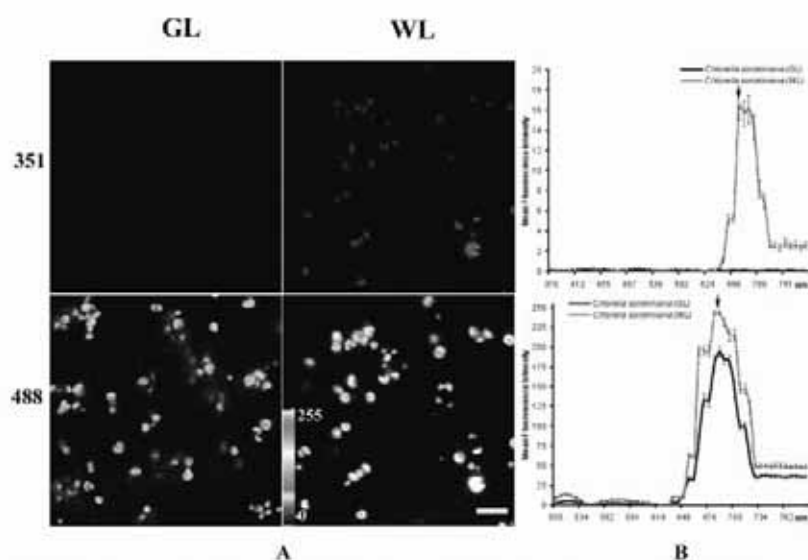


FIG. 4. In vivo CSLM images and lambda scans of *Chlorella sorokiniana*. Optical sections and spectral profiles derived from  $\lambda_{exc}$ s of 351 and 488 nm under WL and GL conditions are shown. (A) False color representation corresponding to the  $\lambda_{exc}$ s autofluorescence of Chl *a* and *b* from WL and GL spectral data sets for each of the two  $\lambda_{exc}$ s. The color key is shown at the bottom right. Optical sections correspond to the maximum peak when excited with the corresponding  $\lambda_{exc}$ s, shown in the plots in B (arrows). (B) Two-dimensional plots representing the MFI spectra for *C. sorokiniana* under WL and GL conditions. Data are the means  $\pm$  standard errors from 20 cells of the three fields examined in each treatment. Note the decrease in MFI of the pigments from GL treatment relative to the WL control. Scale bar, 10  $\mu$ m.

PC and APC emit. Finally, at a  $\lambda_{exc}$  of 543 nm, significant differences in MFI were found for the emission range of 567.8 to 598.8 nm, in which PE emits, 645.3 to 668.6 nm, in which PC and APC emit, and 684.1 nm, in which Chl *a* emits. Statistical analysis confirmed the significance of the results outlined above (Table 2).

**Conclusions.** The observations reported above suggest that GL could prevent the growth of photosynthetic organisms, except for those capable of modifying accessory pigments. However, even biofilms composed of the chromatic adaptable phycoerythrin-containing *G. membranacea* had lower photosynthetic pigment biovolume, smaller thylakoid regions, and a

TABLE 2. Three-way ANOVA of *G. membranacea* and *C. sorokiniana* in the different  $\lambda_{exc}$ s<sup>a</sup>

Organism and factor	$\lambda_{exc}$											
	351 nm				488 nm				543 nm			
	DF	SS	F	P	DF	SS	F	P	DF	SS	F	P
<i>G. membranacea</i>												
Light	1	679.52	50.18	0.000	1	80.669	4.48	0.042	1	294.516	12.32	0.001
Emission	9	430.09	41.11	0.000	13	656.421	128.68	0.000	12	1,276.629	153.28	0.000
Cell	34	460.43	9.29	0.000	34	612.197	46.47	0.000	34	812.562	35.94	0.000
Light and emission	9	551.85	42.07	0.000	13	38,109	7.57	0.000	12	116,083	14.55	0.000
Error	306	445.94			442	171,247			408	271,342		
<i>C. sorokiniana</i>												
Light	1	9,454.32	159.92	0.000	1	314,470	69.19	0.000				
Emission	5	1,122.52	71.16	0.000	7	226,461	82.44	0.000				
Cell	38	2,246.47	18.74	0.000	38	172,715	11.58	0.000				
Light and emission	5	1,123.45	71.22	0.000	7	42,126	15.34	0.000				
Error	190	599.41			266	104,384						

<sup>a</sup> Significant effects ( $P < 0.05$ ) are observed for the three factors (light treatment, wavelength, and cell) for the two species in every excitation line. DF, degrees of freedom; SS, sum of squares; F, experimental result, Fisher's F ratio; P, P value.

weaker MFI in GL than in WL, all of which are signs of retarded growth and thus suggest a possible treatment for preventing photosynthetic biofilm growth. Although laboratory data cannot be extrapolated to natural environments, our results have prompted studies of the application of green light to artificially illuminated works of art.

This work was supported by the EU Programme for Energy, Environment, and Sustainable Development in the CATS Project, contract EVK4-CT-2000-00028.

We thank the Scientific and Technical Services of the University of Barcelona for their excellent technical assistance with the CSLM and the Department of Fluid Mechanics Energy Engineering at the Superior School of Engineering of the University of Seville for their assistance with the spectral measurements of light sources.

## REFERENCES

- Albertano, P. 1991. Effects of monochromatic lights on four species of *Leptolyngbia*. Arch. Hydrobiol. Algal. Stud. 64:199-214.
- Albertano, P., and L. Bruno. 2003. The importance of light in the conservation of hypogean monuments, p. 171-177. In C. Saiz-Jiménez (ed.), Molecular biology and cultural heritage. Swets & Zeitlinger, Lisse, The Netherlands.
- Albertano, P., D. Moscone, G. Palleschi, B. Hermsolin, C. Saiz-Jiménez, S. Sánchez-Moral, M. Hernández-Marín, C. Urzú, I. Groth, V. Schroeckh, J. R. Gallon, F. Grazziotin, F. Bisconti, and R. Giuliani. 2003. Cyanobacteria attack rocks (CATS): control and preventive strategies to avoid damage caused by cyanobacteria and associated microorganisms in Roman hypogean monuments, p. 151-162. In C. Saiz-Jiménez (ed.), Molecular biology and cultural heritage. Swets & Zeitlinger, Lisse, The Netherlands.
- Ariño, X., M. Hernández-Marín, and C. Saiz-Jiménez. 1997. Colonization of Roman tombs by calcifying cyanobacteria. Phycologia 36:366-373.
- Costerton, J. W., P. S. Stewart, and E. P. Greenberg. 1999. Bacterial biofilms: a common cause of persistent infections. Science 284:1318-1322.
- Decho, A. W. 2000. Microbial biofilms in intertidal systems: an overview. Cont. Shelf Res. 20:1257-1273.
- De los Ríos, A., C. Ascaso, J. Wierzbos, E. Fernández-Valiente, and A. Quesada. 2004. Microstructural characterization of cyanobacterial mats from the McMurdo Ice Shelf, Antarctica. Appl. Environ. Microbiol. 70:569-580.
- De Philippis, R., and M. Vicenzini. 1998. Exocellular polysaccharides from cyanobacteria and their possible applications. FEMS Microbiol. Rev. 22:151-175.
- Hauschild, C. A., H. J. McMurter, and F. R. Pick. 1991. Effect of spectral quality on growth and pigmentation of picocyanobacteria. J. Phycol. 27:698-702.
- Hernández-Marín, M., E. Clavero, and M. Roldán. 2003. Why there is such luxurious growth in the hypogean environments. Arch. Hydrobiol. Algal. Stud. 109:229-239.
- Hernández-Marín, M., and M. Roldán. 2005. Adherence of hormogonia to substrata is mediated by polysaccharides produced by necridic cells. Arch. Hydrobiol. Algal. Stud. 117:239-249.
- Heydorn, A., A. T. Nielsen, M. Hentzer, C. Sternberg, M. Givskov, B. K. Ersbøll, and S. Molin. 2000. Quantification of biofilm structures by the novel computer program COMSTAT. Microbiology 146:2395-2407.
- Hoffmann, L. 2002. Caves and other low-light environments: aerophytic photoautotrophic microorganisms, p. 835-843. In G. Bitton (ed.), Encyclopedia of environmental microbiology. John Wiley & Sons, New York, N.Y.
- Kumar, R., and A. Kumar. 1999. Biodeterioration of stone in tropical environments. An overview. The Getty Conservation Institute, Los Angeles, Calif.
- Lefevre, M. 1974. La maladie verte de Lascaux. Stud. Conserv. 19:126-156.
- Lewandowski, Z. 2000. Notes on biofilm porosity. Water Res. 34:2620-2624.
- Millie, D. F., D. A. Ingram, and C. P. Dionigi. 1990. Pigment and photosynthetic responses of *Oscillatoria agardhii* (Cyanophyta) to photon flux density and spectral quality. J. Phycol. 26:660-666.
- Mullineaux, C. W. 2001. How do cyanobacteria sense and respond to light? Mol. Microbiol. 41:965-971.
- Ortega-Calvo, J. J., M. Hernández-Marín, and C. Saiz-Jiménez. 1993. Cyanobacteria and algae on historic buildings and monuments, p. 173-203. In K. L. Garg, H. Arai, and B. Rai (ed.), Recent advances in biodeterioration and biodegradation, vol. 1. Naya Prokash, Calcutta, India.
- Roldán, M., E. Clavero, S. Castel, and M. Hernández-Marín. 2004. Biofilms fluorescence and image analysis in hypogean monuments research. Arch. Hydrobiol. Algal. Stud. 111:127-143.
- Roldán, M., F. Thomas, S. Castel, A. Quesada, and M. Hernández-Marín. 2004. Noninvasive pigment identification in living phototrophic biofilms by confocal imaging spectrophotometry. Appl. Environ. Microbiol. 70:3745-3750.
- Schüller, A., T. Meyer, H. Gehrig, and M. Kluge. 1997. Variations of lectin binding sites in extracellular glycoconjugates during the life cycle of *Nostoc punctiforme*, a potentially endosymbiotic cyanobacterium. Eur. J. Phycol. 32:233-239.
- Talarico, L. 1996. Phycobiliproteins and phycobilisomes in red algae: adaptive responses to light. Sci. Mar. 60:205-222.
- Tamaru, Y., Y. Takani, T. Yoshida, and T. Sakamoto. 2005. Crucial role of extracellular polysaccharides in desiccation and freezing tolerance in the terrestrial cyanobacterium *Nostoc commune*. Appl. Environ. Microbiol. 71:7327-7333.
- Tandieu de Marsac, N., D. Mazel, T. Damerval, G. Guglielmi, V. Capuano, and J. Houmard. 1988. Photoregulation of gene expression in the filamentous cyanobacterium *Calothrix* sp. PCC7601. Photosynth. Res. 18:99-132.
- Thompson, P. A., P. J. Harrison, and J. S. Parslow. 1991. Influence of irradiance on cell volume and carbon quota for ten species of marine phytoplankton. J. Phycol. 27:351-360.
- Vila, X., and C. A. Abella. 2001. Light-harvesting adaptations of planktonic phototrophic microorganisms to different light quality conditions. Hydrobiologia 452:15-30.
- Wotton, R. S. 2004. The ubiquity and many roles of exopolymers (EPS) in aquatic systems. Sci. Mar. 68:13-21.

---

#### 4.9. La influència de la llum verda en la ultraestructura dels cianobacteris: aplicació en ambients de baixa il·luminació

L'objectiu d'aquest estudi va ser avaluar el potencial de la llum verda (GL) per prevenir el creixement de biofilms fotosintètics en ambients hipogeus, que són normalment il·luminats amb llum blanca artificial (WL). Es va comparar la morfologia i la ultraestructura de l'espècie aerofítica *Gloeocapsopsis magma*, aïllada de la cova turística de Collbató (Catalunya, Espanya), en cultius de dos mesos d'edat sota llum verda i llum blanca. A més, es van examinar cultius de sis mesos d'edat sota llum blanca per distingir els efectes causats per llum verda dels provocats per senescència. Les cèl·lules procedents d'ambients naturals contenen alts nivells de ficoeritrina. Les beines de les cèl·lules sota llum verda no eren estratificades, mentre que les de llum blanca presentaven una clara estratificació. Les cèl·lules sota llum verda van ser significativament més llargues que les cèl·lules sota llum blanca de la mateixa edat, però més petites que les cèl·lules de sis mesos d'edat sota llum blanca. Respecte a l'ultraestructura, les cèl·lules sota llum verda contenen només alguns til·lacoids distribuïts a l'atzar i grànuls de cianoficina dispersats pel citoplasma. Les cèl·lules sota llum blanca contenen grups de til·lacoids paral·lels que formen dues meitats.

Els cultius de llum blanca de dos i sis mesos d'edat pràcticament no difereixen en nombre i disposició dels seus til·lacoids. Encara que *Gloeocapsopsis magma* exposada a llum verda sobreviu a la natura i en cultiu, la pèrdua de pigments i el desequilibri de la seva ultraestructura revelen que aquest organisme està al límit de la seva adaptació a aquestes condicions. Actualment, estem explorant aquesta informació per desenvolupar tractaments efectius per controlar el creixement dels biofilms en àrees del patrimoni cultural.

Els resultats detallats d'aquest capítol s'inclouen en el següent article:

The influence of green light on cyanobacterial fine structure: Applicability for dim environments. ***Arch. Hydrobiol. / Algological studies*** (2008), en premsa.

THE INFLUENCE OF GREEN LIGHT ON CYANOBACTERIAL FINE  
STRUCTURE: APPLICABILITY FOR DIM ENVIRONMENTS

Mònica Roldán<sup>1</sup> & Mariona Hernández-Mariné<sup>2</sup>

<sup>1</sup> Universitat Autònoma de Barcelona, Bellaterra, Spain.

<sup>2</sup> Universitat de Barcelona, Barcelona, Spain.

With 4 figures

**Abstract**

The purpose of this study was to evaluate the potential of green light (GL) for preventing biofilm growth in hypogean environments, which are normally illuminated with artificial white light (WL). The morphology and ultrastructure of an aerophytic *Gloeocapsopsis magma*, isolated from the Collbató tourist cave (Catalonia, Spain) was compared in two-month old cultures grown under either GL or WL. In addition, six-month old cultures grown under WL were examined to distinguish those effects caused by GL from those caused by senescence. The wild cells contained high levels of phycoerythrin. The sheaths of GL cells were not clearly layered, in contrast to those of WL cells. GL cells were also significantly larger than WL cells of the same age, but smaller than the six-month old WL cells. Moreover, the GL cells contained only a few randomly distributed thylakoids and cyanophycin granules dispersed throughout the cytoplasm, whereas the WL cells contained clusters of parallel thylakoids that formed two halves. The two-month and six-month old WL cultures did not differ either in the number or disposition of their thylakoids. Although *G. magma* exposed to GL survived in nature and in culture, the loss of pigments and unbalanced fine structure for this organism clearly reveal the limits of its adaptation. We are currently exploiting this information to develop new and more effective treatments to control biofilm growth in areas of cultural patrimony.

Keywords: Biofilms, cave, Confocal scanning laser microscopy, CSLM, cyanobacteria, EPS, green light, hypogean environments, pigments.



## **Introduction**

Photosynthetic organisms are often implicated in the degradation of cultural heritage sites (LEFEVRE 1974, ALBERTANO et al. 2005, GROBBELAAR 2000, HERNÁNDEZ-MARINÉ et al. 2003, HOFFMANN 2002, ORTEGA-CALVO et al. 1995). Artificially illuminated subterranean environments, in particular, are colonized by microbial communities that cause undesirable changes in the properties of materials, ultimately leading to grave economic and social consequences for cultural patrimony. The microorganisms together with the extracellular polymeric substances (EPS) that they produce form a three-dimensional arrangement called biofilm (COSTERTON et al. 1999, ROLDÁN et al. 2003, 2004a, CRISPIM & GAYLARDE 2005). Biofilms manifest as green or dark patina due to the colored sheaths and constituent pigments of the building organisms (ALBERTANO 1993, ARIÑO et al. 1997, GORBUSHINA & PALINSKA 1999, LAMENTI et al. 2000, LEWIN 2006, SAIZ-JIMENEZ 1997, TOMASELLI et al. 2000). Surface deterioration in natural or man-made sites results from biofilm production of acidic/alkaline conditions (ALBERTANO et al. 2000, ASCASO et al. 2002, BÜDEL et al. 2004, CRISPIM et al. 2003), physical penetration into the substratum (GAYLARDE & MORTON 1999, KUMAR & KUMAR 1999, WARSCHIED & BRAAMS 2000), or through repeated shrinking and loosening of surface adhered EPS during drying and rewetting cycles (de los RÍOS et al. 2004, ORTEGA-CALVO et al. 1995).

Controlling biodeterioration in caves should start with preventive measures to minimize conditions that favor the growth of lamp-microflora (ALBERTANO et al. 2005, GROBBELAAR 2000). Unfortunately, traditional chemical treatments are ineffective in the long term against biofilms (KUMAR & KUMAR 1999). Hence there is an ever-increasing interest in alternative strategies for preventing and minimizing biofilm development. In the case of illuminated indoor archaeological or historical sites such as catacombs or tourist caves, biofilms are composed of cosmopolitan, well-adapted, low-diversity communities in which cyanobacteria are the main building group (ALBERTANO et al. 2003, 2005, GARBACKI et al. 1999, ORTEGA-MORALES et al. 2000, ROLDÁN et

---

al. 2003, CRISPIM & GAYLARDE 2005). The survival of these biofilms under varying light conditions depends on structural, behavioral, physiological and chemical factors (RICHARDSON et al. 1983), including several types of light-harvesting pigments, each of which collects photons from a narrow range of the spectrum (RICHARDSON et al. 1983, GANTT 1990, TANDEAU DE MARSAC 2003). Cultures of photosynthetic cyanobacteria have been widely studied, and the metabolic and growth responses to monochromatic light have been well characterized. Monochromatic green light (GL) has been observed to affect the pigment composition (ALBERTANO et al. 2005, GANTT 1980, MULLINEAUX 2001, SUETSUGU & WADA 2003, TANDEAU DE MARSAC et al. 1988), three-dimensional organization, EPS and fluorescence properties of biofilms (ROLDÁN et al. 2006). However, the effects of monochromatic light on the fine structure of biofilm organisms is less understood (ALBERTANO et al. 2003, 2005).

Suggested methods for limiting biofilm growth in illuminated sites include the use of very low intensity light, and/or monochromatic light that doesn't support photosynthesis (ALBERTANO & BRUNO 2003, FAIMON et al. 2003, GROBBELAAR 2000, ROLDÁN et al., 2006).

During an intervention intended to clean biofilms and prevent subsequent biofilm growth in cave surfaces using biocides and monochromatic light, we found resilient colonies of a cyanobacteria that fit the description of *Gloeocapsopsis magma* (BRÉBISSE) KOMÁREK et ANAGNOSTIDIS (KOMÁREK & ANAGNOSTIDIS 1999). As part of the CATS project (ALBERTANO et al. 2003) we have studied the potential of GL for preventing biofilm growth in hypogean environments (ROLDÁN et al. 2006) that are normally illuminated with artificial white light (WL). We chose green wavelengths because they are barely used by phototrophic microorganisms, yet are in the range of human vision and produce minimum distortion of human color perception. We report here an evaluation of the differential effects of commercial GL and WL lamps on the fine structure and viability of the aforementioned cyanobacteria.

### Materials and methods

Samples were collected in the Collbató tourist cave in Montserrat (Catalonia, Spain) on 3 March 2004. A green patina was observed on a stalactite (4a GL) that had been exposed to GL for one year. From this patina were isolated mucilaginous colonies of *Gloeocapsopsis magma*. Similar colonies were identified from plots on the same stalactite, in zones that were simultaneously submitted to GL and a biocide treatment (Preventol®). The cave features relative micro-environmental stability throughout the annual cycle: the mean value of the air temperature was 14.7° C, with an annual variation of 4.1° C; the mean value of the stone temperature was 15.5 ° C, with an annual variation of 1.2° C; the mean ambient humidity was high (RH 90-99.9%) in the sampling zones; and the mean ambient CO<sub>2</sub> concentration was 588.2 ppm.

### Growth conditions

*Gloeocapsopsis magma* was grown and maintained in agarized BG11 (RIPPKA et al. 1988) at 19-22 °C under a dark/light cycle of 12:12 hours of either GL (Narva LT 18 W / 017 green TT, Narva, Czech republic) or WL (Chiyoda F 15 S daylight, Chiyoda Corporation, Japan). The strain was maintained in the above culture conditions for one year before the onset of the study. The respective emission spectra of the lamps were measured with a LICOR Li-1800 (Lincoln, NE, USA) spectroradiometer. The spectral emission of the white fluorescent lamps was characterized by two maximum peaks in the ranges from 600 to 620 nm and 520 to 540 nm (blue-green/green), and included shoulders in the ranges from 435 to 500 nm (blue), 580 to 590 nm (yellow) and 625 to 750 nm (red regions), the most significant of which was at 544 nm (green). The commercial green lamp exhibited a major peak in the green region of the spectrum, with an emission maximum in the range from 520 to 560 nm and different shoulders in the ranges from 425 to 440 nm (violet), 480 to 490 nm

---

(blue), 570 to 590 nm (yellow) and 610 to 630 nm (orange) (ROLDÁN et al. 2006).

### **Microscopy techniques**

The samples were imaged using a Zeiss Axioplan equipped with an MRc5 AxioCam photomicrographic system. Cell culture measurements (e.g., cell diameter) were made based on the optical images. The data used represent the mean  $\pm$  SE from  $n=22$  cells from the different fields examined. The results for each species were processed with a One-Way ANOVA model. Epifluorescence observations were made using a green filter ( $\lambda$  excitation : 546- nm,  $\lambda$  barrier: 580 nm) to visualize pigment autofluorescence.

We used TEM to explore the differences in fine structure between two-month old cultures grown under either GL or WL. We also compared the differences in fine structure between two-month old and six-month old WL cultures. Cells were cryofixed at high pressure (HPF), and then cryosubstituted at  $-93$  °C using 0.5% uranyl acetate in pure methanol (stored over molecular sieves) for 72 h. The temperature was then increased at a rate of 5°C per hour to  $-50$ °C. The samples were transferred to methanol at the same temperature ( $-50$ °C) and rinsed three times over 2h. Embedding in HM20 resin and ultraviolet polymerization at  $-50$ °C for 48 h were then performed. The blocks were then warmed to and kept at 22 °C for 24h. Thin sections were cut on a Reichert Ultracut-E microtome, and placed on slot copper Formvar grids coated with carbon. The sections were contrasted with uranyl acetate and lead citrate, and viewed using a Hitachi H800MT transmission electron microscope operating at 100 kV.

#### *Pigment fluorescence analysis: Lambda-Scans*

To identify pigment signatures used by intact, living samples, we used a fluorescence-based technique (ROLDÁN et al. 2004b) for analysis of the fluorescent pigments from a single cell. The spectral profile was obtained by

confocal scanning laser microscopy (CSLM), using the 488 nm line of an argon laser in combination with spectrofluorometric detection (Leica TCS-SP2 Leica Microsystems, Mannheim, Germany). Each stack was obtained by scanning the same x-y optical section using a bandwidth of 20 nm for the emission (x-y coordinate of an x-y data set). Mean Fluorescence Intensity (MFI) of the x-y data sets was measured using Leica Confocal Software, version 2.0. The data used represent the mean  $\pm$  SE from n=20 cells from three fields examined.

## Results

### Light microscopy

Cultures grown in WL. The colonies of *Gloeocapsopsis magma* grown in WL were bluish-green, rounded or hemispherical, and composed of small groups of cells enveloped by colorless, firm-layered sheaths. The WL cells ( $2.53 \pm 0.07 \mu\text{m}$  x  $2.85 \pm 0.07 \mu\text{m}$ ) were rounded, subspherical, irregularly divided in various planes, and, after division, were either irregular in outline or polygonal (Fig. 1 a-c). The thickness of the sheaths appeared to depend on the position of the cell within the colony, whereby the thinnest sheaths were those of the cells located at the colony extremities. When stained with methylene blue, siblings became visibly surrounded by a layered, compact sheath which covered individual cells or cell couples (Fig. 1c). Binary fission occurred via a constrictive pinching mechanism in which all cell envelope layers grow inwards, thus displacing thylakoid membranes. Under epifluorescence microscopy, the chromatoplasm gave a brilliant red response divided into two halves (Fig. 1b). An area in the cell center that was devoid of pigment fluorescence corresponded to a nucleoid region. Cells from six-month old cultures were irregularly sized (Fig. 1d)—with some reaching 18  $\mu\text{m}$  in diameter—and had light-orange sheaths.

Cultures grown in GL. Colonies grown in GL were yellowish and amorphous. The GL cells ( $4.07 \pm 0.11 \mu\text{m}$  x  $4.63 \pm 0.14 \mu\text{m}$ ) had the same shape and division pattern as the WL cells, but were significantly longer and

wider (Fig. 1 e-g). ). The differences in cell size between GL and WL cells were statistically significant, notably in cell width ( $F_{1, 42} = 164.99$ ,  $P < 0.0001$ ) and length ( $F_{1, 42} = 129.53$ ,  $P < 0.0001$ ).

Methylene blue staining revealed that the GL cells were embedded in less-defined mucilage than were the WL cells. The colonies were heavily populated by bacteria. The thylakoidal region was not clearly seen. Epifluorescence microscopy revealed weak and irregular fluorescence (Fig. 1f). Nearly all GL cells contained granules, and some of them had up to ten, large granules (Fig. 1g).

### **Pigment fluorescence analysis: *Lambda-Scans***

The photosynthetic pigments in intact single cells from wild material fluoresced strongly distributed in two ranges (Fig 2 a). The excitation wavelength at 488 nm, absorbed essentially by phycoerythrin, produced a strong in vivo emission at 572 to 590 nm, indicating that the cells contained high levels of this pigment. Chl a fluoresced less intensely than did other pigments, in the range of 659.3 to 666.4 nm. Moreover, all pigments had lower MFI in GL than in WL (data not shown).

### **Transmission electron microscopy**

Fine structure of *G. magma* was characterized by TEM (Figs. 2 b-d, 4 and 5).

Cultures grown in WL. The WL cells were enveloped by two clearly differentiated layers: a fibrous, web like inner layer (ca. 250 nm thick), and a less-defined outer layer (Figs. 2 b-c and 3a). The cell wall had a thin (ca. 10 nm) peptidoglycan layer (Fig. 3 a-b). Sections parallel to the division plane revealed clusters of thylakoids parallel to the cell wall (Figs. 2c and 3a). Adjacent thylakoids were separated by  $77.4 \pm 5.8$  nm, as measured from lumen center to lumen center (Fig. 3a). Transversal sections revealed that the thylakoid-containing region was centered about the nucleoid and perpendicular to the cell wall (Fig. 3b), and exposed thylakoid-free spaces close to division plane. This

arrangement, which we refer to here as a “coffee bean” motif, delineates the two halves that were observed by optical and epifluorescence microscopies (Fig. 1 a-c). Electron-dense, hemidiscoidal ( $12.2 \pm 0.25$  nm in diameter) (Fig. 4a) or star-shaped phycobilisomes (Fig. 4b) were observed along the thylakoid lamellae, depending on the slice orientation. The cytoplasm contained distinct carboxisomes (Fig 3d). Lipid or cyanophycin granules were rarely observed.

Cultures grown in GL. The GL cells were enveloped by sheaths that were not clearly layered (Figs. 2d and 3 c). The cell walls appeared identical to those of the WL cells. The GL cells only contained a few, randomly distributed thylakoids (Figs 2d, 3c and 4c). There were some phycobilisomes and many glycogen granules in the cytoplasm between the thylakoids (Figs. 3c and 4c). No carboxisomes were observed. Large cyanophycin granules were recorded in each section (Figs. 2d, 3c and 4c).

## Discussion

We used optical microscopy and TEM to explore the differences between two-month old cultures grown under either GL or WL. We also compared the differences between two-month old and six-month old cultures grown exclusively under WL to distinguish effects caused by long-term exposure to GL from those caused by senescence.

At the light microscopy level, the three types of cultures differed in cell size and color, and sheath layering and thickness.

The sheaths in GL cells were thicker than those of WL cells, but not layered, suggesting that production and composition of EPS are affected by the wavelength of ambient light (DE PHILIPPIS & VICENZINI 1998). Variability in width and consistence of the sheath have also been reported in other cyanobacteria grown under different light wavelengths (ALBERTANO 1991) in unfavorable conditions of temperature and light intensities (HERNÁNDEZ-MARINÉ et al. 2001, ROLDÁN et al. 2004a, WILMOTTE 1988) or under similar light conditions to the present work for *Gloeotheca membranacea* (ROLDÁN et al. 2006).

---

GL cells were larger than WL cells of the same age, but smaller than the six-month old WL cells. The six-month old WL cells were viable and grew nearly to the sizes reported for the species in the wild (KOMÁREK & ANAGNOSTIDIS 1999). Cell size was dependent on the relative position of the cell within the colony. Cell size apparently varies to a great degree with simultaneous environmental controls such as light intensity and nutrients (SUNDA & HUNTSMAN 1997), or culture conditions (GARCIA-PICHEL et al. 1998).

The observation of larger cell sizes for GL cultures of *Gloeocapsopsis magma* is in contradiction with studies on *Gloeotheca membranacea*, which are reported to have smaller cell sizes when grown in GL than when grown in WL (ROLDÁN et al. 2006). This apparent contradiction may stem from the differences in GL exposure time for the organisms in each study: in our study, *G. magma* was exposed to GL for over two years (one year in the cave, one year in culture, plus two months), whereas the study on *G. membranacea* only implied two months of exposure. Moreover, GL cells of *G. magma* were characterized by large cyanophycin granules, indicating a tendency to accumulate caused by an inability to divide rapidly (HAUSCHILD et al. 1991) and a partial loss of thylakoids. These are characteristics of heterotrophic cultures kept in total darkness (OHKI & GANTT 1983) or in darkness with a daily pulse of WL (ZSÍROS et al. 2002).

The structure of the phycobilisomes of *G. magma* in WL was similar to that of the phycobilisomes of GL-acclimated *Phormidium* sp. C86 after complementary chromatic adaptation (OHKI & FUJITA, 1992). The dimensions of the phycobilisomes were smaller than those isolated from either the aforementioned GL-adapted *Phormidium* sp. C86 (OHKI & FUJITA, 1992) or from *Tolypothrix*, which can undergo chromatic adaptation to GL (OHKI et al. 1985). We also observed shorter thylakoid separation for *G. magma* than that reported for *Synechocystis* (PINEVITH et al. 2000). The larger phycobilisome size agrees with that reported for GL-adaptation (OHKI & FUJITA 1992). However, due to differences in techniques among our study and others studies, our



measurements for phycobilisomes cannot be precisely compared with published measurements.

The pigment spectra of *G. magma* illustrate that phycoerythrin substantially contributes to the light-harvesting capabilities of cells in the wild. A high content of phycobiliproteins allows the cyanobacteria to grow over long periods at various irradiances or at wavelengths different than those of the natural habitats (ALBERTANO 1991, ALBERTANO et al. 2005, BRUNO & ALBERTANO 1999).

The fact that GL colonies were yellowish, rather than blue-green, as in the case of WL colonies, the loss of fluorescence in long-term cultures, and the scarcity of thylakoids and phycobilisomes in the GL cells examined by TEM, led us to assume that GL had caused degradation of photosynthetic pigments, although the cultures were still able to grow and replicate. Therefore, complementary chromatic adaptation in which GL stimulates PE synthesis (OHKI & FUJITA 1992, PINEVICH et al. 2000, TANDEAU de MARSAC 1977) does not occur in cultures of *G. magma*. However, the low fluorescence of GL cells, and the fact that they lacked carboxisomes, which enhance the fixation of carbon dioxide by RuBisCO (CODD & MARSDEN 1984), suggest mixotrophic growth. Mixotrophic growth has been well studied for versatile cyanobacteria (SCHEENEGURT 1997). Indeed, the pigment spectra of other cyanobacteria have been reported to vary slightly in both mixotrophic and chemoheterotrophic cultures (SCHEENEGURT 1997). The organic compounds required for slow growth are most likely provided by bat excrement, which is ubiquitous in the test cave.

Although *G. magma* exposed to GL survived in nature and in culture, it lost of pigments and had unbalanced fine structure, clearly revealing the limits of its adaptation. Having previously studied the potential of GL treatment for controlling biofilm growth in the Collbató cave, we have shown in this study that long-term exposure to GL has serious consequences for *G. magma*, a constituent of biofilms in the Cave. We are currently exploiting this information

to develop new and more effective treatments to control biofilm growth in areas of cultural patrimony.

### Acknowledgements

This paper is dedicated to Prof. Dr. Komárek of the University of Marburg on the occasion of his 70th birthday. This work was partially supported by the EU Energy, Environment and Sustainable Development Program within the framework of the CATS project, contract EVK4-CT-2000-00028. The TEM and confocal microscopy facilities provided by the Scientific and Technical Services of the University of Barcelona are gratefully acknowledged. The authors also thank Mónica Ramirez for helping with the images.

### References

- ALBERTANO, P. (1991): Effects of monochromatic lights on four species of *Leptolyngbya*. – Arch. Hydrobiol. Algol. Stud. **64**: 199-214.
- ALBERTANO, P. (1993): Epilithic algal communities in hypogean environments. - Giorn. Bot. Ital. **127**: 386-392.
- ALBERTANO, P. & BRUNO, L. (2003): The importance of light in the conservation of hypogean monuments.- In C. Saiz Jiménez (ed.), Molecular Biology and Cultural Heritage. pp. 171-177. Swets & Zeitlinger, Lisse (NL).
- ALBERTANO, P., BRUNO, L. & BELLEZZA, S. (2005): New strategy for the monitoring and control of cyanobacterial films on valuable lithic faces.- Plant Biosystems. **139**: 311-322.
- ALBERTANO, P. MOSCONE, D., PALLESCHI, G., HERMOSIN, B., SAIZ-JIMÉNEZ, C., SÁNCHEZ-MORAL, S., HERNÁNDEZ-MARINÉ, M., URZÍ, C., GROTH, I., SCHROECKH, V., GALLON, J. R., GRAZIOTTIN, F., BISCONTI, F. & GIULIANI, R. (2003): Cyanobacteria attack rocks (CATS): Control and preventive

- strategies to avoid damage caused by cyanobacteria and associated microorganisms in Roman hypogean monuments. - In C. SAIZ-JIMÉNEZ (ed.), *Molecular Biology and Cultural Heritage*. p. 151-162. Swets & Zeitlinger, Lisse.
- ALBERTANO, P., BRUNO, L., D'OTTAVI, D., MOSCONE, D. & PALLESCHI, G. (2000): The effect of photosynthesis on pH variation in cyanobacterial biofilms from Roman catacombs. - *J Appl Phycol* . 12: 379 - 384.
- ARIÑO, X., HERNÁNDEZ-MARINÉ, M. & SAIZ-JIMÉNEZ, C. (1997): Colonization of Roman tombs by calcifying cyanobacteria. - *Phycologia*. **36**: 366-373.
- ASCASO, C., WIERZCHOS, J., SOUZA-EGIPSY, V., DE LOS RÍOS, A. & DELGADO RODRIGUES, J. (2002): In situ evaluation of the biodeteriorating action of microorganisms and the effects of biocides on carbonate rock of the Jeronimos Monastery (Lisbon). - *Int. Biodeter. Biodegr.* **49**: 1-12.
- BRUNO, L. & ALBERTANO, P. (1999): Photoacclimation of sciaphilous epilithic cyanobacteria isolated from Roman hypogea. - *Arch. Hydrobiol., Algological Studies* **94**: 89-103.
- BÜDEL, B., WEBER, B., KÜHL, M., PFANZ, H., SÜLTEMEYER, D. & WESSELS, D. (2004): Reshaping of sandstone surfaces by cryptoendolithic cyanobacteria bioalkalization causes chemical weathering in arid landscapes. - *Geobiology* **2**: 261-268.
- CODD, G. A. & MARSDEN, W. J. N. (1984): The carboxysomes (polyhedral bodies) of autotrophic prokaryotes. - *Biol Rev.* **59**: 389- 422.
- COSTERTON, J. W., STEWART, P. S. & GREENBERG, E. P. (1999): Bacterial biofilms: a common cause of persistent infections. - *Science* **284**: 1318-1322.
- CRISPIM, C. A. & GAYLARDE, C. C. (2005): Cyanobacteria and biodeterioration of cultural heritage: a review. - *Microb. Ecol.* **49**: 1-9.
- CRISPIM, C. A., GAYLARDE, P.M. & GAYLARDE, C. C. (2003): Algal and cyanobacterial biofilms on calcareous historic buildings.- *Curr. Microbiol.* **46**: 79 - 82.

- 
- de los RÍOS, A; GALVAN, V. & ASCASO, C. (2004): In situ microscopical diagnosis of biodeterioration processes at the convent of Santa Cruz la Real, Segovia, Spain. - *Int Biodeter. Biodegr.* **54**: 113 - 20.
- DE PHILIPPIS, R. & VINCENZINI, M. (1998): Exocellular polysaccharides from cyanobacteria and their possible applications. - *FEMS Microbiol. Rev.* **22**: 151-175.
- FAIMON, J., STELCL, J., KUBEŠOVÁ, S. & ZIMÁK J. (2003): Environmentally acceptable effect of hydrogen peroxide on cave "lamp-flora", calcite speleothems and limestones. - *Environ. Pollut.* **122**: 417-422.
- GANTT, E. (1980): Structure and function of phycobilisomes: lightharvesting pigment complexes in red and blue-green algae. - *Int. Rev. Cytol.* **66**: 45-80.
- GANTT, E. (1990): Pigmentation and photoacclimation. In: Cole KM, Sheath KG (eds) *Biology of the red algae*. p. 203–221. Cambridge University Press, Cambridge.
- GARBACKI, N., ECTOR, L., KOSTIKOV, I. & HOFFMANN, L. (1999): Contribution a l'étude de la flore des grottes de Belgique. - *Belg. Journ. Bot.* **123**: 43-76.
- GARCIA-PICHEL, F., NÜBEL, U. & MUYZER, G. (1998): The phylogeny of unicellular, extremely halotolerant cyanobacteria. - *Arch Microbiol* **169**: 469-482.
- GAYLARDE, C. C. & MORTON, L. H. G. (1999): Deteriogenic biofilms on buildings and their control: a review. - *Biofouling* **14**: 59-74.
- GORBUSHINA, A. A. & PALINSKA, K. A. (1999): Biodeteriorative processes on glass: experimental proof of the role of fungi and cyanobacteria.- *Aerobiologia* **15**: 183-191.
- GROBBELAAR, J. U. (2000): Lithophytic algae: A major threat to the karst formation of show caves. - *J. Appl. Phycol.* **12**: 309-315.
- HAUSCHILD, C. A., MCMURTER, H. J. & PICK, F. R. (1991): Effect of spectral quality on growth and pigmentation of picocyanobacteria. - *J. Phycol.* **27**: 698-702.

- HERNÁNDEZ-MARINÉ, M., CLAVERO, E. & ROLDÁN, M. (2003): Why there is such luxurious growth in the hypogean environments. - Arch. Hydrobiol., Algological Studies **148**: 229-239.
- HERNÁNDEZ-MARINÉ, M., ROLDÁN, M., CLAVERO, E., CANALS, A. & ARIÑO, X. (2001): Phototrophic biofilm morphology in dim light. The case of the Puigmoltó sinkhole. - In: ELSTER, J.; SECKBACH, J.; VINCENT, W. P. & LHOTSKÝ, O. (eds.): Algae and extreme environments. - Nova Hedwigia, Beih. **123**: 237-253.
- HOFFMANN, L. (2002): Caves and other low-light environments: Aerophytic photoautotrophic microorganisms. - In G. BITTON (ed.), Encyclopedia of Environmental Microbiology. p. 835-843. John Wiley & Sons, New York.
- KOMÁREK, J. & ANAGNOSTIDIS, K. (1999): Süßwasselflora von Mitteleuropa, **1**: 2-491. Cyanoprokaryota. Teil Chroococcales. - In: Ettl, H., Gartner, G., Heynig, H. & Mollenhauer, D. G. Fischer, Verlag Jena.
- KUMAR, R. & KUMAR, A.V. (1999): Biodeterioration of stone in tropical environments. Los Angeles: Paul Getty Trust.
- LAMENTI, G., TIANO, P. & TOMASELLI L. (2000): Biodeterioration of ornamental marble statues in the Boboli Gardens (Florence, Italy). - J. Appl. Phycol. **12**: 427-433.
- LEFEVRE, M. (1974): La maladie verte de Lascaux. - Stud. Conserv. **19**: 126-156.
- LEWIN, R. A. (2006): Black algae. - J. Appl. Phycol. **18**: 699-702.
- MULLINEAUX, C. W. (2001): How do cyanobacteria sense and respond to light? - Mol. Microbiol. **41**: 965-971.
- OHKI, K. & FUJITA Y. (1992): Photoregulation of phycobilisome structure during complementary chromatic adaptation in the marine cyanophyte phormidium sp. C86.,- J. Phycol. **28**: 803-808.
- OHKI, K., GANTT, E., LIPSCHULTZ, C. A. & ERNST, M. C. (1985): Constant phycobilisome size in chromatically adapted cells of the cyanobacterium *Tolypothrix tenuis*, and variation in *Nostoc* sp. - Plant Physiology. **79**: 943-948.

- 
- OHKI, K. & GANTT, E. (1983): Functional phycobilisomes from *Tolypothrix tenuis* (Cyanophyta) grown heterotrophically in the dark. - J. Phycol. **19**: 359-364.
- ORTEGA-CALVO, J. J., ARIÑO, X., HERNÁNDEZ-MARINÉ, M. & SAIZ-JIMENEZ, C. (1995): Factors affecting the weathering and colonization of monuments by phototrophic microorganisms. - The Science of Total Environment **167**: 329-341.
- ORTEGA-MORALES, O., GUEZENNEC, J., HERNANDEZ-DUQUE, G., GAYLARDE, C.C. & GAYLARDE, P. M. (2000): Phototrophic biofilms on ancient Mayan buildings in Yucatan, Mexico. - Curr. Microbiol. **40**: 81-85.
- PINEVICH, A., MATTHIJS, H., GARCIA-MENDOZA, E & BAZANOVA, A. (2000): The uncommon pigment composition of, and complementary chromatic adaptation in a marine *Synechocystis* sp. - Arch. Hydrobiol./Algological Studies **99**: 67-77.
- RICHARDSON, K., BEARDALL, J. & RAVEN, J. A. (1983) Adaptation of unicellular algae to irradiance: an analysis of strategies. - New Phytologist **93**: 157-191.
- RIPPKA, R. (1988): Isolation and purification of cyanobacteria. In: PACKER, L. & GLAZER, A. N. (eds.), Methods in Enzymology. **167**, p. 3-28, Academic Press, Inc., San Diego.
- ROLDÁN, M., CLAVERO, E. & HERNÁNDEZ-MARINÉ, M. (2003): Aerophytic biofilms in dim habitats. - In: C. SAIZ-JIMÉNEZ (ed.), Molecular Biology and Cultural Heritage, Swets & Zeitlinger, Lisse.
- ROLDÁN, M., CLAVERO, E., CANALS, T, GÓMEZ-BOLEA, A.; ARIÑO, X. & HERNÁNDEZ-MARINÉ, M. (2004a): Distribution of phototrophic biofilms in cavities (Garraf, Spain). - Nova Hedwigia **78**: 329-351.
- ROLDÁN, M., THOMAS, F., CASTEL, S., QUESADA, A. & HERNÁNDEZ-MARINÉ, M. (2004b): Non invasive pigment identification in living phototrophic biofilms by confocal imaging spectrophotometry. - Appl. Environ. Microbiol. **70**: 3745-3750.

- ROLDÁN, M., OLIVA, F., GONZALEZ DEL VALLE, M. A., SAIZ-JIMENEZ, C. & HERNÁNDEZ-MARINÉ, M. (2006): Does green light influence the fluorescence properties and structure of phototrophic biofilms? - Appl. Environ. Microbiol. **72**: 3026-3031.
- SAIZ-JIMENEZ, C. (1997): Biodeterioration vs. biodegradation: the role of microorganisms in the removal of pollutants deposited on historic buildings. - Int. Biodet. Biodegr. **40**: 225- 32.
- SCHEENEGURT, M. A., SHERMAN, D. M. & SHERMAN, L. A. (1997): Growth, physiology, and ultrastructure of a diazotrophic cyanobacterium, *Cyanothece* sp. strain ATCC 51142, in mixotrophic and chemoheterotrophic cultures. - J. Phycol. **33**: 632-642.
- SUETSUGU, N. & WADA, M. (2003): Cryptogam blue-light photoreceptors. - Current Opinion **6**: 91-96.
- SUNDA, W.G. & HUNTSMAN, S.A. (1997): Interrelated influence of iron, light and cell size on marine phytoplankton growth. - Nature **390**: 389-392.
- TANDEAU DE MARSAC, N. (1977): Occurrence and nature of chromatic adaptation in cyanobacteria. - J Bacteriol. **130**: 82-91.
- TANDEAU DE MARSAC, N., MAZEL, D., DAMERVAL, T., GUGLIELMI, G. C. V. & HOUMARD, J. (1988): Photoregulation of gene expression in the filamentous cyanobacterium *Calothrix* sp. PCC7601. - Photosynth. Res. **18**: 99-132.
- TANDEAU DE MARSAC, N. (2003): Phycobiliproteins and phycobilisomes: the early observations. - Photosynth. Res. **76**: 197-205.
- TOMASELLI, L., LAMENTI, G., BOSCO, M. & TIANO, P. (2000): Biodiversity of photosynthetic micro-organisms dwelling on stone monuments. - Int. Biodet. Biodegr. **46**: 251-258.
- WARSCHEID, T. & BRAAMS, J. (2000): Biodeterioration of stone: a review. - Int. Biodet. Biodegr. **46**: 343-368.
- WILMOTTE, A. (1988): Growth and morphological variability of six strains of *Phormidium* cf. *ectocarp*i Gomont (Cyanophyceae) cultivated under

different temperatures and light intensity.,- Arch. Hydrobiol./Algological Studies **50-53**: 35-46.

ZSÍROS, O., KIS, M., MUSTÁRDY, L., FARKAS, T., VÁRKONYI, Z., ZOLTÁN GOMBOS, Z. & SZALONTAI, B. (2002): Light-driven structural changes in thylakoid and cytoplasmic membranes of a cyanobacterium, *Synechocystis* PCC6803. - J. Plant. Physiol. **159**: 403-414.



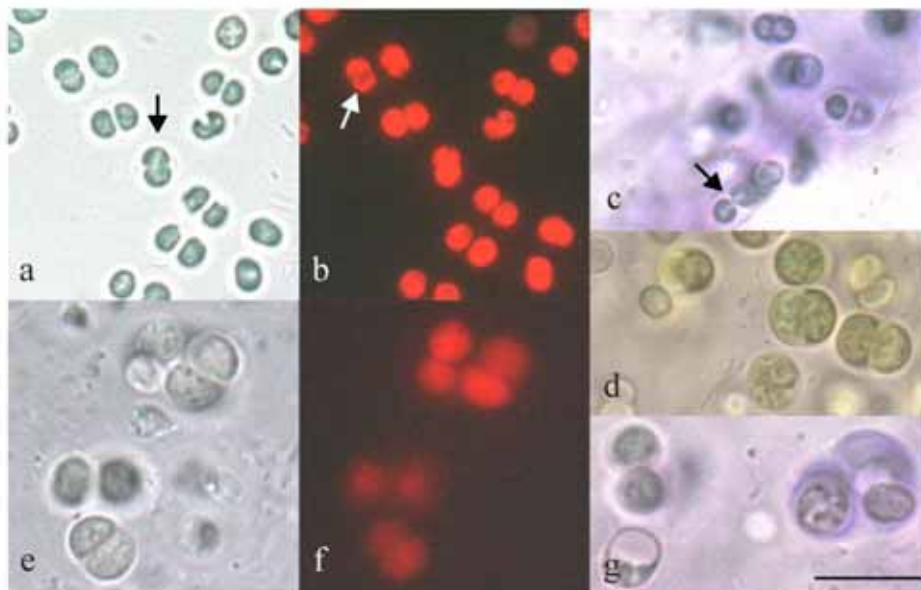


Fig. 1. Optical micrographs of *Gloeocapsopsis magma*. **a-c**, **e-g** - Two-month old cultures. **a-c** - Few-celled colonies grown in WL. Note the halved chromatoplasma (small arrows). **a** - Light micrograph. **b** - Epifluorescence micrograph. **c** - Light micrograph after methylene blue staining. **d** - Irregularly sized cells from six-month old WL cultures. **e-g** - Few-celled colonies grown in GL. **e** - Light micrograph. **f** - epifluorescence micrograph. **g** - Light micrograph after methylene blue staining. [Bar: 10 $\mu$ m]

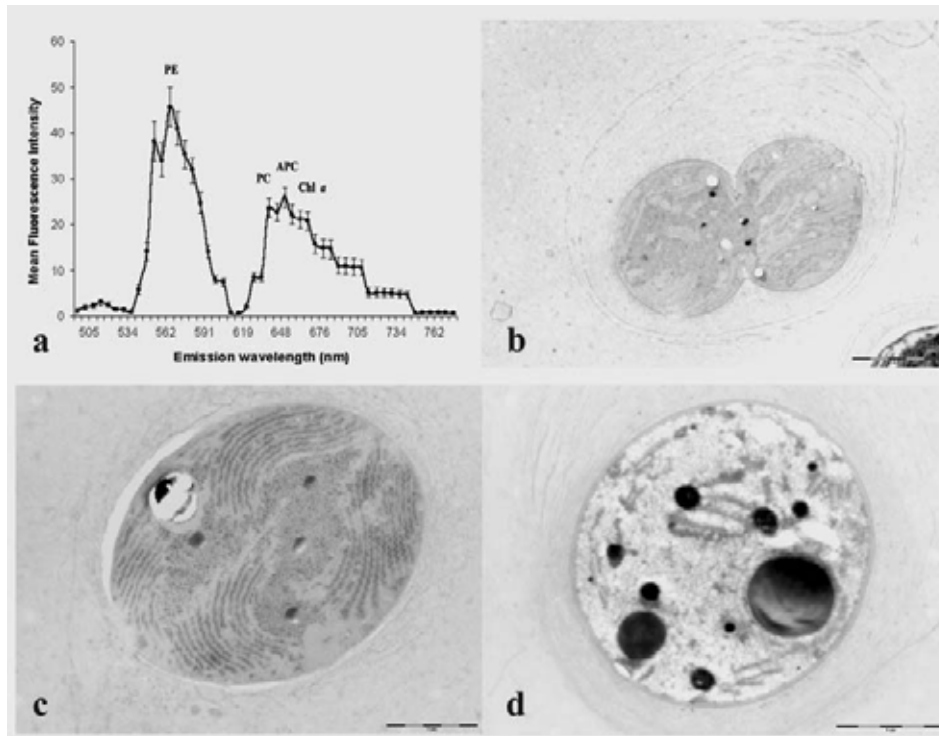


Fig. 2. **a** - Spectral profiles of wild cells of *G. magma*. The image represents the maximum autofluorescence emitted from PE (572 to 577 nm), PC (640 to 645 nm), APC (658 to 664 nm) and Chl a (679 to 684 nm) at an excitation wavelength of 488 nm. The data used represent the mean  $\pm$  SE of  $n = 15$  cells from three fields examined. MFI: mean fluorescence intensity, SE: standard error. **b–d** - Transmission electron micrographs of *G. magma*. **b** - Longitudinal thin section of a cell undergoing binary fission via a constrictive pinching mechanism in which all cell envelope layers grow inwards. **c**- Thin sections of cells from two-month old cultures grown in WL. Thylakoids arranged in clusters parallel or perpendicular to the cell wall. **d**- Thin sections of cells from two-month old cultures grown in GL. Large decrease in the number of thylakoids. [Bars: **b** 2  $\mu\text{m}$ , **c,d** 1  $\mu\text{m}$ ].

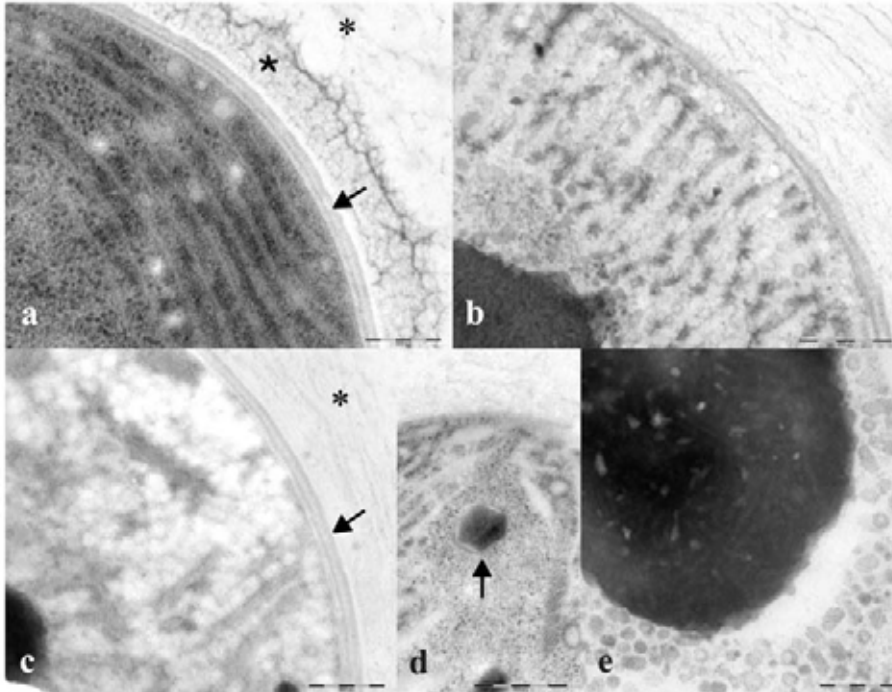


Fig. 3. Transmission electron micrographs of *G. magma*. a - Two-month old cells from cultures grown in WL. Section perpendicular to the thylakoid surface. A fibrous, web like inner layer (star) and a less-defined outer layer of the covering sheath are shown (asterisk). b - Six-month old cells from cultures grown in WL. Changes in thylakoid number or organization were minor. c - Two-month old cells from cultures grown in GL. Scarce thylakoids. The sheath was not clearly layered, and was thick and diffuent (asterisk). d - The carboxisomes in two-month old WL cells were usually large (arrow). e - Typical cyanophycin granule in two-month old GL cells. [Bars: a,c 200 nm, b,d,e 500 nm].

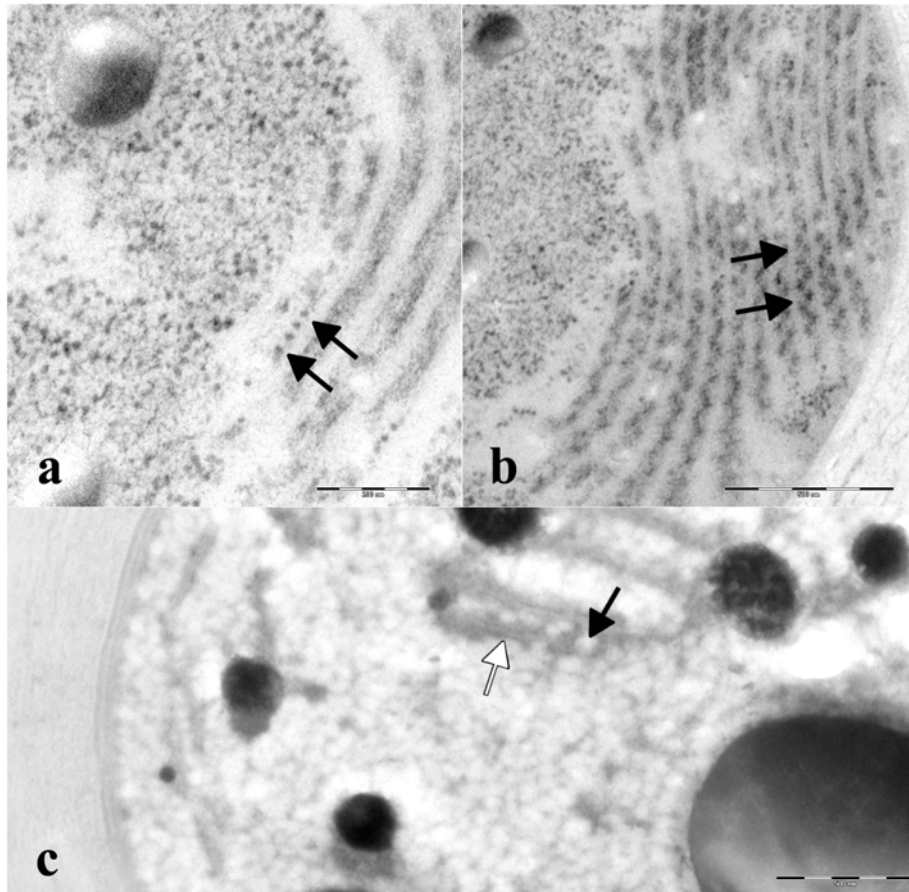


Fig. 4. Transmission electron micrographs of *G. magma*. a,b - Two-month old cells from cultures grown in WL. a - Transversal sections of thylakoids showing phycobilisomes in face view (arrows). b - Sections showing phycobilisomes in side view. The hatched pattern indicates the distribution of phycobilisomes on the thylakoid membrane (arrows). c - Two-month old cells from cultures grown in GL. Large phycobilisomes (white arrow) and glycogen granules (black arrow) were visible between the thylakoids. [Bars: a,c 200 nm, b 500 nm].

*Resultats*

---

---

#### 4.10. La eficàcia dels biocides i els tractaments de neteja en els treballs de restauració de monuments hipogeus

Per a l'estudi de comunitats microbianes en monuments, normalment s'utilitzen mètodes de cultiu tradicionals. Els mètodes més comuns inclouen el recompte de cèl·lules microbianes i l'aïllament i la posterior identificació de cultius purs en el laboratori. Aquests mètodes no només consumeixen molt de temps sinó que requereixen gran quantitat de material i és, per tant, de gran interès trobar metodologies ràpides. L'objectiu d'aquest article és avaluar l'eficiència de les tècniques de neteja utilitzant biocides i identificar un conjunt de metodologies econòmiques per al control de la restauració. S'han realitzat dos estudis diferents.

*Cas 1. Les coves de Collbató, Barcelona, Espanya.* En aquest estudi s'han escollit diferents àrees d'estudi i cadascuna s'ha dividit en quatre quadrants. El quadrant A es va mantenir com a control per tenir una referència dels possibles efectes dels canvis ambientals en el creixement del biofilm durant un any. La resta de quadrants (B, C i D) van ser netejats utilitzant un raspall de dents amb etanol 70 % per eliminar els microorganismes fotosintètics. Els quadrants C i D van ser tractats amb biocides (dues formulacions de clorur de benzoalconi). Paral·lelament es van avaluar els efectes de la il·luminació dels biofilms utilitzant exclusivament làmpades de llum blanca (WL) o de llum verda (GL) en zones properes de les mateixes característiques. Els resultats d'aquest estudi van demostrar que el clorur de benzoalconi redueix els nivells de fluorescència comparat amb els controls. A més, l'abundància de *Scytonema julianum* i altres espècies predominants van disminuir, excepte per a *Nostoc punctiforme* i *Gloeocapsopsis magma*, ambdues cobertes amb polisacàrids extracel·lulars i amb pigments accessoris.

*Cas 2. Pintures murals de la Necròpolis de Carmona, Sevilla, Espanya.* Es va realitzar una restauració que consistia en una neteja de la zona, un tractament amb benzoalconi i una consolidació. Els resultats van mostrar una alta similitud en totes dues comunitats bacteriana i fototròfica, abans i després del procés de restauració. El tipus de seqüències clonades obtingudes de les bandes comunes

procedents de les dues comunitats abans i després del tractament corresponen als gèneres *Chroococciopsis*, *Cyanidium*, *Cyanothece*, etc. La majoria de seqüències obtingudes procedents de les comunitats bacterianes de les mostres investigades presenten homologia amb els microorganismes no cultivats. El conjunt de bacteris pertanyen als gèneres *Propionibacterium*, *Arthrobacter*, *Rubrobacter*, *Micrococcus*, *Mycobacterium*, *Kibdelosporangium* i *Pseudonocardia* (Actinobacteria); *Nordella*, *Mesorhizobium* i *Phyllobacterium* (Alphaproteobacteria); *Salinisphaera* i *Stenotrophomonas* (Gammaproteobacteria).

L'ús correcte de metodologies en el camp de la conservació de monuments pot reduir sensiblement el risc inevitable de danyar les superfícies o la pedra, per intervencions conservatives, i conseqüentment pot dur a un decreixement en els costos de manteniment dels monuments.

Els resultats detallats d'aquest capítol s'inclouen en el següent article:

On the efficiency of biocides and cleaning treatments in restoration works of subterranean monuments. ***Science and Cultural Heritage in the Mediterranean Area. Diagnostic and conservation experiences and proposals for a risk map.*** Palermo Regione Siciliana Assessorato beni Culturali e Ambientali e Pubblica Istruzione. (2008), en premsa.

## ON THE EFFICIENCY OF BIOCIDES AND CLEANING TREATMENTS IN RESTORATION WORKS OF SUBTERRANEAN MONUMENTS

E. Akatova, M. Roldán<sup>1</sup>, M. Hernandez-Marine<sup>1</sup>, J.M. Gonzalez and C. Saiz-Jimenez

Instituto de Recursos Naturales y Agrobiología, CSIC, Apartado 1052, 41080 Sevilla, Spain

<sup>1</sup>Departamento de Productos Naturales, Facultad de Farmacia, 08028 Barcelona, Spain

### INTRODUCTION

The conservation of historical buildings and monuments is a world-wide problem but it is particularly emphasized in Europe where concentrate almost the 70% of these important witness of our cultural heritage. In addition, two countries, Italy and Spain, are characterized for having the largest European Cultural Heritage and face considerable problems for their conservation.

It is now well recognized that microorganisms can be responsible for the destruction of monuments, buildings and cultural heritage assets, including the decay of concrete, cement, stones, mural paintings, woods, metals, glass, paper, etc.

The study of microbial communities in monuments is usually accomplished by using traditional culture methods. Common methods include microbial cell counting or isolation and subsequent identification of laboratory pure cultures. These methods are not only time-consuming but also have the disadvantage that relatively large amounts of sample material are

needed. It is therefore of great interest to provide fast, straightforward methodologies, as conventional microbiological methods are carried out by scientists using complex taxonomic and ecological approaches.

However, it is believed that a very small percentage of the extant microorganisms have been discovered in individual ecosystems, and that culture methods are partially inadequate for studying microbial natural communities. In fact, studies based on 16S ribosomal RNA genes showed a large number of community members which have never been cultured (Ward et al. 1990; Giovannoni et al. 1990).

The same scenario occurs with microbial communities present in cultural assets where traditional culture methods are biased by the limitations imposed by the conservation of the work of art and the very rare availability of often extremely small samples. Therefore, it can be assumed that most of the microorganisms present in cultural assets remain undiscovered. This is



of great importance, as most restoration works apply conventional biocides which probably are not suitable for the unknown and complex microbial communities growing on and beneath the surfaces. Current restoration efforts can have an opposite effect, particularly if these measures use substrates which support the growth of microorganisms and, consequently, accelerate the deterioration process. Consequently the introduction and dissemination of molecular biology and biotechnology techniques in the whole conservation/restoration process of cultural heritage assets will represent a significant advancement in this particular field.

Besides molecular culturing strategies, microscopy can provide with direct examinations of biodeteriorated monuments. The use of recently developed fluorescence microscopical techniques allows to specifically detect autofluorescence produced by phototrophic communities involved in deterioration. This natural autofluorescence is produced by pigments which are a critical component of the photosynthetic machinery in these phototrophic microbes.

The purpose of this paper is to evaluate the efficiency of cleaning techniques by using biocides. The goal is to identify and enhance the use of a set of methodologies affordable for the control of restoration and biocide applications.

#### **CASE STUDY 1. SALPETRE CAVES OF COLLBATO, BARCELONA, SPAIN**

Photosynthetic microorganisms colonize aerophytic environments in a high variety of habitats forming complex communities encased themselves in organic, polymeric matrices known as biofilms. Their microbial activity contributes to the alteration of materials, causes a mechanical deterioration on the stone surface and enhances the loss of particles from the mineral structure. In addition the dusty green color is considered aesthetically unacceptable.

The objective of our study was to ensure cleaning techniques and if the biocide concentrations were appropriate in an intervention proposed to clean affected surfaces in the Salpetre caves of Collbató, Barcelona, and to prevent subsequent biofilm growth by means of environmental friendly techniques.

Caves and other hypogeal environments are usually stable for humidity and temperature whereas light is the main stress factor. Because that, monochromatic light can be applied for control and prevention of biofilm growth on stone. (Albertano et al., 2005).

#### **Material and methods**

The biocide essayed was the quaternary ammonium compound benzalkonium chloride (BC) that has been recognized as a broad spectrum antimicrobial agent. The choice of BC as biocide was based on its relative safety and efficacy as reported in the literature (Ascaso et al. 2002; Bernardini 1993 Kumar and Kumar

1999) and from our own experience (unpublished data).

We use both the commercially available active principle (1%) and the complex commercial organic compound (Preventol R50, 2%). To evaluate the potential inhibitory effect of both formulations on a mixed biofilm and to quantify the fate of the treatments when submitted to green light, *in situ* quantitative assessment of biocide effects were carried out.

To this end, two equivalent testing areas, with a relatively flat topography, were selected inside the Cave in Barcelona. The substrate was a stalactite with clay impurities from decalcification. Each area was divided into four vertically arranged quadrants (Figures 1 and 2).

For each area, one quadrant, denoted quadrant A, was maintained as a control, to have a reference for the possible effects of environmental change on local biofilm growth during the year. The three remaining quadrants (B, C and D) were cleaned using a synthetic brush embedded in 70% alcohol/distilled water to remove photosynthetic organisms and to allow better penetration of biocidal products inside the substrata. Quadrants C and D were then treated with the biocides. In addition we evaluated and compared the effects of illuminating the biofilms using exclusively white light (WL) lamps in one of the sampling zones and green light (GL) lamps (Roldán et al. 2006) in the other.

Small fragments of untreated quadrants were removed before the

cleaning and application of biocides. One year after application, fragments of all the quadrants were also collected for analysis.

Pigment fluorescence can be used as an indicator of photosynthetic processes in plants, algae and cyanobacteria (Eggert et al., 2006; Tomaselli et al., 2002). Therefore, epifluorescence biofilm-monitoring system was used to determine the efficacies of cleaning and biocide formulations and simultaneous effect of GL against new biofilm colonization. The fluorescence emission of photosynthetic pigments (chlorophylls and phycobilins), excited at 546 nm and captured >590nm was directly recorded with a resolution of 1272 x 1017 pixels, using a stereoscopic microscope Leica MZFL3. Photographs were used for computer-assisted quantification of the cover to estimate the degree of colonisation. IMAT software was used to measure fluorescence pixel by pixel. Data sets were exported into Microsoft Excel for analysis. For each image the percentage of fluorescent area (grey pixels in between 70 and 255) with respect to the total area was calculated. Several images for each of the sites and treatments were processed and the media obtained. From each area the average of total number of pixels of all images with fluorescence over the threshold of grey is presented inside parenthesis. Differences among quadrants measured as average of all images from each fluorescent area were used for comparison.

## Results and discussion

The stalactite community forming

biofilms consisted primarily of cyanobacteria and microalgae living on the surface but also in fissures and between crystals (chasmoendoliths). Moss protonemata was also present, depending on light availability.

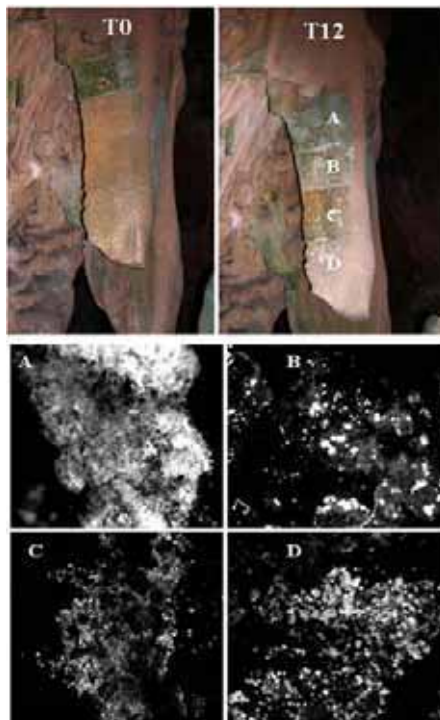


Figure 1. Testing area maintained under white light during 12 months. Treatments A to D as described in Material and methods. Note the decreasing of fluorescence after biocide treatments.

**Testing area under white light** (Figure 1). The control quadrant was covered (83%) by a blue-grey patina, similar to the untreated initial fragments. The main organisms were the filamentous cyanobacteria *Scytonema julianum* and *Leptolyngbya* spp. and diatoms on their surface, while small colonies of

*Nostoc punctiforme* were identified inside the calcite. In the B quadrant the same organisms were observed although impoverished (23%) and, in addition, some moss protonema. The cover of quadrants C (27%) and D (10%) was mainly built by *Nostoc minutissimum* forming brilliant black-green spots, indicating that this is the most resilient organism among those that found in the cave biofilms. Cleaning (quadrant B) and both biocide treatments (quadrants C and D) prevented to a certain extent from biofilm recovering, compared to the control (quadrant A). The change in formulation and the increasing in biocide concentration in quadrant D produced a progressive reduction, but not a total inhibition, of the biofilm development and changes in the biofilms forming organisms.

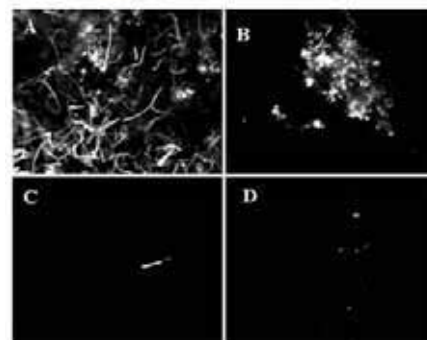
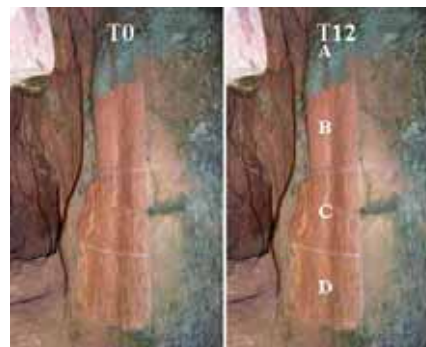


Figure 2. Testing area maintained under green light during 12 months. Treatments A to D as described in Material and methods. Note the almost absence of fluorescence after biocide treatments.

**Testing area under green light** (Figure 2). The control quadrant was covered (48%) by a grey patina consisting on remains of *Scytonema julianum* and other filamentous cyanobacteria and a few colonies of black fungi. Protonema had longer and thinner filaments without plastonemata except for a few wider terminal cells. On B quadrant (19%) were the same organisms as in A although even scarce. On C (9%) and D (6%) quadrants colonization was limited and the fluorescent dots were caused by filamentous remains of *Scytonema julianum* and by *Nostoc punctiforme* and *Gloeocapsopsis magma*.

Results from the study found that BC in both formulations was effective in reducing the levels of fluorescence, compared with controls. In addition, the abundance of *Scytonema julianum* and other predominant species were significantly reduced, except for *Nostoc punctiforme* and *Gloeocapsopsis magma*, both covered by extracellular polysaccharides and with accessory pigments. In the original samples they were mainly restricted to the subsurface. The presence of thick polysaccharidic sheaths might play an important role in the resistance of both organisms to adverse abiotic conditions, including resistance to biocides. As the control quadrants and treated quadrants were subjected

to the same seasonal influences the differences in their photosynthetic coverage can only be attributed to the treatments. Moreover, the observations reported above suggest that GL lighting, instead of WL, could prevent the growth of photosynthetic organisms, even when biofilms were composed of phycoerythrin-containing cyanobacteria, as in this case. The signs of retarded growth suggest that GL is a treatment for preventing photosynthetic biofilm growth in artificially illuminated works of art.

## CASE STUDY 2. MURAL PAINTINGS, NECROPOLIS OF CARMONA, SEVILLA, SPAIN

The Roman Necropolis of Carmona (Seville, Spain) represents one of the most significant burying sites in Southern Spain used during the 1<sup>st</sup> and 2<sup>nd</sup> centuries A.D. It was discovered at the 19<sup>th</sup> century. The Necropolis was formed by a large number of underground tombs excavated in the rock, a highly porous calcarenite, which is easily affected by weathering and processes of microkarstification.



Figure 3. Tomb of Postumio. Note the deterioration of mural paintings and the

abundance of efflorescences.

Within this archaeological site is located the Tomb of Postumio which calcarenite was covered with mural paintings. Due to weathering and efflorescence formation, salts crystallized on the surfaces, only discrete areas of the paintings are preserved (Figure 3).

### Material and methods

Samples were taken from the same efflorescence area in the Tomb of Postumio before (Z26) and after the restoration process (Z26C). The restoration consisted in cleaning, treatment with BC and consolidation. The works were completed in May 2005. Z26C sample was collected two weeks after restoration. Samples were collected under aseptic conditions into sterile tubes and were preserved in the laboratory at -80°C.

Small samples were used for DNA extraction. DNA was extracted using the NucleoSpin Food DNA extraction kit (Macherey-Nagel, Düren, Germany) following the manufacturer's recommendations. DNA was preserved at 4°C until processed.

Amplification of bacterial 16S rRNA fragments was performed by PCR using the primer pair 616F (5'-AGA GTT TGA TYM TGG CTC AG) and 907R (5'-CCC CGT CAA TTC ATT TGA GTT T) from extracted DNA and 616F (Gonzalez et al. 2003). To amplify 16S rRNA gene fragments from Cyanobacteria the universal primer 106F (5'-CGG ACG GGT GAG TAA CGC GTG A-3') and an equimolar mixture of the reverse primers 781Ra (5'-GAC TAC TGG GGT ATC TAA TCC CAT T-3') and

781Rb (5'-GAC TAC AGG GGT ATC TAA TCC CTT T-3') were used. ExTaq (Takara, Shiga, Japan) was the DNA polymerase used for PCR, following the manufacturer's recommendations. Thermal conditions for the amplification reaction consisted on the following steps: 95°C for 2 min; 30 cycles (unless otherwise stated) of 95°C for 15 s, 55°C (60 °C for Cyanobacteria) for 15 s and 72°C for 1 min; and 72°C for 10 min.

Fingerprinting of the microbial communities was obtained by Denaturing Gradient Gel Electrophoresis (DGGE) following the method described by Muyzer et al. (1993) and Gonzalez and Saiz-Jimenez (2004). The primer pair used for amplification of DGGE suitable DNA fragments was: 341F-GC (5'-CC TAC GGG AGG CAG CAG and a GC-rich tail attached at its 5' end) and 518R (5'-TGG TWT TAC CGC GGC GGC TGA-3') (Muyzer et al., 1993; Gonzalez and Saiz-Jimenez, 2005).

Amplification conditions were as described above with the exception of an extension step of only 30 seconds. Migration markers (*Pseudomonas* sp., *Escherichia coli*, *Paenibacillus* sp. and *Streptomyces* sp.) were used throughout this study as reference for locating the position of cloned fragments in a microbial community fingerprint obtained by DGGE and facilitate sample comparisons.

PCR products were purified by the PCR purification kit (JetQuick, Germany) and cloned using the TOPO-TA cloning kit (Invitrogen, Carlsbad, CA, USA). The 16S rRNA libraries obtained were used to

identify the microbial components of the community. A previously described screening method (Gonzalez et al. 2003) was followed with these libraries. Selected clones were sequenced.

Sequence data were edited using the software Chromas, version 1.45 (Technelysium, Tewantin, Australia). Homology searches from the nucleic acid sequences were performed using the Blast algorithm (Altschul et al. 1990) at the NCBI (National Center for Biotechnology Information; <http://www.ncbi.nlm.nih.gov/Blast/>). Sequences were checked for putative chimeras using Ccode as described by Gonzalez et al. (2005).

## Results and Discussion

The results showed a high similarity both between the bacterial communities and phototrophic communities before and after restoration process.

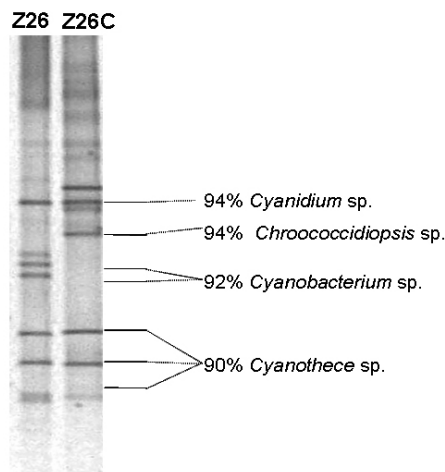


Figure 4. DGGE analysis showing the cyanobacterial communities before (Z26) and after (Z26C) treatment and the

migration of the identified cyanobacteria.

16S rDNA clone libraries revealed phylogenetic information on individual microbial members present in the samples. Obtained cloned sequence types of the common bands from the two communities were affiliated with the genera *Chroococcidiopsis*, *Cyanidium*, *Cyanothece*, etc. (Figure 4).

Cloned sequences obtained from bacterial communities were different in Z26 and Z26C bacterial community. The bacterial community of the sample, taken before restoration treatment (Z26), contained bacteria phylogenetically related to Actinobacteria, Alpha- Beta and Gamma-proteobacteria. The majority of sequences obtained from the bacterial communities of the investigated samples presented homology with uncultured microorganisms. Among the bacteria detected in this study were members of the genera *Propionibacterium*, *Arthrobacter*, *Rubrobacter*, *Micrococcus*, *Mycobacterium*, *Kibdelosporangium*, and *Pseudonocardia* (Actinobacteria); *Nordella*, *Mesorhizobium*, and *Phyllobacterium* (Alphaproteobacteria); *Salinisphaera* and *Stenotrophomonas* (Gammaproteobacteria) (Figure 5).

The presence of Actinobacteria has been previously reported in numerous studies constituting common members of the bacterial community in subterranean monuments (Groth and Saiz-Jimenez, 1999; Laiz et al. 2002). Since the Actinobacteria are heterotrophic microorganisms, their growth must be dependent on inputs

of organic matter into the tombs.

The results suggest that microbial communities were able to colonize the walls of the Tomb of Postumio shortly after restoration, indicating that the

biocide treatment was not effective, probably due to inactivation by biodegradation (Patrauchan and Oriel, 2003), and fast re-colonization of microorganisms.

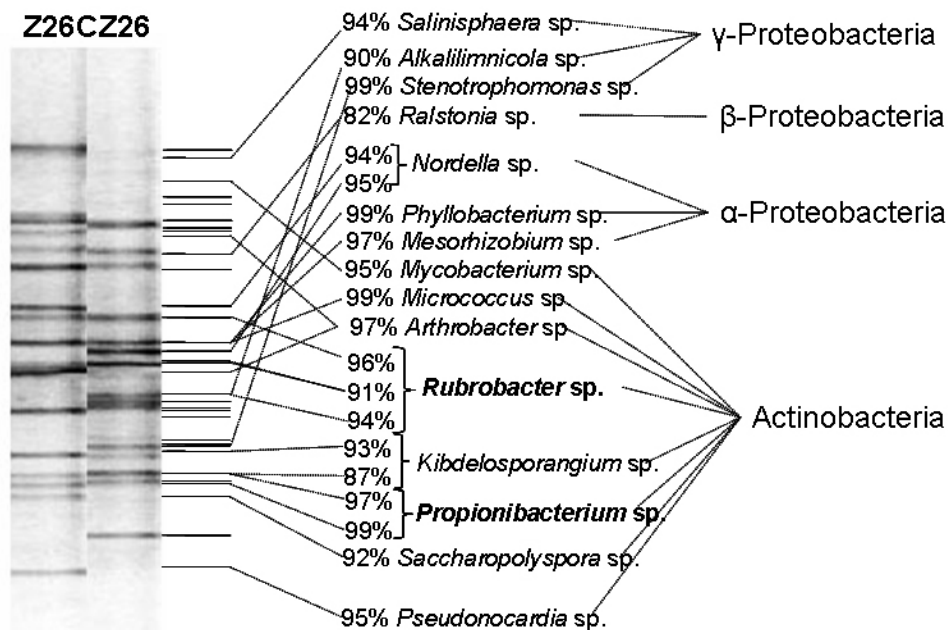


Figure 5. DGGE analysis of the bacterial communities before (Z26) and after (Z26C) treatment and the migration of the identified bacteria in these samples.

## CONCLUSIONS

The technique to evaluate colonization of biofilms *in situ*, based in the fluorescence of pigments, includes the activity of the whole biofilm community under the real environmental conditions. The effectiveness of treatments for the control and prevention of deterioration in dim habitats can be compared in a simple, rapid, and versatile mode.

DGGE analysis allows to monitor changes in community structure, such as those caused by treatments with biocides or any other treatment.

The benefit obtained from the application of these techniques are: i) the minimization of sampling, and ii) the optimization of information in diagnostic studies on microbial contamination of cultural assets, which illustrates the advantages of using molecular techniques for

diagnostic purposes.

The correct use of scientific methodologies in the field of conservation of monumental buildings can sensibly reduce the inevitable risk of stone damage due to empirical conservative interventions, and consequently decrease maintenance cost. Besides, the incorrect or over use of biocide products can lead to an unnecessary rise in maintenance costs.

#### ACKNOWLEDGEMENTS

This work was supported by the European Commission, Marie Curie Actions MEST-CT2004-513915 and Consejería de Innovación, Ciencia y Empresa (project RNM 2318). The facilities provided by the Consejería de Cultura, Junta de Andalucía, the Necropolis de Carmona staff and the corporation of Collbato are gratefully acknowledged.

#### REFERENCES

- Albertano, P., Bruno, L. and Bellezza, S. (2005). *Plant Biosystems*. 139, 311-322.
- Ascaso, C., Wierzchos, J., Souza-Egipsy, V., De los Rios, A. and Delgado Rodrigues, J. (2002). *Int. Biodeter. Biodegr.* 49, 1-12.
- Bernardini, C. (1993). *Kermes* 16, 12-19.
- Eggert, A., Haübner, N., Klausch, Karsten, S. U. and Schumann, R. (2006). *Biofouling* 22, 79-90
- Giovannoni, S.J., Britschgi, T.B., Moyer C.L. and Field. K.G. (1990). *Nature* 345, 60-63.
- Gonzalez J.M. and Saiz-Jimenez C. (2004). *J. Separ. Sci.* 27, 174-180.
- Gonzalez, J.M. and Saiz-Jimenez, C. (2005). *Int. Microbiol.* 8, 189-194.
- Gonzalez J. M., Ortiz-Martinez A., Gonzalez-delValle M. A., Laiz L. and Saiz-Jimenez C. (2003). *J. Microbiol. Meth.* 55, 459-463.
- Gonzalez, J.M., Zimmermann, J. and Saiz-Jimenez, C. (2005). *Bioinformatics* 21, 333-337.
- Groth I. and Saiz-Jimenez C. (1999). *Geomicrobiol. J.* 16, 1-8.
- Kumar, R., Kumar, A.V. (1999). *Research in Conservation, Getty Conservation Institute, Los Angeles*, 85 pp.
- Laiz L., Hermosin B., Caballero B. and Saiz-Jimenez C. (2002). In: Galan E. and Zezza F. (eds.), *Protection and Conservation of the Cultural Heritage of the Mediterranean Cities*, pp. 173-178. Balkema, Lisse.
- Muyzer G., de Waal E. C. and Uitterlinden A.G. (1993). *Appl. Environ. Microbiol.* 59, 695-700.
- Patrauchan, M.A. and P.J. Oriel, P.J. (2003). *J. Appl. Microbiol.* 2003, 94, 266–272.
- Roldán M., Oliva F., González del Valle M. A., Saiz-Jimenez C., and Hernández-Mariné M. (2006). *Appl. Environ. Microbiol.* 72, 3026-3031
- Tomaselli, L., Lamenti, G. and Tiano, P. (2002). *Ann. Microbiol.*, 52, 197-206
- Ward, D.M., Weller, R. and Bateson, M.M. (1990). *Nature* 345, 63-65.



